On the Performance of In-Band Full-Duplex Cooperative Communications

Thesis by

Mohammad Galal Mostafa Khafagy, B.Sc., M.Sc.

In Partial Fulfillment of the Requirements

For the Degree of

Doctor of Philosophy

(Electrical Engineering Program)

Division of Computer, Electrical, and Mathematical Sciences and Engineering (CEMSE)

King Abdullah University of Science and Technology (KAUST)

Thuwal, Makkah Province, Kingdom of Saudi Arabia

The thesis of Mohammad Galal Mostafa Khafagy is approved by the examination committee

Committee Chairperson:	Prof. Mohamed-Slim Alouini
Committee Member:	Prof. Ahmed K. Sultan Salem
Committee Member:	Prof. Basem Shihada
Committee Member:	Prof. Jeff S. Shamma
Committee Member:	Prof. Geoffrey Ye Li

DEDICATION

To my lovely daughter, Nada.

ABSTRACT

On the Performance of In-Band Full-Duplex Cooperative Communications

Mohammad Galal Mostafa Khafagy

In-band full-duplex, by which radios may simultaneously transmit and receive over the same channel, has been always considered practically-unfeasible due to the prohibitively strong self-interference. Indeed, a freshly-generated transmit signal power is typically ten orders of magnitude higher than that of a naturally-attenuated received signal. While unable to manage such an overwhelming interference, wireless communications resorted to half-duplex operation, transmitting and receiving over orthogonal channel resources. Recent research has demonstrated the practical feasibility of full-duplexing via successive sophisticated stages of signal suppression/cancellation, bringing this long-held assumption down and reviving the promising full-duplex potentials. Full-duplex relaying (FDR), where intermediate nodes may now support source-destination communication via simultaneous listening/-forwarding, represents one of two full-duplex settings currently recommended for deployment in future fifth-generation (5G) systems. Theoretically, it has been widely accepted that FDR potentially doubles the channel capacity when compared to its half-duplex counterpart. Although FDR doubles the multiplexing gain, the effective signal-to-noise ratio (SNR) can be significantly degraded due to the residual self-interference (RSI) if not properly handled.

In this work, efficient protocols are devised for different FDR settings. *Selective cooperation* is proposed for the canonical three-terminal FDR channel with RSI, which exploits the *cooperative diversity* offered by the independently fading source/relay message replicas arriving at the destination. Closed-form expressions are derived for the end-to-end SNR cumulative distribution function (CDF) under Rayleigh and Nakagami-m fading. Further, the offered diversity gain is presented as a function of the RSI scaling trend with the relay power. We show that the existing diversity problem in simple FDR protocols can be considerably fixed via block transmission with selective cooperation. Beyond the single-relay setting, the outage performance of different opportunistic full-duplex relay selection (FDRS) protocols is also evaluated under Rayleigh and Nakagami-m fading. It is shown that, with state-of-the-art adaptive self-interference cancellation techniques, FDRS can offer the same diversity order of its half-duplex rival while supporting a higher level of spectral efficiency. FDRS is also analyzed when adopted by a spectrum-sharing secondary system while the primary spectrum user imposes an additional interference constraint. Finally, *buffer-aided* hybrid half-/full-duplex cooperation is addressed. To maximize the end-to-end throughput, joint duplexing mode and link selection is studied where the system leverages the buffer and outage state information at the transmitters. All theoretic findings are corroborated with numerical simulations, with comparisons to existing protocols.

ACKNOWLEDGEMENTS

First and foremost, all the praise and acknowledgements be to Allah, the Most Gracious, the Most Merciful. Alhamdulillah, by the grace of almighty Allah, it has been destined for this thesis to be accomplished. Such a milestone is only one of His countless blessings and bounties that one may never find sufficient words to describe or enumerate.

I would like to express my heartfelt gratitude to my thesis adviser, Prof. Mohamed-Slim Alouini, for the continued and unconditional support he offered me throughout the years I spent in KAUST. I am deeply indebted to his advice, patience, trust, and such a caring attitude he always offered. Without his continued guidance and encouragement, this thesis would have faced several hurdles. I am grateful to my initial adviser in the early stages of my extended stay, Prof. Sonia Aïssa, who also remained as my co-adviser after leaving KAUST. I would like to greatly acknowledge the smooth transition she offered at that time and always cared to maintain. I feel greatly indebted to Prof. Ahmed Kamal Sultan for his continued advice, research collaboration, and the many rich discussions I have always enjoyed and benefited from. I have been truly blessed to have him as a mentor throughout different milestones, and he will always remain to me as a true inspiration when it comes to diligence, hard work, and dedication. Also, I would like to gratefully thank my examination committee for the time and effort they spent in proofreading the presented thesis.

I would like to thank several professors, postdoctoral fellows, and student colleagues with whom I have had several collaboration opportunities, fruitful discussions, and technical advice. First, I want to thank Dr. Amr Ismail, with whom I had my very first fruitful collaboration in the thesis work, while also being very good friends on the personal level. Also, I would like to sincerely thank Dr. Osama Amin, Dr. Walid Abediseid, Dr. Ahmed Bader, Prof. George Turkiyyah, Dr. Ammar Zafar, Dr. Imran Shafique Ansari, Mohamed Gaafar, Ahmed El Shafie (UT Dallas) and Dr. Elsayed

Ahmed (Qualcomm Inc.). I would also like to thank several professors who I attended/audited the courses they offered and greatly benefited from their knowledge; Prof. Ahmed K. Sultan, Prof. Basem Shihada, Prof. Tareq Al-Naffouri, Prof. Klaus Gärtner (Weierstrass Institute), Prof. Diogo Aguiar Gomes, Prof. Jeff S. Shamma, and Prof. Giuseppe Caire (USC). I would have missed a great part of the intellectually-rich research environment if it was lacking the input of several group research scientists, postdoctoral fellows and fellow students; Prof. Sameh Sorour, Prof. Mohamed Farouk Agamy, Dr. Hesham ElSawy, Dr. Ali Chelli, Prof. Minghua Xia, Dr. Tarig Ballal, Dr. Anas Chaaban, Prof. Hayssam Dahrouj, Prof. Zouheir Rezki, Lokman Sboui, Dr. Doha Hamza, Houssem Sifaou, Amr Abdelhady, Ahmed AlAmmouri, Marwen Zorgui, Dr. Mehdi Ben Ghorbel, Mohamed Gharbieh, Rabe Arshad and Ahmad Alsharaa.

A special applause needs to be dedicated to my friends here at KAUST for the great time we had together. I would like to thank Mohamed Nasr, Mohamed Ibrahim, Hassan AbouEisha, Moataz Hammouda, Anas Ismail, Usama Elnily, Mohamed Elshenawy, Ahmed Seif, Mohamed Ghoneim, Amr Ismail, Sameh Sorour, Mohamed Agamy, Hesham ElSawy, Nasr Hassanein, Hatem Selim, Amr El Rasad, Hesham Omran, Mahmoud Ouda, Ayman El Khodeiry, Haitham Ashour, Ahmed Abdelrahman, Ahmed Bahgat, Amin Allam, Amir Nabil, Ahmed Abbas, Ahmed Saad, Ahmed Nafe, Karim Awara, Khaled Ramadan, Maged Abdelsamie, Mohamed Barakat, Ahmed Magdy, Tarek Nasr, Mahmoud Nafe, and Ramy El Afandy. I would also like to sincerely thank the KAUST community for all the support they offered. Such a life milestone, with all its joys and hardships, would have been missing a lot without you all. Everyone I met during my extended stay has engraved a mark that helped enriching my experiences, reshaping my vision, and shall never be forgotten. Please excuse me if I have missed anyone, and thank you for being of great support.

Finally, I would like to thank my family; my lovely daughter, my wife, my father, my aunt, my sisters and their families. It suffices to say that the essence of life may easily go astray without a truly loving, caring, and warmhearted family. Thank you.

TABLE OF CONTENTS

Examination Committee Approval **2**

Dedication **3**

Abstract **4**

Acknowledgements **6**

List of Abbreviations **14**

List of Symbols **17**

List of Figures **18**

List of Tables **20**

I Introduction and Background **21**

1 Introduction **22**

1.1 Motivation 22

1.1.1 Traffic Growth in Next-Generation Networks 23

1.1.2 Envisioned Future Trends: Coping with Traffic Growth 24

1.1.3 Full-Duplexing and Next-Generation Specifications 25

1.1.4 Full-Duplex Cooperation 25

1.2 Full-Duplex Relaying Challenges 26

1.3 Thesis Objectives and Contributions 26

1.4 Thesis Outline 28

2 Background **30**

2.1 The Full-Duplex Self-Interference Channel 30

2.2 Self-Interference Suppression/Cancellation 31
2.2.1 Passive Suppression: Physical Isolation 32
2.2.2 Active Cancellation: Analog Cancellation 32
2.2.3 Active Cancellation: Digital Cancellation 34
2.3 Modeling of the Residual Self-Interference 35
2.3.1 Distribution of the Self-Interference Channel 35
2.3.2 Scaling with Relay Transmit Power 35
2.4 Half-Duplex/Full-Duplex Comparison 36
2.5 Typical Values Used in the Thesis 36

II Buffer-less Relaying **38**

3 Full-Duplex Cooperative Communication **39**
3.1 The Full-Duplex Relay Channel 39
3.1.1 System Model 41
3.2 The Full-Duplex Multi-Hop Channel 43
3.2.1 Outage Performance of MHDF-FDR 44
3.2.2 Outage Performance of MHDF-HDR 47
3.2.3 Source/Relay Power Optimization in MHDF-FDR 47
3.2.4 Comparison of MHDF-FDR and MHDF-HDR 48
3.2.5 Diversity Order Problem 50
3.3 Improper Gaussian Signaling in MHDF-FDR 51
3.3.1 End-to-End Outage Performance Upper Bound 52
3.3.2 Circularity Coefficient Optimization 53
3.3.3 Comparison to MHDF-FDR with PGS 54
3.4 Block Transmission in the Full-Duplex Relay Channel 55
3.4.1 End-to-End Outage Performace 56
3.4.2 Diversity Order of BMSC-FDR 57
3.4.3 Comparison to MRC-HDR 58

Appendices **60**
Appendix 3.A Unimodality of MHDF-FDR Outage Probability in the Source and Relay Power 60
Appendix 3.B Quasiconvexity of Outage Upper Bound in the Relay's Circularity Coefficient 61

4 Selective Full-Duplex Relaying **63**
4.1 Related Work . . . 63
4.2 Block Transmission Scheme . . . 64
4.2.1 Cooperative Mode . . . 65
4.2.2 Non-Cooperative Mode . . . 66
4.2.3 Instantaneous Link Capacities . . . 66
4.3 Selective/Incremental Full-Duplex Cooperation . . . 68
4.4 Outage Performance . . . 69
4.4.1 Rayleigh Fading . . . 71
4.4.2 Nakagami-m Fading . . . 72
4.5 SNR Performance . . . 73
4.5.1 ISDF-FDR . . . 73
4.5.2 SDF-FDR . . . 75
4.5.3 SDF/ISDF-FDR SNR Performance Comparison . . . 76
4.6 Diversity Analysis of SDF-FDR . . . 79
4.7 Hybrid MHDF-FDR/DT . . . 80
4.7.1 Outage Performance . . . 80
4.7.2 Diversity Analysis . . . 81
4.8 Summary . . . 82
4.8.1 A Summary of Protocols . . . 82
4.8.2 A Summary of Results . . . 84
4.9 Numerical Evaluation . . . 85
4.9.1 Simulation Setup . . . 85
4.9.2 Diversity Order: Outage vs. Transmit SNR . . . 87
4.9.3 Outage vs. Rate . . . 88
4.9.4 Outage vs. RSI Link Gain . . . 88
4.9.5 Outage vs. First and Second Hop Gains . . . 89
4.10 Concluding Remarks . . . 90

Appendices **92**
Appendix 4.A Eigenvalues of $H^H H$ . . . 92
Appendix 4.B Derivation of $F(x|A_2)$ . . . 94

5 Full-Duplex Relay Selection **98**
5.1 Introduction . . . 98
5.2 MHDF-FDRS . . . 99
5.2.1 System Model . . . 100

5.2.2 Outage Analysis of MHDF-FDRS . . . 101
5.2.3 Diversity Analysis of MHDF-FDRS . . . 108
5.3 SDF-FDRS . . . 110
5.3.1 Rayleigh Fading . . . 111
5.3.2 Nakagami-m Fading . . . 112
5.3.3 Diversity Analysis . . . 114
5.3.4 Summary of FDRS Diversity Results . . . 114
5.4 Numerical Evaluation . . . 115
5.4.1 End-to-End CDF . . . 115
5.4.2 Outage Probability vs. No. of Relays . . . 116
5.4.3 Diversity Order: Outage Probability vs. Transmit SNR . . . 116
5.4.4 Throughput vs. Source Rate . . . 117
5.5 Conclusion . . . 118

6 Full-Duplex Cooperation in Underlay Cognitive Networks 120
6.1 Spectrum Sharing with Full-Duplex Relaying . . . 121
6.2 System Model . . . 122
6.2.1 Channel Model . . . 122
6.2.2 Signal Model . . . 124
6.3 Performance Analysis . . . 124
6.3.1 No Direct $S-D$ Link . . . 124
6.3.2 Leveraging Direct $S-D$ Link . . . 129
6.4 Numerical Evaluation . . . 130
6.4.1 End-to-End CDF . . . 130
6.4.2 Outage Probability vs. No. of Relays . . . 131
6.5 Conclusion . . . 132

III Buffer-Aided Relaying 133

7 Buffer-Aided Half-Duplex Relaying 134
7.1 Related Work . . . 135
7.1.1 Potentials of Leveraging BSI . . . 136
7.1.2 Leveraging BSI in Fixed-Rate Transmission . . . 137
7.1.3 Contribution . . . 137
7.2 System Model . . . 138
7.2.1 Channel Model . . . 138

7.2.2 Signal Model . . . 139
7.3 Transmission Scheduling Scheme . . . 139
7.3.1 Transmit BSI/No Transmit CSI . . . 140
7.3.2 Transmit BSI/Partial Transmit CSI . . . 142
7.4 End-to-End Throughput Maximization . . . 143
7.4.1 Transmit BSI/No Transmit CSI . . . 143
7.4.2 Transmit BSI/Partial Transmit CSI . . . 145
7.4.3 Partial Transmit CSI only . . . 148
7.5 Numerical Results . . . 148
7.5.1 Throughput vs. Buffer Size . . . 148
7.5.2 Throughput vs. Source Rate . . . 150
7.6 Conclusion . . . 151

Appendices **152**
Appendix 7.A Source/Destination Throughput . . . 152

8 Buffer-Aided Full-Duplex Relaying **153**
8.1 System Model . . . 153
8.2 Transmission Scheduling Protocol . . . 155
8.3 End-to-End Throughput Maximization . . . 158
8.3.1 BSI and CSI at the Transmitter Side . . . 158
8.3.2 CSI Only at the Transmitter Side . . . 162
8.4 Numerical Results . . . 162
8.5 Conclusion . . . 166

Appendices **167**
Appendix 8.A R − D Outage Probability Given S − D outage . . . 167

IV General Conclusion and Future Work **168**

9 Conclusion **169**
9.1 Summary of Results . . . 169
9.2 Future Research Work . . . 170

Appendices **172**

A Useful Probability Distributions **172**

A.1 Sum of Two RVs: $S = X_1 + X_2$ 172
A.1.1 Gamma Distributed X_1 and X_2 172
A.1.2 Exponentially Distributed X_1 and X_2 173
A.2 Ratio of Two RVs: $Z = X_1/(X_2 + 1)$ 173
A.2.1 Gamma-Distributed X_1 and X_2 173
A.2.2 Gamma-Distributed X_1 and Exponentially-Distributed X_2 174
A.2.3 Exponentially-Distributed X_1 and X_2 174

B Papers Submitted and Under Preparation **175**

References **177**

LIST OF ABBREVIATIONS

5G	Fifth-Generation
ACK	Acknowledgment
ADC	Analog-to-Digital Converter
AF	Amplify-and-Forward
AWGN	Additive White Gaussian Noise
BALUN	Balanced/Unbalanced Transformer
BMSC	Block Markov Superposition Coding
bpcu	Bits per Channel Use
BS	Base Station
BSI	Buffer State Information
CDF	Cumulative Distribution Function
CSI	Channel State Information
DF	Decode-and-Forward
DL	Downlink
DT	Direct Transmission
FD	Full-Duplex
FDR	Full-Duplex Relaying
FDRS	Full-Duplex Relay Selection
HD	Half-Duplex
HDR	Half-Duplex Relaying
HDRS	Half-Duplex Relay Selection

i.i.d.	Independent and Identically Distributed
i.n.i.d.	independent but not identically distributed
ICIC	Inter-Cell Interference Coordination
IDF	Incremental Decode-and-Forward
IDL	Interfering Direct Link
IGS	Improper Gaussian Signaling
IMT	International Mobile Telecommunication
IMT-2020	IMT for 2020 and beyond
ISDF	Incremental Selective Decode-and-Forward
ITU	International Telecommunication Union
ITU-R	ITU Radiocommunications Sector
LoS	Line-of-Sight
MBB	Mobile Broadband
MHDF	Multi-Hop Decode-and-Forward
MIMO	Multiple-Input Multiple-Output
MISO	Multiple-Input Single-Output
MRC	Maximum-Ratio Combining
NACK	Negative Acknowledgment
NDL	No Direct Link
PDF	Probability Density Function
PGS	Proper Gaussian Signaling
QoS	Quality-of-Service
RF	Radio Frequency
RSI	Residual Self-Interference
RV	Random Variable
SC	Selective Combining
SDF	Selective Decode-and-Forward
SINR	Signal-to-Interference-plus-Noise Ratio
SISO	Single-Input Single-Output

SNR	Signal-to-Noise Ratio
STR	Simultaneous Transmission and Reception
UE	User Equipment
UL	Uplink
UN	United Nations
w.r.t.	with respect to

LIST OF SYMBOLS

$\boldsymbol{\mathcal{B}}(a,b)$	Beta Function
$\boldsymbol{\Gamma}(a)$	Gamma Function
$\boldsymbol{\gamma}(a,b)$	Lower Incomplete Gamma Function
$\boldsymbol{\Gamma}(a,b)$	Upper Incomplete Gamma Function
${}_{\mathbf{1}}\boldsymbol{F}_{\mathbf{1}}(a;b;c)$	Kummer's Function
$\boldsymbol{U}(a,b,c)$	Tricomi's Function
$\boldsymbol{W}_{a,b}(c)$	Whittaker's Function
B	Source Codeword Block Length in Symbols
$\mathcal{C}$	Source Code Book
D	Destination Node
$\mathcal{E}$	Source Encoding Function
g_{ij}	Channel Gain from node i to node j
h_{ij}	Complex Channel Coefficient from node i to node j
M	Source Message
$\mathcal{M}$	Source Message Book
π_{ij}	Average Channel Gain from node i to node j
R	Relay Node
R	Source Rate
S	Source Node

LIST OF FIGURES

3.1 Full-Duplex vs. Half-Duplex Cooperation 40
3.2 A full-duplex cooperative setting in coverage extension scenarios where direct source transmissions are treated as interference at the destination. 44
3.3 Relative Performance of MHDF-HDR/-FDR protocols over Rayleigh fading links, for $\pi_{\mathrm{SR}} = \pi_{\mathrm{RD}} = 20$ dB, $\pi_{\mathrm{RR}} = 8$ dB, $\pi_{\mathrm{SD}} = 0$ dB, and $\delta = 1$. 49
3.4 Outage vs. Power over Rayleigh fading links, for $\pi_{\mathrm{SR}} = \pi_{\mathrm{RD}} = 20$ dB, $\pi_{\mathrm{RR}} = 8$ dB, $\pi_{\mathrm{SD}} = 0$ dB and $R = 1$ bpcu. 54
3.5 A general full-duplex cooperative setting where direct source transmission is exploited as a diversity branch at the destination. 55
3.6 End-to-End Performance of BMSC-FDR and MRC-HDR protocols over Rayleigh fading links, for $\pi_{\mathrm{SR}} = \pi_{\mathrm{RD}} = 20$ dB, $\pi_{\mathrm{RR}} = 2$ dB, $\delta = 1$ and $\pi_{\mathrm{SD}} = 5$ dB. . . 59

4.1 SDF-FDR block transmission scheme, where $\boldsymbol{x}_{\mathrm{S}}[b]$, $b \in \{1, 2, \cdots, L\}$, is the b^{th} B-dimensional codeword transmitted by the source. 64
4.2 CDF of the end-to-end SNR. 77
4.3 Percentage of relay cooperation/power expenditure, for $\pi_{\mathrm{SD}} = 10$ dB, $\pi_{\mathrm{SR}} = \pi_{\mathrm{RD}} = 20$ dB, $\pi_{\mathrm{RR}} = 10$ dB and $m_{\mathrm{SR}} = m_{\mathrm{RR}} = m_{\mathrm{RD}} = m_{\mathrm{SD}} = 1$. 77
4.4 Outage prob. vs. $P_{\mathrm{S}} = P_{\mathrm{R}} = P$, for $\pi_{\mathrm{SR}} = \pi_{\mathrm{RD}} = 15$ dB, $\pi_{\mathrm{SD}} = 0$ dB, $m_{\mathrm{SR}} = m_{\mathrm{RD}} = m_{\mathrm{RR}} = m_{\mathrm{SD}} = 1$ and $R = 2$ bpcu. 86
4.5 Outage probability vs. rate, for $\pi_{\mathrm{SR}} = \pi_{\mathrm{RD}} = 20$ dB, $\pi_{\mathrm{RR}} = 3$ dB, $m_{\mathrm{SR}} = 3$, $m_{\mathrm{RR}} = m_{\mathrm{RD}} = 2$, and $m_{\mathrm{SD}} = 1$. 88
4.6 Outage prob. vs. π_{RR}, for $\pi_{\mathrm{SR}} = \pi_{\mathrm{RD}} = 20$ dB, $\pi_{\mathrm{SD}} = 3$ dB, $m_{\mathrm{SR}} = 3$, $m_{\mathrm{RR}} = m_{\mathrm{RD}} = 2$, $m_{\mathrm{SD}} = 1$ and $R = 1$ bpcu. 89
4.7 Outage prob. vs. π_{SR} and π_{RD}, for $\pi_{\mathrm{RR}} = 3$ dB, $\pi_{\mathrm{SD}} = 5$ dB, $m_{\mathrm{SR}} = m_{\mathrm{RD}} = 2$, $m_{\mathrm{RR}} = m_{\mathrm{SD}} = 1$ and $R = 1.5$ bpcu. 89
4.8 Integration regions: a) $x < \eta$ (checkerboard), b) $x > \eta$ (dotted). 94

5.1 A full-duplex cooperative setting with opportunistic relay selection. 99

5.2 CDF of the end-to-end SNR, for $\pi_{\mathrm{SR}} = \pi_{\mathrm{RD}} = 15$ dB, $\pi_{\mathrm{RR}} = \pi_{\mathrm{SD}} = 5$ dB, $m_{\mathrm{SR}} = m_{\mathrm{RD}} = 2$, $m_{\mathrm{RR}} = m_{\mathrm{SD}} = 1$, $\delta = 1$, $P_{\mathrm{S}} = P_{\mathrm{R}} = 1$, and $K = 5$ relays. . . 115
5.3 Outage probability vs. No. of Relays, for $\pi_{\mathrm{SR}} = \pi_{\mathrm{RD}} = 10$ dB, $\pi_{\mathrm{RR}} = 3$ dB, $\pi_{\mathrm{SD}} = 5$ dB, $m_{\mathrm{SR}} = m_{\mathrm{RD}} = m_{\mathrm{RR}} = m_{\mathrm{SD}} = 2$, $\delta = 1$, $P_{\mathrm{S}} = P_{\mathrm{R}} = 1$, and $R = 1$ bpcu. 116
5.4 Outage probability vs. Transmit Power, for $\pi_{\mathrm{SR}} = \pi_{\mathrm{RD}} = 15$ dB, $\pi_{\mathrm{RR}} = \pi_{\mathrm{SD}} = 4$ dB, $m_{\mathrm{SR}} = m_{\mathrm{RD}} = m_{\mathrm{RR}} = m_{\mathrm{SD}} = 1$, $K = 3$, and $R = 2$ bpcu. 117
5.5 Throughput vs. rate, for $(\pi_{\mathrm{SR}}, \pi_{\mathrm{RD}}, \pi_{\mathrm{RR}}, \pi_{\mathrm{SD}}) = (15, 15, 4, 4)$ dB, $(m_{\mathrm{SR}}, m_{\mathrm{RD}}, m_{\mathrm{RR}}, m_{\mathrm{SD}}) = (2, 2, 3, 1)$, $\delta = 1$, $P_{\mathrm{S}} = P_{\mathrm{R}} = 1$, and $K = 4$ relays. . . . 118

6.1 Spectrum sharing network with full-duplex relaying. 123
6.2 CDF of the end-to-end SNR, for $\pi_{\mathrm{SR}} = \pi_{\mathrm{RD}} = 15$ dB, $\pi_{\mathrm{RR}} = \pi_{\mathrm{SD}} = 5$ dB, $\pi_{\mathrm{SP}} = 2$ dB, $\pi_{\mathrm{RP}} = 4$ dB, $I_{\mathrm{th}} = 6$ dB, $m_{\mathrm{SR}} = m_{\mathrm{RD}} = 2$, $m_{\mathrm{RR}} = m_{\mathrm{SD}} = m_{\mathrm{SP}} = m_{\mathrm{RP}} = 1$, $\delta = 1$, $P_{\mathrm{S}} = P_{\mathrm{R}} = 1$, and $K = 5$ relays. 131
6.3 Outage probability vs. No. of Relays, for $\pi_{\mathrm{SR}} = \pi_{\mathrm{RD}} = 25$ dB, $\pi_{\mathrm{RR}} = 3$ dB, $\pi_{\mathrm{SD}} = 5$ dB, $\pi_{\mathrm{SP}} = 0$ dB, $\pi_{\mathrm{RP}} = 1$ dB, $m_{\mathrm{SR}} = m_{\mathrm{RD}} = m_{\mathrm{RR}} = m_{\mathrm{SD}} = m_{\mathrm{SP}} = m_{\mathrm{RP}} = 2$, $\delta = 1$, $P_{\mathrm{S}} = P_{\mathrm{R}} = 1$, $I_{\mathrm{th}} \in \{4, 6, 8\}$ dB, and $R = 1$ bpcu. 132

7.1 A buffer-aided half-duplex relay channel. 138
7.2 Birth-death Markov process. Transitions from a state to itself are omitted for visual clarity. 140
7.3 Throughput vs. buffer size. 148
7.4 Throughput vs. rate for $N = 4$ packets, $\gamma_{\mathrm{SR}} = 15$ dB, $\gamma_{\mathrm{RD}} = 15$ dB and $\gamma_{\mathrm{SD}} = 2$ dB. 150

8.1 A buffer-aided full-duplex relay channel with self-interference. 153
8.2 Throughput vs. source rate, for $\pi_{\mathrm{SR}} = \pi_{\mathrm{RD}} = 15$ dB, $\pi_{\mathrm{RR}} = 5$ dB, $\pi_{\mathrm{SD}} = 3$ dB, and $N = 4$ packets. 164
8.3 Throughput vs. buffer size, for $\pi_{\mathrm{SR}} = \pi_{\mathrm{RD}} = 15$ dB, $\pi_{\mathrm{RR}} = 5$ dB, $\pi_{\mathrm{SD}} = 3$ dB, and $R = 1$ bits/sec/Hz. 165

LIST OF TABLES

4.1 A summary of theoretic outage probability and diversity order for the different protocols under consideration. 85

5.1 Diversity order of Full-Duplex Relay Selection Protocols with K Relays . . . 114

8.1 Proposed Transmission Scheduling Protocol 155

Part I

Introduction and Background

Chapter 1

Introduction

1.1 Motivation

Since their first generation in the 1980s, the international mobile telecommunication (IMT) systems have continued to witness rapid developments in wireless services and their substantially growing quality-of-service (QoS) demands. Over the years, such growing demands influenced massive developments in the employed technologies along with the network infrastructure in order to offer *better* and *wider* mobile network connectivity. According to recent statistics, mobile subscriptions has exceeded the current world's population, with about 7.5 billion mobile subscriptions, including machine-to-machine, in May 2015 [1]. Out of this huge number of subscriptions, at least 30% are data ones. Indeed, due to the widespread use of smart hand-held devices, and the revolutionary developments in video streaming applications, even the air interface connecting mobile users to the core network is experiencing growing demands to support bandwidth-intensive data applications. Given the known inherent imperfections in wireless links, e.g., spectrum scarcity, interference, and fading, great challenges are continuously imposed on the wireless communications research community to devise novel and efficient techniques to cope up with these demands. These challenges include maintaining ubiquitous connectivity for the growing number of mobile users, their

high data rate support, in addition to supporting high level of communication reliability, among others.

Currently, and since the beginning of the decade, the world is diligently moving towards fifth-generation (5G) mobile networks. For instance, the International Telecommunication Union (ITU), the international United Nations (UN) specialized agency, has already begun to set the stage for 5G mobile network specifications, in preparation to come into action by the year 2020. For this reason, the upcoming IMT system's set of requirements for 5G networks is termed by the ITU as IMT for 2020 and beyond (IMT-2020). Also, numerous focused articles are being published by experts from both the industry and the academia, discussing the future estimated trends of the evolving applications, demands, candidate technologies, and network infrastructure modifications. Despite being still underway, communications experts from both industry and academia have already started to discuss the set of challenges 5G networks are envisioned to tackle [2, 3, 4, 5]. This includes the support of different traffic types with diverse demands, better sustainability via reduced energy consumption, along with higher quality of user experience. In addition to the efforts coordinated by the UN-based ITU, there are multiple other international/cosmopolitan groups/projects/consortia/fora which race and complement one another to develop and promote for next-generation requirements and specifications. Other international players include 3GPP, a collaboration between multiple telecommunications associations, IEEE, the international standardization organization, as well as the NGMN Alliance, an association of international mobile network operators. Also, examples of partnership projects in the European Union only are 5GNOW, FANTASTIC-5G, and H2020 5GPPP with its METIS, METIS-II, 5G NORMA, and mmMAGIC projects.

1.1.1 Traffic Growth in Next-Generation Networks

The evolution of IMT systems towards mobile broadband (MBB) imposes growing demands for heavier and geographically wider spectrum usage. Multiple studies have been conducted

by the ITU to assess and forecast the traffic growth over the upcoming years, estimating the growth trend till 2020 in [6, 7], and from 2020 to 2030 in [1]. Several drivers impact such a traffic growth, including the growing audio-visual media streaming, device proliferation, and application uptake, among others [1].

For instance, video streaming accounts for around two-thirds of the total mobile traffic in 2016, as per a study by Bell Labs. Also, it is estimated that the total mobile traffic will continue to grow with an annual rate of 54% from 2020 to 2030. This is an estimated growth figure from a traffic amount perspective.

Also, the number of mobile subscriptions is expected to almost double to 13.8 billion in 2025 compared to that in 2015, and to continue growing to 17.1 billion in 2030. Moreover, the number of non-smart-phones/devices is expected to continue declining and being replaced by smart-devices, to the extent it will totally disappear by the year 2025 due to the appeal of the latter to the users. This gives a growth estimate for the traffic from a different perspective, namely, a more connected society with traffic spread over wider geographic areas. More detailed information about the estimated traffic trends and key drivers can be found in [1].

1.1.2 Envisioned Future Trends: Coping with Traffic Growth

To meet such challenges in 5G networks, and as per the recent ITU report of future technology trends[8], next generation networks are anticipated to adopt an extensive reshaping of its infrastructure along with employing novel radio technologies that offer high efficiency from both spectral and energy perspectives. For instance, an infrastructure densification is expected in which heterogeneous deployments of macrocells, picocells and relays are jointly utilized to enhance the end-user experience [3]. Technologies to enhance the current radio interface are also expected to be employed such as Massive MIMO, flexible spectrum usage via cognitive radio techniques, and simultaneous transmission and reception (STR), to name a few. Further, new bands above 6 GHz are being explored for potential usage in future IMT systems, also known as mmWave communications [9].

1.1.3 Full-Duplexing and Next-Generation Specifications

Beyond the currently employed conventional half-duplex radio, supporting STR over the same channel via in-band full-duplex transceivers represents a strong radio technology candidate [4, 5]. Full-duplex operation has been always considered unfeasible due to the very strong and prohibitive interference imposed by the transmitter on the receiver of full-duplex nodes. Recent studies, however, showed that full-duplex radios can be efficiently implemented, and since then, a strong body of literature has been published on the different full-duplex aspects, including its radio frequency (RF) engineering, hardware developments, and protocol design [10, 11, 12]. In addition to the other technology candidates for 5G, full-duplex radio contributes to the support of the growing traffic demand by potentially doubling the spectral efficiency. This motivated the ITU Radiocommunications Sector (ITU-R) to consider two candidate settings where full-duplex operation (also known as STR) can be leveraged in its very recent report and recommendation for 5G networks [13, 8], namely, 1) supporting simultaneous uplink/downlink via full-duplex base stations, and 2) supporting simultaneous listening/forwarding via full-duplex relay cooperation.

1.1.4 Full-Duplex Cooperation

Multi-hop communication represents one promising, cost-effective, approach to meet some of the future network requirements through the deployment of intermediate relay nodes [14]. The assistance of relays can offer numerous advantages including the extension of network coverage, higher efficiency in transmit power consumption and enhancement of the communication link reliability via providing signal diversity. Despite its offered performance gains, half-duplex relaying (HDR) is known to suffer from an inherent spectral efficiency loss when compared to direct transmission (DT). This is owing to its nature of allocating orthogonal listening/forwarding phases at the relay. Full-duplex relaying (FDR), on the other hand, overcomes this inefficiency by allowing the relay to simultaneously transmit and

receive over the same channel [15].

1.2 Full-Duplex Relaying Challenges

Although *ideal* FDR clearly offers a spectral-efficiency gain by eliminating the known prelog factor from the capacity expressions of relay channels [15], performance can be significantly degraded in practice from a different perspective. Indeed, since the relay transmits and receives over the same channel resource, an interference link, called loopback or echo interference link, is introduced from the relay transmitter to its receiver, and this loopback interference level can reach 100 dB higher than the desired signal at the relay. Thus, this loopback interference defines a major practical challenge for FDR implementation that needs to be adequately suppressed. Early FDR performance evaluation attempts, however, assumed *perfect isolation* of the relay's receive antenna from its own overwhelming transmissions, which overestimates its actual performance merits [16]. In practice, even with recent advances in prototyping full-duplex nodes, all known analog, digital and spatial isolation/cancellation techniques cannot guarantee perfect isolation [17, 18]. As a result, a level of residual self-interference (RSI) persists. Moreover, the adverse effect of RSI proportionally grows with the relay transmit power. Hence, a clear tradeoff exists in FDR between its gained temporal efficiency and the corresponding degradation due to RSI, which is directly controlled by the relay power. This fact motivates further studies to revisit the available literature originally developed for *ideal* FDR in order to account for the RSI and study its effect. Also, it is desirable to design novel techniques to alleviate this adverse effect on the end-to-end performance.

1.3 Thesis Objectives and Contributions

In this work, we seek to devise efficient cooperation techniques for different full-duplex relay-assisted communication settings and evaluate their performance while taking the mentioned

leakage effect into account. These cooperation techniques are primarily required to seek reducing the effect of the RSI on the end-to-end performance. The efficiency of the sought techniques will be evaluated according to their offered end-to-end performance including outage, throughput, their required amount of channel knowledge, complexity in addition to their power consumption.

The contribution in this work is two-fold:

- **Buffer-less Cooperation:** In this regard, no packet queuing is allowed at the relay due to the nonavailability of a queuing buffer. Hence, upon relay cooperation, only instantaneous forwarding is allowed, taking processing delay into account. For buffer-less full-duplex cooperation, the following is studied.
  - **The basic three-terminal full-duplex relay channel:** We study the performance and devise efficient cooperation protocols for the three-terminal FDR channel with non-negligible direct source-destination link gain. These cooperation protocols seek to relieve the RSI effect on the end-to-end performance, and utilize the diversity branch via the direct link. The performance of the proposed protocols is evaluated relative to known full-duplex and half-duplex cooperation protocols in the literature. Closed-form expressions are presented for the outage performance/throughput of the proposed protocols under Rayleigh and Nakagami-m fading. Also, beyond conventional transmission with proper Gaussian signaling, some gains are shown due to the employment of improper signaling, even for simple transmission approaches which consider the direct link as interference.
  - **Full-duplex relay selection:** Relay selection is addressed in settings where a cluster of full-duplex relays exist between the source and the destination, with the study of its effect on the minimization of the RSI effect. The potential performance merits of relay selection is also studied while taking the direct link into account. The end-to-end outage performance is evaluated in closed-form under Rayleigh

and Nakagami-m fading. Diversity analysis is also performed, where it is shown that significant diversity enhancements can be attained by considering the direct transmission as an additional diversity branch to the available multi-hop paths, even with simple cooperation schemes that treat the direct link as interference to each multi-hop path.

  - **Full-duplex cooperation in cognitive radio settings:** In secondary systems of underlay cognitive networks, FDR can offer better outage/throughput performance than HDR. However, unlike in HDR, the employment of FDR by the secondary system imposes higher interference at the primary system due to simultaneous secondary source/relay transmission. Closed-form expressions are presented for full-duplex relay selection in underlay networks, comparing its performance to its HDR counterpart.

- **Buffer-Aided Cooperation:** Buffer-aided relaying is recently shown to offer higher throughput performance compared to buffer-less systems. A buffer-aided relaying scheme is proposed for *pure* HDR and FDR cooperation, as well as *hybrid* schemes that switch between FDR, HDR and DT based on the channel state information (CSI). The proposed relaying schemes seek to maximize the end-to-end throughput, also making use of the relay's buffer state information (BSI) that is assumed available at the source.

1.4 Thesis Outline

The thesis content is outlined as follows, where it is divided into three main parts:

Part I is dedicated to provide all the necessary introduction and background information to serve the two subsequent parts. Specifically, as already noticed, Chapter 1 draws the broad context where the study is primarily addressing, specifies the thesis topic under discussion and its significance, enumerates the thesis objectives, contribution, and finally outlines the rest of the thesis. Chapter 2 provides background information and further di-

rections for the practical hardware-level aspects of full-duplex communication, discussiing the self-interference channel, the different techniques for interference cancellation, the modeling of the residual self-interference, and some notes pertaining to the comparison between full-duplex and half-duplex systems.

Part II addresses *bufferless* full-duplex cooperative systems where the relay node has the limitation of instantaneously forwarding the decoded source message. In Chapter 3, the basic three-terminal full-duplex cooperative setting is explained in comparison to its half-duplex counterpart. Existing protocols and their related literature are explained, also in comparison to their half-duplex rivals. The chapter also discusses the challenges and performance limitations experienced by these protocols, highlighting also some performance evaluation and optimization contributions. In order to alleviate the aforementioned limitations, Chapter 4 proposes two selective full-duplex relaying protocols and evaluates their performance relative to the existing full-duplex and half-duplex ones under different fading scenarios. Moving to multi-relay settings, Chapter 5 studies the full-duplex relay selection problem, followed by the problem solution in underlay cognitive settings in Chapter 6.

Part III moves to cooperative settings where the relay is equipped with a *buffering facility* to queue its incoming packets. Chapter 7 introduces the related literature on buffer-aided half-duplex relaying, and proposes a random access scheme that offers end-to-end throughput enhancements. The proposed scheme probabilistically schedules the source/relay transmissions based on the available buffer and/or channel state information. Chapter 8 generalizes such a transmission scheduling mechanism to hybrid half-/full-duplex cooperative settings where also duplexing mode selection is jointly addressed.

Part IV concludes the presented thesis. In chapter 9, general conclusions for the entire thesis are summarized, followed by highlighting open research directions that are yet to be investigated.

Chapter 2

Background

Over the last few years, several extensive studies have been conducted on the different ways to efficiently suppress and/or cancel the in-band full-duplex self-interference. This chapter focuses on providing the necessary background related to full-duplex self-interference, its cancellation, in addition to the modeling adopted in this thesis for the residual interference after cancellation. It also discusses some fairness aspects related to the comparison between full-duplex and half-duplex systems. More detailed information can be found in the following published surveys/tutorials/magazine articles [5, 10, 19], focused papers [17, 18, 20, 21, 22, 23, 24, 25, 26], and theses [27, 28, 29, 30].

2.1 The Full-Duplex Self-Interference Channel

As a motivating example [10], we discuss the challenge that would be experienced by a typical *full-duplex* node, either a base station (BS) or a user equipment (UE), in a contemporary femto-cell cellular system. A transmitter in such a system typically transmits at about 20 dBm, while the noise floor is at -90 to -100 dBm, with around 110 to 120 dB gap. Assuming a 10-15 dB isolation between transmit and receive chains, the receive antenna of a full-duplex node would experience an overwhelming level of self-interference of about 110 dB above the noise level, which accordingly prohibits any successful reception. Of course, if

we go beyond femto-cell systems, the transmit power level will be typically higher, and such an overwhelming level can grow larger. It is clear that, for such a full-duplex femto-cell to be operational, efficient techniques should be applied to suppress/cancel such a prohibitive self-interference level to attempt to bring it as close as possible to the noise floor. A similar figure which considers a WiFi 802.11ac setup is also explained in details in [22].

According to the recent literature on state-of-the-art suppression/cancellation techniques, such a cancellation task is very challenging and cannot be accomplished by one single method. Instead, multiple techniques have to be successively applied to the interfering signal on top of one another, with suppression amounts adding up and approaching the desired noise level when aggregated. For instance, it should be carefully taken into consideration that the receiver's analog-to-digital converter (ADC) circuit does not get saturated. For 12 bit ADCs, while typically leaving 2 bits of margin, a dynamic range of up to only 60 dB is allowed at the receiver. Hence, out of this 110 to 120 dB gap, 50 to 60 dB should be suppressed before passing through the ADC to avoid receiver saturation, and accordingly the distortion of the signal. Also, the feasibility of each technique depends on the adopted hardware design for full-duplex radios, e.g., using either a single antenna or two separate antennas for transmission and reception.

2.2 Self-Interference Suppression/Cancellation

Recently, remarkable research efforts have been exerted to alleviate this echo interference on the hardware-level through several techniques, namely, 1) physical isolation, 2) analog cancellation, and 3) digital cancellation. In the following, we briefly go over each of these techniques.

2.2.1 Passive Suppression: Physical Isolation

Physical isolation techniques attempt to physically prevent the full-duplex node transmissions from reaching its receiver end via different approaches [30]. This may include: 1) the placement of shielding plates between the transmitter and receiver sides, 2) the employment of directive transmit antennas with nulls spatially projected at the receive antennas, 3) the use of orthogonally polarized transmit and receive antennas, and 4) the physical separation between the transmit and receive arrays, e.g., in the case of coverage extension inside a tunnel. It is worth mentioning that some passive suppression techniques, such as shielding placement, are only feasible in full-duplex designs with two separate antennas. Although the mentioned physical isolation techniques significantly reduce the loopback interference, additional mitigation is usually required due to the overwhelming strength of the interfering signal.

2.2.2 Active Cancellation: Analog Cancellation

The second stage of mitigation is performed by processing the RF signal at the full-duplex node. The necessity of the analog suppression techniques arises from the fact that due to the interference strength, it may saturate the ADC circuitry because of its limited resolution which renders the useful signal unrecoverable. Several analog/RF suppression techniques have been proposed in the literature namely, 1) antennas cancellation [17], 2) analog cancellation by vector modulation [27], and 3) analog cancellation by signal inversion [20]. Antenna cancellation uses an extra transmit antenna at the full-duplex node in addition to the existing one transmit and one receive antennas. In this setting, the transmitted signal from the second antenna is delayed from the original signal such that they add destructively at the receiver antenna. The destructive phase shift may be achieved through physical positioning of the transmit antennas by placing the second transmit antennas at $d + \lambda/2$ from the desired receiver where d denotes the distance between the desired receiver and the first

transmit antenna, while λ denotes the transmitted wavelength. The above approach suffers from two major drawbacks, namely, the sensitivity to the loopback channel estimation errors and to the transmitted signal bandwidth. In fact, as the paths from the two transmit antennas to the desired receiver are of different lengths, each transmit signal will experience a different path loss leading to different signal amplitudes at the receiver, and causing a reduced efficacy of destructive combining. For this purpose, the original signal needs to be attenuated to match the amplitude of the delayed replica for efficient self-interference suppression. Moreover, the transmitted signal usually spans a bandwidth B whereas the phase shift is designed for a specific frequency (typically the central frequency), therefore the self-interference suppression is not the same for all the frequency components of the transmitted signal due the induced mismatch in the antennas placement. The sensitivity to the channel estimation errors may be alleviated by using equidistant transmit antennas from the desired receiver and introducing a wired phase offset.

Another approach is to suppress the interference by creating a signal replica with inverse sign at the receiver [20, 27]. This is achieved through the so-called vector modulation. The original transmitted signal is fed to the vector modulation chip which rotates and scales its input signal to cancel the interference signal at the desired receiver. For this purpose, the vector modulating chip creates a quadrature component of its input signal, scales it to match the attenuation experienced by the interfering signal and adjust its phase to cancel the self-interference. However, the quadrature component is nothing more than a delayed version of the input signal by $\lambda/4$ and thus bandwidth sensitivity is persistent. In order to alleviate this bandwidth sensitivity, the phase dependent cancellation has to be avoided. This is achieved by using a balanced/unbalanced transformer (BALUN) at the transmitting side with conjunction of an attenuator to simulate the propagation loss between the transmitting and the receiving side of the full-duplex node. Simulation results have shown that using the BALUN significantly reduces the bandwidth sensitivity. However, the self-interference suppression could not be uniformly performed over the whole bandwidth since the frequency

response of the BALUN is not flat. A more recent design in [22] uses a dynamic and tunable tapping circuit with multiple delay lines that can offer up to 60 dB of analog cancellation. Also, wider bands of up to 80 MHz were shown to be supported.

2.2.3 Active Cancellation: Digital Cancellation

Although the aforementioned techniques can significantly reduce the deleterious effect of the loopback interference, additional steps are indispensable for practical considerations. For this purpose, one resorts to apply supplementary countermeasures on the digital/baseband signal. The straightforward approach is the so-called time-domain cancellation which cancels the self-interference by reproducing the interfering signal and feeding its inverse back to the relay's input. Obviously, the efficiency of this approach heavily relies on the quality of the available channel estimates under the assumption that the relay knows accurately its own transmitted signal. Also, in the case of multiple-input multiple-output (MIMO) FDR, a judicious choice is to apply spatial cancellation techniques in conjunction with the time-domain cancellation [31].

However, despite all the mentioned efforts to alleviate the echo interference level, relay transmissions cannot be *perfectly* prevented from leaking towards the receive antenna and causing undesirable interference. In fact, a level of RSI persists and adversely affects the effective signal-to-noise ratio (SNR) inside the capacity logarithm. Thus, increasing the relay transmit power does not necessarily help in boosting the end-to-end performance due to the existing trade-off between the spectral efficiency gain and the growing RSI, which defines a real challenge in practical FDR channels. Thus, it is desirable to additionally devise novel techniques to further alleviate this adverse effect.

2.3 Modeling of the Residual Self-Interference

2.3.1 Distribution of the Self-Interference Channel

In the available literature, this specific issue has not been extensively investigated. Based on the experiment-driven results reported in [21], the magnitude distribution for the self-interference channel differs according to the employed isolation/cancellation techniques. Specifically, it was reported in [21] that after passive isolation, and before active cancellation, the RSI channel is found as a *fading channel* with strong line-of-sight (LoS) effects. Accordingly, it was suggested that the RSI magnitude can be modeled to follow a Rician distribution with large K-factor. Also, after active cancellation, the LoS effect is reduced, and the magnitude was found to follow a Rician distribution with smaller K-factor. Also, according to the results in [24, 26] when strong passive suppression is employed, the LoS component is efficiently suppressed, and the RSI channel can be regarded as Rayleigh-fading.

2.3.2 Scaling with Relay Transmit Power

It is also of great importance to account for how the RSI average gain scales with the increase in the relay's transmit power. This issue also heavily relies on the adopted suppression and cancellation techniques. In earlier suppression approaches [17, 18, 20], the RSI power follows a linear trend with the increase in the relay's power, as reported later in [22]. However, with the suppression advancement, highly adaptive suppression/cancellation techniques like those in [22, 25] can actually maintain a nearly constant level of RSI with a growing relay power, although till some limits.

Based on the previous discussion, and throughout the thesis, we consider the RSI channel model to be on the form of $\sqrt{P_{\mathrm{R}}^{\delta}}h_{\mathrm{RR}}$, as suggested in [32], where P_{R} is the relay's transmit power, h_{RR} accounts for the fading coefficient of the RSI link after undergoing all suppression techniques, while δ is a power scaling factor ranging from 0 to 1 to cover a wide range of

power scaling, namely, constant, linear, and sublinear scaling.

2.4 Half-Duplex/Full-Duplex Comparison

The first implementations of full-duplex radios used separate antennas for transmission and reception [17, 18, 20, 21]. Specifically, a transmit RF chain is connected to a transmit antenna, while a receive RF chain is connected to the receive antenna, with a cancellation circuit that lies in between. More recently, it has been shown in [22] that single-antenna full-duplex radios are possible.

While comparing full-duplex to half-duplex nodes, it is often questionable how many antennas/RF chains should be allocated for each. In a study for multiple-antenna channels in [33], two approaches were suggested; namely, an *antenna-conserved* scenario versus an *RF-chain-conserved scenario*. In the antenna-conserved scenario, the number of antennas is kept fixed in half-/full-duplex settings, regardless of the number of RF chains utilized in both systems. Alternatively, and in agreement with recent studies on the topic [34], we adopt herein the RF-chain-conserved approach where the relay is equipped with the same number of RF chains (one for transmission and another one for reception). This approach neglects the fact that half-duplex is basically equipped with a single antenna for both transmission and reception as opposed to two antennas in full-duplex, one for each task, as long as they have the same number of RF chains. This argument is further supported by the previous discussion on the feasibility of single-antenna full-duplex radios.

2.5 Typical Values Used in the Thesis

Noise Power: As highlighted earlier, the noise level is typically in the range of -90 dBm or 1 picowatt. Throughout the thesis, we usually normalize the noise power to 1, while all other values are calculated relative to this level.

Average Desired Channel Gains: When the transmit power is kept constant, we

typically normalize it to 1, while assuming the average channel gains to absorb the aggregate effect of transmit power, path loss, in addition to fading. A typical received signal SNR level is in the range of 10 to 30 dB. Hence, the channel gains are usually assumed in the range of 10 to 30 dB above the normalized 0 dB noise floor. A weak channel gain is assumed below this range, i.e., from 0 to 10 dB.

Average RSI Channel Gain: As per recent loopback interference cancellation techniques, some architectures/designs may reach down to 1 or 2 dB above the noise floor such as in [22] in certain communication scenarios and up to certain transmit power ranges. To account for more general scenarios, we typically adopt an RSI link of an average gain π_{RR} that is in the range from 0 to 10 dB above noise floor.

Transmit Power: As the base effect of the transmit power is accounted for inside the average channel gains, we reserve the transmit power P_{S} and P_{R} to account for any further *relative* scaling to demonstrate effects such as the diversity order of the system. As noted earlier, if no scaling of transmit power takes place, the transmit power is simply set to a unity factor.

After the previous introduction to full-duplex communications, we proceed in the next part with buffer-less full-duplex cooperation.

Part II

Buffer-less Relaying

Chapter 3

Full-Duplex Cooperative Communication

After the earlier introduction to full-duplex communication with glimpses of its practical aspects, this chapter leads off the discussion on full-duplex *cooperation*. Specifically, it focuses on the canonical three-terminal communication channel which comprises an information source node, a full-duplex relay, and a destination node. In Section 3.1, we first explain the fundamental changes in the system model by moving from half-duplex to full-duplex operation at the relay.

3.1 The Full-Duplex Relay Channel

The full-duplex and half-duplex cooperative settings are depicted side-by-side in Fig. 3.1. From a signal transmission perspective, FDR differs from its half-duplex rival in two fundamental aspects as shown in Fig. 3.1a and Fig. 3.1b:

1. The source and the full-duplex relay simultaneously access the channel, thereby resulting in a superposition of their received signals at the destination. Resource-orthogonal transmissions in HDR allow for exploiting both message replicas in providing higher

communication reliability via signal combining. On the contrary, direct source transmissions in FDR can be problematic at the destination; not only they cannot be easily combined due to non-orthogonality, but also they may further act as an interferer to the stronger relay transmissions when instantaneous decoding is adopted.

2. The full-duplex relay itself simultaneously transmits and receives, which imposes self-interference in practice as discussed earlier. Such a residual interference, if not adequately taken into account, may waste the gains of FDR due to the recovered spectral efficiency (the prelog factor) since the effective SNR inside the capacity logarithm of the first hop is deteriorated.

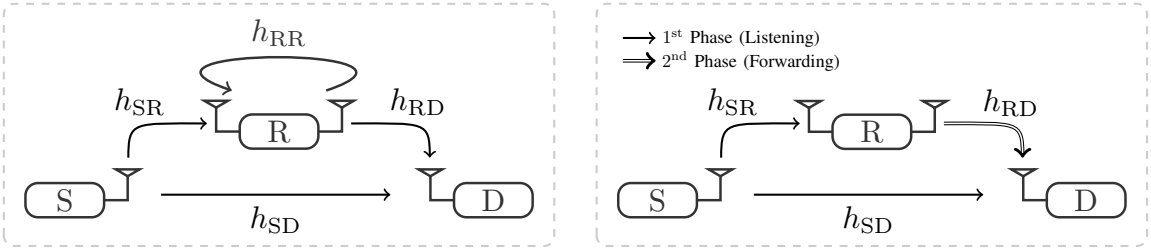

(a) Full-Duplex Relaying. (b) Half-Duplex Relaying.

Figure 3.1: Full-Duplex vs. Half-Duplex Cooperation

Such interactions at the signal level in FDR suggest different cooperation protocols which vary in their error performance, required amount of channel state information, and encoding/decoding complexity, among others. In what follows, the discussion starts with a simple protocol in terms of complexity and knowledge of the channel state, however it accordingly offers a limited error performance. The discussion then proceeds in an ascending order of performance and complexity.

Before proceeding, we first formally define the basic system model which is adopted in all the discussed protocols, then highlight the differences in their respective sections.

3.1.1 System Model

In Fig. 3.1a, a source (S) intends to communicate with a destination (D) via a full-duplex relay (R). The source message, $M \in \mathcal{M} = \{1, 2, \cdots, 2^{BR}\}$, is encoded using an encoding function $\mathcal{E} : \mathcal{M} \to \mathcal{C}$ with a fixed rate R bits per channel use (bpcu) into a codeword $\boldsymbol{x}_{\mathrm{S}} \in \mathcal{C}$ of length B symbols, where $\mathcal{C}$ is the source codebook with cardinality $|\mathcal{C}| = |\mathcal{M}| = 2^{BR}$. At the relay, a decode-and-forward (DF) strategy is employed. Therefore, the relay attempts to decode the source message from its received signal and re-encode it into $\boldsymbol{x}_{\mathrm{R}} \in \mathcal{C}$. It is assumed that B is fairly large, thereby validating the use of information theoretic tools. In what follows, the adopted channel and signal models are detailed.

Channel Model

We denote the channel between node $i \in \{\mathrm{S}, \mathrm{R}\}$ and node $j \in \{\mathrm{R}, \mathrm{D}\}$ by h_{ij}. As mentioned earlier, the relay loopback channel introduces self-interference that cannot be perfectly cancelled in practice. For notational convenience, we assume that h_{RR} denotes the RSI channel after undergoing all known practical isolation and cancellation techniques, see [20, 18, 34, 35, 36] and the references therein. We use $g_{ij} = |h_{ij}|^2$ to denote the $i{-}j$ link gain, for $i \in \{\mathrm{S}, \mathrm{R}\}$ and $j \in \{\mathrm{R}, \mathrm{D}\}$.

We assume all the links experience block fading. Thus, h_{ij} remains constant over one block, and varies independently from one block to another following some probability distribution. Two distributions are mainly considered in this thesis; Rayleigh and Nakagami-m fading.

In Rayleigh fading, the $i{-}j$ link gain g_{ij} is exponentially distributed with an average gain of π_{ij}. For such, we use the shorthand notation $g_{ij} \sim \mathrm{Exp}\,(\pi_{\mathrm{ij}})$. The probability density function (PDF) and cumulative distribution function (CDF) of an exponential random

variable (RV) $X \sim \text{Exp}(\pi)$ for $x \geq 0$ are given, respectively, by

$$f_X(x;\pi) = \frac{1}{\pi}\exp\left(-\frac{x}{\pi}\right), \tag{3.1}$$

$$F_X(x;\pi) = 1-\exp\left(-\frac{x}{\pi}\right). \tag{3.2}$$

On the other hand, when the links are experiencing Nakagami-m fading [37, 38], the $i-j$ link gain g_{ij} is Gamma distributed with an average gain of π_{ij}, in addition to a shape parameter denoted by m_{ij}. We use the shorthand notation $g_{ij} \sim \mathcal{G}(m_{ij}, \theta_{ij})$, where $\theta_{ij} = \frac{\pi_{ij}}{m_{ij}}$ is called the scale parameter. For a Gamma RV $X \sim \mathcal{G}(m,\theta)$, the PDF and CDF are given, respectively, by

$$f_X(x;m,\theta) = \frac{x^{m-1}e^{-\frac{x}{\theta}}}{\mathbf{\Gamma}(m)\theta^m}, \tag{3.3}$$

$$F_X(x;m,\theta) = \frac{\boldsymbol{\gamma}\left(m,\frac{x}{\theta}\right)}{\mathbf{\Gamma}(m)}, \tag{3.4}$$

where $\boldsymbol{\gamma}(a,b) = \int_0^b t^{a-1}e^{-t}dt$ denotes the lower incomplete Gamma function, while $\mathbf{\Gamma}(a)$ denotes the Gamma function [39]. The Nakagami-m fading model spans a wide range of fading scenarios that subsumes Rayleigh fading as a special case when $m = 1$. Also, for $m > 1$, a one-to-one mapping exists between its m parameter and the Rician K factor, which allows it to closely approximate the Rician distribution and accordingly capture LoS effects [38].

Signal Model

Due to simultaneous source/relay transmissions, the received signals at R and D at time t are given, respectively, by

$$y_{\text{R}}[t] = \sqrt{P_{\text{S}}}h_{\text{SR}}x_{\text{S}}[t] + \sqrt{P_{\text{R}}^{\delta}}h_{\text{RR}}x_{\text{R}}[t] + n_{\text{R}}[t], \tag{3.5}$$

$$y_{\text{D}}[t] = \sqrt{P_{\text{R}}}h_{\text{RD}}x_{\text{R}}[t] + \sqrt{P_{\text{S}}}h_{\text{SD}}x_{\text{S}}[t] + n_{\text{D}}[t], \tag{3.6}$$

where P_i and $x_i[t]$ denote the transmit power and the transmit symbol at time t at node $i \in \{\mathrm{S}, \mathrm{R}\}$, respectively, while $n_i[t]$ represents the additive white Gaussian noise (AWGN) component at node $i \in \{\mathrm{R}, \mathrm{D}\}$ at time t. Following from the earlier discussion on the RSI link modeling, it is assumed that the RSI term proportionally scales with P_{R}^{δ}, where $0 \leq \delta \leq 1$, covering the range from constant to linear scaling with the relay power. Without loss of generality, all AWGN components are assumed of unit variance.

As mentioned earlier, FDR can yield different levels of performance depending on how the received signals given in (3.5) and (3.6) are processed at the respective receivers. In other words, the performance depends on the adopted *cooperation protocol*, which is the subject under discussion in the following.

3.2 The Full-Duplex Multi-Hop Channel

A multi-hop channel and a relay channel are often distinguished from one another. On the one hand, a multi-hop channel is a channel where the destination receives and decodes the source message only via its relay-forwarded replica, i.e., that passing through the multi-hop path. Thus, it is assumed that no information can be distilled via the direct source-destination link. On the other hand, a relay channel is a channel where the destination receives the source message via the multi-hop path passing through the relay as well as that arriving directly from the source.

We first consider the simple full-duplex cooperative setting depicted in Fig. 3.2. In this setting, the destination distills the source message only via the multi-hop path. Following the previous discussion, this protocol is commonly called in the literature as the multi-hop decode-and-forward (MHDF) FDR protocol [40]. By simply using the same codebook of the source at the DF relay, and assuming successful reception at the relay, the relay's transmit signal is given by

$$\boldsymbol{x}_{\mathrm{R}}[b] = \boldsymbol{x}_{\mathrm{S}}[b - D], \tag{3.7}$$

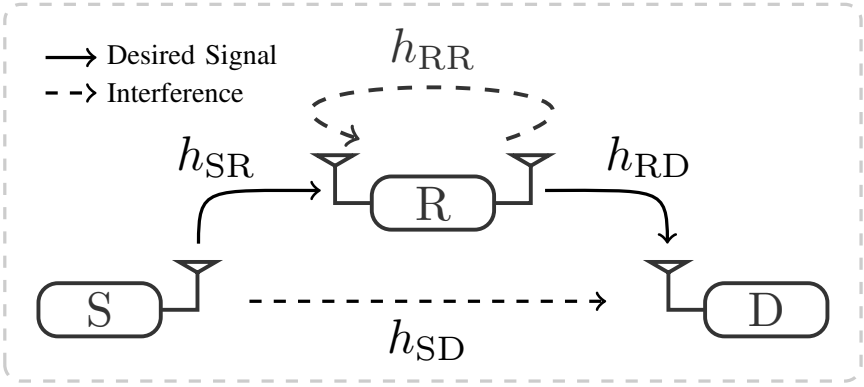

Figure 3.2: A full-duplex cooperative setting in coverage extension scenarios where direct source transmissions are treated as interference at the destination.

with b being the time index of the codeword block while D denotes the processing delay at the relay in codeword blocks. In the MHDF-FDR protocol, simple instantaneous decoding is adopted. Hence, as clear from (3.6) and (3.7), either $\boldsymbol{x}_{\mathrm{S}}$ or $\boldsymbol{x}_{\mathrm{R}}$ can be decoded, treating the other as interference. Since using a relay implicitly implies a weaker direct link gain than those of the aiding multi-hop path, the direct source signal is treated as interference to the stronger relay signal. Clearly, such a MHDF-FDR protocol is best-suited to coverage extension scenarios where the direct source-destination link is either absent due to deep shadowing effects, or having a very weak gain.

3.2.1 Outage Performance of MHDF-FDR

According to the earlier explanation of the MHDF-FDR protocol, the received signal-to-interference-plus-noise ratio (SINR) at R and D are given, respectively, by

$$\gamma_{\mathrm{SR}} = \frac{P_{\mathrm{S}} g_{\mathrm{SR}}}{P_{\mathrm{R}}^{\delta} g_{\mathrm{RR}} + 1}, \qquad \gamma_{\mathrm{RD}} = \frac{P_{\mathrm{R}} g_{\mathrm{RD}}}{P_{\mathrm{S}} g_{\mathrm{SD}} + 1}. \tag{3.8}$$

In (3.8), $x_i[t]$ is assumed to have an average power of unity. The end-to-end outage probability using MHDF-FDR, assuming complex Gaussian channel inputs and unit bandwidth,

is simply given by

$$\mathcal{P}_{\text{out}} \;=\; 1-\overline{\mathcal{P}_{\text{SR}}}\;\overline{\mathcal{P}_{\text{RD}}}, \tag{3.9}$$

with

$$\mathcal{P}_{ij} \;=\; \mathbb{P}\left\{C_{ij}<R\right\}, \tag{3.10}$$

representing the probability of outage in the $i-j$ link, and $\mathbb{P}\{A\}$ denoting the probability of occurrence of event A. In (3.10), $C_{ij}=\log_2\left(1+\gamma_{ij}\right)$ bpcu is the instantaneous capacity of the $i-j$ link

Rayleigh Fading

When the links are Rayleigh-fading, the link gain g_{ij} is exponentially distributed as given by (3.1) and (3.2). It follows that the outage in the first and second hop are obtained as given in [41], respectively, by

$$\mathcal{P}_{\text{SR}} \;=1-\frac{P_{\text{S}}\pi_{\text{SR}}\exp\left(-\frac{\eta}{P_{\text{S}}\pi_{\text{SR}}}\right)}{P_{\text{S}}\pi_{\text{SR}}+\eta P_{\text{R}}^{\delta}\pi_{\text{RR}}} \;=1-\frac{\exp\left(-\frac{\eta}{P_{\text{S}}\pi_{\text{SR}}}\right)}{1+\eta\frac{P_{\text{R}}^{\delta}\pi_{\text{RR}}}{P_{\text{S}}\pi_{\text{SR}}}}, \tag{3.11}$$

$$\mathcal{P}_{\text{RD}} \;\;=1-\frac{P_{\text{R}}\pi_{\text{RD}}e^{-\frac{\eta}{P_{\text{R}}\pi_{\text{RD}}}}}{P_{\text{R}}\pi_{\text{RD}}+\eta P_{\text{S}}\pi_{\text{SD}}} \;\;=1-\frac{\exp\left(-\frac{\eta}{P_{\text{R}}\pi_{\text{RD}}}\right)}{1+\eta\frac{P_{\text{S}}\pi_{\text{SD}}}{P_{\text{R}}\pi_{\text{RD}}}}, \tag{3.12}$$

where $\eta=2^R-1$. It is clear from (3.11) and (3.12) that the outage probability increase due to interference is captured by scaling down the exponential term in the CDF of the first and second hop by the factors $\frac{1}{1+\eta\frac{P_{\text{R}}^{\delta}\pi_{\text{RR}}}{P_{\text{S}}\pi_{\text{SR}}}}$ and $\frac{1}{1+\eta\frac{P_{\text{S}}\pi_{\text{SD}}}{P_{\text{R}}\pi_{\text{RD}}}}$, respectively. These scaling factors are functions of the relative average received power of the desired and interference signals, in addition to the source rate. It follows that the end-to-end outage probability for MHDF-FDR

is simply given as

$$\mathcal{P}_{\text{out}} = 1 - \frac{\exp\left(-\frac{\eta}{P_{\text{S}}\pi_{\text{SR}}}\right)}{1+\eta\frac{P_{\text{R}}^{\delta}\pi_{\text{RR}}}{P_{\text{S}}\pi_{\text{SR}}}} \frac{\exp\left(-\frac{\eta}{P_{\text{R}}\pi_{\text{RD}}}\right)}{1+\eta\frac{P_{\text{S}}\pi_{\text{SD}}}{P_{\text{R}}\pi_{\text{RD}}}}. \tag{3.13}$$

Nakagami-m Fading

Under Nakagami-m fading, the SINR in each hop is an RV on the form $\frac{X_1}{X_2+1}$, where $X_1 \sim \mathcal{G}(m_1,\theta_1)$ and $X_2 \sim \mathcal{G}(m_2,\theta_2)$. To obtain the outage probability in the first and second hops, we make use of the the following remark.

Remark 1 (CDF of $Z = \frac{X_1}{X_2+1}$)**.** *For two independent Gamma RVs, $X_1 \sim \mathcal{G}(m_1,\theta_1)$ and $X_2 \sim \mathcal{G}(m_2,\theta_2)$, with integer shape parameters and possibly distinct scale parameters, $Z = \frac{X_1}{X_2+1}$ has the following CDF [42, 43]:*

$$F_Z(z;\boldsymbol{p}) = \frac{\boldsymbol{\gamma}\left(m_1, \frac{z}{\theta_1}\right)}{\boldsymbol{\Gamma}(m_1)} + B\sum_{k=0}^{m_2-1}\frac{c^{-d}}{{\theta_2}^k}\boldsymbol{W}_{a,b}(c), \tag{3.14}$$

where $\boldsymbol{p} = (m_1,\theta_1,m_2,\theta_2)$ is a vector holding the shape and scale parameters, $\boldsymbol{W}_{a,b}(c)$ is the Whittaker function [39, Eq. 13.1.33], $a = \frac{m_1-k-1}{2}$, $b = \frac{-m_1-k}{2}$, $c = \frac{z}{\theta_1}+\frac{1}{\theta_2}$, $d = \frac{m_1+k+1}{2}$ and

$$B = \frac{\exp\left(-\frac{1}{2}\left(\frac{z}{\theta_1}-\frac{1}{\theta_2}\right)\right)}{\boldsymbol{\Gamma}(m_1)}\left(\frac{z}{\theta_1}\right)^{m_1}. \tag{3.15}$$

It should be noted that, if a Gamma RV $X \sim \mathcal{G}(m,\theta)$ is scaled by a constant α, then $Y = \alpha X \sim \mathcal{G}(m,\alpha\theta)$. Thus, it follows from Remark 1 that the end-to-end outage probability for MHDF-FDR under Nakagami-m fading is given by

$$\mathcal{P}_{\text{out}} = 1 - \left(1 - F_Z(\eta;\boldsymbol{p}_1)\right)\left(1 - F_Z(\eta;\boldsymbol{p}_2)\right), \tag{3.16}$$

with $\boldsymbol{p}_1 = (m_{\text{SR}}, P_{\text{S}}\theta_{\text{SR}}, m_{\text{RR}}, P_{\text{R}}^{\delta}\theta_{\text{RR}})$ and $\boldsymbol{p}_2 = (m_{\text{RD}}, P_{\text{R}}\theta_{\text{RD}}, m_{\text{SD}}, P_{\text{S}}\theta_{\text{SD}})$.

3.2.2 Outage Performance of MHDF-HDR

For the sake of comparison, we write down here the expressions for the end-to-end outage probability of MHDF-HDR, the half-duplex version of the MHDF-FDR. In this protocol, the source message is only distilled from the multi-hop path without combining the direct link signal. It should be noted that, for fair outage performance comparison, we need to account for the difference in multiplexing gains between HDR and FDR, i.e., to take the prelog factor of $\frac{1}{2}$ in HDR into account. Thus, the source in HDR transmits with double the rate of that of FDR, i.e., $2R$, and hence $\eta_{\rm HD} = 2^{2R}-1$. The end-to-end outage performance of MHDF-HDR is given in (3.17) and (3.18) under Rayleigh and Nakagami-m fading, respectively.

Rayleigh Fading

$$\mathcal{P}_{\rm out} \;=\; 1-\exp\left(-\frac{\eta_{\rm HD}}{P_{\rm S}\pi_{\rm SR}}\right)\;\exp\left(-\frac{\eta_{\rm HD}}{P_{\rm R}\pi_{\rm RD}}\right). \tag{3.17}$$

Nakagami-m Fading

$$\mathcal{P}_{\rm out} \;=\; 1-\frac{\mathbf{\Gamma}\left(m_{\rm SR},\frac{\eta_{\rm HD}}{P_{\rm S}\theta_{\rm SR}}\right)}{\mathbf{\Gamma}\left(m_{\rm SR}\right)}\;\frac{\mathbf{\Gamma}\left(m_{\rm RD},\frac{\eta_{\rm HD}}{P_{\rm R}\theta_{\rm RD}}\right)}{\mathbf{\Gamma}\left(m_{\rm RD}\right)}, \tag{3.18}$$

with $\mathbf{\Gamma}\left(a,b\right)=\int_b^\infty t^{a-1}e^{-t}dt=\mathbf{\Gamma}\left(a\right)-\boldsymbol{\gamma}\left(a,b\right)$ denoting the upper incomplete Gamma function.

3.2.3 Source/Relay Power Optimization in MHDF-FDR

It is straightforward in HDR to show that the higher the transmit power of the source and/or the relay, the better the end-to-end error performance. Accordingly, for the considered simple three-terminal setting, transmission with maximum power in HDR always yields the best error performance. Unfortunately, this is not the case in FDR, and especially for MHDF-

FDR. This stems from the fact that increasing the transmit power of any of the nodes boosts the desired signal power at one receiver end, however it also increases the interference power at another as clearly seen from (3.8). Given the individual power constraints $0 \leq P_{\mathrm{S}} \leq P_{\mathrm{S}}^{\max}$ and $0 \leq P_{\mathrm{R}} \leq P_{\mathrm{R}}^{\max}$, it is important to find the pair $(P_{\mathrm{S}}^*, P_{\mathrm{R}}^*)$ that minimizes the end-to-end outage probability. For the Rayleigh-fading scenario, it is proposed in [44] that such a pair, for $P_{\mathrm{S}}^{\max} = P_{\mathrm{R}}^{\max} = P_{\mathrm{m}}$ and $\delta = 1$, is given by

$$(P_{\mathrm{S}}^*, P_{\mathrm{R}}^*) = \begin{cases} (P_{\mathrm{m}}, P_{\mathrm{m}}), & \text{if } P_{\mathrm{m}} < \min\left(P_{\mathrm{S}}^{\mathrm{opt}}(P_{\mathrm{m}}), P_{\mathrm{R}}^{\mathrm{opt}}(P_{\mathrm{m}})\right), \\ (P_{\mathrm{S}}^{\mathrm{opt}}(P_{\mathrm{m}}), P_{\mathrm{m}}), & \text{if } P_{\mathrm{S}}^{\mathrm{opt}}(P_{\mathrm{m}}) \leq P_{\mathrm{m}} \leq P_{\mathrm{R}}^{\mathrm{opt}}(P_{\mathrm{m}}), \\ (P_{\mathrm{m}}, P_{\mathrm{R}}^{\mathrm{opt}}(P_{\mathrm{m}})), & \text{if } P_{\mathrm{R}}^{\mathrm{opt}}(P_{\mathrm{m}}) \leq P_{\mathrm{m}} \leq P_{\mathrm{S}}^{\mathrm{opt}}(P_{\mathrm{m}}), \end{cases} \tag{3.19}$$

where $P_{\mathrm{S}}^{\mathrm{opt}}(P_{\mathrm{m}})$ and $P_{\mathrm{R}}^{\mathrm{opt}}(P_{\mathrm{m}})$ are the solutions to the cubic equations obtained from differentiating (3.13) with respect to (w.r.t.) P_{S} and P_{R}, respectively, with setting the other transmit power to P_{m}. However, no discussion was provided in [44] on the existence and nature of the roots for the given cubic equations. We show in Appendix 3.A that the end-to-end outage probability in MHDF-FDR is actually unimodal in the source power and in the relay power. Hence, the solution (3.19) given in [44] is the optimal solution. Although the objective function is nonconvex, the optimization can be also performed numerically due to unimodality using the bisection method, since unimodality implies quasiconvexity.

3.2.4 Comparison of MHDF-FDR and MHDF-HDR

In Fig. 3.3, the performance of the MHDF is compared for HDR and FDR, also against that of DT. For DT, we consider two settings: 1) a single-input single-output (SISO) setting where the source is equipped with only one transmit antenna, and 2) a multiple-input single-output (MISO) 2×1 setting with a two-antenna source, which provides transmit diversity using the celebrated Alamouti space-time coding scheme taking the slow fading channel assumption into account. In the MISO setting, the first and second antennas are allocated power of P_{S}

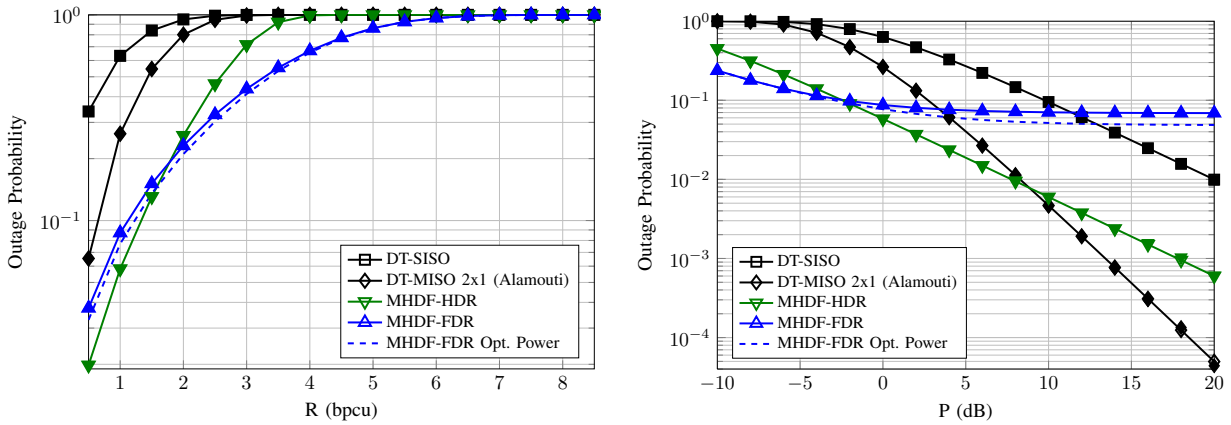

(a) Outage vs. Rate, for $P_{\mathrm{S}} = P_{\mathrm{R}} = P = 1$.

(b) Outage vs. Power, for $R = 1$ bpcu.

Figure 3.3: Relative Performance of MHDF-HDR/-FDR protocols over Rayleigh fading links, for $\pi_{\mathrm{SR}} = \pi_{\mathrm{RD}} = 20$ dB, $\pi_{\mathrm{RR}} = 8$ dB, $\pi_{\mathrm{SD}} = 0$ dB, and $\delta = 1$.

and P_{R}, respectively. In Fig. 3.3a, we can observe that MHDF-FDR outperforms MHDF-HDR as the rate R increases, and vice versa. It can be seen also that power optimization offers a better performance in MHDF-FDR, implying that transmission with maximum power can be performance-limiting. The relative performance depends on the values of π_{RR} and π_{SD} since the MHDF-HDR protocol is indifferent to them, while the MHDF-FDR performance is worsened as their values increase. In Fig. 3.3b, the outage performance is shown against $P_{\mathrm{S}} = P_{\mathrm{R}} = P$ to give an idea about the diversity of the protocols. It is clear that the curve of MHDF-HDR has the same slope as that of DT, implying it has a diversity of order 1. On the other hand, the MHDF-FDR protocol suffers from an error floor, implying a zero diversity order. It can be also observed that although power optimization can enhance the error floor value, it cannot get around this diversity order problem. In the following, we analytically show that the diversity gain is equal to zero, and analyze the causes for such a performance.

3.2.5 Diversity Order Problem

By setting $P_{\mathrm{S}} = P_{\mathrm{R}} = P$ in (3.13), the outage probability for MHDF-FDR under Rayleigh fading is given by

$$\mathcal{P}_{\mathrm{out}} = 1 - \frac{\exp\left(-\frac{1}{P}\left(\frac{\eta}{\pi_{\mathrm{SR}}} + \frac{\eta}{\pi_{\mathrm{RD}}}\right)\right)}{\left(1 + \eta\frac{\pi_{\mathrm{RR}}}{\pi_{\mathrm{SR}}}P^{\delta-1}\right)\left(1 + \eta\frac{\pi_{\mathrm{SD}}}{\pi_{\mathrm{RD}}}\right)}. \tag{3.20}$$

The diversity order [45] is defined as

$$\mathcal{D} = \lim_{P\to\infty} -\frac{\log\left(\mathcal{P}_{\mathrm{out}}\right)}{\log\left(P\right)}. \tag{3.21}$$

For large P, $1 - \exp\left(-\frac{1}{P}\left(\frac{\eta}{\pi_{\mathrm{SR}}} + \frac{\eta}{\pi_{\mathrm{RD}}}\right)\right)$ approaches $\frac{1}{P}\left(\frac{\eta}{\pi_{\mathrm{SR}}} + \frac{\eta}{\pi_{\mathrm{RD}}}\right)$ as in [45]. Thus,

$$\mathcal{D} = \lim_{P\to\infty} -\frac{\log\left(1 - \frac{1 - \frac{1}{P}\left(\frac{\eta}{\pi_{\mathrm{SR}}} + \frac{\eta}{\pi_{\mathrm{RD}}}\right)}{\left(1+\eta\frac{\pi_{\mathrm{RR}}}{\pi_{\mathrm{SR}}}P^{\delta-1}\right)\left(1+\eta\frac{\pi_{\mathrm{SD}}}{\pi_{\mathrm{RD}}}\right)}\right)}{\log\left(P\right)} \tag{3.22}$$

$$= \lim_{P\to\infty} -\frac{\log\left(\frac{\eta\frac{\pi_{\mathrm{SD}}}{\pi_{\mathrm{RD}}}P + \eta\frac{\pi_{\mathrm{RR}}}{\pi_{\mathrm{SR}}}\left(1+\eta\frac{\pi_{\mathrm{SD}}}{\pi_{\mathrm{RD}}}\right)P^{\delta} + \left(\frac{\eta}{\pi_{\mathrm{SR}}} + \frac{\eta}{\pi_{\mathrm{RD}}}\right)}{\left(P+\eta\frac{\pi_{\mathrm{RR}}}{\pi_{\mathrm{SR}}}P^{\delta}\right)\left(1+\eta\frac{\pi_{\mathrm{SD}}}{\pi_{\mathrm{RD}}}\right)}\right)}{\log\left(P\right)} \tag{3.23}$$

$$= 1 - \lim_{P\to\infty} \frac{\log\left(\eta\frac{\pi_{\mathrm{SD}}}{\pi_{\mathrm{RD}}}P + \eta\frac{\pi_{\mathrm{RR}}}{\pi_{\mathrm{SR}}}\left(1+\eta\frac{\pi_{\mathrm{SD}}}{\pi_{\mathrm{RD}}}\right)P^{\delta} + \left(\frac{\eta}{\pi_{\mathrm{SR}}} + \frac{\eta}{\pi_{\mathrm{RD}}}\right)\right)}{\log\left(P\right)}, \tag{3.24}$$

where the logarithm of the ratio in the numerator of (3.23) is written on the form of the difference of logarithms, then the limit is applied to the subtrahend terms. It can be noticed that the limit of the logarithm ratio in (3.24) always goes to 1, hence yielding a zero diversity order, unless all the P-dependent terms in the numerator vanish. Specifically, we can notice that the limit drops to zero when $\pi_{\mathrm{SD}} = \pi_{\mathrm{RR}} = 0$. It can be also noticed that the limit goes to δ when $\pi_{\mathrm{SD}} = 0$ but $\pi_{\mathrm{RR}} \neq 0$, hence yielding a diversity order of $1 - \delta$. In summary, the

diversity order of MHDF-FDR is given by

$$\mathcal{D} = \begin{cases} 1, & \text{if } \pi_{\mathrm{SD}} = \pi_{\mathrm{RR}} = 0, \\ 1-\delta, & \text{if } \pi_{\mathrm{SD}} = 0, \pi_{\mathrm{RR}} \neq 0, \\ 0, & \text{elsewhere.} \end{cases} \tag{3.25}$$

This aforementioned error floor result explains the noticed trend in Fig. 3.3b. It also agrees with recent results in the amplify-and-forward (AF) FDR literature [46]. With the analyzed diversity order now in hand, we can conclude the following from (3.25):

- For any nonzero value of π_{SD}, the diversity order of MHDF-FDR drops to zero regardless of the RSI link gain or how the RSI scales with the relay power. Although the $\mathrm{S}-\mathrm{D}$ link bears useful information, not only it cannot be exploited by the MHDF-FDR protocol, but also it worsens the performance as its gain increases.

- For nonzero RSI that is linearly-scaling with P_{R}, i.e., $\delta = 1$, the diversity order of MHDF-FDR is equal to zero no matter what the value of π_{SD} is, being zero or nonzero.

- In order to have a diversity order of MHDF-FDR equal to that of MHDF-HDR, i.e., diversity order of 1, two conditions should be simultaneously maintained: 1) no direct link exists ($\pi_{\mathrm{SD}} = 0$), and 2) no RSI exists or the RSI does not scale with the relay power P_{R} at all (the RSI link can be still a fading link, but the average is constant w.r.t. P_{R}, i.e., $\delta = 0$).

As noticed, instantaneous decoding did not allow MHDF-FDR to exploit the direct link, and caused a diversity order problem.

3.3 Improper Gaussian Signaling in MHDF-FDR

In an attempt to *statistically* mitigate the effect of the RSI link on the end-to-end performance of MHDF-FDR, we examine the potential merits of allowing the relay to more generally use

improper Gaussian signaling (IGS) [47]. Proper Gaussian signaling (PGS) assume that zero-mean complex transmit signals are statistically circularly symmetric with uncorrelated real and imaginary components. On the other hand, IGS is a more general class of signals where circularity and uncorrelatedness conditions can be relaxed, subsuming PGS as a special case. For Gaussian channels, and within the class of Gaussian signals, PGS has been widely accepted and adopted in the literature as the best Gaussian signaling scheme for different communication settings. This common assumption was primarily motivated by the fact that PGS is known to maximize the achievable rates in point-to-point, multiple access, and broadcast channels. However, recent work on the interference channel showed that, in general, IGS can actually support higher rates in certain interference-limited scenarios [48]. These results motivate the need to further study the potential gains of IGS in communication scenarios where interference imposes a noticeable limitation.

The potential gains of IGS have been also recently studied in [49] for the MIMO relay channel when a partial DF strategy is adopted. In such a relaying strategy, the relay only decodes a part of the message, while the rest of the message is treated as an additional interference term. It was shown in [49] that PGS achieves the highest rate within the class of Gaussian signals. However, the work in [49] assumed an ideal full-duplex relay channel, where the self-interference imposed by the relay's transmitter on its own receiver is perfectly canceled.

3.3.1 End-to-End Outage Performance Upper Bound

As derived in [50], when PGS and IGS are employed at the source and the relay, respectively, the end-to-end upper bound on the outage probability under Rayleigh fading can be obtained from Theorem 1.

Theorem 1. *Using MHDF-FDR cooperation with IGS adopted at the relay, the end-to-end outage probability under Rayleigh fading as a function of the relay's transmit power and*

circularity coefficient can be upper bounded by

$$\mathcal{P}_{\text{out}}^{\text{UB}}\left(P_{\text{R}}, C_{\text{R}}\right) = 1 - \frac{e^{-\left(\frac{1}{P_{\text{R}}\pi_{\text{RD}}}\frac{\Psi(C_{\text{R}})}{\left(1-C_{\text{R}}^2\right)}+\frac{P_{\text{R}}^{\delta}\pi_{\text{RR}}+1}{P_{\text{S}}\pi_{\text{SR}}}\Psi\left(\frac{P_{\text{R}}^{\delta}\pi_{\text{RR}}}{P_{\text{R}}^{\delta}\pi_{\text{RR}}+1}C_{\text{R}}\right)\right)}}{\frac{P_{\text{S}}\pi_{\text{SD}}}{P_{\text{R}}\pi_{\text{RD}}}\frac{\Psi(C_{\text{R}})}{\left(1-C_{\text{R}}^2\right)}+1}. \tag{3.26}$$

where

$$\Psi\left(x\right) = \sqrt{1+\eta_{\text{HD}}\left(1-x^2\right)} - 1. \tag{3.27}$$

3.3.2 Circularity Coefficient Optimization

In order to investigate the merits of IGS over conventional PGS in MHDF-FDR, we aim at finding the optimal circularity coefficient value that minimizes the end-to-end outage probability upper bound. Specifically, we aim at solving the following optimization problem:

$$\begin{aligned} \min_{C_{\text{R}}} \quad & \mathcal{P}_{\text{out}}^{\text{UB}}\left(P_{\text{R}}, C_{\text{R}}\right) \\ \text{s.t.} \quad & 0 \leq C_{\text{R}} \leq 1. \end{aligned} \tag{3.28}$$

In order to solve the optimization problem, we analyze the convexity properties of the objective function $\mathcal{P}_{\text{out}}^{\text{UB}}\left(P_{\text{R}}, C_{\text{R}}\right)$. In general, the function is found to be non-convex due to the indefinite sign of the second derivative. However, other desirable properties that allow us to find the global optimal point are presented in the following theorem.

Theorem 2. *When IGS is employed at the relay, the upper bound of the end-to-end outage probability is either a monotonic or a unimodal function in C_{R} over the interior of the region of interest, $0 \leq C_{\text{R}} \leq 1$.*

Proof. The proof is provided in Appendix 3.B. □

Since monotonicity and unimodality are special cases of quasi-convexity, such a result allows for the use of quasi-convex optimization algorithms. For instance, the optimal C_{R} can

be numerically obtained using the well-known bisection method operating on its derivative given in Appendix 3.B.

3.3.3 Comparison to MHDF-FDR with PGS

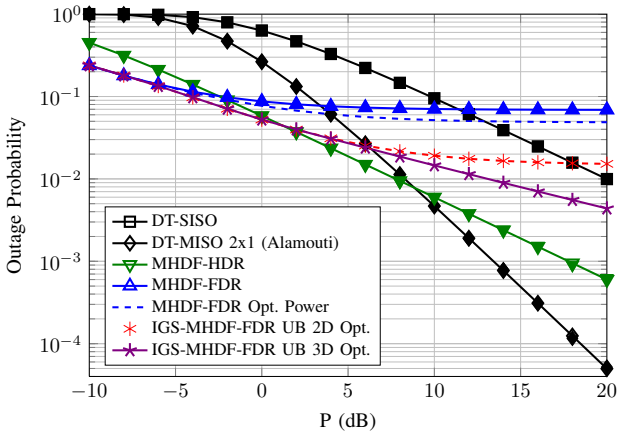

Figure 3.4: Outage vs. Power over Rayleigh fading links, for $\pi_{\mathrm{SR}} = \pi_{\mathrm{RD}} = 20$ dB, $\pi_{\mathrm{RR}} = 8$ dB, $\pi_{\mathrm{SD}} = 0$ dB and $R = 1$ bpcu.

In Fig. 3.4, we compare the performance of the system by employing IGS at the relay to that with PGS. In addition to the optimization over the relay's circularity coefficient, we also jointly optimize over the relay's power, i.e., by not necessarily transmitting with full power at the relay. The two-dimensional optimization for the upper bound is performed using two methods: 1) a grid search plotted with marks, and 2) a two-dimensional bisection algorithm operating in an iterative and alternating fashion on the relay's power and circularity coefficients. From the numerical results, it can be easily noticed that IGS improves the end-to-end outage probability relative to the previous optimized PGS scheme. However, such an improvement does not enhance the diversity order of the system as shown. A three-dimensional grid search that additionally includes the optimization over the source power is also shown in Fig. 3.4. As noticed, further improvements are offered to the system performance. Although the performance of the latter curve is shown to steadily improve, a plateau is eventually reached, even though at higher power, reflecting the persistence of

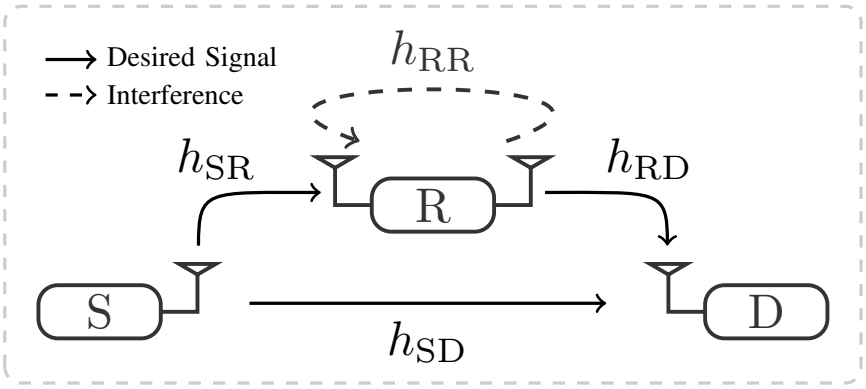

Figure 3.5: A general full-duplex cooperative setting where direct source transmission is exploited as a diversity branch at the destination.

the same diversity problem. It remains interesting to study the performance of MHDF-FDR when IGS is employed at both the source and the relay.

3.4 Block Transmission in the Full-Duplex Relay Channel

In contrast to the setting shown in Fig. 3.2 where the direct $\mathrm{S}-\mathrm{D}$ link is treated as interference, the setting shown in Fig. 3.5 attempts to exploit it as a diversity branch. As noticed in the previous sections, instantaneous decoding at the destination did not allow for leveraging the direct link. Alternatively, a block transmission scheme can be adopted where a sequence of codewords can be *jointly* or *conditionally* decoded to make use of the diversity in the two arriving replicas at the destination.

In the earlier FDR literature with perfect self-interference cancellation, a cooperation protocol based on block Markov superposition coding (BMSC) [51, 52, and the references therein] attains the best known achievable rates among fixed DF protocols. This BMSC-FDR protocol was further applied and analyzed for FDR channels with RSI in [40, 43] over Rayleigh and Nakagami-m fading channels. There exist several decoding techniques for BMSC that are explained in [52], e.g., sliding-window decoding and backward decoding.

3.4.1 End-to-End Outage Performace

The end-to-end outage probability for the BMSC-FDR protocol is given under Rayleigh [40] and Nakagami-m [43] fading as follows.

Rayleigh Fading

$$\mathcal{P}_{\text{out}} \;=\; 1 - \frac{e^{-\frac{\eta}{P_{\text{S}}\pi_{\text{SR}}(1-\rho^2)}}}{1+\frac{\eta}{1-\rho^2}\frac{P_{\text{R}}^{\delta}\pi_{\text{RR}}}{P_{\text{S}}\pi_{\text{SR}}}}\frac{\alpha e^{-\frac{\eta}{\alpha}} - \beta e^{-\frac{\eta}{\beta}}}{\alpha-\beta}, \tag{3.29}$$

where $\alpha = \frac{a}{2} + \sqrt{b}$, $\beta = \frac{a}{2} - \sqrt{b}$, $a = P_{\text{R}}\pi_{\text{RD}} + P_{\text{S}}\pi_{\text{SD}}$, and $b = \frac{a^2}{4} - P_{\text{S}}\pi_{\text{SD}}P_{\text{R}}\pi_{\text{RD}}(1-\rho^2)$, while ρ is the correlation coefficient between the source and relay messages, which can be designed to maximize the end-to-end mutual information.

Nakagami-m Fading

The approximate end-to-end outage probability for the BMSC-FDR protocol under Nakagami-m fading is given in [43] by

$$\begin{aligned}\mathcal{P}_{\text{out}} \;\approx\; & 1 - \frac{\boldsymbol{\Gamma}\left(m, \frac{\eta}{\theta}\right)}{\boldsymbol{\Gamma}(m)}\sum_{k=0}^{m_{\text{SR}}-1}\frac{1}{\boldsymbol{\Gamma}(k+1)}\left(\frac{1}{P_{\text{R}}^{\delta}\theta_{\text{RR}}}\right)^{m_{\text{RR}}}\left(\frac{\eta}{(1-\rho^2)P_{\text{S}}\theta_{\text{SR}}}\right)^{k} \\ & \times e^{-\frac{\eta}{(1-\rho^2)P_{\text{S}}\theta_{\text{SR}}}} U\left(m_{\text{RR}}, k+m_{\text{RR}}+1, \frac{1}{P_{\text{R}}^{\delta}\theta_{\text{RR}}} + \frac{\eta}{(1-\rho^2)P_{\text{S}}\theta_{\text{SR}}}\right),\end{aligned} \tag{3.30}$$

where

$$\xi = \left(\frac{\mathbf{\Gamma}\left(m_{\mathrm{SD}}\right)\mathbf{\Gamma}\left(m_{\mathrm{SD}}+1\right)\mathbf{\Gamma}\left(m_{\mathrm{RD}}\right)\mathbf{\Gamma}\left(m_{\mathrm{RD}}+1\right)}{\mathbf{\Gamma}\left(m_{\mathrm{SD}}+\frac{1}{2}\right)^2\mathbf{\Gamma}\left(m_{\mathrm{RD}}+\frac{1}{2}\right)^2} - 1 \right)^{-1}, \tag{3.31}$$

$$\varrho = \sqrt{\theta_{\mathrm{SD}}\theta_{\mathrm{RD}}}\frac{\mathbf{\Gamma}\left(m_{\mathrm{SD}}+\frac{1}{2}\right)\mathbf{\Gamma}\left(m_{\mathrm{RD}}+\frac{1}{2}\right)}{\mathbf{\Gamma}\left(m_{\mathrm{SD}}\right)\mathbf{\Gamma}\left(m_{\mathrm{RD}}\right)}\frac{1}{\xi}, \tag{3.32}$$

$$\Omega = P_{\mathrm{S}}\theta_{\mathrm{SD}}m_{\mathrm{SD}} + P_{\mathrm{R}}\theta_{\mathrm{RD}}m_{\mathrm{RD}} + 2\sqrt{P_{\mathrm{S}}P_{\mathrm{R}}}\,\rho\,\xi\,\varrho, \tag{3.33}$$

$$m = \left(\frac{(P_{\mathrm{S}}\theta_{\mathrm{SD}})^2 m_{\mathrm{SD}} + (P_{\mathrm{R}}\theta_{\mathrm{RD}})^2 m_{\mathrm{RD}} + 4P_{\mathrm{S}}P_{\mathrm{R}}\,\rho^2\,\xi\,\varrho^2}{\Omega^2} \right)^{-1}, \tag{3.34}$$

$$\theta = \frac{\Omega}{m}. \tag{3.35}$$

In (3.30), $U(\cdot,\cdot,\cdot)$ denotes the confluent hypergeometric function of the second kind (Tricomi's function) [39, Eq. 13.2.5].

3.4.2 Diversity Order of BMSC-FDR

Here, we derive the diversity order of the BMSC-FDR protocol. Under Rayleigh fading, and for $P_{\mathrm{S}} = P_{\mathrm{R}} = P$, it can be easily verified that the fraction $\frac{\alpha e^{-\frac{\eta}{\alpha}} - \beta e^{-\frac{\eta}{\beta}}}{\alpha-\beta}$ in (3.29) goes to 1 as P increases, using the approximation $e^{-\frac{x}{P}} \approx 1 - \frac{x}{P}$. Hence the diversity order, also using the same previous approximation, is on the form

$$\mathcal{D} = \lim_{P\to\infty} -\frac{\log\left(\frac{\tilde{a}P^{-1}+\tilde{b}P^{\delta-1}}{1+\tilde{b}P^{\delta-1}}\right)}{\log\left(P\right)} \tag{3.36}$$

$$= \lim_{P\to\infty} \frac{\log\left(P+\tilde{b}P^{\delta}\right) - \log\left(\tilde{a}+\tilde{b}P^{\delta}\right)}{\log\left(P\right)} \tag{3.37}$$

$$= 1-\delta, \tag{3.38}$$

with $\tilde{a} = \frac{\eta}{\pi_{\mathrm{SR}}(1-\rho^2)}$ and $\tilde{b} = \frac{\eta}{1-\rho^2}\frac{\pi_{\mathrm{RR}}}{\pi_{\mathrm{SR}}}$.

From the derived diversity order, we can see that it is enhanced due to considering block transmission and the conditional decoding employed in BMSC-FDR. Specifically, it is no longer limited by the direct link, since the information arriving directly from the source is

now leveraged rather than being treated as interference. However, it is still limited by the RSI and how it scales with the relay power.

3.4.3 Comparison to MRC-HDR

Although BMSC-FDR exploits the direct link and offers a better diversity order than that of MHDF-FDR in the case of non-negligible direct link gain, it still suffers from a diversity problem as that experienced by maximum-ratio combining (MRC)-HDR. Unlike MHDF-HDR, MRC-HDR does not neglect the replica arriving directly from the source. On the contrary, MRC-HDR combines both direct and multi-hop replicas to offer better performance. Nonetheless, from a diversity point of view, it is known from [45] that MRC-HDR does not offer any diversity gain, yielding a diversity order that is equal to 1. This result is due to the fact that the performance of MRC-HDR is limited by that of the first hop. Using *fixed* relaying in which the relay always cooperates, even with combining, renders the first hop as a single point of failure in the system. In other words, if the relay decodes incorrectly due to an outage in the first hop, it will forward a *logically corrupted* message. Combining such a corrupted signal with that correctly, but weakly, arriving directly from the source will still count as an error event due to erroneous decoding with high probability.

For the sake of comparison, the outage performance of MRC-HDR under Nakagami-m fading is given as follows. For Rayleigh fading, m is simply set to 1.

$$\mathcal{P}_{\text{out}} \;=\; 1-\left(1-F_X\left(\eta_{\text{HD}};m_{\text{SR}},\theta_{\text{SR}}\right)\right)\left(1-F_S\left(\eta_{\text{HD}};\boldsymbol{p}_2\right)\right), \tag{3.39}$$

where $\boldsymbol{p}_2=(m_{\text{RD}},P_{\text{R}}\theta_{\text{RD}},m_{\text{SD}},P_{\text{S}}\theta_{\text{SD}})$.

The previous discussion is numerically illustrated in Fig. 3.6. As shown, BMSC-FDR offers better error performance than that of MHDF-FDR due to leveraging the direct link. However, as noticed in Fig. 3.6b, it still suffers from an error floor when $\delta=1$. When $\delta=0$, the diversity gain improves for BMSC-FDR from 0 to 1 as shown in 3.6c, which

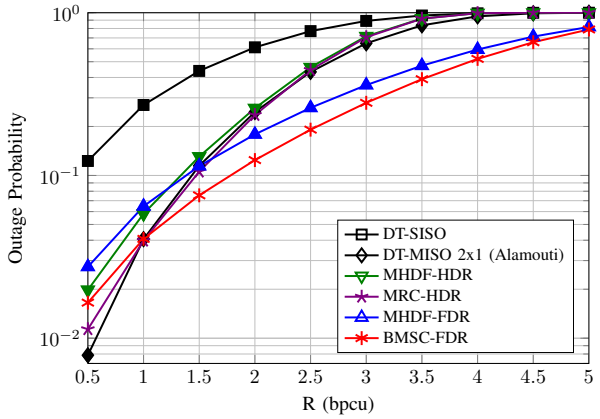

(a) Outage vs. Rate, for $P_{\mathrm{S}} = P_{\mathrm{R}} = P = 1$ and $\delta = 1$.

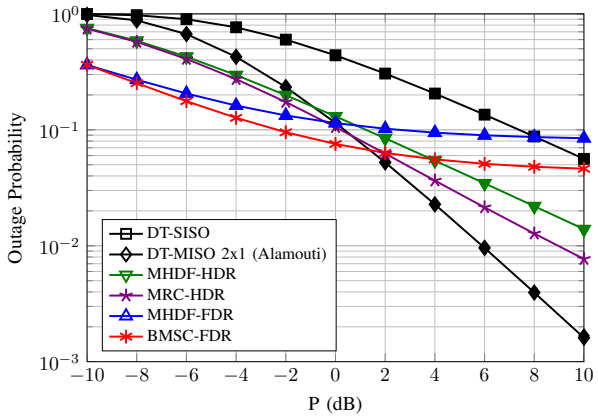

(b) Outage vs. Power, for $R = 1.5$ bpcu and $\delta = 1$.

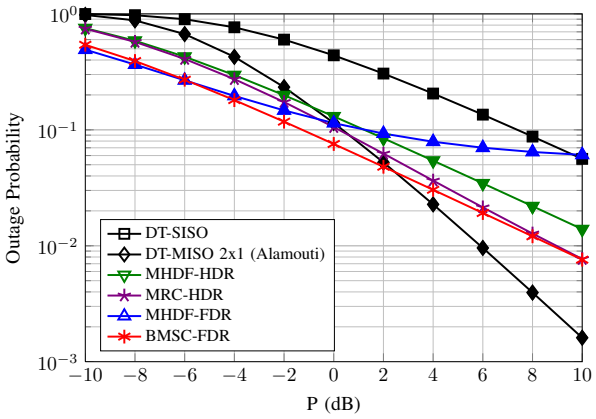

(c) Outage vs. Power, for $R = 1.5$ bpcu and $\delta = 0$.

Figure 3.6: End-to-End Performance of BMSC-FDR and MRC-HDR protocols over Rayleigh fading links, for $\pi_{\mathrm{SR}} = \pi_{\mathrm{RD}} = 20$ dB, $\pi_{\mathrm{RR}} = 2$ dB, $\delta = 1$ and $\pi_{\mathrm{SD}} = 5$ dB.

agrees with the results derived earlier. The performance of MRC-HDR is also shown relative to MHDF-HDR, indicating an improvement in error performance, without any improvement in the diversity gain. As shown, the Alamouti 2×1 scheme attains the best performance due to the full diversity gain it provides.

From the shown figure, it is clear that more efficient cooperative protocols still need be devised and investigated to demonstrate the gains of FDR. In the next chapter, we propose to relax the limitation of adopting *fixed* relaying, and investigate the entailed performance gains.

Appendix

Appendix 3.A Unimodality of MHDF-FDR Outage Probability in the Source and Relay Power

By differentiating $\mathcal{P}_{\text{out}}$ in (3.13) w.r.t. P_{S} while setting $P_{\text{R}} = P_{\text{m}}$, we get

$$\frac{\partial \mathcal{P}_{\text{out}}}{\partial P_{\text{S}}} = -\frac{\eta P_{\text{m}} \pi_{\text{RD}} \exp\left(-\eta\left(\frac{1}{P_{\text{S}}\pi_{\text{SR}}} + \frac{1}{P_{\text{m}}\pi_{\text{RD}}}\right)\right)\left(a_1 P_{\text{S}}^3 + b_1 P_{\text{S}}^2 + c_1 P_{\text{S}} + d_1\right)}{P_{\text{S}}\left(P_{\text{S}}\pi_{\text{SR}} + \eta P_{\text{m}}\pi_{\text{RR}}\right)^2\left(P_{\text{m}}\pi_{\text{RD}} + \eta P_{\text{S}}\pi_{\text{SD}}\right)^2}, \tag{3.40}$$

where $a_1 = -{\pi_{\text{SR}}}^2\pi_{\text{SD}}$, $b_1 = \eta\pi_{\text{SR}}\pi_{\text{SD}}$, $c_1 = (P_{\text{m}}\pi_{\text{SR}}\pi_{\text{RD}} + P_{\text{m}}^2\pi_{\text{SR}}\pi_{\text{RR}}\pi_{\text{RD}} + P_{\text{m}}\pi_{\text{RR}}\pi_{\text{SD}}\eta^2)$, and $d_1 = \eta P_{\text{m}}^2\pi_{\text{RR}}\pi_{\text{RD}}$. It is clear that the exponential term and the denominator are always positive, implying that any sign change of the derivative is due to the cubic equation in the numerator. Here, since the transmit power can only take positive real values, we make use of Descartes rule of signs [53] to find the number of positive roots for the cubic equation. Specifically, for the sequence formed by the descending order of the cubic equation coefficients, i.e., the sequence $\{a_1, b_1, c_1, d_1\}$, the number of sign changes is only one. For our real cubic polynomial, this determines the number of positive roots to be exactly one root, which implies that the interior of the function $\mathcal{P}_{\text{out}}$ in (3.13) is unimodal in $P_{\text{S}} > 0$. Hence, this single positive root of the equation $a_1 P_{\text{S}}^3 + b_1 P_{\text{S}}^2 + c_1 P_{\text{S}} + d_1$ yields $P_{\text{S}}^{\text{opt}}(P_{\text{m}})$. It should be noted that the unimodality property in P_{S} is preserved for general $0 \leq \delta \leq 1$.

Similarly, and due to symmetry in the case of $\delta = 1$, differentiating $\mathcal{P}_{\text{out}}$ in (3.13) w.r.t.

P_{R} while setting $P_{\mathrm{S}} = P_{\mathrm{m}}$, we get

$$\frac{\partial \mathcal{P}_{\mathrm{out}}}{\partial P_{\mathrm{R}}} = -\frac{\eta P_{\mathrm{m}} \pi_{\mathrm{SR}} \exp\left(-\eta\left(\frac{1}{P_{\mathrm{m}}\pi_{\mathrm{SR}}} + \frac{1}{P_{\mathrm{R}}\pi_{\mathrm{RD}}}\right)\right)\left(a_2 P_{\mathrm{R}}^3 + b_2 P_{\mathrm{R}}^2 + c_2 P_{\mathrm{R}} + d_2\right)}{P_{\mathrm{R}}\left(P_{\mathrm{m}}\pi_{\mathrm{SR}} + \eta P_{\mathrm{R}}\pi_{\mathrm{RR}}\right)^2\left(P_{\mathrm{R}}\pi_{\mathrm{RD}} + \eta P_{\mathrm{m}}\pi_{\mathrm{SD}}\right)^2}, \tag{3.41}$$

where $a_2 = -{\pi_{\mathrm{RD}}}^2\pi_{\mathrm{RR}}$, $b_2 = \eta\pi_{\mathrm{RD}}\pi_{\mathrm{RR}}$, $c_2 = (P_{\mathrm{m}}\pi_{\mathrm{SR}}\pi_{\mathrm{RD}} + P_{\mathrm{m}}^2\pi_{\mathrm{SR}}\pi_{\mathrm{SD}}\pi_{\mathrm{RD}} + P_{\mathrm{m}}\pi_{\mathrm{RR}}\pi_{\mathrm{SD}}\eta^2)$, and $d_2 = \eta P_{\mathrm{m}}^2\pi_{\mathrm{SD}}\pi_{\mathrm{SR}}$. The same unimodality property follows in $P_{\mathrm{R}} > 0$, and hence, the single positive root of the equation $a_2 P_{\mathrm{R}}^3 + b_2 P_{\mathrm{R}}^2 + c_2 P_{\mathrm{R}} + d_2$ yields $P_{\mathrm{R}}^{\mathrm{opt}}(P_{\mathrm{m}})$.

Appendix 3.B Quasiconvexity of Outage Upper Bound in the Relay's Circularity Coefficient

The derived outage probability upper bound as a function of the relay's circularity coefficient is given on the form:

$$f(x) = 1 - \frac{e^{-a\frac{\Psi(x)}{(1-x^2)} - b\Psi(cx)}}{d\frac{\Psi(x)}{(1-x^2)} + 1}, \tag{3.42}$$

where $0 \leq x \leq 1$, $a = \frac{1}{P_{\mathrm{R}}\pi_{\mathrm{RD}}}$, $b = \frac{P_{\mathrm{R}}^{\delta}\pi_{\mathrm{RR}}+1}{P_{\mathrm{S}}\pi_{\mathrm{SR}}}$, $c = \frac{P_{\mathrm{R}}^{\delta}\pi_{\mathrm{RR}}}{P_{\mathrm{R}}^{\delta}\pi_{\mathrm{RR}}+1}$, and $d = \frac{P_{\mathrm{S}}\pi_{\mathrm{SD}}}{P_{\mathrm{R}}\pi_{\mathrm{RD}}}$. We analyze the stationary points of $\overline{f}(x) = 1 - f(x)$. Its derivative is given by

$$\frac{d\overline{f}(x)}{dx} = x\frac{e^{-a\frac{\Psi(x)}{1-x^2} - b\Psi(cx)}}{\left(d\frac{\Psi(x)}{1-x^2} + 1\right)^2}S(x), \tag{3.43}$$

where

$$\begin{aligned} S(x) = &\left(d\frac{\Psi(x)}{1-x^2} + 1\right)\left(\frac{a\left(2\Psi(x) + \eta_{\mathrm{HD}}\left(x^2-1\right)\right)}{\left(\Psi(x)+1\right)\left(1-x^2\right)^2} + \frac{b\eta_{\mathrm{HD}}c^2}{\Psi(cx)+1}\right) \\ &+ \frac{\eta_{\mathrm{HD}}d}{\left(\Psi(x)+1\right)\left(1-x^2\right)} - \frac{2d\Psi(x)}{\left(1-x^2\right)^2}. \end{aligned} \tag{3.44}$$

From the given form, and in addition to the roots of $S(x)$, it is clear that $\frac{d\overline{f}(x)}{dx}$ admits only a zero at $x = 0$. Now, we investigate the roots for $S(x)$, and use the change of variables, $z = \Psi(x) + 2$. Hence, $1 - x^2 = \frac{z(z-2)}{\eta_{\rm HD}}$. After substitution and some manipulations, $S(z)$ is hence given for our region of interest, $2 \leq z \leq 1 + \sqrt{1 + \eta_{\rm HD}}$, by

$$S(z) = \left(d\frac{\eta_{\rm HD}}{z} + 1\right)\left(\frac{-a\eta_{\rm HD}^2}{z^2(z-1)} + \frac{b\eta_{\rm HD}c^2}{\Psi(cx)+1}\right) - \frac{\eta_{\rm HD}^2 d}{z^2(z-1)}. \tag{3.45}$$

Since $0 < c < 1$, we know that $1 - c^2x^2 \geq 1 - x^2$. Hence, $\Psi(cx) + 1 \geq \Psi(x) + 1 = z - 1$. Let $\Psi(cx) + 1 = t_z(z-1)$, where $t_z \geq 1$. Therefore,

$$S(z) \;=\; \frac{(d\eta_{\rm HD} + z)(-a\eta_{\rm HD}^2 t_z + b\eta_{\rm HD}c^2z^2) - \eta_{\rm HD}^2 d t_z z}{t_z z^3(z-1)}. \tag{3.46}$$

The numerator is a cubic polynomial in z which is given by

$$T(z) = bc^2\eta_{\rm HD}z^3 + bc^2d\eta_{\rm HD}^2z^2 - (a+d)\eta_{\rm HD}^2 t_z z - ad\eta_{\rm HD}^3 t_z. \tag{3.47}$$

To find the number of positive roots for $T(z)$, we use Descartes rule of signs [53]. Specifically, for the sequence formed by the descending order of the cubic equation coefficients, i.e., the sequence $\{bc^2\eta_{\rm HD}, bc^2d\eta_{\rm HD}^2, -(a+d)\eta_{\rm HD}^2 t_z, -ad\eta_{\rm HD}^3 t_z\}$, the number of sign changes is only one. For our real cubic polynomial, this determines the number of positive roots to be exactly one root. Hence, in the positive region of interest, $2 \leq z \leq 1 + \sqrt{1 + \eta_{\rm HD}}$, either one or no *feasible* roots exist for $T(z)$, and hence for $S(z)$. This shows that $\overline{f}(x)$ is either monotonic or unimodal due to the existence of one root at maximum in its interior. If unimodal, the global optimal point can be numerically obtained via the bisection method operating on the derivative function.

Chapter 4

Selective Full-Duplex Relaying

4.1 Related Work

In HDR, there exist different protocols in the existing literature that can offer a better diversity order than that of MRC-HDR. In [45], Laneman *et al.* proposed several HDR protocols and studied their outage performance. Among these protocols is the selective decode-and-forward (SDF) protocol in which the relay assists only when the source-relay link is not in outage. Thus, SDF avoids as much as possible forwarding mere interference to the destination, giving the latter a chance to recover the message from the direct link. Also proposed in [45] is the incremental decode-and-forward (IDF) protocol where the relay only assists upon the reception of a one-bit feedback from the destination declaring an outage in the direct source-destination link. This protocol was proposed to primarily alleviate the inherent rate loss in HDR by allowing the destination to solely rely on the direct link as long as it is in a good condition, and hence it avoids the dedication of a time slot for relay forwarding.

In addition to their rate enhancement to HDR systems, SDF and IDF also offer a diversity gain by no longer having the first hop as the system's single point of failure. Indeed, at high SNR, the error probability is inversely proportional to the SNR squared as derived in [45],

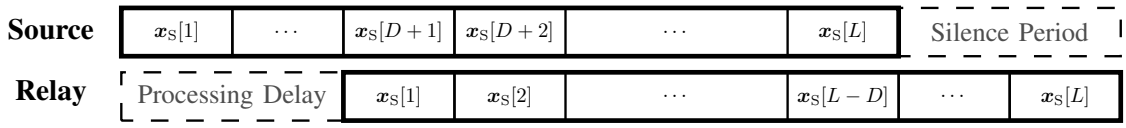

Figure 4.1: SDF-FDR block transmission scheme, where $\boldsymbol{x}_S[b]$, $b \in \{1, 2, \cdots, L\}$, is the b^{th} B-dimensional codeword transmitted by the source.

implying a diversity of order 2.

In what follows, and in order to capture the direct link benefits, we first propose to adopt a block transmission scheme where both message replicas (the direct and multi-hop replicas) can be leveraged at the destination. In such a block transmission, we revisit the SDF and IDF protocols proposed for HDR, and propose two protocols that can be employed in FDR. Unlike in *fixed* relaying, the proposed *selective* FDR protocols have the potential to offer higher diversity as will be shortly discussed.

4.2 Block Transmission Scheme

We consider the block transmission scheme in Fig. 4.1. As shown, communication takes place over one super-block, which is composed of $L + D$ blocks. All channel gains are assumed to remain constant over the entire super-block. Unlike in MHDF-FDR, and similar to BMSC-FDR, here the destination node D attempts decoding only after the reception of the whole super-block. This ensures that the destination has received the two replicas via the direct and multi-hop paths, although they are not well-aligned as shown.

For each set of channel realizations, the system selects to operate in either a cooperative or non-cooperative mode. In the cooperative mode, it is assumed that the relay is able to successfully decode and simply reencode the source message with the same encoding function used by the source, taking its processing delay into account. In what follows, we discuss the signal model with and without relay assistance.

4.2.1 Cooperative Mode

Taking the relay processing delay of D codewords into account, the relay simultaneously forwards $\boldsymbol{x}_{\mathrm{R}}[b] = \boldsymbol{x}_{\mathrm{S}}[b-D]$, which imposes self-interference. Thus, the B-dimensional received signals at R and D at block b are given,respectively, by

$$\boldsymbol{y}_{\mathrm{R}}[b] = \sqrt{P_{\mathrm{S}}} h_{\mathrm{SR}} \boldsymbol{x}_{\mathrm{S}}[b] + \sqrt{P_{\mathrm{R}}^{\delta}} h_{\mathrm{RR}} \boldsymbol{x}_{\mathrm{S}}[b-D] + \boldsymbol{n}_{\mathrm{R}}[b], \tag{4.1}$$

$$\boldsymbol{y}_{\mathrm{D}}[b] = \sqrt{P_{\mathrm{S}}} h_{\mathrm{SD}} \boldsymbol{x}_{\mathrm{S}}[b] + \sqrt{P_{\mathrm{R}}} h_{\mathrm{RD}} \boldsymbol{x}_{\mathrm{S}}[b-D] + \boldsymbol{n}_{\mathrm{D}}[b], \tag{4.2}$$

where $\boldsymbol{n}_{\mathrm{R}}[b] \in \mathbb{C}^{B\times 1}$ and $\boldsymbol{n}_{\mathrm{D}}[b] \in \mathbb{C}^{B\times 1}$ denote the relay and destination noise at block b, respectively. We rewrite (4.2) in vector form to jointly account for the $L+D$ signals received over the entire super-block as

$$\boldsymbol{y}_{\mathrm{D}} = \boldsymbol{H}\boldsymbol{x}_{\mathrm{S}} + \boldsymbol{n}_{\mathrm{D}}, \tag{4.3}$$

where

$$\boldsymbol{y}_{\mathrm{D}} = \left(\boldsymbol{y}_{\mathrm{D}}[1]^T, \ldots, \boldsymbol{y}_{\mathrm{D}}[L+D]^T\right)^T, \tag{4.4}$$

$$\boldsymbol{x}_{\mathrm{S}} = \left(\boldsymbol{x}_{\mathrm{S}}[1]^T, \ldots, \boldsymbol{x}_{\mathrm{S}}[L]^T\right)^T, \tag{4.5}$$

$$\boldsymbol{n}_{\mathrm{D}} = \left(\boldsymbol{n}_{\mathrm{D}}[1]^T, \ldots, \boldsymbol{n}_{\mathrm{D}}[L+D]^T\right)^T, \tag{4.6}$$

and

$$\boldsymbol{H} = \sqrt{P_{\mathrm{S}}} h_{\mathrm{SD}} \begin{bmatrix} \boldsymbol{I}_{BL} \\ \boldsymbol{0}_{BD\times BL} \end{bmatrix} + \sqrt{P_{\mathrm{R}}} h_{\mathrm{RD}} \begin{bmatrix} \boldsymbol{0}_{BD\times BL} \\ \boldsymbol{I}_{BL} \end{bmatrix}. \tag{4.7}$$

4.2.2 Non-Cooperative Mode

In this case, the relay does not assist. Thus, the received signal at the destination at block b is given by

$$\boldsymbol{y}_{\mathrm{D}}[b] \;=\; \sqrt{P_{\mathrm{S}}}h_{\mathrm{SD}}\boldsymbol{x}_{\mathrm{S}}[b] + \boldsymbol{n}_{\mathrm{D}}[b]. \tag{4.8}$$

For large $\frac{L}{D}$, in order to keep the same block structure adopted in the no-outage case, it is equivalent to use the vector form in (4.3) with the value of P_{R} or π_{RD} set to zero.

4.2.3 Instantaneous Link Capacities

To analyze the end-to-end channel outage, the instantaneous capacities of the individual links need to be first provided. Assuming complex Gaussian channel inputs and unit bandwidth, the information capacity of the $i-j$ link is given by

$$C_{ij} \;=\; \log_2\left(1+\gamma_{ij}\right) \text{ bpcu}, \tag{4.9}$$

where $\gamma_{\mathrm{SD}} = P_{\mathrm{S}}g_{\mathrm{SD}}$ and $\gamma_{\mathrm{RD}} = P_{\mathrm{R}}g_{\mathrm{RD}}$, while $\gamma_{\mathrm{SR}} = \frac{P_{\mathrm{S}}g_{\mathrm{SR}}}{P_{\mathrm{R}}^{\delta}g_{\mathrm{RR}}+1}$ denotes the SINR in the $\mathrm{S}-\mathrm{R}$ link with the RSI effect taken into account as an additional noise term.

At the destination, we use $C_{(\mathrm{S,R})\to\mathrm{D}}$ to denote the information capacity per super-block in the virtual MISO channel formed by S and R as the transmitter side and by D as the receiver side. It is worth mentioning that no channel state information is assumed at the transmitter side, and hence, no power or rate adaptation is possible. Again, assuming complex Gaussian inputs and unit bandwidth, it is readily given by

$$C_{(\mathrm{S,R})\to\mathrm{D}} = \log_2 \det\left\{\boldsymbol{I}_{BL} + \boldsymbol{H}^H\boldsymbol{H}\right\} = \log_2 \prod_{i=1}^{BL}\left(1+\lambda_i\right), \tag{4.10}$$

where

$$\boldsymbol{H}^H\boldsymbol{H} \;=\; \alpha\boldsymbol{I}_{BL} + \beta{\boldsymbol{B}_{BL}}^{BD} + \beta^*{\boldsymbol{F}_{BL}}^{BD}, \tag{4.11}$$

with $\alpha = P_{\rm S}g_{\rm SD} + P_{\rm R}g_{\rm RD} = \gamma_{\rm SD} + \gamma_{\rm RD}$ and $\beta = h^*_{\rm SD}h_{\rm RD}$, while $\boldsymbol{B}_\ell$ ($\boldsymbol{F}_\ell$) denotes a square backward (forward) shift matrix of size ℓ, with ones only on the first subdiagonal (superdiagonal) and zeros elsewhere. Also, $\{\lambda_i\}_{i=1}^{BL}$ denote the BL eigenvalues of $\boldsymbol{H}^H\boldsymbol{H}$. For the special case of $D = B = 1$, $\boldsymbol{H}^H\boldsymbol{H}$ is an $L \times L$ tridiagonal Toeplitz matrix, whose L eigenvalues are known in closed-form, [54, pp. 80], as

$$\lambda_i = \alpha + 2|\beta|\cos\frac{i\pi}{L+1}, \quad i \in \{1, 2, \cdots, L\}. \tag{4.12}$$

We show in Appendix 4.A that for $L = kD$ with $k \in \mathbb{Z}^+$, and for general $B \in \mathbb{Z}^+$, the BL eigenvalues are generalized to:

$$\lambda_{BD(i-1)+1:BDi} = \alpha + 2|\beta|\cos\frac{iD\pi}{L+D}, \quad i \in \{1, 2, \cdots, k\}, \tag{4.13}$$

where $\lambda_{i:j}$ denotes the set of eigenvalues $\{\lambda_i, \lambda_{i+1}, \cdots, \lambda_j\}$. That is, the BL eigenvalues of $\boldsymbol{H}^H\boldsymbol{H}$ are only k distinct eigenvalues, each with a multiplicity of BD.

From (4.13), it follows that

$$C_{\rm (S,R)\to D} \;=\; \log_2\prod_{i=1}^{k}\left(1 + \alpha + 2|\beta|\cos\frac{iD\pi}{L+D}\right)^{BD} \tag{4.14}$$

$$\;=\; BL\log_2(1+\alpha) + BD\sum_{i=1}^{k}\log_2\left(1 + \frac{2|\beta|\cos\frac{i\pi}{k+1}}{1+\alpha}\right). \tag{4.15}$$

Thanks to the arithmetic-geometric mean inequality, we know that $2|\beta| \le \alpha$, and hence, $2|\beta|\cos\frac{i\pi}{k+1} < 2|\beta| \le \alpha < \alpha + 1$. Thus, in the second term of (4.15), $|\frac{2|\beta|\cos\frac{i\pi}{k+1}}{1+\alpha}| < 1$. For mathematical tractability, we only use the first order Taylor expansion that $\ln(1+x) \approx x$, or alternatively, $\log_2(1+x) \approx \frac{x}{\ln(2)}$. Noting that $\sum_{i=1}^{k}\cos\frac{i\pi}{k+1} = 0$, the second term in (4.15)

vanishes. Hence,

$$C_{(\mathrm{S,R})\to\mathrm{D}} \approx BL\log_2(1+\alpha) \text{ bpcu.} \tag{4.16}$$

Recalling that $\alpha = P_{\mathrm{S}}g_{\mathrm{SD}}+P_{\mathrm{R}}g_{\mathrm{RD}}$, this previous approximation offers an interesting intuition. That is, by employing block decoding using the proposed block transmission scheme, the effective SINR per block is approximately equal to the sum of those obtained via the $\mathrm{S}-\mathrm{D}$ and $\mathrm{R}-\mathrm{D}$ links. This appears of an equivalent effect as if maximum-ratio combining is applied on the two signal replicas. Thus, although the two signals are non-orthogonal in time and frequency due to simultaneous transmission, block transmission and decoding allowed for an MRC-like effect. Clearly, this comes at the expense of D wasted blocks for alignment, in addition to the higher decoding complexity. It should be also noted that due to the special structure of the channel matrix, the source codewords in the super-block can be grouped into k disjoint sets that can be separately decoded without loss of performance, thus reducing the decoding complexity.

4.3 Selective/Incremental Full-Duplex Cooperation

Two selective cooperation protocol variants are proposed based on the aforementioned block transmission scheme, namely, SDF-FDR and incremental selective decode-and-forward (ISDF)-FDR.

- In SDF-FDR, the system operates in the cooperative mode as long as the relay is able to decode the source message. It is assumed that the outage event dominates the error event. Thus, the relay successfully decodes the source message as long as its received SINR exceeds the threshold $\eta = 2^R - 1$. Otherwise, the relay does not cooperate, and the destination attempts to decode only from the directly received signal. According to the defined SDF-FDR cooperation policy, and based on the result in (4.16), the effective SNR profile at the destination node, denoted by γ_{e2e}, can be approximately

given by

$$\gamma_{\text{e2e}} \approx \begin{cases} \gamma_{\text{SD}}, & \mathcal{O}_{\text{SR}}, \\ \gamma_{\text{SD}} + \gamma_{\text{RD}}, & \overline{\mathcal{O}_{\text{SR}}}. \end{cases} \tag{4.17}$$

where $\mathcal{O}_{ij}$ denotes the outage event in the $i-j$ link, with $\overline{\mathcal{O}_{ij}}$ denoting its complement.

- In ISDF-FDR, the system favors non-cooperative mode as long as the direct $\text{S}-\text{D}$ link is outage-free. When the $\text{S}-\text{D}$ link falls in outage, the relay starts to cooperate when the $\text{S}-\text{R}$ link is outage-free. This offers better energy-efficiency in terms of putting the relay to sleep as long as the direct link is operational. Also, simpler instantaneous decoding can be performed at the destination when receiving directly from the source. The received SNR profile of ISDF-FDR is approximately given by

$$\gamma_{\text{e2e}} \approx \begin{cases} \gamma_{\text{SD}}, & \overline{\mathcal{O}_{\text{SD}}} \cup (\mathcal{O}_{\text{SR}} \cap \mathcal{O}_{\text{SD}}), \\ \gamma_{\text{SD}} + \gamma_{\text{RD}}, & \overline{\mathcal{O}_{\text{SR}}} \cap \mathcal{O}_{\text{SD}}. \end{cases} \tag{4.18}$$

In what follows we analyze the performance of the two protocol variants under both Rayleigh and Nakagami-m fading.

4.4 Outage Performance

In SDF-FDR, cooperation takes place only when the $\text{S}-\text{R}$ link is not in outage. Accordingly, an outage is declared when one of two events occurs: 1) the $\text{S}-\text{R}$ link is in outage, hence no cooperation takes place, while the $\text{S}-\text{D}$ link goes into an outage state, or 2) the $\text{S}-\text{R}$ link is not in outage, thus relay assistance is available, but an outage occurs in the MISO channel. This is more formally defined as

$$\mathcal{P}_{\text{out}} = \mathcal{P}_{\text{SR}}\mathcal{P}_{\text{SD}} + (1 - \mathcal{P}_{\text{SR}})\,\mathcal{P}_{(\text{S,R})\to\text{D}}, \tag{4.19}$$

where $\mathcal{P}_{\mathrm{SR}}$ and $\mathcal{P}_{\mathrm{SD}}$ are the outage probabilities of the $\mathrm{S}-\mathrm{R}$ and $\mathrm{S}-\mathrm{D}$ links, respectively, which are given by

$$\mathcal{P}_{\mathrm{SR}} = \mathbb{P}\left\{C_{\mathrm{SR}} < R\right\}, \qquad \text{and} \qquad \mathcal{P}_{\mathrm{SD}} = \mathbb{P}\left\{C_{\mathrm{SD}} < R\right\}. \tag{4.20}$$

In (4.19), $\mathcal{P}_{(\mathrm{S,R})\to\mathrm{D}}$ is the probability of outage in the virtual MISO channel. Noting that $C_{(\mathrm{S,R})\to\mathrm{D}}$ denotes the information capacity per super-block, $\mathcal{P}_{(\mathrm{S,R})\to\mathrm{D}}$ is defined as

$$\mathcal{P}_{(\mathrm{S,R})\to\mathrm{D}} \;=\; \mathbb{P}\left\{\frac{C_{(\mathrm{S,R})\to\mathrm{D}}}{B(L+D)} < \frac{BL}{B(L+D)}R\right\}, \tag{4.21}$$

where the factor $\frac{BL}{B(L+D)}$ accounts for the fact that the source only transmits in L out of $L+D$ blocks. Using (4.16), we get

$$\mathcal{P}_{(\mathrm{S,R})\to\mathrm{D}} \;\approx\; \mathbb{P}\left\{\gamma_{\mathrm{RD}} + \gamma_{\mathrm{SD}} < \eta\right\}. \tag{4.22}$$

The ISDF-FDR protocol seeks further relay power savings. The selective part in its name comes from the same relay selectivity in forwarding the source message depending on the outage state of the $\mathrm{S}-\mathrm{R}$ link. However, the relay does not need to always forward when it successfully decodes. Instead, relay assistance becomes necessary only upon the reception of a one-bit feedback from the destination at the beginning of the super-block declaring an outage and asking for assistance. Therefore, an end-to-end outage occurs when one of two events occurs: 1) the $\mathrm{S}-\mathrm{D}$ link goes in outage, while the $\mathrm{S}-\mathrm{R}$ link is in outage. In this case, the relay is unable to assist and outage occurs with probability $\mathcal{P}_{\mathrm{SR}}\mathcal{P}_{\mathrm{SD}}$ due to the independence of channel fading coefficients, or 2) the $\mathrm{S}-\mathrm{D}$ link goes in outage while the $\mathrm{S}-\mathrm{R}$ link is not in outage, but the cooperative MISO channel is in outage. The latter outage event represents an intersection of three events. We know that the event of no outage in the $\mathrm{S}-\mathrm{R}$ link is independent of the $\mathrm{S}-\mathrm{D}$ and the MISO channel outage events. Also, we know that cooperation cannot decrease the mutual information, and thus, the outage capacity of

the MISO channel is at least equal to that of the $\mathrm{S}-\mathrm{D}$ link. Hence, the intersection of the outage events in the $\mathrm{S}-\mathrm{D}$ and the MISO channel is the outage event in the MISO channel itself. Therefore, the probability of this event is equal to $\overline{\mathcal{P}_{\mathrm{SR}}}\,\mathcal{P}_{(\mathrm{S,R})\to\mathrm{D}}$. As such, the outage probability of ISDF-FDR is exactly equal to that given in (4.19) for the SDF-FDR protocol. In what follows we derive the end-to-end outage probability for the proposed protocols.

4.4.1 Rayleigh Fading

Under Rayleigh fading, $\mathcal{P}_{\mathrm{SR}}$ and $\mathcal{P}_{\mathrm{SD}}$ are easily derived starting from (4.1) and (4.8), see [41, 40], to be:

$$\mathcal{P}_{\mathrm{SR}} = \quad \mathbb{P}\left\{C_{\mathrm{SR}} < R\right\} \quad = 1 - \frac{P_{\mathrm{S}}\pi_{\mathrm{SR}} e^{-\frac{\eta}{P_{\mathrm{S}}\pi_{\mathrm{SR}}}}}{\eta P_{\mathrm{R}}^{\delta}\pi_{\mathrm{RR}} + P_{\mathrm{S}}\pi_{\mathrm{SR}}}, \tag{4.23}$$

$$\mathcal{P}_{\mathrm{SD}} = \quad \mathbb{P}\left\{C_{\mathrm{SD}} < R\right\} \quad = 1 - e^{-\frac{\eta}{P_{\mathrm{S}}\pi_{\mathrm{SD}}}}. \tag{4.24}$$

From (4.22), we know that $\mathcal{P}_{(\mathrm{S,R})\to\mathrm{D}}$ is approximated by the CDF of $\alpha = \gamma_{\mathrm{SD}} + \gamma_{\mathrm{RD}}$ evaluated at η. Since γ_{SD} and γ_{RD} are independent exponential random variables with mean parameters $P_{\mathrm{S}}\pi_{\mathrm{SD}}$ and $P_{\mathrm{R}}\pi_{\mathrm{RD}}$, respectively, α is a hypoexponential random variable with two rate parameters, $\frac{1}{P_{\mathrm{S}}\pi_{\mathrm{SD}}}$ and $\frac{1}{P_{\mathrm{R}}\pi_{\mathrm{RD}}}$. Thus, according to [55, Eq. (5.9)], its CDF is given by:

$$F_{\alpha}(x) \quad = \quad 1 - \frac{P_{\mathrm{R}}\pi_{\mathrm{RD}} e^{-\frac{x}{P_{\mathrm{R}}\pi_{\mathrm{RD}}}} - P_{\mathrm{S}}\pi_{\mathrm{SD}} e^{-\frac{x}{P_{\mathrm{S}}\pi_{\mathrm{SD}}}}}{P_{\mathrm{R}}\pi_{\mathrm{RD}} - P_{\mathrm{S}}\pi_{\mathrm{SD}}}. \tag{4.25}$$

Now, substituting (4.22), (4.23), (4.24), and (4.25) into (4.19), and performing some manipulations, the overall outage probability of proposed SDF-FDR/ISDF-FDR protocol variants is obtained as:

$$\mathcal{P}_{\mathrm{out}} \;\approx\; 1 - e^{-\frac{\eta}{P_{\mathrm{S}}\pi_{\mathrm{SD}}}} - \frac{P_{\mathrm{S}}\pi_{\mathrm{SR}} e^{-\frac{\eta}{P_{\mathrm{S}}\pi_{\mathrm{SR}}}} \times P_{\mathrm{R}}\pi_{\mathrm{RD}}\left(e^{-\frac{\eta}{P_{\mathrm{R}}\pi_{\mathrm{RD}}}} - e^{-\frac{\eta}{P_{\mathrm{S}}\pi_{\mathrm{SD}}}}\right)}{\left(\eta P_{\mathrm{R}}^{\delta}\pi_{\mathrm{RR}} + P_{\mathrm{S}}\pi_{\mathrm{SR}}\right) \times \left(P_{\mathrm{R}}\pi_{\mathrm{RD}} - P_{\mathrm{S}}\pi_{\mathrm{SD}}\right)}. \tag{4.26}$$

4.4.2 Nakagami-m Fading

Since the SNRs γ_{SD} and γ_{RD} are respectively $\mathcal{G}\left(m_{\mathrm{SD}}, P_{\mathrm{S}}\theta_{\mathrm{SD}}\right)$ and $\mathcal{G}\left(m_{\mathrm{RD}}, P_{\mathrm{R}}\theta_{\mathrm{RD}}\right)$ distributed, it follows from (3.4) that for $i \in \{\mathrm{S}, \mathrm{R}\}$ the SNR CDF is given by

$$F_{\gamma_{i\mathrm{D}}}(x) \;=\; F_X\left(x; m_{i\mathrm{D}}, P_i\theta_{i\mathrm{D}}\right). \tag{4.27}$$

Also, since $\gamma_{\mathrm{SR}} = \frac{P_{\mathrm{S}}g_{\mathrm{SR}}}{P_{\mathrm{R}}^{\delta}g_{\mathrm{RR}}+1}$, it follows from (3.14) in Remark 1 that the CDF of the received SNR via the $\mathrm{S}-\mathrm{R}$ link is given by

$$F_{\gamma_{\mathrm{SR}}}(x) \;=\; F_Z\left(x; \boldsymbol{p}_1\right), \tag{4.28}$$

with $\boldsymbol{p}_1 = (m_{\mathrm{SR}}, P_{\mathrm{S}}\theta_{\mathrm{SR}}, m_{\mathrm{RR}}, P_{\mathrm{R}}^{\delta}\theta_{\mathrm{RR}})$. To find $\mathcal{P}_{(\mathrm{S,R})\to\mathrm{D}}$, we need to know the CDF of $\alpha = \gamma_{\mathrm{SD}} + \gamma_{\mathrm{RD}}$. Since γ_{SD} and γ_{RD} are independent Gamma RVs, we make use of the following remark on the CDF of their sum.

Remark 2 (CDF of $S = X_1 + X_2$)**.** *For two independent Gamma RVs, $X_1 \sim \mathcal{G}\left(m_1, \theta_1\right)$ and $X_2 \sim \mathcal{G}\left(m_2, \theta_2\right)$, with integer shape parameters and possibly distinct scale parameters, $S = X_1 + X_2$ has the following CDF [56]:*

$$F_S\left(s; \boldsymbol{p}\right) = \frac{\boldsymbol{\gamma}\left(m_2, \frac{s}{\theta_2}\right)}{\boldsymbol{\Gamma}\left(m_2\right)} - \sum_{k=0}^{m_1-1} \frac{A}{\boldsymbol{\Gamma}\left(v\right)} \left(\frac{s}{\theta_1}\right)^k {}_1\boldsymbol{F}_1\left(u; v; w\right), \tag{4.29}$$

where $\boldsymbol{p} = (m_1, \theta_1, m_2, \theta_2)$ is a vector holding the shape and scale parameters, $A = \left(\frac{s}{\theta_2}\right)^{m_2} \exp\left(-\frac{s}{\theta_2}\right)$, $u = k+1$, $v = m_2 + k + 1$, $w = \frac{\theta_1-\theta_2}{\theta_1\theta_2}s$ and ${}_1\boldsymbol{F}_1\left(u; v; w\right)$ is the Kummer's confluent hypergeometric function [39, Eq. 13.1.2].

Since γ_{SD} and γ_{RD} are independent and respectively distributed as $\mathcal{G}\left(m_{\mathrm{SD}}, P_{\mathrm{S}}\theta_{\mathrm{SD}}\right)$ and $\mathcal{G}\left(m_{\mathrm{RD}}, P_{\mathrm{R}}\theta_{\mathrm{RD}}\right)$, it follows from (A.1) that the CDF of the SNR in the MISO channel,

denoted as $F_{(\mathrm{S,R})\to\mathrm{D}}(x)$, is approximately given as

$$F_{(\mathrm{S,R})\to\mathrm{D}}(x) \approx \mathbb{P}\{\alpha \leq x\} = F_S\left(x; \boldsymbol{p}_2\right), \tag{4.30}$$

with $\boldsymbol{p}_2 = (m_{\mathrm{RD}}, P_{\mathrm{R}}\theta_{\mathrm{RD}}, m_{\mathrm{SD}}, P_{\mathrm{S}}\theta_{\mathrm{SD}})$. Hence, $\mathcal{P}_{(\mathrm{S,R})\to\mathrm{D}}$ is then given for the Nakagami-m fading scenario by evaluating the CDF at η as

$$\mathcal{P}_{(\mathrm{S,R})\to\mathrm{D}} \;\approx\; F_S\left(\eta; \boldsymbol{p}_2\right). \tag{4.31}$$

4.5 SNR Performance

It can be noticed from (4.17) and (4.18) that the SDF-FDR protocol offers extra relay cooperation in the particular non-outage event of $\overline{\mathcal{O}_{\mathrm{SR}}} \cap \overline{\mathcal{O}_{\mathrm{SD}}}$ that does not matter in terms of the outage performance. Since we can expect that SDF-FDR can offer higher performance beyond the outage metric due to the more cooperation it offers, outage analysis does not suffice to capture and distinguish the relative performance of both protocols. Now, we analyze the end-to-end SNR performance of each of the two protocols.

4.5.1 ISDF-FDR

Let $\{A_i\}_{i=1}^{4}$ denote some intersections of outage events which are defined, along with their probabilities, as follows:

$$\begin{aligned}
A_1 &\triangleq \mathcal{O}_{\mathrm{SR}} \cap \mathcal{O}_{\mathrm{SD}}, \quad \mathbb{P}\{A_1\} = \mathcal{P}_{\mathrm{SR}}\mathcal{P}_{\mathrm{SD}}, \\
A_2 &\triangleq \overline{\mathcal{O}_{\mathrm{SR}}} \cap \mathcal{O}_{\mathrm{SD}}, \quad \mathbb{P}\{A_2\} = \overline{\mathcal{P}_{\mathrm{SR}}}\mathcal{P}_{\mathrm{SD}}, \\
A_3 &\triangleq \mathcal{O}_{\mathrm{SR}} \cap \overline{\mathcal{O}_{\mathrm{SD}}}, \quad \mathbb{P}\{A_3\} = \mathcal{P}_{\mathrm{SR}}\overline{\mathcal{P}_{\mathrm{SD}}}, \\
A_4 &\triangleq \overline{\mathcal{O}_{\mathrm{SR}}} \cap \overline{\mathcal{O}_{\mathrm{SD}}}, \quad \mathbb{P}\{A_4\} = \overline{\mathcal{P}_{\mathrm{SR}}\mathcal{P}_{\mathrm{SD}}}.
\end{aligned} \tag{4.32}$$

Clearly, $\{A_i\}_{i=1}^4$ are mutually exclusive events that jointly span the whole probability space, and hence, they form a partitioned space. Therefore, we can use the total probability theorem to get the distribution of the end-to-end SNR γ_{e2e} as:

$$F_{\gamma_{\text{e2e}}}(x) \;=\; \sum_{i=1}^{4} F(x|A_i)\mathbb{P}\{A_i\}, \tag{4.33}$$

where

$$F(x|A_1) \;=\; \begin{cases} \frac{F_{\gamma_{\text{SD}}}(x)}{\mathcal{P}_{\text{SD}}}, & 0 < x < \eta, \\ 1, & \text{elsewhere}, \end{cases} \tag{4.34}$$

and

$$F(x|A_3) = F(x|A_4) \;=\; \begin{cases} \frac{F_{\gamma_{\text{SD}}}(x) - \mathcal{P}_{\text{SD}}}{1-\mathcal{P}_{\text{SD}}}, & \eta < x < \infty, \\ 0, & \text{elsewhere}. \end{cases} \tag{4.35}$$

We show in Appendix 4.B that

$$F(x|A_2) \;\approx\; \begin{cases} F_1(x), & 0 < x < \eta, \\ F_2(x), & \eta < x < \infty, \end{cases} \tag{4.36}$$

where $F_1(x)$ and $F_2(x)$ are given in (4.37) and (4.38), respectively, as

$$F_1(x) \;=\; \frac{F_X(x;m_{\text{SD}},P_{\text{S}}\theta_{\text{SD}})}{\mathcal{P}_{\text{SD}}} - \sum_{m=0}^{m_{\text{RD}}-1} \frac{x^{m_{\text{SD}}+m} e^{-\frac{x}{P_{\text{R}}\theta_{\text{RD}}}}\, {}_1\boldsymbol{F}_1\left(m_{\text{SD}};m_{\text{SD}}+m+1;\left(\frac{1}{P_{\text{R}}\theta_{\text{RD}}}-\frac{1}{P_{\text{S}}\theta_{\text{SD}}}\right)x\right)}{\mathcal{P}_{\text{SD}}\boldsymbol{\Gamma}(m_{\text{SD}}+m+1)(P_{\text{R}}\theta_{\text{RD}})^m(P_{\text{S}}\theta_{\text{SD}})^{m_{\text{SD}}}} = \frac{F_S(x;\boldsymbol{p_2})}{\mathcal{P}_{\text{SD}}}, \tag{4.37}$$

$$F_2(x) \;=\; 1 - \sum_{m=0}^{m_{\text{RD}}-1} \sum_{k=0}^{m} \frac{(x-\eta)^{m-k}\eta^{m_{\text{SD}}+k} e^{-\frac{\eta}{P_{\text{R}}\theta_{\text{RD}}}}\, {}_1\boldsymbol{F}_1\left(m_{\text{SD}};m_{\text{SD}}+k+1;\left(\frac{1}{P_{\text{R}}\theta_{\text{RD}}}-\frac{1}{P_{\text{S}}\theta_{\text{SD}}}\right)\eta\right)}{\mathcal{P}_{\text{SD}}\boldsymbol{\Gamma}(m_{\text{SD}}+k+1)\boldsymbol{\Gamma}(m-k+1)(P_{\text{R}}\theta_{\text{RD}})^m(P_{\text{S}}\theta_{\text{SD}})^{m_{\text{SD}}}}. \tag{4.38}$$

Substituting (4.34)-(4.38) into (4.33), we get $F_{\gamma_{\text{e2e}}}(x)$ for ISDF-FDR.

4.5.2 SDF-FDR

In SDF-FDR, the relay cooperates regardless of the outage state of the S − D link. Thus, the CDF of the end-to-end SNR can be expressed as:

$$\begin{aligned} F_{\gamma_{\text{e2e}}}(x) &= F(x|\mathcal{O}_{\text{SR}})\mathcal{P}_{\text{SR}} + F(x|\overline{\mathcal{O}_{\text{SR}}})\overline{\mathcal{P}_{\text{SR}}} \\ &= F_{\gamma_{\text{SD}}}(x)\mathcal{P}_{\text{SR}} + F_{(\text{S,R})\to\text{D}}(x)\overline{\mathcal{P}_{\text{SR}}}. \end{aligned} \tag{4.39}$$

By substituting (4.27), (4.28) and (4.30) in (4.39) we get $F_{\gamma_{\text{e2e}}}(x)$ for SDF-FDR.

As shown in the last section, both SDF-FDR and ISDF-FDR yield the same outage performance. However, as shown in this section, SDF-FDR has a higher end-to-end SNR profile when compared to ISDF-FDR due to the more relay cooperation SDF-FDR offers. To motivate their inherent performance difference in light of the above, consider the following illustrative variable-rate scenario where the end-to-end communication has R as a lower acceptable rate limit below which an outage is defined and declared. However, when the channel is not in outage with respect to this lower limit, the source is now allowed to freely increase its rate to only approach the verge of outage without falling into it. In this scenario, it is clear that the outage performance will remain the same for both SDF-FDR and ISDF-FDR since the outage threshold is exactly the same. However, it also becomes clear that the protocol which offers a higher end-to-end SNR profile will attain higher rates. Thus, as it will be shown in the subsequent numerical evaluations, ISDF-FDR offers additional power savings when compared to SDF-FDR while maintaining the same outage performance at the only expense of a one-bit feedback provided that a fixed-rate transmission is adopted. When variable-rate transmission is allowed, assuming channel state information is provided to the transmitters, this power saving can come at an additional expense of a lower end-to-end throughput.

4.5.3 SDF/ISDF-FDR SNR Performance Comparison

CDF

In Fig. 4.2, we compare the empirical CDF of the end-to-end SNR with that obtained from the derived expressions for three schemes; namely, (i) DT, (ii) ISDF and (iii) SDF. As depicted in Fig. 4.2, the CDF of ISDF lies between DT and SDF, and the degree of proximity from either DT or SDF performance is found to depend on the average direct link gain. Specifically, as the direct link gain increases, the ISDF performance gets closer to that of DT due to limited cooperation as in Fig. 4.2a. This happens for the reason that ISDF does not activate the relay for cooperation as long as the destination can retrieve the source message by solely relying on the direct link. On the other hand, as the direct link gain becomes weaker, the performance of ISDF approaches that of SDF due to the unreliability of the direct link as for instance in Fig. 4.2b. This is due to the fact that the destination cannot decode from the source directly, leading to always triggering the relay to cooperate whenever it can decode, which is basically what SDF does. We can also notice that the curves of SDF and ISDF overlap till reaching $\eta = 10\log_{10}(2^{R(L+D)/L} - 1)$ dB. This confirms what was reached earlier in the outage analysis section that both protocols yield the same outage performance. In Fig. 4.2a, we kept $m_{\mathrm{SD}} = 1$ which is reasonable for the direct $\mathrm{S} - \mathrm{D}$ link, while evaluating the performance for $m_{\mathrm{SR}} = m_{\mathrm{RR}} = m_{\mathrm{RD}} = m \in \{1, 3\}$. We can notice that as m increases, the SNR probability distribution shifts to higher values indicating an improvement in performance. However, in contrast to increasing either m_{SR} or m_{SD}, which naturally boosts the performance due to decreasing the severity of fading over the multi-hop path, one would expect that increasing m_{RR} should cause a performance degradation due to the introduction of LoS effects to the RSI component. We study this effect in particular in Fig. 4.2b by fixing $m_{\mathrm{SR}} = m_{\mathrm{SD}} = m_{\mathrm{RD}} = 1$ and plotting for $m_{\mathrm{RR}} \in \{1, 4\}$. We found that the effect of increasing m_{RR} for the same set of average channel gains in Fig. 4.2a could not be distinguished. In order to distinguish the said effect, we had to significantly

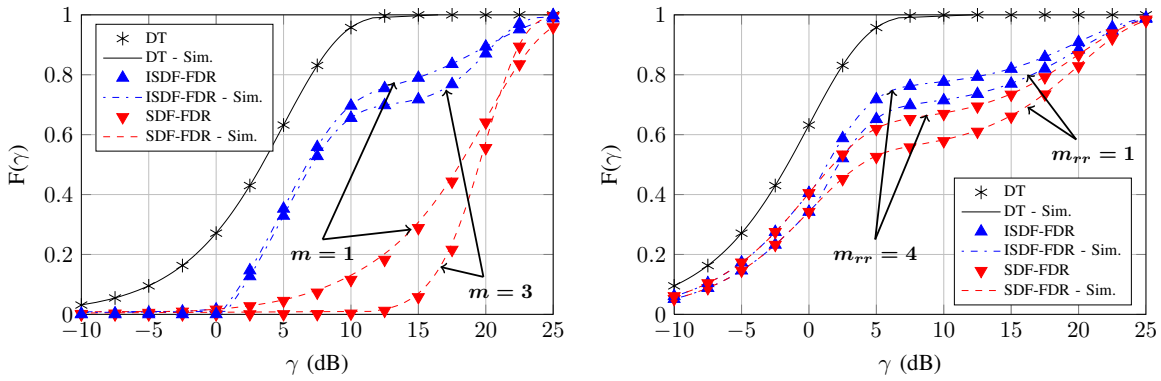

(a) $\pi_{\mathrm{SD}} = 5$ dB, $\pi_{\mathrm{RD}} = \pi_{\mathrm{SR}} = 20$ dB, $\pi_{\mathrm{RR}} = 6$ dB, $m_{\mathrm{SD}} = 1$, $m_{\mathrm{SR}} = m_{\mathrm{RR}} = m_{\mathrm{RD}} = m \in \{1, 3\}$ and $R = 1$ bpcu.

(b) $\pi_{\mathrm{SD}} = 0$ dB, $\pi_{\mathrm{SR}} = \pi_{\mathrm{RR}} = \pi_{\mathrm{RD}} = 20$ dB, $m_{\mathrm{SD}} = m_{\mathrm{SR}} = m_{\mathrm{RD}} = 1$, $m_{\mathrm{RR}} \in \{1, 4\}$ and $R = 1$ bpcu.

Figure 4.2: CDF of the end-to-end SNR.

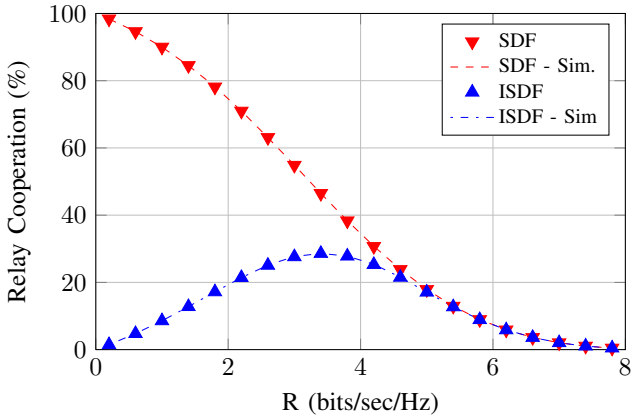

Figure 4.3: Percentage of relay cooperation/power expenditure, for $\pi_{\mathrm{SD}} = 10$ dB, $\pi_{\mathrm{SR}} = \pi_{\mathrm{RD}} = 20$ dB, $\pi_{\mathrm{RR}} = 10$ dB and $m_{\mathrm{SR}} = m_{\mathrm{RR}} = m_{\mathrm{RD}} = m_{\mathrm{SD}} = 1$.

magnify the effect of the RSI channel on the end-to-end performance as shown in Fig. 4.2b by simultaneously decreasing the direct link gain to $\pi_{\mathrm{SD}} = 0$ dB and considerably increasing the RSI link gain to $\pi_{\mathrm{RR}} = 20$ dB. From the shown results, we conclude that the impact of m_{RR} can be negligible as long as π_{RR} has a reasonable value that is well below π_{SR}.

Relative Relay Power Expenditure

In Fig. 4.3, we plot the percentage of relay power expenditure/relay cooperation obtained via simulation for the SDF-FDR/ISDF-FDR protocols. We also compare them with their theoretic values of $(1 - \mathcal{P}_{\mathrm{SR}}) \times 100$ % and $(1 - \mathcal{P}_{\mathrm{SR}})\mathcal{P}_{\mathrm{SD}} \times 100$ % for SDF and ISDF,

respectively. As observed from the figure, relay power expenditure in SDF steadily decreases with the increase in the attempted source rate. The reason is that, as the source increases its information rate, the relay ability of properly decoding the source message decreases since $\mathrm{S}-\mathrm{R}$ link outage occurs more frequently. Thus, less cooperation takes place as the rate increases, and hence, the destination gradually proceeds towards relying more on direct source transmissions. On the other hand, ISDF gives a different performance trend, in which the expended relay power increases starting from zero. After some point, it starts its decreasing trend and meets that of SDF until both reach zero power again at high rates. This is due to the fact that, at very low rates, the destination can anyway decode when solely receiving via the direct link. As the rate increases, the direct link starts to fail more frequently, thereby activating the relay cooperation when no outage occurs in the $\mathrm{S}-\mathrm{R}$ link. As we further increase the rate, outage in the $\mathrm{S}-\mathrm{R}$ link takes place with higher probability and the relay becomes unable to assist regardless of the direct link's outage state.

In summary, in Fig. 4.3, there exists at lower rates a non-negligible probability that the $\mathrm{S}-\mathrm{D}$ link does not fall into outage, i.e., $1-\mathcal{P}_{\mathrm{SD}}$ has a non-negligible value. Hence, relay cooperation is less needed which favors ISDF over SDF since it yields the same outage performance at a lower power consumption. This clearly comes at the expense of a lower SNR profile in the no-outage events for ISDF when compared to SDF, and consequently a lower capacity if a variable rate transmission was allowed. For high rates, the direct link falls into outage with very high probability, i.e., $\mathcal{P}_{\mathrm{SD}} \approx 1$. Hence, the relay assists in both protocols whenever it can successfully decode, yielding similar performance for SDF and ISDF as shown.

4.6 Diversity Analysis of SDF-FDR

Under Rayleigh fading, and for $P_{\mathrm{S}} = P_{\mathrm{R}} = P$, the outage probability is approximately given as

$$\mathcal{P}_{\text{out}} \approx 1 - \exp(-\frac{\eta}{P\pi_{\mathrm{SD}}}) - \frac{\exp\left(-\frac{\eta}{P\pi_{\mathrm{SR}}}\right)}{\left(1+\eta\frac{\pi_{\mathrm{RR}}}{\pi_{\mathrm{SR}}}P^{\delta-1}\right)} \frac{\overbrace{\left(\exp\left(-\frac{\eta}{P\pi_{\mathrm{RD}}}\right) - \exp\left(-\frac{\eta}{P\pi_{\mathrm{SD}}}\right)\right)}^{\mathcal{A}(P)}}{\left(1-\frac{\pi_{\mathrm{SD}}}{\pi_{\mathrm{RD}}}\right)}. \tag{4.40}$$

It can be easily shown that $\mathcal{A}(P)$ is always positive since the numerator and denominator change their sign simultaneously around the point $\pi_{\mathrm{SD}} = \pi_{\mathrm{RD}}$. It can be noticed that $1 - \exp(-\frac{\eta}{P\pi_{\mathrm{SD}}})$ and $\mathcal{A}(P)$ vanish as P increases for nonzero direct link gain, leading to a vanishing $\mathcal{P}_{\text{out}}$ as $P \to \infty$. Thus, it is guaranteed that SDF-FDR has a nonzero diversity order, which gets around the error floor phenomenon in MHDF-FDR even in the presence of self-interference. Now, we quantify the exact diversity order of the SDF-FDR protocol. As P increases, we can well-approximate $1 - \exp(-\frac{x}{P})$ as $\frac{x}{P}$. Hence,

$$\begin{aligned}
\mathcal{D} &= \lim_{P\to\infty} -\frac{\log\left(\frac{\eta}{P\pi_{\mathrm{SD}}} - \frac{1-\frac{\eta}{P\pi_{\mathrm{SR}}}}{\left(1+\eta\frac{\pi_{\mathrm{RR}}}{\pi_{\mathrm{SR}}}P^{\delta-1}\right)}\frac{\frac{\eta}{P\pi_{\mathrm{SD}}}-\frac{\eta}{P\pi_{\mathrm{RD}}}}{1-\frac{\pi_{\mathrm{SD}}}{\pi_{\mathrm{RD}}}}\right)}{\log(P)} \\
&= \lim_{P\to\infty} -\frac{\log\left(\frac{\eta}{P\pi_{\mathrm{SD}}}\left(\frac{\eta+\eta\pi_{\mathrm{RR}}P^{\delta}}{P\pi_{\mathrm{SR}}+\eta\pi_{\mathrm{RR}}P^{\delta}}\right)\right)}{\log(P)},
\end{aligned} \tag{4.41}$$

where $\mathcal{A}(P) \approx \frac{\frac{\eta}{P\pi_{\mathrm{SD}}}-\frac{\eta}{P\pi_{\mathrm{RD}}}}{1-\frac{\pi_{\mathrm{SD}}}{\pi_{\mathrm{RD}}}} = \frac{\eta}{P\pi_{\mathrm{SD}}}$. Hence,

$$\mathcal{D} = 1 + \lim_{P\to\infty} \frac{\log\left(P\pi_{\mathrm{SR}} + \eta\pi_{\mathrm{RR}}P^{\delta}\right) - \log\left(\eta + \eta\pi_{\mathrm{RR}}P^{\delta}\right)}{\log(P)} \tag{4.42}$$

$$= 1 + \lim_{P\to\infty} \frac{\log(P) - \log\left(P^{\delta}\right)}{\log(P)} = 2 - \delta. \tag{4.43}$$

It is thereby shown that the SDF-FDR protocol can at least maintain a unity diversity order even in the presence of a self-interference link with a gain that scales linearly with the relay

power, while it can achieve a diversity of order 2 when the self-interference vanishes (or has a constant mean value that does not grow with the relay power). Hence, as in the other FDR protocols, the diversity also depends on the quality of the adopted loopback isolation and cancellation techniques.

4.7 Hybrid MHDF-FDR/DT

In this section, we also study a hybrid scheme that switches between the simple MHDF-FDR and DT. Specifically, as long as the direct link is not in outage, the system resorts to DT. Otherwise, MHDF-FDR is adopted. In essence, this system is similar to ISDF-FDR in that it favors DT as long as the direct link is outage-free. However, its performance is worse when outage occurs in the direct link since the direct link is treated as interference instead of being utilized.

4.7.1 Outage Performance

The outage probability is given as

$$\mathcal{P}_{\text{out}} \;=\; \mathcal{P}_{\text{SD}}\,(1-\overline{\mathcal{P}_{\text{SR}}}\;\overline{\mathcal{P}'_{\text{RD}}}), \tag{4.44}$$

where $\mathcal{P}'_{\text{RD}}=1-\overline{\mathcal{P}'_{\text{RD}}}$ is the outage probability in the $\text{R}-\text{D}$ link with direct link treated as interference conditioned on $\text{S}-\text{D}$ link outage. It is shown in Appendix 8.A that it is given under Rayleigh fading by

$$\mathcal{P}'_{\text{RD}} \;=\; 1-\frac{e^{-\frac{\eta}{P_{\text{R}}\pi_{\text{RD}}}}\left(1-e^{-\eta\left(\frac{\eta}{P_{\text{R}}\pi_{\text{RD}}}+\frac{1}{P_{\text{S}}\pi_{\text{SD}}}\right)}\right)}{P_{\text{S}}\pi_{\text{SD}}\left(\frac{\eta}{P_{\text{R}}\pi_{\text{RD}}}+\frac{1}{P_{\text{S}}\pi_{\text{SD}}}\right)\left(1-e^{-\frac{\eta}{P_{\text{S}}\pi_{\text{SD}}}}\right)}. \tag{4.45}$$

Hence, substituting (3.11), (4.24), and (4.45) in (4.44), the end-to-end outage probability of the hybrid MHDF-FDR/DT is given as

$$\mathcal{P}_{\text{out}} = 1 - e^{-\frac{\eta}{P_{\text{S}}\pi_{\text{SD}}}} - \frac{e^{-\eta\left(\frac{1}{P_{\text{S}}\pi_{\text{SR}}}+\frac{1}{P_{\text{R}}\pi_{\text{RD}}}\right)}\left(1 - e^{-\eta\left(\frac{\eta}{P_{\text{R}}\pi_{\text{RD}}}+\frac{1}{P_{\text{S}}\pi_{\text{SD}}}\right)}\right)}{\left(1+\eta\frac{P_{\text{R}}^{\delta}\pi_{\text{RR}}}{P_{\text{S}}\pi_{\text{SR}}}\right)\left(1+\eta\frac{P_{\text{S}}\pi_{\text{SD}}}{P_{\text{R}}\pi_{\text{RD}}}\right)}. \tag{4.46}$$

4.7.2 Diversity Analysis

First, we set $P_{\text{S}} = P_{\text{R}} = P$. As P increases, $1-e^{-\eta\left(\frac{\eta}{P\pi_{\text{RD}}}+\frac{1}{P\pi_{\text{SD}}}\right)}$ approaches $\eta\left(\frac{\eta}{P\pi_{\text{RD}}}+\frac{1}{P\pi_{\text{SD}}}\right)$. Knowing that $\frac{\eta\left(\frac{\eta}{P\pi_{\text{RD}}}+\frac{1}{P\pi_{\text{SD}}}\right)}{1+\eta\frac{P_{\text{S}}\pi_{\text{SD}}}{P_{\text{R}}\pi_{\text{RD}}}} = \frac{\eta}{P_{\text{S}}\pi_{\text{SD}}}$, and using the approximation $1-\exp(-\frac{x}{P}) \approx \frac{x}{P}$ as P increases, the diversity order is given by

$$\begin{aligned}
\mathcal{D} &= \lim_{P\to\infty} -\frac{\log\left(aP^{-1} - \frac{\left(1-bP^{-1}\right)aP^{-1}}{1+cP^{\delta-1}}\right)}{\log(P)} && (4.47)\\
&= \lim_{P\to\infty} -\frac{\log\left(aP^{-1}\left(\frac{cP^{\delta-1}+bP^{-1}}{1+cP^{\delta-1}}\right)\right)}{\log(P)} && (4.48)\\
&= \lim_{P\to\infty} -\frac{\log\left(aP^{-1}\right)+\log\left(cP^{\delta-1}+bP^{-1}\right)-\log\left(1+cP^{\delta-1}\right)}{\log(P)} && (4.49)\\
&= 2-\delta, && (4.50)
\end{aligned}$$

where $a = \frac{\eta}{\pi_{\text{SD}}}$, $b = \eta\left(\frac{1}{\pi_{\text{SR}}}+\frac{1}{\pi_{\text{RD}}}\right)$, and $c = \eta\frac{\pi_{\text{RR}}}{\pi_{\text{SR}}}$. The previous result shows that a hybrid scheme that opportunistically switches between MHDF-FDR and DT achieves the same diversity order of the proposed selective relaying protocols. However, SDF-FDR still offers better outage performance due to the reasons explained earlier. This results emphasizes the message that selectivity between cooperation and direct transmission is crucial in FDR systems.

4.8 Summary

4.8.1 A Summary of Protocols

Here, we summarize the protocols considered for comparison in the next section. We take DT as a baseline with rate R bpcu. The protocols are classified under three main categories; namely, 1) multi-hop protocols in which the desired information is only distilled from the multi-hop path while the direct link is neglected/treated as interference, 2) combining protocols where both the multi-hop and direct paths are non-selectively combined, and finally, 3) selective relaying protocols in which combining is applied only when the relay performs successful decoding, while the direct link is solely leveraged otherwise. We start by specifying the HDR protocols and their inherent differences in the following progressive way.

HDR Protocols

a) MHDF-HDR: Direct source transmissions are totally ignored. An outage is declared unless the $\mathrm{S}-\mathrm{R}$ and $\mathrm{R}-\mathrm{D}$ links are simultaneously outage-free.

b) MRC-HDR [45]: It allows *combining* of the direct signal with that arriving via the multi-hop path. Yet, combining might still cause undesirable loss of performance due to the occasional interference from the multi-hop path when an outage occurs in the $\mathrm{S}-\mathrm{R}$ link. The end-to-end SNR is given in [45, 34] by $\min\{\gamma_{\mathrm{SR}}, \gamma_{\mathrm{RD}}+\gamma_{\mathrm{SD}}\}$, which can be easily shown to yield the outage probability in Table 4.1.

c) SDF-HDR [45, 40]: It overcomes the performance limitation in MRC-HDR by allowing the relay to forward only when the $\mathrm{S}-\mathrm{R}$ link is not in outage, thereby improving the combining step. However, when the relay does not forward, about half of the time becomes unutilized due to the orthogonal nature of source/relay transmissions. The expression in Table 4.1 follows from [45], taking power normalization into account.

Due to the rate penalty of 1/2 which all the previous HDR protocols suffer, the trans-

mitters need to signal with a rate of $2R$ to maintain the same rate adopted by the DT baseline.

d) IDF-HDR [45, 40]: To solve the under-utilization problem in SDF-HDR, the source continues its transmission over the previously dedicated time for relay forwarding as long as the $\mathrm{S}-\mathrm{D}$ link is not in outage. Hence, IDF-HDR is a hybrid scheme that switches between DT and HDR based on the $\mathrm{S}-\mathrm{D}$ link outage state. In [45], the source transmits with a constant rate, R_{I}, regardless of the $\mathrm{S}-\mathrm{D}$ link state. The effective rate with rate penalties taken into account is equal to $R_{\mathrm{I}} \times 1 \times (1-\mathcal{P}_{\mathrm{SD}}) + R_{\mathrm{I}} \times \frac{1}{2} \times \mathcal{P}_{\mathrm{SD}}$, with $\mathcal{P}_{\mathrm{SD}}$ now calculated for the source rate R_{I}. Taking DT as a baseline, this should be equal to R. Hence, R_{I} can be calculated by numerically solving the nonlinear equation:

$$R_{\mathrm{I}}: \quad \left(1 - F_X\left(2^{R_{\mathrm{I}}} - 1; m_{\mathrm{SD}}, \theta_{\mathrm{SD}}\right)/2\right) R_{\mathrm{I}} = R. \tag{4.51}$$

It is clear that $R \leq R_{\mathrm{I}} \leq 2R$ with the lower and upper limits attained at zero and almost sure direct link outage, respectively.

Next, we discuss the FDR protocols.

FDR Protocols

Although FDR versions of the above-listed protocols now exist, their effect on the performance is quite different due to two main reasons; the non-orthogonal source/relay transmission in FDR, and the RSI link that affects the first hop.

e) MHDF-FDR [36, 34, 35, 42]: The multi-hop approach in FDR now imposes undesirable source interference at the destination via the direct link. This comes in addition to the inherent drawback of FDR where a higher outage probability is incurred in the multi-hop path due to the RSI affecting the $\mathrm{S}-\mathrm{R}$ link. Except for the small delay between source/relay transmissions to maintain causality, MHDF-FDR does not incur a rate penalty in comparison to DT due to its instantaneous decoding at the destination.

f) BMSC-FDR [40, 43]: Among fixed DF protocols, BMSC [51] attains the best known achievable rates. However, due to its non-selective relaying nature, it falls to some degree under the category of combining protocols which suffer from undesirable loss of performance due to possibly superimposing mere interference from the multi-hop path when $\mathrm{S}-\mathrm{R}$ link outage occurs. Also, since BMSC-FDR adopts a block transmission scheme, it incurs a rate penalty of $1/(L+1)$.

g) SDF-FDR/ISDF-FDR: SDF does not suffer from resource under-utilization anymore since the source almost transmits all the time for large L/D, yet its selective nature in the $\mathrm{S}-\mathrm{R}$ link alleviates the RSI adverse effect on the end-to-end performance. Nonetheless, we modify its rate to $R(L+D)/L$ to account for the rate penalty it incurs due to the delay in block transmission. It is worth mentioning that the simple repetition-based selective cooperation protocols considered herein are only meant to show the effect of selective relaying on the end-to-end performance. Selective cooperation versions of higher rate protocols such as BMSC can be still adopted where it is straightforward to expect their superior performance to their non-selective versions.

h) Hybrid MHDF-FDR/DT: This protocol gets around the error floor problem in MHDF-FDR by switching to DT whenever the direct link is outage free. SDF-FDR, however, still offers better error performance due to jointly leveraging the $\mathrm{S}-\mathrm{D}$ and $\mathrm{R}-\mathrm{D}$ links in the second hop when the $\mathrm{S}-\mathrm{R}$ link is outage-free.

4.8.2 A Summary of Results

The considered protocols and their end-to-end outage probability are summarized in Table 4.1, with $\eta_{\mathrm{I}}=2^{R_{\mathrm{I}}}-1$ and $\acute{\eta}=2^{\frac{L+D}{L}R}-1$.

Mode	Protocol	Rate	Theoretic Outage Probability	Diversity
DT		R	$F_X\left(\eta; m_{\mathrm{SD}}, P_{\mathrm{S}}\theta_{\mathrm{SD}}\right)$	1
HDR	MHDF	$2R$	$1-\overline{F_X}\left(\eta_{\mathrm{HD}}; m_{\mathrm{SR}}, P_{\mathrm{S}}\theta_{\mathrm{SR}}\right)\overline{F_X}\left(\eta_{\mathrm{HD}}; m_{\mathrm{RD}}, P_{\mathrm{R}}\theta_{\mathrm{RD}}\right)$	1
	MRC	$2R$	$1-\overline{F_X}\left(\eta_{\mathrm{HD}}; m_{\mathrm{SR}}, P_{\mathrm{S}}\theta_{\mathrm{SR}}\right)\overline{F_S}\left(\eta_{\mathrm{HD}}; \boldsymbol{p}_2\right)$	1
	SDF	$2R$	$F_X\left(\eta_{\mathrm{HD}}; m_{\mathrm{SR}}, P_{\mathrm{S}}\theta_{\mathrm{SR}}\right)F_X\left(\eta_{\mathrm{HD}}; m_{\mathrm{SD}}, P_{\mathrm{S}}\theta_{\mathrm{SD}}\right)$ $+\overline{F_X}\left(\eta_{\mathrm{HD}}; m_{\mathrm{SR}}, P_{\mathrm{S}}\theta_{\mathrm{SR}}\right)F_S\left(\eta_{\mathrm{HD}}; \boldsymbol{p}_2\right)$	2
	IDF	R_{I} (4.51)	$F_X\left(\eta_{\mathrm{I}}; m_{\mathrm{SR}}, P_{\mathrm{S}}\theta_{\mathrm{SR}}\right)F_X\left(\eta_{\mathrm{I}}; m_{\mathrm{SD}}, P_{\mathrm{S}}\theta_{\mathrm{SD}}\right)$ $+\overline{F_X}\left(\eta_{\mathrm{I}}; m_{\mathrm{SR}}, P_{\mathrm{S}}\theta_{\mathrm{SR}}\right)F_S\left(\eta_{\mathrm{I}}; \boldsymbol{p}_2\right)$	2
FDR	MHDF	R	$1-\overline{F_Z}\left(\eta; \boldsymbol{p}_1\right)\overline{F_Z}\left(\eta; \boldsymbol{p}_2\right)$	$\begin{cases}1-\delta, & \text{if } \pi_{\mathrm{SD}}=0,\\ 0, & \text{if } \pi_{\mathrm{SD}}\neq 0\end{cases}$
	BMSC	$\frac{L+1}{L}R$	Eq. 3.30 with the optimization of ρ [43]	$1-\delta$
	SDF	$\frac{L+D}{L}R$	$F_Z\left(\acute{\eta}; \boldsymbol{p}_1\right)F_X\left(\acute{\eta}; m_{\mathrm{SD}}, P_{\mathrm{S}}\theta_{\mathrm{SD}}\right)+\overline{F_Z}\left(\acute{\eta}; \boldsymbol{p}_1\right)F_S\left(\acute{\eta}; \boldsymbol{p}_2\right)$	$2-\delta$

Table 4.1: A summary of theoretic outage probability and diversity order for the different protocols under consideration.

4.9 Numerical Evaluation

4.9.1 Simulation Setup

We generate 10^7 sets of channel realizations according to the channel model described in previous sections for $L = 20$ blocks per super-block and $D = 2$ blocks, i.e., $k = \frac{L}{D} = 10$. In each set of channel realizations, we exactly calculate $C_{(\mathrm{S,R})\to\mathrm{D}}$ for SDF-FDR/ISDF-FDR as given in (4.10) without undergoing any approximations. We define the effective end-to-end SNR per symbol in the equivalent single-antenna channel as

$$\gamma_{\mathrm{eff}} = 2^{\frac{C_{(\mathrm{S,R})\to\mathrm{D}}}{BL}} - 1. \tag{4.52}$$

This comes from the equivalence we mentioned earlier between the actual virtual MISO channel and another point-to-point single-antenna channel that can be carefully explained as follows. In the virtual MISO channel, noting that $C_{(\mathrm{S,R})\to\mathrm{D}}$ denotes the exact mutual information per super-block, the mutual information per symbol time can be clearly obtained as $\frac{1}{B(L+D)}C_{(\mathrm{S,R})\to\mathrm{D}}$ since the transmission of L codewords actually spans $L + D$ blocks. On the other hand, a prelog factor of $\frac{BL}{B(L+D)}$ is accordingly introduced in the equivalent single-

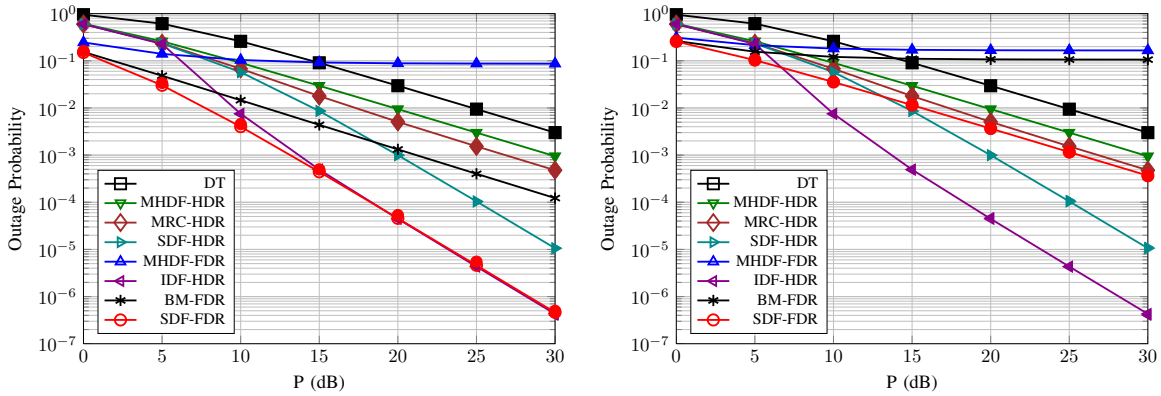

(a) No loopback interference link ($\pi_{\mathrm{RR}} = 0$) and large k.

(b) $\pi_{\mathrm{RR}} = 0$ dB, and linearly scaling with P ($\delta = 1$).

Figure 4.4: Outage prob. vs. $P_{\mathrm{S}} = P_{\mathrm{R}} = P$, for $\pi_{\mathrm{SR}} = \pi_{\mathrm{RD}} = 15$ dB, $\pi_{\mathrm{SD}} = 0$ dB, $m_{\mathrm{SR}} = m_{\mathrm{RD}} = m_{\mathrm{RR}} = m_{\mathrm{SD}} = 1$ and $R = 2$ bpcu.

antenna channel due to the inactivity of the source over the last D blocks, and hence the mutual information per symbol time is given in terms of γ_{eff} as $\frac{L}{L+D}\log_2(1+\gamma_{\mathrm{eff}})$. Thus,

$$\frac{1}{B(L+D)}C_{(\mathrm{S,R})\to\mathrm{D}} \quad = \quad \frac{BL}{B(L+D)}\log_2(1+\gamma_{\mathrm{eff}}),$$

which yields the expression in (4.52). We compare the empirical probability distribution of this γ_{eff} with those theoretical results obtained in previous sections. For all the figures we present, we include all used simulation parameters in their caption.

In the following figures, we compare the relative outage performance of the FDR and HDR protocols summarized in the previous section. Connected lines with unfilled plot marks of different shapes are dedicated to the theoretic outage probability for each of the protocols, while filled marks of the same respective shape represent the values obtained via simulations. Thus, an appropriately filled mark reflects the quality of matching between theoretical and simulation results. Also, since SDF-FDR and ISDF-FDR yield the same outage performance, we only plot one curve for both to which we refer as SDF-FDR.

4.9.2 Diversity Order: Outage vs. Transmit SNR

In Fig. 4.4, we plot the outage probability versus the transmit SNR level at the source and the relay, with both set to P, in order to evaluate the diversity order of the different schemes. In Fig. 4.4a, we neglect the RSI link for all FDR schemes. As shown, even in the absence of the loopback interference, the MHDF-FDR scheme suffers an error floor as discussed earlier due to the existence of a nonzero direct link gain. The non-selective HDR schemes, MHDF-HDR and MRC-HDR, in addition to the BMSC-FDR scheme have the same slope of the DT scheme indicating a unity diversity order. This is due to the fact that the three previous schemes have the $\mathrm{S}-\mathrm{R}$ link as a single-point of failure. When only the $\mathrm{S}-\mathrm{R}$ link goes into outage, all these three schemes drop into outage as can be noticed from their analytical expressions. On the other hand, the incremental/selective HDR and FDR schemes all enjoy a diversity of order 2. This agrees with the diversity results noted earlier, where the multi-hop and direct paths should both fall into outage for an end-to-end outage to occur. It can be seen also that SDF-FDR/ISDF-FDR further outperform the selective/incremental HDR at low-to-moderate (practical) transmit power values.

In Fig. 4.4b, we account for the loopback interference link whose gain scales linearly with the relay transmit power. We can notice that the diversity order of the full-duplex schemes drops by 1, i.e., BMSC-FDR experiences an error floor while the SDF-FDR/ISDF-FDR schemes have a unity diversity order which agrees with the results noted earlier. However, as discussed earlier, the performance of the FDR schemes can be significantly enhanced if the loopback interference isolation and cancellation techniques can control its growth to be rather *sublinear* with an exponent $0 < \delta < 1$, i.e., scales with P^{δ}. In this case, the diversity order of the SDF-FDR/ISDF-FDR schemes becomes equal to $2 - \delta$. Even in this case of linearly scaling loopback interference link, the FDR schemes can still offer better performance than that offered by the HDR schemes at practical transmit power values as shown in previous figures.

4.9.3 Outage vs. Rate

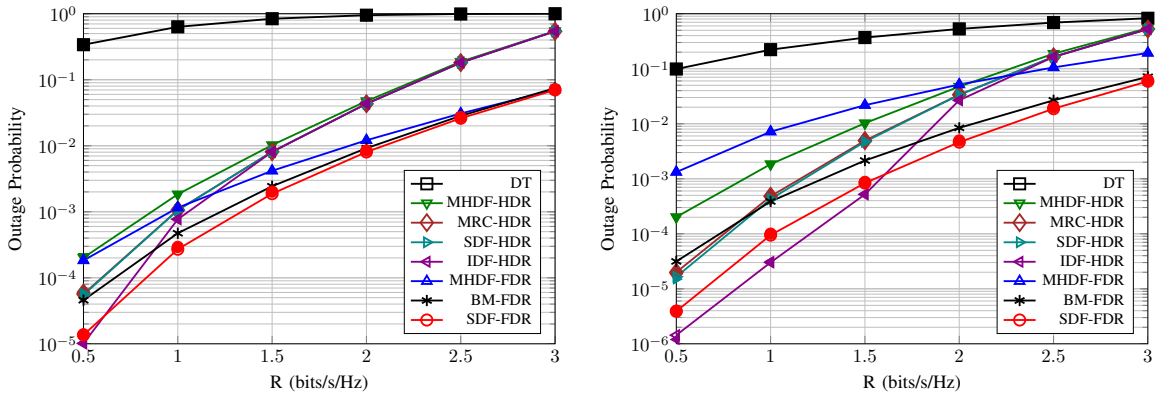

(a) $\pi_{\mathrm{SD}} = 0$ dB (b) $\pi_{\mathrm{SD}} = 6$ dB

Figure 4.5: Outage probability vs. rate, for $\pi_{\mathrm{SR}} = \pi_{\mathrm{RD}} = 20$ dB, $\pi_{\mathrm{RR}} = 3$ dB, $m_{\mathrm{SR}} = 3$, $m_{\mathrm{RR}} = m_{\mathrm{RD}} = 2$, and $m_{\mathrm{SD}} = 1$.

In Fig. 4.5, we plot the outage performance versus the source rate of the DT baseline, denoted by R, which also represents the attempted level of spectral efficiency. As shown in Fig. 4.5a, SDF-FDR indeed offers better outage performance than all existing schemes for reasonable RSI levels and low direct link gains. As the direct link gain increases, we start to notice in Fig. 4.5b that the performance of IDF-HDR is enhanced. This is due to the fact that its rate/spectral efficiency is significantly enhanced and approaches that of DT as the direct link outage probability decreases, yet it does not suffer from any RSI in the events of direct link outage. Thus, its performance curve shifts down as well as to the right as we increase the direct link gain, and we find that IDF-HDR becomes more desirable for low attempted rates while SDF-FDR remains of better performance for higher rates.

4.9.4 Outage vs. RSI Link Gain

We further clarify the aforementioned observation from a different perspective in Fig. 4.6, where we plot the outage probability versus π_{RR}. It can be easily expected that the performance of all HDR protocols remains unchanged as no simultaneous source/relay transmission occurs, while that of FDR protocols suffers gradual deterioration and intersects with the dif-

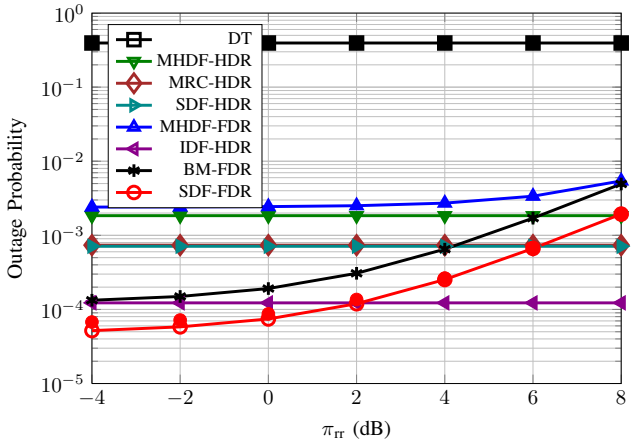

Figure 4.6: Outage prob. vs. π_{RR}, for $\pi_{\mathrm{SR}} = \pi_{\mathrm{RD}} = 20$ dB, $\pi_{\mathrm{SD}} = 3$ dB, $m_{\mathrm{SR}} = 3$, $m_{\mathrm{RR}} = m_{\mathrm{RD}} = 2$, $m_{\mathrm{SD}} = 1$ and $R = 1$ bpcu.

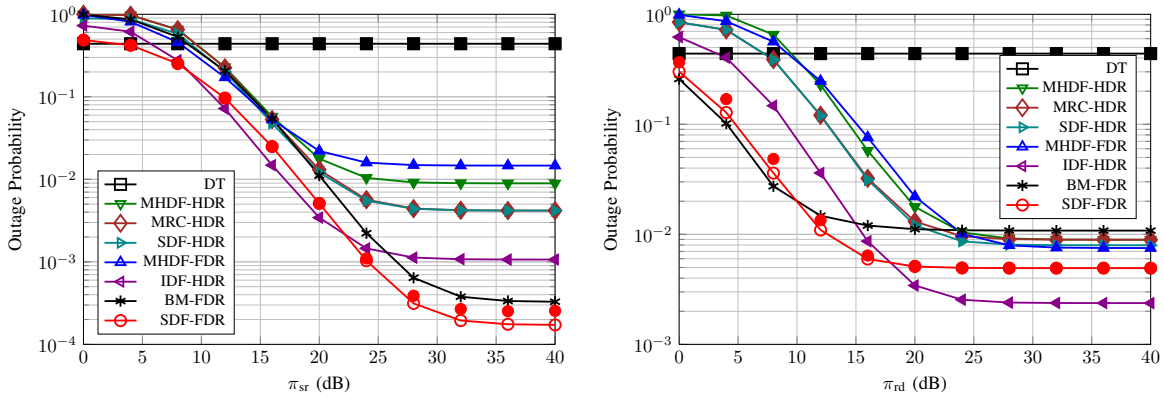

(a) $\pi_{\mathrm{RD}} = 20$ dB (b) $\pi_{\mathrm{SR}} = 20$ dB

Figure 4.7: Outage prob. vs. π_{SR} and π_{RD}, for $\pi_{\mathrm{RR}} = 3$ dB, $\pi_{\mathrm{SD}} = 5$ dB, $m_{\mathrm{SR}} = m_{\mathrm{RD}} = 2$, $m_{\mathrm{RR}} = m_{\mathrm{SD}} = 1$ and $R = 1.5$ bpcu.

ferent HDR protocols at different π_{RR} levels for any given set of channel parameters. This is obviously caused by the deterioration of the multi-hop path due to the increased level of self-interference.

4.9.5 Outage vs. First and Second Hop Gains

In Fig. 4.7a and Fig. 4.7b, the outage probability is plotted versus π_{SR} and π_{RD}, respectively. The general trend is as shown where the performance is enhanced till reaching the bottleneck of the multi-hop path defined by the other hop, set to 20 dB in both figures. We noticed however that the relative performance of the incremental/selective HDR and FDR schemes

heavily depends on the direct link gain and the targeted spectral efficiency level as previously discussed in Fig. 4.5. Specifically, the IDF-HDR scheme is significantly improved as the direct link gain increases since its rate R_{I} approaches that of the DT. It is also improved as the the spectral efficiency level, R, decreases. On the other hand, the SDF-FDR/ISDF-FDR scheme offer superior performance as the spectral efficiency level decreases.

4.10 Concluding Remarks

- When comparing the outage performance of HDR protocols, we can easily notice as expected that MRC-HDR uniformly dominates MHDF-HDR owing to leveraging the redundant information that arrives via the direct path. Further, SDF-HDR by its turn also uniformly dominates MRC-HDR since it still enjoys the benefits of signal combining, yet it further eliminates unnecessary interference components from the combining stage when the $\mathrm{S}-\mathrm{R}$ link falls into an outage state. IDF-HDR offers further performance enhancements by simultaneously eliminating the resource under-utilization in SDF-HDR and adjusting its source rate to meet the same level of attempted information rate. Since R_{I} is upper bounded by $2R$, IDF-HDR replaces η_{HD} in the outage expression of SDF-HDR by $\eta_{\mathrm{I}} \leq \eta_{\mathrm{HD}}$, and hence, it yields lower outage probability. Indeed, it is worth mentioning that besides the rate adjustment which IDF-HDR offers, it simultaneously captures the gain of selective relaying in SDF-HDR too. This is due to the fact that, due to the incremental nature of IDF-HDR, an event where the multi-hop path disturbs a possibly outage-free direct path can never occur.

- On the other hand, FDR protocols demand about half the source rate of their HDR counterparts to communicate the same amount of information, which should yield a lower outage probability in ideal conditions. Nonetheless, RSI jumps into the picture as an additional challenge that draws the $\mathrm{S}-\mathrm{R}$ link, and consequently the multi-hop path, into outage more frequently than its HDR counterpart. Thus, an efficient FDR

protocol is desirable in which two requirements are simultaneously attained, namely, a) mitigation of the multi-hop path adverse effect on the end-to-end performance in the event of $S-R$ link outage, and b) leveraging of the channel diversity elsewhere. From the shown results, we can notice that both requirements are not met in MHDF-FDR, only the second is met in BMSC-FDR regardless of the $S-R$ link state, while both are attained by SDF-FDR/ISDF-FDR.

- In comparing HDR and FDR protocols, the additionally introduced RSI level in FDR plays a pivotal role in determining which of the two modes might be preferable over the other, which comes in agreement with recent studies [34]. Indeed, in the absence of RSI, SDF-FDR/ISDF-FDR outperform all existing HDR and FDR protocols in terms of outage for all possible channel parameters. Yet, depending on the level of RSI, the performance of IDF-HDR gradually improves and can outperform all FDR protocols as we increase the direct link gain or by increasing the source power.

Appendix

Appendix 4.A Eigenvalues of $H^H H$

Let $\ell = kd,\ k \in \mathbb{Z}^+$, and consider a family of square matrices $\boldsymbol{A}(\alpha;\beta;\ell;d) = (\boldsymbol{a}_1, \cdots, \boldsymbol{a}_\ell)$ of the form:

$$\boldsymbol{A}(\alpha;\beta;\ell;d) \;\; = \;\; \alpha \boldsymbol{I}_\ell + \beta {\boldsymbol{B}_\ell}^d + \beta^* {\boldsymbol{F}_\ell}^d, \tag{4.53}$$

where $\alpha \in \mathbb{R}^+$, $\beta \in \mathbb{C}$, while $\boldsymbol{B}_\ell$ ($\boldsymbol{F}_\ell$) denotes a square backward (forward) shift matrix of size ℓ, with ones only on the first subdiagonal (superdiagonal) and zeros elsewhere. Consider the eigenvalue problem:

$$\boldsymbol{A}\boldsymbol{u} = \lambda \boldsymbol{u}. \tag{4.54}$$

It can be noticed that the nonzero elements of $\boldsymbol{A}$ are limited to positions on the form $(id + j, j),\ \forall\ j \in \{1, \cdots, \ell\},\ i \in \{-1, 0, 1\}$, and $1 \leq id + j \leq \ell$. This makes a column linearly dependent only on its two neighboring d-spaced columns and orthogonal on all others. Motivated by this special structure, we can split $\boldsymbol{A}$ as the sum of d matrices with orthogonal column spaces:

$$\boldsymbol{A} = \sum_{j=1}^{d} \boldsymbol{A}_j, \tag{4.55}$$

where the matrix $\boldsymbol{A}_j$ holds only k nonzero columns corresponding to the k d-spaced columns of $\boldsymbol{A}$ with shift j, i.e., $\{\boldsymbol{a}_{(i-1)d+j}\}_{i=1}^{k}$, at their respective positions, while the remaining columns are all zeros. Similarly, let us project the $\ell \times 1$ eigenvector $\boldsymbol{u} = (u[1], \cdots, u[\ell])^T$ onto d orthogonal subspaces, such that:

$$\boldsymbol{u} = \sum_{j=1}^{d} \boldsymbol{u}_j, \tag{4.56}$$

where the vector $\boldsymbol{u}_j$ holds only k nonzero elements corresponding to the k d-spaced elements of $\boldsymbol{u}$ with shift j, i.e., $\{u[(i-1)d+j]\}_{i=1}^{k}$, at their respective positions, while the remaining elements are all zeros. Thus, the eigenvalue problem can be rewritten as

$$\sum_{j=1}^{d} \boldsymbol{A}_j \sum_{j=1}^{d} \boldsymbol{u}_j = \lambda \sum_{j=1}^{d} \boldsymbol{u}_j, \tag{4.57}$$

It is clear that $\boldsymbol{u}_i$ lies in the nullspace of $\boldsymbol{A}_j \ \forall \ i \neq j$. Hence, due to orthogonality, the eigenvalue problem can be split into d eigenvalue problems:

$$\boldsymbol{A}_j \boldsymbol{u}_j = \lambda \boldsymbol{u}_j, \ \forall j \in \{1, \cdots, d\}. \tag{4.58}$$

Since the $\ell \times \ell$ $\boldsymbol{A}_j$ has zero rows and columns corresponding to the zero elements of $\boldsymbol{u}_j$, we can eliminate them and alternatively solve the reduced k-dimensional eigenvalue problem:

$$\tilde{\boldsymbol{A}}_j \tilde{\boldsymbol{u}}_j = \lambda \tilde{\boldsymbol{u}}_j, \ \forall j \in \{1, \cdots, d\}, \tag{4.59}$$

where $\tilde{\boldsymbol{A}}_j$ and $\tilde{\boldsymbol{u}}_j$ are $k \times k$ and $k \times 1$, respectively. We can easily notice that $\tilde{\boldsymbol{A}}_j = \boldsymbol{A}(\alpha; \beta; \frac{\ell}{d}, 1), \forall j \in \{1, \cdots, d\}$, which is a a tridiagonal Toeplitz matrix with known k eigenvalues as given in (4.12). Thus, $\boldsymbol{A}(\alpha; \beta; \ell, d)$ has the k eigenvalues of $\boldsymbol{A}(\alpha; \beta; k, 1)$, each with multiplicity d, i.e.,

$$\lambda_{d(i-1)+1:di} = \alpha + 2|\beta| \cos \frac{i\pi}{k+1}, \quad i \in \{1, 2, \cdots, k\}. \tag{4.60}$$

Accordingly, its determinant is that of $\boldsymbol{A}(\alpha;\beta;k,1)$ raised to the d^{th} power. For $B \in \mathbb{Z}^+$, substituting with $\ell = BL$ and $d = BD$ in (4.60) gives the expression in (4.13).

Appendix 4.B Derivation of $F(x|A_2)$

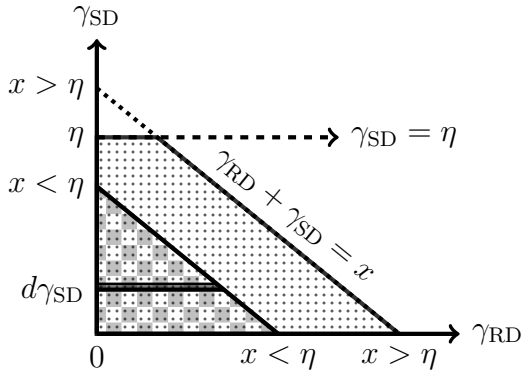

Figure 4.8: Integration regions: a) $x < \eta$ (checkerboard), b) $x > \eta$ (dotted).

Given A_2, γ_{SD} is confined to the range $0 < x < \eta$, thus having the distribution:

$$f_{\gamma_{\mathrm{SD}}}(x|A_2) = \begin{cases} \frac{f_{\gamma_{\mathrm{SD}}}(x)}{\mathcal{P}_{\mathrm{SD}}}, & 0 < x < \eta, \\ 0, & \text{elsewhere}, \end{cases} \tag{4.61}$$

while γ_{RD} remains as $\mathcal{G}\left(m_{\mathrm{RD}}, P_{\mathrm{R}}\theta_{\mathrm{RD}}\right)$ RV due to independence. Thus, with the regions of integration depicted in Fig. 4.8, the CDF of γ_{e2e} conditioned on A_2 is given by:

$$\begin{aligned} F_{\gamma_{\mathrm{e2e}}}(x|A_2) &\approx \mathbb{P}\{\gamma_{\mathrm{SD}} + \gamma_{\mathrm{RD}} < x|A_2\} \\ &= \begin{cases} F_1(x), & 0 < x < \eta, \\ F_2(x), & \eta \leq x < \infty, \end{cases} \end{aligned} \tag{4.62}$$

where

$$F_1(x) = \int_{\gamma_{\rm SD}=0}^{x} f_{\gamma_{\rm SD}}(\gamma_{\rm SD}|A_2) F_{\gamma_{\rm RD}}(x-\gamma_{\rm SD}) d\gamma_{\rm SD}, \tag{4.63}$$

$$F_2(x) = \int_{\gamma_{\rm SD}=0}^{\eta} f_{\gamma_{\rm SD}}(\gamma_{\rm SD}|A_2) F_{\gamma_{\rm RD}}(x-\gamma_{\rm SD}) d\gamma_{\rm SD}. \tag{4.64}$$

Substituting (3.4) and (4.61) in (4.63), we get

$$F_1(x) = \int_{\gamma_{\rm SD}=0}^{x} \frac{\gamma_{\rm SD}^{m_{\rm SD}-1} e^{-\frac{\gamma_{\rm SD}}{P_{\rm S}\theta_{\rm SD}}} \boldsymbol{\gamma}\left(m_{\rm RD}, \frac{x-\gamma_{\rm SD}}{P_{\rm R}\theta_{\rm RD}}\right)}{\mathcal{P}_{\rm SD}(P_{\rm S}\theta_{\rm SD})^{m_{\rm SD}} \boldsymbol{\Gamma}(m_{\rm SD}) \boldsymbol{\Gamma}(m_{\rm RD})} d\gamma_{\rm SD}. \tag{4.65}$$

For integer $m_{\rm RD}$, we can use the following series expansion of the lower incomplete Gamma function [57, Eq. 8.352-1]:

$$\frac{\boldsymbol{\gamma}\left(m_{\rm RD}, \frac{x-\gamma_{\rm SD}}{P_{\rm R}\theta_{\rm RD}}\right)}{\boldsymbol{\Gamma}\left(m_{\rm RD}\right)} = 1 - e^{-\frac{x-\gamma_{\rm SD}}{P_{\rm R}\theta_{\rm RD}}} \sum_{m=0}^{m_{\rm RD}-1} \frac{\left(\frac{x-\gamma_{\rm SD}}{P_{\rm R}\theta_{\rm RD}}\right)^m}{\boldsymbol{\Gamma}\left(m+1\right)}. \tag{4.66}$$

Substituting (4.66) in (4.65), and by the Riemann-Liouville integral form in [57, Eq. 3.383-1] we get

$$F_1(x) = \frac{I_{11} - I_{12}}{\mathcal{P}_{\rm SD}(P_{\rm S}\theta_{\rm SD})^{m_{\rm SD}} \boldsymbol{\Gamma}\left(m_{\rm SD}\right)}, \tag{4.67}$$

where

$$\begin{aligned} I_{11} &= \int_{\gamma_{\rm SD}=0}^{x} \gamma_{\rm SD}^{m_{\rm SD}-1} e^{-\frac{\gamma_{\rm SD}}{P_{\rm S}\theta_{\rm SD}}} d\gamma_{\rm SD} \\ &= \boldsymbol{\mathcal{B}}\left(1, m_{\rm SD}\right) x^{m_{\rm SD}} {}_{\mathbf{1}}\boldsymbol{F}_{\mathbf{1}}\left(m_{\rm SD}; m_{\rm SD}+1; -\frac{x}{P_{\rm S}\theta_{\rm SD}}\right) \end{aligned} \tag{4.68}$$

and

$$
\begin{aligned}
I_{12} &= \int_{\gamma_{\mathrm{SD}}=0}^{x} \gamma_{\mathrm{SD}}^{m_{\mathrm{SD}}-1} e^{-\frac{\gamma_{\mathrm{SD}}}{P_{\mathrm{S}}\theta_{\mathrm{SD}}}} e^{-\frac{x-\gamma_{\mathrm{SD}}}{P_{\mathrm{R}}\theta_{\mathrm{RD}}}} \sum_{m=0}^{m_{\mathrm{RD}}-1} \frac{\left(\frac{x-\gamma_{\mathrm{SD}}}{P_{\mathrm{R}}\theta_{\mathrm{RD}}}\right)^m}{\mathbf{\Gamma}(m+1)} d\gamma_{\mathrm{SD}} \\
&= \sum_{m=0}^{m_{\mathrm{RD}}-1} \frac{e^{-\frac{x}{P_{\mathrm{R}}\theta_{\mathrm{RD}}}}}{\mathbf{\Gamma}(m+1)(P_{\mathrm{R}}\theta_{\mathrm{RD}})^m} \int_{\gamma_{\mathrm{SD}}=0}^{x} \gamma_{\mathrm{SD}}^{m_{\mathrm{SD}}-1} (x-\gamma_{\mathrm{SD}})^m e^{\frac{P_{\mathrm{S}}\theta_{\mathrm{SD}}-P_{\mathrm{R}}\theta_{\mathrm{RD}}}{P_{\mathrm{S}}\theta_{\mathrm{SD}}P_{\mathrm{R}}\theta_{\mathrm{RD}}}\gamma_{\mathrm{SD}}} d\gamma_{\mathrm{SD}} \\
&= \sum_{m=0}^{m_{\mathrm{RD}}-1} \frac{e^{-\frac{x}{P_{\mathrm{R}}\theta_{\mathrm{RD}}}} \boldsymbol{\mathcal{B}}(m+1,m_{\mathrm{SD}}) x^{m_{\mathrm{SD}}+m}}{\mathbf{\Gamma}(m+1)(P_{\mathrm{R}}\theta_{\mathrm{RD}})^m} \\
&\quad \times {}_1\boldsymbol{F}_1\left(m_{\mathrm{SD}}; m_{\mathrm{SD}}+m+1; \left(\frac{1}{P_{\mathrm{R}}\theta_{\mathrm{RD}}} - \frac{1}{P_{\mathrm{S}}\theta_{\mathrm{SD}}}\right) x\right),
\end{aligned} \tag{4.69}
$$

with

$$
\boldsymbol{\mathcal{B}}(x,y) = \frac{\mathbf{\Gamma}(x)\mathbf{\Gamma}(y)}{\mathbf{\Gamma}(x+y)} \tag{4.70}
$$

denoting the beta function [57, Eq. 8.384-1]. Substituting (4.68) and (4.69) in (4.67) we obtain (4.37). Similarly,

$$
F_2(x) = \frac{I_{21} - I_{22}}{\mathcal{P}_{\mathrm{SD}}(P_{\mathrm{S}}\theta_{\mathrm{SD}})^{m_{\mathrm{SD}}}\mathbf{\Gamma}(m_{\mathrm{SD}})}, \tag{4.71}
$$

where

$$
I_{21} = \boldsymbol{\mathcal{B}}(1, m_{\mathrm{SD}}) \eta^{m_{\mathrm{SD}}} {}_1\boldsymbol{F}_1\left(m_{\mathrm{SD}}; m_{\mathrm{SD}}+1; -\frac{\eta}{P_{\mathrm{S}}\theta_{\mathrm{SD}}}\right) \tag{4.72}
$$

and

$$
\begin{aligned}
I_{22} &= \sum_{m=0}^{m_{\mathrm{RD}}-1} \int_{\gamma_{\mathrm{SD}}=0}^{\eta} \frac{e^{-\frac{x}{P_{\mathrm{R}}\theta_{\mathrm{RD}}}} \gamma_{\mathrm{SD}}^{m_{\mathrm{SD}}-1} (\eta-\gamma_{\mathrm{SD}}+x-\eta)^m e^{\frac{P_{\mathrm{S}}\theta_{\mathrm{SD}}-P_{\mathrm{R}}\theta_{\mathrm{RD}}}{P_{\mathrm{S}}\theta_{\mathrm{SD}}P_{\mathrm{R}}\theta_{\mathrm{RD}}}\gamma_{\mathrm{SD}}}}{\mathbf{\Gamma}(m+1)(P_{\mathrm{R}}\theta_{\mathrm{RD}})^m} d\gamma_{\mathrm{SD}} \\
&= \sum_{m=0}^{m_{\mathrm{RD}}-1} \sum_{k=0}^{m} \frac{\binom{m}{k}(x-\eta)^{m-k} e^{-\frac{x}{P_{\mathrm{R}}\theta_{\mathrm{RD}}}} \boldsymbol{\mathcal{B}}(k+1,m_{\mathrm{SD}}) \eta^{m_{\mathrm{SD}}+k}}{\mathbf{\Gamma}(m+1)(P_{\mathrm{R}}\theta_{\mathrm{RD}})^m} \\
&\quad \times {}_1\boldsymbol{F}_1\left(m_{\mathrm{SD}}; m_{\mathrm{SD}}+k+1; \left(\frac{1}{P_{\mathrm{R}}\theta_{\mathrm{RD}}} - \frac{1}{P_{\mathrm{S}}\theta_{\mathrm{SD}}}\right)\eta\right).
\end{aligned} \tag{4.73}
$$

In (4.73), we replaced $(x-\gamma_{\mathrm{SD}})$ by $[(x-\eta)+(\eta-\gamma_{\mathrm{SD}})]$ and then used the binomial theorem to put the integral on the Riemann-Liouville form in [57, Eq. 3.383-1]. With the substitution of (4.72) and (4.73) in (4.71) and after some manipulations, we get (4.38). In the first term of (4.37) and (4.38), we used the relation between the confluent hypergeometric function and the lower incomplete gamma function in [39, Eq. 6.5.12]. Also, in (4.38) we used [39, Eq. 13.1.27] to put it on the form in (A.1).

Chapter 5

Full-Duplex Relay Selection

5.1 Introduction

All the work in the previous chapters considered the simpler setting where only a single relay node is available for cooperation. In order to further boost the end-to-end performance, multiple relay cooperation is known to offer a higher diversity gain with the adoption of sophisticated space-time coding/beamforming techniques. Unlike multi-relay cooperative diversity systems where all intermediate relays cooperate, single relay selection has been proposed in [58, 59] in order to offer an enhanced end-to-end performance relative to single relay settings. Specifically, it was shown in [58, 59] that single relay selection achieves an equal diversity order to that of cooperative diversity systems while maintaining a simple single relay cooperation.

Following the work in [58, 59], several contributions have been published to analyze the end-to-end outage performance of AF and DFhalf-duplex relay selection (HDRS) systems. For DF relaying, the end-to-end performance of opportunistic relay selection has been analyzed under Rayleigh [60, 61, 62] and Nakagami-m [63, 64] fading, when either selective combining (SC) or MRC is applied to the direct link and the best-relayed link. Recently, full-duplex relay selection (FDRS) has been investigated for AF networks in [65, 66].

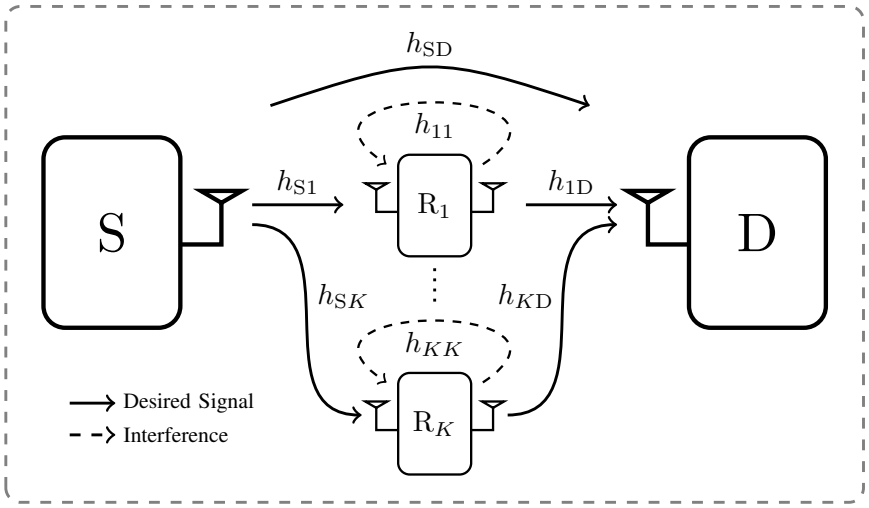

Figure 5.1: A full-duplex cooperative setting with opportunistic relay selection.

In this work, we evaluate the performance of opportunistic DF FDRS with fading RSI and direct links for the MHDF-FDR and SDF-FDR protocols. For both protocols, we present a closed-form expression for the end-to-end SINR CDF which readily yields the outage probability and system throughput for fixed-rate transmission systems. Also, we derive the exact SNR CDF for the hybrid MHDF-FDR/DT scheme that exploits the direct link as an additional diversity branch. Furthermore, we derive the diversity order of each of the FDRS protocols as a function of the RSI scaling exponent, δ. Finally, and via numerical simulations, we validate our theoretical results, and assess the effect of the severity of fading on the residual self-interference link.

5.2 MHDF-FDRS

We consider the communication setting depicted in Fig. 5.1, where the source S intends to communicate with the destination D via a full-duplex relay. In order to boost the system performance and alleviate the aforementioned RSI effect, the source may select one relay out of a cluster of K full-duplex relays, $\mathcal{R} = \{\mathrm{R}_1, \mathrm{R}_2, \cdots, \mathrm{R}_K\}$.

5.2.1 System Model

Channel Model

The fading coefficient of the $i-j$ link is denoted by h_{ij}, for $i \in \{\mathrm{S}, 1, 2, \cdots, K\}$ and $j \in \{1, 2, \cdots, K, \mathrm{D}\}$, with $k \in \mathcal{K}$ denotes the relay index, with $\mathcal{K} = \{1, 2, \cdots, K\}$ being the set of all possible relay indices. Moreover, the $i-j$ link gain is denoted by $g_{ij} = |h_{ij}|^2$. All channels are assumed to follow a block fading model, where h_{ij} remains constant over one block, and varies independently from one block to another following a Nakagami-m fading model with shape parameter m_{ij} and average power $\mathbb{E}\{g_{ij}\} = \pi_{ij}$.

All channel fading gains are assumed to be mutually independent. The source and the k^{th} relay powers are denoted by P_{S} and P_k, respectively. Also, n_k and n_{D} denote the complex AWGN components at the k^{th} relay and the destination, with variance σ_k^2 and σ_{D}^2, respectively.

As commonly assumed in the literature, for instance in [67], we assume the relays are clustered somewhere between the source and the destination. Hence, the distances among the relays are much shorter than those between the relays and the source/destination. Thus, it is reasonable to assume the following symmetric scenario where all source-relay links have an average gain of $\mathbb{E}\{g_{\mathrm{S}k}\} = \pi_{\mathrm{SR}}$, while all relay-destination links have an average gain of $\mathbb{E}\{g_{k\mathrm{D}}\} = \pi_{\mathrm{RD}}$, $\forall k \in \mathcal{K}$. Also, we assume that all relays have their RSI links with the same average gain, i.e., $\mathbb{E}\{g_{kk}\} = \pi_{\mathrm{RR}}$. Further, it is assumed that $m_{\mathrm{S}k} = m_{\mathrm{SR}}$, $m_{k\mathrm{D}} = m_{\mathrm{RD}}$ and $m_{kk} = m_{\mathrm{RR}}$ for all $k \in \mathcal{K}$. Although the analysis of asymmetric scenarios remains possible, the previous assumptions allow for simpler final expressions, and yet maintain the same diversity order of the system. Therefore, it follows that $\theta_{\mathrm{S}k} = \theta_{\mathrm{SR}}$, $\theta_{k\mathrm{D}} = \theta_{\mathrm{RD}}$ and $\theta_{kk} = \theta_{\mathrm{RR}}$ for all $k \in \mathcal{K}$. Finally, we assume that $\sigma_k^2 = \sigma_{\mathrm{D}}^2 = 1$, while all relays have the same transmit power $P_k = P_{\mathrm{R}}$.

Signal Model

When the k^{th} relay is selected, and following the same model in (3.5) and (3.6), the received signals at the k^{th} relay and destination at time t are given, respectively, by

$$y_k[t] = \sqrt{P_{\text{S}}} h_{\text{S}k} x_{\text{S}}[t] + \sqrt{P_{\text{R}}^{\delta}} h_{kk} x_k[t] + n_k[t], \tag{5.1}$$

$$y_{\text{D}}[t] = \sqrt{P_{\text{R}}} h_{k\text{D}} x_k[t] + \sqrt{P_{\text{S}}} h_{\text{SD}} x_{\text{S}}[t] + n_{\text{D}}[t]. \tag{5.2}$$

The system is assumed to adopt the simple MHDF protocol, where the signal transmitted by the relay (source) is considered as an additional noise term at the relay (destination) as commonly treated in the related literature [34]. Accordingly, the received SINRs at the k^{th} relay and at the destination are given respectively by

$$\gamma_{\text{S}k} = \frac{P_{\text{S}} g_{\text{S}k}}{P_{\text{R}}^{\delta} g_{kk} + 1} \text{ and } \gamma_{k\text{D}} = \frac{P_{\text{R}} g_{k\text{D}}}{P_{\text{S}} g_{\text{SD}} + 1}. \tag{5.3}$$

In the following, we analyze the performance of opportunistic FDRS in the absence/presence of a direct $\text{S} - \text{D}$ link.

5.2.2 Outage Analysis of MHDF-FDRS

In this section, we derive the end-to-end SINR CDF for opportunistic FDRS with/without a direct $\text{S} - \text{D}$ link. Specifically, when K DF full-duplex relays are available, the end-to-end SINR is given by

$$\gamma_{\text{e2e}} = \max_{k \in \mathcal{K}} \{\gamma_k\}, \tag{5.4}$$

where

$$\gamma_k = \min \{\gamma_{\text{S}k}, \gamma_{k\text{D}}\}. \tag{5.5}$$

In the absence of a direct link, $\gamma_{k\mathrm{D}}$ is calculated for $\gamma_{\mathrm{SD}} = P_{\mathrm{S}} g_{\mathrm{SD}} = 0$. The expression in (5.4) also applies to the scenario where the direct link exists, yet it is treated as mere interference. Alternatively, if direct transmission is taken into account as a possible diversity branch, the end-to-end SINR is given by

$$\gamma_{\mathrm{e2e}} \;=\; \max\left\{\max_{k\in\mathcal{K}}\left\{\gamma_k\right\}, \gamma_{\mathrm{SD}}\right\}. \tag{5.6}$$

In what follows, we derive the exact end-to-end SINR CDF for three MHDF scenarios; 1) no direct link (NDL), 2) interfering direct link (IDL) and 3) hybrid IDL/DT.

CDF of Link SINRs

First hop: According to the channel model explained in Section 5.2.1, the CDF of the SINR pertaining to the first hop of the k^{th} path follows from Theorem 4 and Corollary 2 in Appendix A for the cases of Nakagami-m and Rayleigh fading RSI channel, respectively, as

$$F_{\gamma_{\mathrm{S}k}}(x) = F_Z(x;\boldsymbol{p}_1) \quad \text{and} \quad F_{\gamma_{\mathrm{S}k}}(x) = F_Z(x;\boldsymbol{v}_1), \tag{5.7}$$

where $\boldsymbol{p}_1 = \left(m_{\mathrm{SR}}, P_{\mathrm{S}}\theta_{\mathrm{SR}}, m_{\mathrm{RR}}, P_{\mathrm{R}}^{\delta}\theta_{\mathrm{RR}}\right)$ and $\boldsymbol{v}_1 = \left(m_{\mathrm{SR}}, P_{\mathrm{S}}\theta_{\mathrm{SR}}, 1, P_{\mathrm{R}}^{\delta}\pi_{\mathrm{RR}}\right)$. Depending on the communication setup, it is recently shown that passive cancellation in recent implementations can provide up to 65 dB cancellation, which eliminates the LoS effects and renders Rayleigh fading a quite reasonable model for the residual channel [24, 26]. For such scenarios, the latter distribution, $F_Z(x;\boldsymbol{v}_1)$, given in Corollary 2 yields simpler expressions.

Second hop: Since the direct link SNR, γ_{SD}, is a common RV among all the multi-hop paths, all the second-hop gains are clearly correlated. However, they are conditionally independent given $\gamma_{\mathrm{SD}} = \beta$. Thus, in the presence of a direct link, we are only interested in the conditional distributions of the second-hop gains given $\gamma_{\mathrm{SD}} = \beta$, which follow $\gamma_{k\mathrm{D}}|\gamma_{\mathrm{SD}} \sim \mathcal{G}\left(m_{\mathrm{RD}}, \frac{P_{\mathrm{R}}\theta_{\mathrm{RD}}}{\beta+1}\right)$, $\forall k \in \mathcal{K}$. On the other hand, when no direct link exists, it is clear that $\gamma_{k\mathrm{D}}|\gamma_{\mathrm{SD}} \sim \mathcal{G}\left(m_{\mathrm{RD}}, P_{\mathrm{R}}\theta_{\mathrm{RD}}\right)$.

The k^{th} multi-hop path: According to (5.5) and with the above-mentioned distributions of the hop SINRs, the conditional CDF of the SINR over the k^{th} path given the direct link SNR $\gamma_{\mathrm{SD}} = \beta$ is given by

$$F_{\gamma_k|\gamma_{\mathrm{SD}}}(x|\beta) = 1 - \overline{F_Z}\left(x; \boldsymbol{p}_1\right) \overline{F_X}\left(x; m_{\mathrm{RD}}, \frac{P_{\mathrm{R}}\theta_{\mathrm{RD}}}{\beta+1}\right), \tag{5.8}$$

where $\overline{F}(\cdot) = 1 - F(\cdot)$ denotes the complementary CDF. It is clear that in the absence of a direct link, the CDF of the k^{th} path SINR is given by

$$F_{\gamma_k}(x) = 1 - \overline{F_Z}\left(x; \boldsymbol{p}_1\right) \overline{F_X}\left(x; m_{\mathrm{RD}}, P_{\mathrm{R}}\theta_{\mathrm{RD}}\right). \tag{5.9}$$

End-to-end SINR CDF

No direct link: In the absence of a direct $\mathrm{S}-\mathrm{D}$ link, the end-to-end SINR CDF has the following simple form:

$$F^{\mathrm{NDL}}_{\gamma_{\mathrm{e2e}}}(x) = F_{\gamma_k}(x)^K = \left(1 - \overline{F_Z}\left(x; \boldsymbol{p}_1\right) \overline{F_X}\left(x; m_{\mathrm{RD}}, P_{\mathrm{R}}\theta_{\mathrm{RD}}\right)\right)^K, \tag{5.10}$$

which is explicitly given in (5.11) for real-valued m_{SR} and m_{RD}, and integer-valued m_{RR}.

$$\begin{aligned} F^{\mathrm{NDL}}_{\gamma_{\mathrm{e2e}}}(x) = \Bigg(1 - \frac{\boldsymbol{\Gamma}\left(m_{\mathrm{RD}}, \frac{x}{P_{\mathrm{R}}\theta_{\mathrm{RD}}}\right)}{\boldsymbol{\Gamma}\left(m_{\mathrm{SR}}\right)\boldsymbol{\Gamma}\left(m_{\mathrm{RD}}\right)} \Bigg(\boldsymbol{\Gamma}\left(m_{\mathrm{SR}}, \frac{x}{P_{\mathrm{S}}\theta_{\mathrm{SR}}}\right) - e^{-\frac{1}{2}\left(\frac{x}{P_{\mathrm{S}}\theta_{\mathrm{SR}}} - \frac{1}{P^{\delta}_{\mathrm{R}}\theta_{\mathrm{RR}}}\right)} \left(\frac{x}{P_{\mathrm{S}}\theta_{\mathrm{SR}}}\right)^{m_{\mathrm{SR}}} \\ \times \sum_{l=0}^{m_{\mathrm{RR}}-1} \frac{\left(\frac{x}{P_{\mathrm{S}}\theta_{\mathrm{SR}}} + \frac{1}{P^{\delta}_{\mathrm{R}}\theta_{\mathrm{RR}}}\right)^{-\frac{m_{\mathrm{SR}}+l+1}{2}}}{\left(P^{\delta}_{\mathrm{R}}\theta_{\mathrm{RR}}\right)^l} \boldsymbol{W}_{\frac{m_{\mathrm{SR}}-l-1}{2}, \frac{-m_{\mathrm{SR}}-l}{2}}\left(\frac{x}{P_{\mathrm{S}}\theta_{\mathrm{SR}}} + \frac{1}{P^{\delta}_{\mathrm{R}}\theta_{\mathrm{RR}}}\right)\Bigg)\Bigg)^K. \end{aligned} \tag{5.11}$$

For $m_{\mathrm{RR}} = 1$, we get the simpler form in (5.12) via Corollary 2 as

$$F_{\gamma_{\mathrm{e2e}}}^{\mathrm{NDL}}(x)=\left(1-\left(\mathbf{\Gamma}\left(m_{\mathrm{SR}},\frac{x}{P_{\mathrm{S}}\theta_{\mathrm{SR}}}\right)-\frac{e^{\frac{1}{P_{\mathrm{R}}^{\delta}\pi_{\mathrm{RR}}}}\left(xP_{\mathrm{R}}^{\delta}\pi_{\mathrm{RR}}\right)^{m_{\mathrm{SR}}}\mathbf{\Gamma}\left(m_{\mathrm{SR}},\frac{P_{\mathrm{S}}\theta_{\mathrm{SR}}+xP_{\mathrm{R}}^{\delta}\pi_{\mathrm{RR}}}{P_{\mathrm{S}}P_{\mathrm{R}}^{\delta}\theta_{\mathrm{SR}}\pi_{\mathrm{RR}}}\right)}{\left(P_{\mathrm{S}}\theta_{\mathrm{SR}}+xP_{\mathrm{R}}^{\delta}\pi_{\mathrm{RR}}\right)^{m_{\mathrm{SR}}}}\right)\frac{\mathbf{\Gamma}\left(m_{\mathrm{RD}},\frac{x}{P_{\mathrm{R}}\theta_{\mathrm{RD}}}\right)}{\mathbf{\Gamma}\left(m_{\mathrm{SR}}\right)\mathbf{\Gamma}\left(m_{\mathrm{RD}}\right)}\right)^{K}. \quad (5.12)$$

Further, under Rayleigh fading, i.e., $m_{\mathrm{SR}}=m_{\mathrm{RR}}=m_{\mathrm{RD}}=m_{\mathrm{SD}}=1$, we get

$$F_{\gamma_{\mathrm{e2e}}}^{\mathrm{NDL}}(x)=\left(1-\frac{e^{-x\left(\frac{1}{P_{\mathrm{S}}\pi_{\mathrm{SR}}}+\frac{1}{P_{\mathrm{R}}\pi_{\mathrm{RD}}}\right)}}{1+x\frac{P_{\mathrm{R}}^{\delta}\pi_{\mathrm{RR}}}{P_{\mathrm{S}}\pi_{\mathrm{SR}}}}\right)^{K}. \quad (5.13)$$

Interfering direct link: In this scenario, the end-to-end SINR CDF is given by

$$\begin{aligned}F_{\gamma_{\mathrm{e2e}}}^{\mathrm{IDL}}(x) &= \int_{0}^{\infty}F_{\gamma_k|\gamma_{\mathrm{SD}}}(x|\beta)^{K}f_x\left(\beta;m_{\mathrm{SD}},P_{\mathrm{S}}\theta_{\mathrm{SD}}\right)\mathrm{d}\beta\\ &= \sum_{k=0}^{K}C(x,k)\underbrace{\int_{0}^{\infty}\frac{\mathbf{\Gamma}\left(m_{\mathrm{RD}},\frac{x(\beta+1)}{P_{\mathrm{R}}\theta_{\mathrm{RD}}}\right)^{k}}{\mathbf{\Gamma}\left(m_{\mathrm{RD}}\right)^{k}}\beta^{m_{\mathrm{SD}}-1}e^{-\frac{\beta}{P_{\mathrm{S}}\theta_{\mathrm{SD}}}}\mathrm{d}\beta}_{\mathcal{I}_1},\end{aligned}$$

with

$$C(x,k)=\binom{K}{k}\frac{\left(-\overline{F_Z}\left(x;\boldsymbol{p}_1\right)\right)^{k}}{\mathbf{\Gamma}\left(m_{\mathrm{SD}}\right)\left(P_{\mathrm{S}}\theta_{\mathrm{SD}}\right)^{m_{\mathrm{SD}}}}, \quad (5.14)$$

where the binomial expansion is exploited in the last step. We are now interested in solving the integral $\mathcal{I}_1$. Using the finite series expansion of the upper incomplete Gamma function in [57, Eq. 8.352-2], for integer values of m_{RD}, we get

$$\begin{aligned}\mathcal{I}_1 &= \int_{0}^{\infty}\left(e^{-\frac{x(\beta+1)}{P_{\mathrm{R}}\theta_{\mathrm{RD}}}}\sum_{n=1}^{m_{\mathrm{RD}}}\frac{\left(\frac{x(\beta+1)}{P_{\mathrm{R}}\theta_{\mathrm{RD}}}\right)^{n-1}}{\mathbf{\Gamma}\left(n\right)}\right)^{k}\beta^{m_{\mathrm{SD}}-1}e^{-\frac{\beta}{P_{\mathrm{S}}\theta_{\mathrm{SD}}}}\mathrm{d}\beta\\ &= e^{-\frac{xk}{P_{\mathrm{R}}\theta_{\mathrm{RD}}}}\sum_{\sum_{n=1}^{m_{\mathrm{RD}}}k_n=k}C_{\{k_n\}}\mathcal{I}_2, \quad (5.15)\end{aligned}$$

where

$$\mathcal{I}_2 = \int_0^\infty (\beta+1)^{D_{\{k_n\}}} \beta^{m_{\mathrm{SD}}-1} e^{-\beta\eta_k} \mathrm{d}\beta, \tag{5.16}$$

$$\eta_k = \left(\frac{1}{P_{\mathrm{S}}\theta_{\mathrm{SD}}} + \frac{xk}{P_{\mathrm{R}}\theta_{\mathrm{RD}}} \right), \tag{5.17}$$

$$C_{\{k_n\}} = \frac{\mathbf{\Gamma}\left(k+1\right)\left(\frac{x}{P_{\mathrm{R}}\theta_{\mathrm{RD}}}\right)^{\sum_{n=1}^{m_{\mathrm{RD}}} k_n(n-1)}}{\prod_{n=1}^{m_{\mathrm{RD}}} \left(\mathbf{\Gamma}\left(k_n+1\right)\mathbf{\Gamma}\left(n\right)^{k_n}\right)}, \tag{5.18}$$

$$D_{\{k_n\}} = \sum_{n=1}^{m_{\mathrm{RD}}} k_n(n-1), \tag{5.19}$$

with (5.15) obtained via the multinomial theorem [39, Section 24.1.2]. By substitution of variables, $y = \beta+1$, the integral $\mathcal{I}_2$ in (5.16) is on the form of the Riemann-Liouville integral in [57, Eq. 3.383-4]. Hence,

$$\begin{aligned} \mathcal{I}_2 &= e^{\eta_k} \int_1^\infty y^{D_{\{k_n\}}} (y-1)^{m_{\mathrm{SD}}-1} e^{-y\eta_k} \mathrm{d}y \\ &= e^{\frac{\eta_k}{2}} \eta_k^{-\frac{m_{\mathrm{SD}}+D_{\{k_n\}}+1}{2}} \mathbf{\Gamma}\left(m_{\mathrm{SD}}\right) \boldsymbol{W}_{\frac{D_{\{k_n\}}-m_{\mathrm{SD}}+1}{2}, -\frac{m_{\mathrm{SD}}+D_{\{k_n\}}}{2}}\left(\eta_k\right). \end{aligned} \tag{5.20}$$

Accordingly, $F_{\gamma_{\mathrm{e2e}}}^{\mathrm{IDL}}(x)$ is given by (5.21) for integer-valued m_{RR} and m_{RD}, and real-valued m_{SR} and m_{SD}.

$$\begin{aligned} F_{\gamma_{\mathrm{e2e}}}^{\mathrm{IDL}}(x) = &\sum_{k=0}^{K} \binom{K}{k} \frac{e^{\left(\frac{1}{2P_{\mathrm{S}}\theta_{\mathrm{SD}}} - \frac{xk}{2P_{\mathrm{R}}\theta_{\mathrm{RD}}}\right)}}{\left(P_{\mathrm{S}}\theta_{\mathrm{SD}}\right)^{m_{\mathrm{SD}}} \mathbf{\Gamma}\left(m_{\mathrm{SR}}\right)^k} \Bigg(e^{-\frac{1}{2}\left(\frac{x}{P_{\mathrm{S}}\theta_{\mathrm{SR}}} - \frac{1}{P_{\mathrm{R}}^{\delta}\theta_{\mathrm{RR}}}\right)} \left(\frac{x}{P_{\mathrm{S}}\theta_{\mathrm{SR}}}\right)^{m_{\mathrm{SR}}} \\ &\times \sum_{l=0}^{m_{\mathrm{RR}}-1} \frac{\left(\frac{x}{P_{\mathrm{S}}\theta_{\mathrm{SR}}} + \frac{1}{P_{\mathrm{R}}^{\delta}\theta_{\mathrm{RR}}}\right)^{-\frac{m_{\mathrm{SR}}+l+1}{2}}}{\left(P_{\mathrm{R}}^{\delta}\theta_{\mathrm{RR}}\right)^{l}} \boldsymbol{W}_{\frac{m_{\mathrm{SR}}-l-1}{2}, \frac{-m_{\mathrm{SR}}-l}{2}}\left(\frac{x}{P_{\mathrm{S}}\theta_{\mathrm{SR}}} + \frac{1}{P_{\mathrm{R}}^{\delta}\theta_{\mathrm{RR}}}\right) - \mathbf{\Gamma}\left(m_{\mathrm{SR}}, \frac{x}{P_{\mathrm{S}}\theta_{\mathrm{SR}}}\right) \Bigg)^k \\ &\times \sum_{\sum_{n=1}^{m_{\mathrm{RD}}} k_n = k} \frac{\mathbf{\Gamma}\left(k+1\right)\left(\frac{x}{P_{\mathrm{R}}\theta_{\mathrm{RD}}}\right)^{\sum_{n=1}^{m_{\mathrm{RD}}} k_n(n-1)}}{\prod_{n=1}^{m_{\mathrm{RD}}} \left(\mathbf{\Gamma}\left(k_n+1\right)\mathbf{\Gamma}\left(n\right)^{k_n}\right)} \eta_k^{-\frac{m_{\mathrm{SD}}+\sum_{n=1}^{m_{\mathrm{RD}}} k_n(n-1)+1}{2}} \\ &\times \boldsymbol{W}_{\frac{\sum_{n=1}^{m_{\mathrm{RD}}} k_n(n-1)-m_{\mathrm{SD}}+1}{2}, -\frac{m_{\mathrm{SD}}+\sum_{n=1}^{m_{\mathrm{RD}}} k_n(n-1)}{2}}\left(\eta_k\right). \end{aligned} \tag{5.21}$$

In the special case when the R−D link is Rayleigh-fading, i.e., $m_{\mathrm{RD}} = 1$, much simpler expressions can be obtained which also avoids the use of the multinomial theorem. Specifically, the integral $\mathcal{I}_1$ reduces to

$$\mathcal{I}_1 = e^{-\frac{xk}{P_{\mathrm{R}}\theta_{\mathrm{RD}}}} \int_0^{\infty} \beta^{m_{\mathrm{SD}}-1} e^{-\beta\eta_k} \mathrm{d}\beta = e^{-\frac{xk}{P_{\mathrm{R}}\theta_{\mathrm{RD}}}} \mathbf{\Gamma}\left(m_{\mathrm{SD}}\right) \eta_k^{-m_{\mathrm{SD}}}, \tag{5.22}$$

using [57, Eq. 3.351-3].

Furthermore, in the case when all links are Rayleigh-fading, i.e., $m_{\mathrm{SR}} = m_{\mathrm{RR}} = m_{\mathrm{RD}} = m_{\mathrm{SD}} = 1$, then

$$F_{\gamma_{\mathrm{e2e}}}^{\mathrm{IDL}}(x) = \int_{\beta=0}^{\infty} \left(1 - \frac{e^{-x\left(\frac{1}{P_{\mathrm{S}}\pi_{\mathrm{SR}}} + \frac{\beta+1}{P_{\mathrm{R}}\pi_{\mathrm{RD}}}\right)}}{(1 + x\frac{P_{\mathrm{R}}^{\delta}\pi_{\mathrm{RR}}}{P_{\mathrm{S}}\pi_{\mathrm{SR}}})}\right)^{K} \frac{e^{-\frac{\beta}{P_{\mathrm{S}}\pi_{\mathrm{SD}}}}}{P_{\mathrm{S}}\pi_{\mathrm{SD}}} \mathrm{d}\beta. \tag{5.23}$$

Using the binomial expansion, and after integration, we get

$$F_{\gamma_{\mathrm{e2e}}}^{\mathrm{IDL}}(x) = \sum_{k=0}^{K} \binom{K}{k} \left(\frac{-e^{-x\left(\frac{1}{P_{\mathrm{S}}\pi_{\mathrm{SR}}} + \frac{1}{P_{\mathrm{R}}\pi_{\mathrm{RD}}}\right)}}{(1 + x\frac{P_{\mathrm{R}}^{\delta}\pi_{\mathrm{RR}}}{P_{\mathrm{S}}\pi_{\mathrm{SR}}})}\right)^{k} \frac{1}{\left(1 + xk\frac{P_{\mathrm{S}}\pi_{\mathrm{SD}}}{P_{\mathrm{R}}\pi_{\mathrm{RD}}}\right)}. \tag{5.24}$$

Hybrid multi-hop/direct transmission: When the direct S − D link is leveraged as an additional diversity path, $\gamma_{\mathrm{SD}} = \beta$ is bounded above by x. Hence, the CDF expression is similar to that of the IDL case, however with the upper integration limit changed to x. That is,

$$F_{\gamma_{\mathrm{e2e}}}^{\mathrm{IDL/DT}}(x) \;\; = \;\; \int_0^{x} F_{\gamma_k|\gamma_{\mathrm{SD}}}(x|\beta)^{K} f_x\left(\beta; m_{\mathrm{SD}}, P_{\mathrm{S}}\theta_{\mathrm{SD}}\right) \mathrm{d}\beta. \tag{5.25}$$

The evaluation of such an integral follows the same steps, except that the integral $\mathcal{I}_2$ is

changed to

$$\tilde{\mathcal{I}}_2 = \int_0^x (\beta+1)^{D_{\{k_n\}}} \beta^{m_{\mathrm{SD}}-1} e^{-\beta\eta_k} \mathrm{d}\beta \tag{5.26}$$

$$= \sum_{r=0}^{D_{\{k_n\}}} \binom{D_{\{k_n\}}}{r} \int_0^x \beta^{r+m_{\mathrm{SD}}-1} e^{-\beta\eta_k} \mathrm{d}\beta \tag{5.27}$$

$$= \sum_{r=0}^{D_{\{k_n\}}} \binom{D_{\{k_n\}}}{r} \eta_k^{-(r+m_{\mathrm{SD}})} \boldsymbol{\gamma}\left(r+m_{\mathrm{SD}}, x\eta_k\right), \tag{5.28}$$

for integer-valued m_{SD} due to the use of the binomial theorem, with the last integral evaluated using [57, Eq. 3.381-1]. Hence, $F_{\gamma_{\mathrm{e2e}}}^{\mathrm{IDL/DT}}(x)$ is finally given by (5.29) for real-valued m_{SR} and integer-valued m_{RR}, m_{RD} and m_{SD}.

$$\begin{aligned} F_{\gamma_{\mathrm{e2e}}}^{\mathrm{IDL/DT}}(x) = & \sum_{k=0}^{K} \binom{K}{k} \frac{e^{-\frac{xk}{P_{\mathrm{R}}\theta_{\mathrm{RD}}}}}{\boldsymbol{\Gamma}\left(m_{\mathrm{SD}}\right)\left(P_{\mathrm{S}}\theta_{\mathrm{SD}}\right)^{m_{\mathrm{SD}}} \boldsymbol{\Gamma}\left(m_{\mathrm{SR}}\right)^k} \left(e^{-\frac{1}{2}\left(\frac{x}{P_{\mathrm{S}}\theta_{\mathrm{SR}}} - \frac{1}{P_{\mathrm{R}}^{\delta}\theta_{\mathrm{RR}}}\right)} \left(\frac{x}{P_{\mathrm{S}}\theta_{\mathrm{SR}}}\right)^{m_{\mathrm{SR}}} \right. \\ & \times \left. \sum_{l=0}^{m_{\mathrm{RR}}-1} \frac{\left(\frac{x}{P_{\mathrm{S}}\theta_{\mathrm{SR}}} + \frac{1}{P_{\mathrm{R}}^{\delta}\theta_{\mathrm{RR}}}\right)^{-\frac{m_{\mathrm{SR}}+l+1}{2}}}{\left(P_{\mathrm{R}}^{\delta}\theta_{\mathrm{RR}}\right)^{l}} \boldsymbol{W}_{\frac{m_{\mathrm{SR}}-l-1}{2}, \frac{-m_{\mathrm{SR}}-l}{2}}\left(\frac{x}{P_{\mathrm{S}}\theta_{\mathrm{SR}}} + \frac{1}{P_{\mathrm{R}}^{\delta}\theta_{\mathrm{RR}}}\right) - \boldsymbol{\Gamma}\left(m_{\mathrm{SR}}, \frac{x}{P_{\mathrm{S}}\theta_{\mathrm{SR}}}\right) \right)^k \\ & \times \sum_{\sum_{n=1}^{m_{\mathrm{RD}}} k_n = k} \frac{\boldsymbol{\Gamma}\left(k+1\right)\left(\frac{x}{P_{\mathrm{R}}\theta_{\mathrm{RD}}}\right)^{\sum_{n=1}^{m_{\mathrm{RD}}} k_n(n-1)}}{\prod_{n=1}^{m_{\mathrm{RD}}}\left(\boldsymbol{\Gamma}\left(k_n+1\right)\boldsymbol{\Gamma}\left(n\right)^{k_n}\right)} \\ & \times \sum_{r=0}^{\sum_{n=1}^{m_{\mathrm{RD}}} k_n(n-1)} \binom{\sum_{n=1}^{m_{\mathrm{RD}}} k_n(n-1)}{r} \eta_k^{-(r+m_{\mathrm{SD}})} \boldsymbol{\gamma}\left(r+m_{\mathrm{SD}}, x\eta_k\right). \end{aligned} \tag{5.29}$$

Also, simpler expressions can be obtained in the special case when $m_{\mathrm{RD}} = 1$ since the integral $\tilde{\mathcal{I}}_1$ ($\mathcal{I}_1$ with the upper integral changed to x) reduces to

$$\tilde{\mathcal{I}}_1 \quad = e^{-\frac{xk}{P_{\mathrm{R}}\theta_{\mathrm{RD}}}} \int_0^x \beta^{m_{\mathrm{SD}}-1} e^{-\beta\eta_k} \mathrm{d}\beta \tag{5.30}$$

$$= e^{-\frac{xk}{P_{\mathrm{R}}\theta_{\mathrm{RD}}}} \boldsymbol{\gamma}\left(m_{\mathrm{SD}}, x\eta_k\right) \eta_k^{-m_{\mathrm{SD}}}, \tag{5.31}$$

using [57, Eq. 3.351-1].

In the Rayleigh-fading scenario, it can be verified that the expression simplifies to

$$F_{\gamma_{\mathrm{e2e}}}^{\mathrm{IDL/DT}}(x) = \int_{\beta=0}^{x} \left(1 - \frac{e^{-x\left(\frac{1}{P_{\mathrm{S}}\pi_{\mathrm{SR}}}+\frac{\beta+1}{P_{\mathrm{R}}\pi_{\mathrm{RD}}}\right)}}{(1+x\frac{P_{\mathrm{R}}^{\delta}\pi_{\mathrm{RR}}}{P_{\mathrm{S}}\pi_{\mathrm{SR}}})}\right)^{K} \frac{e^{-\frac{\beta}{P_{\mathrm{S}}\pi_{\mathrm{SD}}}}}{P_{\mathrm{S}}\pi_{\mathrm{SD}}}\mathrm{d}\beta. \tag{5.32}$$

Again, using the binomial expansion, and after integration, we get

$$F_{\gamma_{\mathrm{e2e}}}^{\mathrm{IDL/DT}}(x) = \sum_{k=0}^{K}\binom{K}{k}\left(\frac{-e^{-x\left(\frac{1}{P_{\mathrm{S}}\pi_{\mathrm{SR}}}+\frac{1}{P_{\mathrm{R}}\pi_{\mathrm{RD}}}\right)}}{(1+x\frac{P_{\mathrm{R}}^{\delta}\pi_{\mathrm{RR}}}{P_{\mathrm{S}}\pi_{\mathrm{SR}}})}\right)^{k} \frac{\left(1-e^{-x\left(\frac{xk}{P_{\mathrm{R}}\pi_{\mathrm{RD}}}+\frac{1}{P_{\mathrm{S}}\pi_{\mathrm{SD}}}\right)}\right)}{\left(1+xk\frac{P_{\mathrm{S}}\pi_{\mathrm{SD}}}{P_{\mathrm{R}}\pi_{\mathrm{RD}}}\right)}. \tag{5.33}$$

5.2.3 Diversity Analysis of MHDF-FDRS

MHDF-NDL

By setting $P_{\mathrm{S}} = P_{\mathrm{R}} = P$, and by substituting the outage threshold η into the derived CDF expression in (5.13), the outage probability under Rayleigh fading is given by

$$\mathcal{P}_{\mathrm{out}}^{\mathrm{NDL}}(P) \;=\; \left(1 - \frac{e^{-\frac{a}{P}}}{1+bP^{\delta-1}}\right)^{K}. \tag{5.34}$$

where $a = \eta\left(\frac{1}{\pi_{\mathrm{SR}}}+\frac{1}{\pi_{\mathrm{RD}}}\right)$ and $b = \eta\frac{\pi_{\mathrm{RR}}}{\pi_{\mathrm{SR}}}$. As P increases, $e^{-\frac{a}{P}}$ approaches $1-\frac{a}{P}$. Hence,

$$\mathcal{P}_{\mathrm{out}}^{\mathrm{NDL}}(P) \;\approx\; \left(\frac{bP^{\delta}+a}{bP^{\delta}+P}\right)^{K}. \tag{5.35}$$

Therefore, the diversity order is given by

$$\mathcal{D}^{\mathrm{NDL}} = \lim_{P\to\infty} K\frac{\left(\frac{b+P^{1-\delta}}{b+aP^{-\delta}}\right)}{\log(P)} = K(1-\delta). \tag{5.36}$$

MHDF-IDL

By substituting $P_{\mathrm{S}} = P_{\mathrm{R}} = P$ and $x = \eta$ in (5.24), we get

$$\mathcal{P}_{\mathrm{out}}^{\mathrm{IDL}}(P) = \sum_{k=0}^{K} \binom{K}{k} \frac{\left(\frac{-e^{-\frac{a}{P}}}{1+bP^{\delta-1}}\right)^k}{c_k} \approx \sum_{k=0}^{K} \binom{K}{k} \frac{\left(\frac{aP^{-1}-1}{bP^{\delta-1}-1}\right)^k}{c_k}, \tag{5.37}$$

where $c_k = \eta k \frac{\pi_{\mathrm{SD}}}{\pi_{\mathrm{RD}}} + 1$. Hence,

$$\mathcal{D}^{\mathrm{IDL}} \underset{P\to\infty}{=} \lim - \frac{\log\left(\sum_{k=0}^{K} \binom{K}{k} \frac{\left(\frac{aP^{-1}-1}{bP^{\delta-1}+1}\right)^k}{c_k}\right)}{\log(P)} = 0, \tag{5.38}$$

regardless of the exact value of $0 \leq \delta \leq 1$, since $\mathcal{P}_{\mathrm{out}}^{\mathrm{IDL}}(P)$ is finite and not a function of P as $P \to \infty$.

IDL/DT

Substituting $P_{\mathrm{S}} = P_{\mathrm{R}} = P$ and $x = \eta$ in (5.33) yields

$$\begin{aligned}
\mathcal{P}_{\mathrm{out}}^{\mathrm{IDL/DT}}(P) &= \sum_{k=0}^{K} \binom{K}{k} \left(\frac{-e^{-\frac{a}{P}}}{bP^{\delta-1}+1}\right)^k \frac{\left(1-e^{-\frac{d_k}{P}}\right)}{c_k} && (5.39)\\
&\approx \sum_{k=0}^{K} \binom{K}{k} \left(\frac{a-P}{bP^{\delta}+P}\right)^k \frac{\eta}{\pi_{\mathrm{SD}}} \frac{1}{P} && (5.40)\\
&= \frac{\eta}{\pi_{\mathrm{SD}}} \frac{1}{P} \left(1 + \frac{a-P}{bP^{\delta}+P}\right)^K && (5.41)\\
&= \frac{\eta}{\pi_{\mathrm{SD}}} \frac{1}{P} \left(\frac{b+aP^{-\delta}}{b+P^{1-\delta}}\right)^K, && (5.42)
\end{aligned}$$

with $d_k = \eta\left(\frac{\eta k}{\pi_{\mathrm{RD}}} + \frac{1}{\pi_{\mathrm{SD}}}\right)$, $\frac{d_k}{c_k} = \frac{\eta}{\pi_{\mathrm{SD}}}$, while (5.41) follows from the binomial theorem. Hence, the diversity gain is given by

$$\mathcal{D}^{\mathrm{IDL/DT}} = \lim_{P\to\infty} -\frac{\log\left(\frac{\eta}{\pi_{\mathrm{SD}}}\frac{1}{P}\left(\frac{b+aP^{-\delta}}{b+P^{1-\delta}}\right)^{K}\right)}{\log(P)} \tag{5.43}$$

$$= K(1-\delta)+1. \tag{5.44}$$

5.3 SDF-FDRS

When SDF is adopted, the instantaneous SNR in the first hop via the k^{th} relay, its virtual MISO channel, and the direct link are given, respectively, by

$$\gamma_{\mathrm{S}k} = \frac{P_{\mathrm{S}} g_{\mathrm{S}k}}{P_{\mathrm{R}}^{\delta} g_{kk} + 1}, \tag{5.45}$$

$$\gamma_{(\mathrm{S},k)\to\mathrm{D}} \approx P_{\mathrm{R}} g_{k\mathrm{D}} + P_{\mathrm{S}} g_{\mathrm{SD}}, \tag{5.46}$$

$$\gamma_{\mathrm{SD}} = P_{\mathrm{S}} g_{\mathrm{SD}}. \tag{5.47}$$

Seeking the highest instantaneous SNR when opportunistic relay selection is adopted, the end-to-end SNR via the best relay is given by

$$\gamma_{\mathrm{e2e}} = \max\left\{\max_{k\in\mathcal{K}}\left\{\min\left\{\gamma_{\mathrm{S}k}, \gamma_{(\mathrm{S},k)\to\mathrm{D}}\right\}\right\}, \gamma_{\mathrm{SD}}\right\}. \tag{5.48}$$

Now, we need to characterize the CDF of γ_{e2e}. From the link gains independence assumption, we can notice that the end-to-end SNRs of all K paths are conditionally independent given the direct link SNR γ_{SD}. Thus, the end-to-end SNR CDF is given by

$$F_{\gamma_{\mathrm{e2e}}}^{\mathrm{SDF}}(x) = \int_0^{\infty} \left(F_{\gamma_k|\gamma_{\mathrm{SD}}}^{\mathrm{SDF}}(x|\beta)\right)^{K} \mathbb{P}\left\{\gamma_{\mathrm{SD}} < x | \gamma_{\mathrm{SD}} = \beta\right\} f_{\gamma_{\mathrm{SD}}}(\beta)\mathrm{d}\beta, \tag{5.49}$$

where $F^{\mathrm{SDF}}_{\gamma_k|\gamma_{\mathrm{SD}}}(x|\beta)$ is raised to the K^{th} power due to the independent and identically distributed (i.i.d.) link gains assumption. It can be easily seen that

$$\mathbb{P}\left\{\gamma_{\mathrm{SD}} < x|\gamma_{\mathrm{SD}} = \beta\right\} = \begin{cases} 1, & \beta < x, \\ 0, & \text{elsewhere.} \end{cases} \tag{5.50}$$

Hence,

$$F^{\mathrm{SDF}}_{\gamma_{\mathrm{e2e}}}(x) = \int_0^x \left(F^{\mathrm{SDF}}_{\gamma_k|\gamma_{\mathrm{SD}}}(x|\beta)\right)^K f_{\gamma_{\mathrm{SD}}}(\beta)\mathrm{d}\beta. \tag{5.51}$$

5.3.1 Rayleigh Fading

The conditional CDF of the k^{th} path given the direct link gain is given by

$$\begin{aligned} F^{\mathrm{SDF}}_{\gamma_k|\gamma_{\mathrm{SD}}}(x|\beta) &= \mathbb{P}\left\{\min\left\{\gamma_{\mathrm{S}k}, \gamma_{(\mathrm{S},k)\to\mathrm{D}}\right\} < x|\gamma_{\mathrm{SD}} = \beta\right\} && (5.52)\\ &= 1 - \overline{F^{\mathrm{SDF}}_{\gamma_{\mathrm{S}k}|\gamma_{\mathrm{SD}}}}(x|\beta)\overline{F^{\mathrm{SDF}}_{\gamma_{(\mathrm{S},k)\to\mathrm{D}}|\gamma_{\mathrm{SD}}}}(x|\beta) && (5.53)\\ &\approx \begin{cases} 1 - \left(\frac{e^{-\frac{x}{P_{\mathrm{S}}\pi_{\mathrm{SR}}}}}{x\frac{P^{\delta}_{\mathrm{R}}\pi_{\mathrm{RR}}}{P_{\mathrm{S}}\pi_{\mathrm{SR}}}+1}\right)\left(e^{-\frac{(x-\beta)}{P_{\mathrm{R}}\pi_{\mathrm{RD}}}}\right), & x > \beta, \\ 1 - \left(\frac{e^{-\frac{x}{P_{\mathrm{S}}\pi_{\mathrm{SR}}}}}{x\frac{P^{\delta}_{\mathrm{R}}\pi_{\mathrm{RR}}}{P_{\mathrm{S}}\pi_{\mathrm{SR}}}+1}\right), & \text{elsewhere,} \end{cases} && (5.54) \end{aligned}$$

since $\gamma_{(\mathrm{S},k)\to\mathrm{D}} \approx \gamma_{\mathrm{RD}} + \gamma_{\mathrm{SD}} \geq \gamma_{\mathrm{SD}}$. Hence,

$$\begin{aligned} F^{\mathrm{SDF}}_{\gamma_{\mathrm{e2e}}}(x) &\approx \int_0^x \left(1 - \frac{e^{-\frac{x}{P_{\mathrm{S}}\pi_{\mathrm{SR}}} - \frac{(x-\beta)}{P_{\mathrm{R}}\pi_{\mathrm{RD}}}}}{x\frac{P^{\delta}_{\mathrm{R}}\pi_{\mathrm{RR}}}{P_{\mathrm{S}}\pi_{\mathrm{SR}}}+1}\right)^K \frac{e^{-\frac{\beta}{P_{\mathrm{S}}\pi_{\mathrm{SD}}}}}{P_{\mathrm{S}}\pi_{\mathrm{SD}}}\mathrm{d}\beta \\ &= \sum_{k=0}^{K}\binom{K}{k}\left(-\frac{e^{-x\left(\frac{1}{P_{\mathrm{S}}\pi_{\mathrm{SR}}}+\frac{1}{P_{\mathrm{R}}\pi_{\mathrm{RD}}}\right)}}{x\frac{P^{\delta}_{\mathrm{R}}\pi_{\mathrm{RR}}}{P_{\mathrm{S}}\pi_{\mathrm{SR}}}+1}\right)^k \int_0^x \frac{e^{-\beta\left(\frac{1}{P_{\mathrm{S}}\pi_{\mathrm{SD}}}-\frac{k}{P_{\mathrm{R}}\pi_{\mathrm{RD}}}\right)}}{P_{\mathrm{S}}\pi_{\mathrm{SD}}}\mathrm{d}\beta \\ &= \sum_{k=0}^{K}\binom{K}{k}\left(-\frac{e^{-x\left(\frac{1}{P_{\mathrm{S}}\pi_{\mathrm{SR}}}+\frac{1}{P_{\mathrm{R}}\pi_{\mathrm{RD}}}\right)}}{x\frac{P^{\delta}_{\mathrm{R}}\pi_{\mathrm{RR}}}{P_{\mathrm{S}}\pi_{\mathrm{SR}}}+1}\right)^k \frac{1 - e^{-x\left(\frac{1}{P_{\mathrm{S}}\pi_{\mathrm{SD}}}-\frac{k}{P_{\mathrm{R}}\pi_{\mathrm{RD}}}\right)}}{1 - k\frac{P_{\mathrm{S}}\pi_{\mathrm{SD}}}{P_{\mathrm{R}}\pi_{\mathrm{RD}}}}. \end{aligned} \tag{5.55}$$

It can be verified from (5.55) that when no relays exist, i.e., $K = 0$, the end-to-end SNR CDF boils down to the CDF of the direct link.

5.3.2 Nakagami-m Fading

The conditional CDF of the k^{th} path given the direct link gain, using (4.27) and (4.28), is given by

$$\begin{aligned} F^{\text{SDF}}_{\gamma_k|\gamma_{\text{SD}}}(x|\beta) &= 1 - \overline{F^{\text{SDF}}_{\gamma_{\text{S}k}|\gamma_{\text{SD}}}}(x|\beta)\overline{F^{\text{SDF}}_{\gamma_{(\text{S},k)\to\text{D}}|\gamma_{\text{SD}}}}(x|\beta) \\ &\approx \begin{cases} 1 - \overline{F_Z}\left(x;\boldsymbol{p}_1\right)\overline{F_X}\left(x-\beta; m_{\text{RD}}, P_{\text{R}}\theta_{\text{RD}}\right), & x > \beta, \\ 1 - \overline{F_Z}\left(x;\boldsymbol{p}_1\right), & \text{elsewhere}, \end{cases} \end{aligned} \tag{5.56}$$

also since $\gamma_{(\text{S},k)\to\text{D}} \approx \gamma_{\text{RD}} + \gamma_{\text{SD}} \geq \gamma_{\text{SD}}$. Hence,

$$F^{\text{SDF}}_{\gamma_{\text{e2e}}}(x) \approx \int_0^x \left(1 - \overline{F_Z}\left(x;\boldsymbol{p}_1\right)\frac{\boldsymbol{\Gamma}\left(m_{\text{RD}}, \frac{x-\beta}{P_{\text{R}}\theta_{\text{RD}}}\right)}{\boldsymbol{\Gamma}\left(m_{\text{RD}}\right)}\right)^K \frac{\beta^{m_{\text{SD}}-1}e^{-\frac{\beta}{P_{\text{S}}\theta_{\text{SD}}}}}{\boldsymbol{\Gamma}\left(m_{\text{SD}}\right)\left(P_{\text{S}}\theta_{\text{SD}}\right)^{m_{\text{SD}}}}\text{d}\beta \tag{5.57}$$

$$\begin{aligned} &= \sum_{k=0}^{K}\binom{K}{k}\left(-\overline{F_Z}\left(x;\boldsymbol{p}_1\right)\right)^k \frac{1}{\boldsymbol{\Gamma}\left(m_{\text{SD}}\right)\left(P_{\text{S}}\theta_{\text{SD}}\right)^{m_{\text{SD}}}} \\ &\quad \times \underbrace{\int_0^x \left(\frac{\boldsymbol{\Gamma}\left(m_{\text{RD}}, \frac{x-\beta}{P_{\text{R}}\theta_{\text{RD}}}\right)}{\boldsymbol{\Gamma}\left(m_{\text{RD}}\right)}\right)^k \beta^{m_{\text{SD}}-1}e^{-\frac{\beta}{P_{\text{S}}\theta_{\text{SD}}}}\text{d}\beta}_{\hat{\mathcal{I}}_1}, \end{aligned} \tag{5.58}$$

where the binomial theorem is utilized in the last step. For integer m_{RD}, we can use the following series expansion for the upper regularized Gamma function [57, Eq. 8.352-2]:

$$\frac{\boldsymbol{\Gamma}\left(m_{\text{RD}}, \frac{x-\beta}{P_{\text{R}}\theta_{\text{RD}}}\right)}{\boldsymbol{\Gamma}\left(m_{\text{RD}}\right)} = e^{-\frac{x-\beta}{P_{\text{R}}\theta_{\text{RD}}}}\sum_{m=0}^{m_{\text{RD}}-1}\frac{\left(\frac{x-\beta}{P_{\text{R}}\theta_{\text{RD}}}\right)^m}{\boldsymbol{\Gamma}\left(m+1\right)}. \tag{5.59}$$

Hence,

$$\hat{\mathcal{I}}_1 = e^{-\frac{kx}{P_{\mathrm{R}}\theta_{\mathrm{RD}}}} \int_0^x \left(\sum_{n=1}^{m_{\mathrm{RD}}} \frac{\left(\frac{x-\beta}{P_{\mathrm{R}}\theta_{\mathrm{RD}}}\right)^{n-1}}{\mathbf{\Gamma}(n)} \right)^k \beta^{m_{\mathrm{SD}}-1} e^{-\beta\left(\frac{1}{P_{\mathrm{S}}\theta_{\mathrm{SD}}} - \frac{k}{P_{\mathrm{R}}\theta_{\mathrm{RD}}}\right)} \mathrm{d}\beta \tag{5.60}$$

$$= e^{-\frac{kx}{P_{\mathrm{R}}\theta_{\mathrm{RD}}}} \sum_{\sum_{n=1}^{m_{\mathrm{RD}}} \hat{k}_n = k} \hat{C}_{\{\hat{k}_n\}} \hat{\mathcal{I}}_2, \tag{5.61}$$

where

$$\hat{\mathcal{I}}_2 = \int_0^x (x-\beta)^{\hat{D}_{\{\hat{k}_n\}}} \beta^{m_{\mathrm{SD}}-1} e^{-\beta\hat{\eta}_k} \mathrm{d}\beta, \tag{5.62}$$

$$\hat{\eta}_k = \left(\frac{1}{P_{\mathrm{S}}\theta_{\mathrm{SD}}} - \frac{k}{P_{\mathrm{R}}\theta_{\mathrm{RD}}} \right), \tag{5.63}$$

$$\hat{C}_{\{\hat{k}_n\}} = \frac{\mathbf{\Gamma}(k+1) \left(\frac{1}{P_{\mathrm{R}}\theta_{\mathrm{RD}}}\right)^{\sum_{n=1}^{m_{\mathrm{RD}}} \hat{k}_n(n-1)}}{\prod_{n=1}^{m_{\mathrm{RD}}} \left(\mathbf{\Gamma}\left(\hat{k}_n + 1\right) \mathbf{\Gamma}(n)^{\hat{k}_n} \right)}, \tag{5.64}$$

$$\hat{D}_{\{\hat{k}_n\}} = \sum_{n=1}^{m_{\mathrm{RD}}} \hat{k}_n (n-1), \tag{5.65}$$

with (6.13) obtained via the multinomial theorem [39, Section 24.1.2]. Now, the integral $\hat{\mathcal{I}}_2$ in (5.62) is on the form of the Riemann-Liouville integral in [57, Eq. 3.383-1] when $\hat{\eta}_k \leq 0$. Hence,

$$\hat{\mathcal{I}}_2 = x^{\hat{D}_{\{\hat{k}_n\}} + m_{\mathrm{SD}}} \boldsymbol{\mathcal{B}}\left(\hat{D}_{\{\hat{k}_n\}} + 1, m_{\mathrm{SD}}\right) {}_1\boldsymbol{F}_1\left(m_{\mathrm{SD}}; \hat{D}_{\{\hat{k}_n\}} + m_{\mathrm{SD}} + 1; -x\hat{\eta}_k\right). \tag{5.66}$$

On the other hand, when $\hat{\eta}_k > 0$, we can use the change of variables $y = x - \beta$ and again use [57, Eq. 3.383-1] to get

$$\hat{\mathcal{I}}_2 = e^{-x\hat{\eta}_k} x^{\hat{D}_{\{\hat{k}_n\}} + m_{\mathrm{SD}}} \boldsymbol{\mathcal{B}}\left(m_{\mathrm{SD}}, \hat{D}_{\{\hat{k}_n\}} + 1\right) {}_1\boldsymbol{F}_1\left(\hat{D}_{\{\hat{k}_n\}} + 1; \hat{D}_{\{\hat{k}_n\}} + m_{\mathrm{SD}} + 1; x\hat{\eta}_k\right). \tag{5.67}$$

Finally, substituting back, we get

$$F_{\gamma_{\mathrm{e2e}}}^{\mathrm{SDF}}(x) \approx \sum_{k=0}^{K}\binom{K}{k}\Bigg(-\frac{\mathbf{\Gamma}\left(m_{\mathrm{SR}},\frac{x}{P_{\mathrm{S}}\theta_{\mathrm{SR}}}\right)}{\mathbf{\Gamma}\left(m_{\mathrm{SR}}\right)} + \frac{\exp\left(-\frac{1}{2}\left(\frac{x}{P_{\mathrm{S}}\theta_{\mathrm{SR}}}-\frac{1}{P_{\mathrm{R}}^{\delta}\theta_{\mathrm{RR}}}\right)\right)}{\mathbf{\Gamma}\left(m_{\mathrm{SR}}\right)}\left(\frac{x}{P_{\mathrm{S}}\theta_{\mathrm{SR}}}\right)^{m_{\mathrm{SR}}}$$
$$\times \sum_{l=0}^{m_{\mathrm{RR}}-1}\frac{\left(\frac{x}{P_{\mathrm{S}}\theta_{\mathrm{SR}}}+\frac{1}{P_{\mathrm{R}}^{\delta}\theta_{\mathrm{RR}}}\right)^{-\frac{m_{\mathrm{SR}}+l+1}{2}}}{\left(P_{\mathrm{R}}^{\delta}\theta_{\mathrm{RR}}\right)^{l}}\boldsymbol{W}_{\frac{m_{\mathrm{SR}}-l-1}{2},\frac{-m_{\mathrm{SR}}-l}{2}}\left(\frac{x}{P_{\mathrm{S}}\theta_{\mathrm{SR}}}+\frac{1}{P_{\mathrm{R}}^{\delta}\theta_{\mathrm{RR}}}\right)\Bigg)^{k}$$
$$\times\frac{1}{\mathbf{\Gamma}\left(m_{\mathrm{SD}}\right)\left(P_{\mathrm{S}}\theta_{\mathrm{SD}}\right)^{m_{\mathrm{SD}}}}e^{-\frac{kx}{P_{\mathrm{R}}\theta_{\mathrm{RD}}}}\sum_{\sum_{n=1}^{m_{\mathrm{RD}}}\hat{k}_n=k}\hat{C}_{\{\hat{k}_n\}}\hat{\mathcal{I}}_2. \tag{5.68}$$

5.3.3 Diversity Analysis

In the Rayleigh-fading scenario with $P_{\mathrm{S}}=P_{\mathrm{R}}=P$, we have

$$\mathcal{P}_{\mathrm{out}}^{\mathrm{SDF}}(P) \approx \sum_{k=0}^{K}\binom{K}{k}\left(-\frac{e^{-\frac{a}{P}}}{bP^{\delta-1}+1}\right)^{k}\frac{1-e^{-\frac{p_k}{P}}}{q_k} \tag{5.69}$$

$$\approx \sum_{k=0}^{K}\binom{K}{k}\left(-\frac{1-\frac{a}{P}}{bP^{\delta-1}+1}\right)^{k}\frac{x}{P_{\mathrm{S}}\pi_{\mathrm{SD}}}\frac{1}{P}, \tag{5.70}$$

where $p_k = x\left(\frac{1}{P_{\mathrm{S}}\pi_{\mathrm{SD}}}-\frac{k}{P_{\mathrm{R}}\pi_{\mathrm{RD}}}\right)$ and $q_k = 1-k\frac{P_{\mathrm{S}}\pi_{\mathrm{SD}}}{P_{\mathrm{R}}\pi_{\mathrm{RD}}}$, also using the same approximation for large P in (5.70). Clearly, this yields the same diversity order of the hybrid IDL/DT protocol. That is,

$$\mathcal{D}^{\mathrm{SDF}} = K(1-\delta)+1. \tag{5.71}$$

5.3.4 Summary of FDRS Diversity Results

Table 5.1: Diversity order of Full-Duplex Relay Selection Protocols with K Relays

Protocol/Scenario		Diversity Order
MHDF	NDL	K(1-δ)
	IDL	0
	IDL/DT	K(1-δ) + 1
SDF		K(1-δ) + 1

5.4 Numerical Evaluation

In this section, we numerically evaluate the performance of FDRS, and verify the theoretical findings derived in previous sections. All numerical results are evaluated by averaging over 10^7 sets of channel realizations with the parameters summarized in the caption of each figure. Also, for clarity of presentation, solid lines with unfilled marks are used to plot the theoretical results, while the same filled marks with no connecting lines are used for simulation results. Hence, curves with solid lines and filled marks indicate perfect matching between theoretical and simulation results.

5.4.1 End-to-End CDF

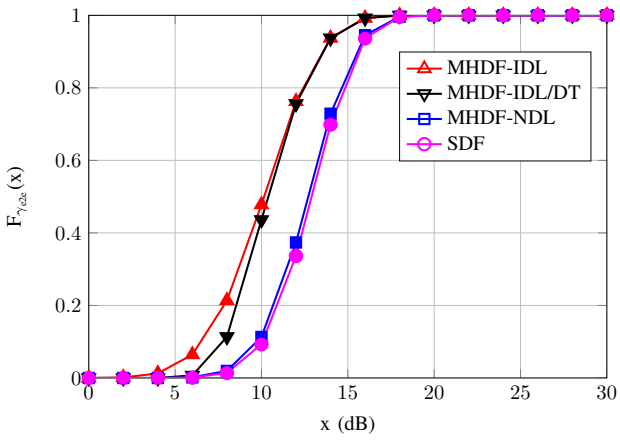

Figure 5.2: CDF of the end-to-end SNR, for $\pi_{\mathrm{SR}} = \pi_{\mathrm{RD}} = 15$ dB, $\pi_{\mathrm{RR}} = \pi_{\mathrm{SD}} = 5$ dB, $m_{\mathrm{SR}} = m_{\mathrm{RD}} = 2$, $m_{\mathrm{RR}} = m_{\mathrm{SD}} = 1$, $\delta = 1$, $P_{\mathrm{S}} = P_{\mathrm{R}} = 1$, and $K = 5$ relays.

The end-to-end SNR CDF of the derived expressions for MHDF-FDRS and SDF-FDRS are shown in Fig. 5.2. The empirical CDFs are also plotted for validation, and as shown, they perfectly match with theory.

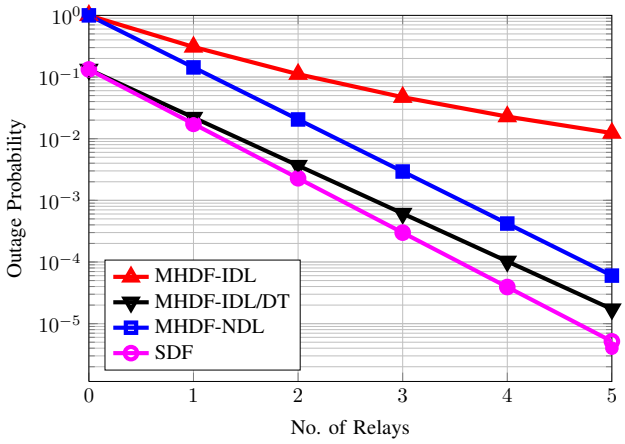

Figure 5.3: Outage probability vs. No. of Relays, for $\pi_{\mathrm{SR}} = \pi_{\mathrm{RD}} = 10$ dB, $\pi_{\mathrm{RR}} = 3$ dB, $\pi_{\mathrm{SD}} = 5$ dB, $m_{\mathrm{SR}} = m_{\mathrm{RD}} = m_{\mathrm{RR}} = m_{\mathrm{SD}} = 2$, $\delta = 1$, $P_{\mathrm{S}} = P_{\mathrm{R}} = 1$, and $R = 1$ bpcu.

5.4.2 Outage Probability vs. No. of Relays

In Fig. 5.3, the outage performance is shown versus K for the three scenarios of MHDF-FDRS under consideration, as well as that of SDF-FDRS. As expected, when opportunistic relay selection is considered only among the available K dual-hop paths, the performance of the system can be seriously degraded as soon as a direct link starts to get into the picture. This can be seen from the relative performance of the NDL and IDL schemes, which is caused by the introduced direct-link interference in all second hops. It can be also noticed that the performance enhancement in IDL due to additional relays has diminishing returns. This is due to the fact that is performance is primarily limited by the average gain of the interfering direct link. On the other hand, when DT is also considered as an additional diversity branch, the performance can be significantly enhanced to the extent that the hybrid IDL/DT scheme may even outperform the NDL case depending on the average direct link gain.

5.4.3 Diversity Order: Outage Probability vs. Transmit SNR

In Fig. 5.4, the outage performance is plotted versus the transmit power, P, for $K = 3$. For a linearly-scaling RSI, i.e., $\delta = 1$, both the NDL and IDL scenarios suffer from an error floor indicating a zero diversity order as shown in Fig. 5.4a. However, the schemes which exploit

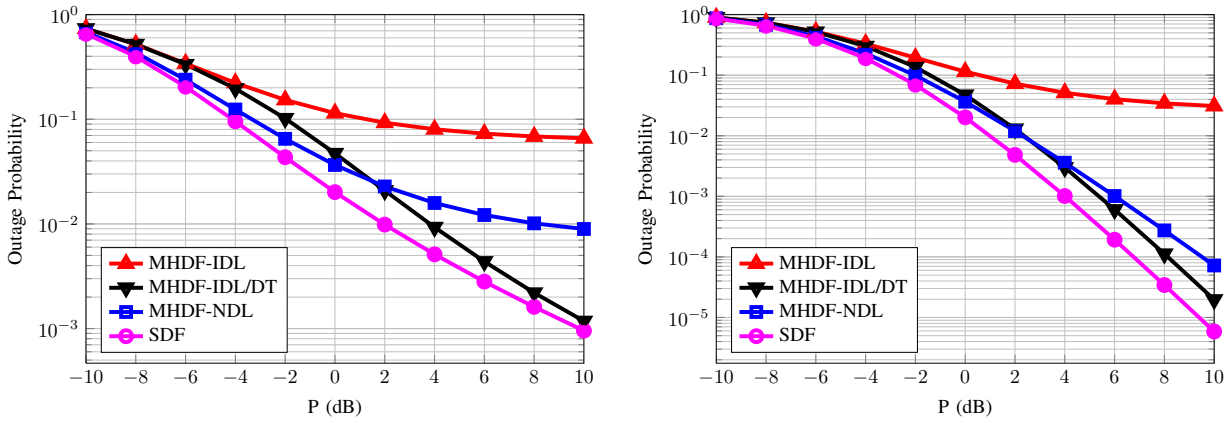

(a) $\delta = 1$. (b) $\delta = 0$.

Figure 5.4: Outage probability vs. Transmit Power, for $\pi_{\text{SR}} = \pi_{\text{RD}} = 15$ dB, $\pi_{\text{RR}} = \pi_{\text{SD}} = 4$ dB, $m_{\text{SR}} = m_{\text{RD}} = m_{\text{RR}} = m_{\text{SD}} = 1$, $K = 3$, and $R = 2$ bpcu.

the direct link (IDL/DT and SDF) maintain a minimum diversity of order 1 regardless of the RSI scaling factor. On the other hand, the diversity gain of IDL/DT and SDF grows as shown to $3(1-\delta)+1 = 4$, while that of the NDL reaches 3, which agrees with the earlier analysis. The diversity of the IDL scenario remains of zero order since selection is performed among K zero-order branches.

5.4.4 Throughput vs. Source Rate

In Fig. 5.5, we plot the throughput versus the fixed transmission rate of the source in bpcu. For fixed-rate transmission, the end-to-end throughput, $\mathcal{T}$, is obtained simply as

$$\mathcal{T} = R(1 - \mathcal{P}_{\text{out}}) \text{ bpcu}, \tag{5.72}$$

where R is the fixed source transmission rate in bpcu, and $\mathcal{P}_{\text{out}}$ is the end-to-end outage probability when the source rate is equal to *Rate*. The shown figure emphasizes the performance gap between the NDL and IDL scenarios. As shown, exploiting the direct link as an additional non-cooperative path in the hybrid IDL/DT scheme offers throughput enhancements relative to the IDL scheme even with treating direct link as interference to all other

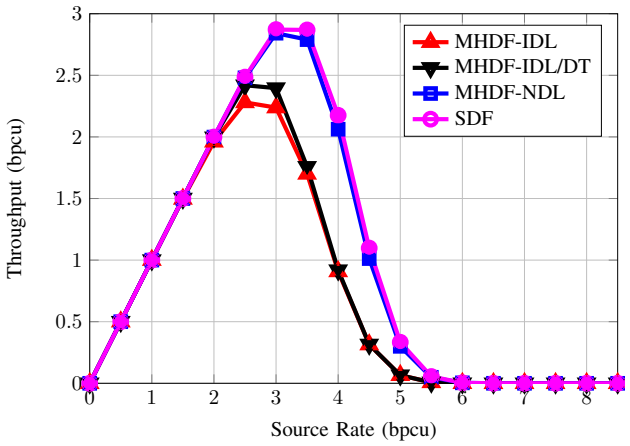

Figure 5.5: Throughput vs. rate, for $(\pi_{\mathrm{SR}}, \pi_{\mathrm{RD}}, \pi_{\mathrm{RR}}, \pi_{\mathrm{SD}}) = (15, 15, 4, 4)$ dB, $(m_{\mathrm{SR}}, m_{\mathrm{RD}}, m_{\mathrm{RR}}, m_{\mathrm{SD}}) = (2, 2, 3, 1)$, $\delta = 1$, $P_{\mathrm{S}} = P_{\mathrm{R}} = 1$, and $K = 4$ relays.

dual-hop paths. This is due to the elimination of the particular error event caused by having large-valued realizations of the direct-link gain which prohibits the communication via all cooperative dual-hop paths while DT can take place.

It has been found that the fading severity of the RSI link, m_{RR}, is of minimal effect on the end-to-end performance in the scenarios of practical interest. Specifically, when the average gain of the first hop is well above that of the RSI link, it was found that the outage performance almost does not change. The performance can be slightly affected only in the scenarios where the RSI link gain approaches that of the $\mathrm{S}-\mathrm{R}$ link. However, the end-to-end communication in the latter scenarios tends to fail due to the communication failure in the first hop. This result agrees with a recent result that has been reported in [68] for the single relay scenario.

5.5 Conclusion

In this chapter, closed-form expressions for the CDF of the end-to-end SNR were derived for opportunistic DF FDRS, taking the self-interference of the relays into account. The performance was analyzed when the different links experience general Nakagami-m fading, and compared in the scenarios where either coverage extension or throughput enhancement is

targeted. The derived analytical results were shown to perfectly match with those obtained via numerical simulations. In the scenarios where a direct source-to-destination link exists, and even when the direct link is treated as interference to all dual-hop paths, it was shown that considering direct transmission as a possible diversity branch has the potential to offer significant performance enhancements that can reach and may exceed the scenario with no direct link.

Chapter 6

Full-Duplex Cooperation in Underlay Cognitive Networks

Spectrum sharing represents one network paradigm for the now celebrated cognitive radio technology in which adequate means are offered to resolve the scarcity problem of wireless resources [69, 70]. Also known as underlay cognitive radio, spectrum sharing allows the traffic of secondary *cognitive* users to coexist with that of the primary spectrum users as long as a certain interference level is not exceeded. In particular, when the secondary source and destination are spatially isolated, relay assistance becomes inevitable to establish successful communication via relay listening/forwarding, while satisfying the coexistence constraints with the primary user. Cognitive relay networks continue to draw a noticeable interest of the wireless communications community for its coverage extension capabilities under an efficient spectrum usage [71].

Adhering to the interference constraints in underlay networks, however, can considerably limit the throughput of the secondary system, especially when a single relay is leveraged to assist the communication between the secondary source and its far destination. To tackle such a challenge, relay selection [58, 59, 60] was introduced to underlay cognitive relay networks, and it was shown to offer remarkable performance gains relative to its fixed relaying

counterpart. Cognitive relay selection was fairly investigated in the literature under the relaying strategies of AF [72, 73, 74, 75] and DF [76, 67, 77, 78, 79].

6.1 Spectrum Sharing with Full-Duplex Relaying

All the aforementioned efforts considered relays to operate in the conventional half-duplex mode. However, as discussed earlier, HDR is known to suffer from a spectral efficiency loss when compared to DT due to its time-orthogonal relay listening/forwarding. Recent efforts were directed to study FDR in cognitive radio networks [80, 81, 82, 83]. Contrary to HDR, FDR enables simultaneous listening/forwarding at the secondary relay, thereby allowing for a higher spectral efficiency. However, since the source and relay simultaneously transmit in FDR, their superimposed signal at the primary receiver should now satisfy the existing interference constraint which can considerably limit the secondary network throughput.

In [82], a cognitive underlay setting is studied in which a secondary system shares the spectrum with a primary system under a certain interference constraint. The secondary system comprises a source, a destination and a full-duplex DF relay. Under the aforementioned interference constraint, optimal source and relay power allocation was investigated with the objective to minimize the end-to-end outage probability.

Despite its anticipated performance merits, the incorporation of relay selection techniques into cognitive full-duplex relay networks remained untackled before this work. In this work, we aim at bridging this gap by introducing relay selection to cognitive full-duplex relay networks and analyzing its offered performance gains. In underlay settings with FDR, the performance of the secondary users can be seriously limited due to the fact that now the superimposed source and relay interference components should satisfy the existing interference constraint which was previously imposed in HDR on each transmitting node at a time. In this regard, relay selection techniques can offer an adequate solution to boost the secondary network throughput. Unlike in underlay HDRS settings, since the source interference signal

is a common random variable when any of the K relays is selected, the superimposed interference signals at the primary receiver are not independent. In this work, we derive the exact CDF of the end-to-end SNR for opportunistic FDRS in an underlay cognitive system when an interference constraint is imposed by the primary user.

6.2 System Model

We consider the underlay cognitive setting depicted in Fig. 6.1. As shown, a secondary source S intends to communicate with a secondary destination D in the presence of a primary receiver P. In agreement to similar recent studies of underlay cognitive settings, for instance in [67], the primary source is assumed to be far enough that its interference effect on the secondary system can be reasonably ignored. The direct secondary source-destination link is assumed of a relatively weak gain due to distance and shadowing effects. Hence, a full-duplex relay is utilized to assist the end-to-end secondary communication, taking the interference constraint on the primary receiver into account. Although FDR can offer higher spectral efficiency when compared to its half-duplex counterpart, it introduces an additional challenge in cognitive settings where higher interference levels may be experienced by the primary user of the spectrum band, due to simultaneous source/relay transmissions. Also, FDR suffers from a residual self-interference level which imposes an additional communication challenge.

6.2.1 Channel Model

The fading coefficient of the $i-j$ link is denoted by h_{ij}, for $i \in \{\mathrm{S}, 1, 2, \cdots, K\}$ and $j \in \{1, 2, \cdots, K, \mathrm{D}, \mathrm{P}\}$, where $k \in \{1, 2, \cdots, K\}$ denotes the relay index. Moreover, the $i-j$ link gain is denoted by $g_{ij} = |h_{ij}|^2$. All channels are assumed to follow a block fading model, where h_{ij} remains constant over one block, and varies independently from one block to another following a Nakagami-m fading model with shape parameter m_{ij} and average power $\mathbb{E}\{g_{ij}\} = \pi_{ij}$. Accordingly, $|h_{ij}|$ is Rayleigh distributed, while g_{ij} follows an exponential distribution

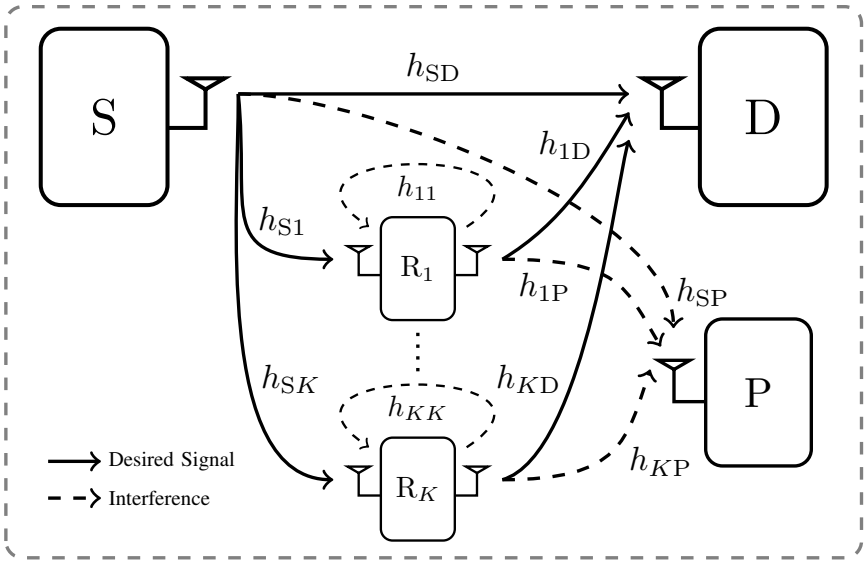

Figure 6.1: Spectrum sharing network with full-duplex relaying.

with mean π_{ij}. All channel fading gains are assumed to be mutually independent. The relays operate in a full-duplex mode where simultaneous listening/forwarding is allowed with an introduced level of loopback interference. The link gain h_{kk} is assumed to represent the residual self-interference after undergoing all possible isolation and cancellation techniques, as for instance [34] and the references therein. The source and the k^{th} relay powers are denoted by P_{S} and P_k, respectively. Also, n_k and n_{D} denote the complex AWGN components at the k^{th} relay and the destination, with variance σ_k^2 and σ_{D}^2, respectively.

As commonly assumed in the literature, for instance in [67], we assume the relays are clustered somewhere between the source and the destination. Hence, the distances among the relays are much shorter than those between the relays and the source/destination. In this setting, it is reasonable to assume the following symmetric scenario where all source-relay links have an average gain of $\mathbb{E}\{g_{\mathrm{S}k}\} = \pi_{\mathrm{SR}}$, while all relay-destination links have an average gain of $\mathbb{E}\{g_{k\mathrm{D}}\} = \pi_{\mathrm{RD}}$, $\forall k \in \{1, 2, \cdots, K\}$. Also, all relays have the same average gain to the primary receiver, denoted as π_{RP}. Moreover, we assume that all relays have their loopback interference links with the same average gain, i.e., $\mathbb{E}\{g_{kk}\} = \pi_{\mathrm{RR}}$. Although the analysis of asymmetric scenarios remains possible, the previous assumptions allow for simpler final expressions, and yet maintain the same diversity order of the system. Finally, we assume

that $\sigma_k^2 = \sigma_{\mathrm{D}}^2 = 1$ and $P_k = P_{\mathrm{R}}$ for ease of notation.

6.2.2 Signal Model

The adopted signal model follows directly from that in section 5.2.1. However, in an underlay setting, the introduced interference level on the primary receiver is constrained not to exceed a certain threshold, I_{th}. Thus, when the k^{th} relay is selected, the interference constraint is given by

$$I_k = I_{\mathrm{SP}} + I_{k\mathrm{P}} \leq I_{\mathrm{th}}, \tag{6.1}$$

where $I_{\mathrm{SP}} = P_{\mathrm{S}} g_{\mathrm{SP}}$ and $I_{k\mathrm{P}} = P_{\mathrm{R}} g_{k\mathrm{P}}$ are the interference components imposed on the primary receiver due to the source and the k^{th} relay, respectively, while I_k denotes their sum. When no relays are selected while a direct source-destination link exists, the interference constraint is simply given by

$$I_{\mathrm{SP}} \leq I_{\mathrm{th}}. \tag{6.2}$$

6.3 Performance Analysis

There exists an interference threshold, I_{th}, that the secondary system cannot exceed. Now, we are interested in the probability to have L out of the K available relays that satisfy the interference constraint I_{th}. Let us denote this probability by $\mathcal{P}_L$. We first start with the NDL scenario.

6.3.1 No Direct $\mathrm{S} - \mathrm{D}$ Link

The end-to-end SNR CDF when no direct $\mathrm{S} - \mathrm{D}$ link exists is given as

$$F_{\gamma_{\mathrm{e2e}}}^{\mathrm{NDL}}(x) \;=\; \sum_{L=0}^{K} F_{\gamma_{\mathrm{e2e}}}^{\mathrm{NDL}}(x|L)\mathcal{P}_L, \tag{6.3}$$

where $F^{\mathrm{NDL}}_{\gamma_{\mathrm{e2e}}}(x|L)$ is that derived in the previous chapter when L relays are available. Now, we derive $\mathcal{P}_L$. The same expression also applies to the IDL scenario where the direct link is not leveraged. Specifically,

$$F^{\mathrm{IDL}}_{\gamma_{\mathrm{e2e}}}(x) = \sum_{L=0}^{K} F^{\mathrm{IDL}}_{\gamma_{\mathrm{e2e}}}(x|L)\mathcal{P}_L, \tag{6.4}$$

We now need to derive the probability of L feasible relays, $\mathcal{P}_L$.

Rayleigh Fading

When the k^{th} relay is active, the interference constraint is given by (6.1). Unlike half-duplex cognitive relay settings, full-duplex operation causes a superposition of the source and relay interference at the primary receiver. Since the source interference is a common random variable when any of the K relays is selected, the superimposed interference signals are correlated. However, they are conditionally independent given I_{SP}. Conditioned on $I_{\mathrm{SP}} = \beta \geq 0$, the probability that the k^{th} relay is feasible is given by

$$F_{I_k|I_{\mathrm{SP}}}(I_{\mathrm{th}}|\beta) = \begin{cases} 1 - e^{-\frac{I_{\mathrm{th}}-\beta}{P_{\mathrm{R}}\pi_{\mathrm{RP}}}}, & \text{if } I_{\mathrm{th}} > \beta, \\ 0, & \text{elsewhere.} \end{cases} \tag{6.5}$$

Accordingly, conditioned on $I_{\mathrm{SP}} = \beta$ for $0 \leq \beta \leq I_{\mathrm{th}}$, and due to the considered symmetric scenario, $\mathcal{P}_{L|I_{\mathrm{SP}}}(\beta)$ is given in terms of a binomial distribution as

$$\mathcal{P}_{L|I_{\mathrm{SP}}}(\beta) = \binom{K}{L}\left(1 - e^{-\frac{I_{\mathrm{th}}-\beta}{P_{\mathrm{R}}\pi_{\mathrm{RP}}}}\right)^{L}\left(e^{-\frac{I_{\mathrm{th}}-\beta}{P_{\mathrm{R}}\pi_{\mathrm{RP}}}}\right)^{K-L} \tag{6.6}$$

$$= \binom{K}{L}\sum_{l=0}^{L}\binom{L}{l}(-1)^l e^{-\frac{(K-L+l)(I_{\mathrm{th}}-\beta)}{P_{\mathrm{R}}\pi_{\mathrm{RP}}}}, \tag{6.7}$$

where the binomial expansion is again utilized. It is straightforward to see that when $\beta > I_{\mathrm{th}}$, $\mathcal{P}_{L|I_{\mathrm{SP}}}(\beta) = 0$ for $L = 1, 2, \cdots, K$, while $\mathcal{P}_{L|I_{\mathrm{SP}}}(\beta) = 1$ for $L = 0$. Hence, for the case when $L = 0$, the support of β is $0 \leq \beta \leq \infty$, while it is $0 \leq \beta \leq I_{\mathrm{th}}$ for $1 \leq L \leq K$. Now, we can

obtain $\mathcal{P}_L$ for $L = 1, 2, \cdots, K$ as

$$\mathcal{P}_L = \int_0^{\infty} \mathcal{P}_{L|I_{\rm SP}}(\beta) \frac{e^{-\frac{\beta}{P_{\rm S}\pi_{\rm SP}}}}{P_{\rm S}\pi_{\rm SP}} \mathrm{d}\beta = \int_0^{I_{\rm th}} \mathcal{P}_{L|I_{\rm SP}}(\beta) \frac{e^{-\frac{\beta}{P_{\rm S}\pi_{\rm SP}}}}{P_{\rm S}\pi_{\rm SP}} \mathrm{d}\beta \tag{6.8}$$

$$= \binom{K}{L} \sum_{l=0}^{L} \binom{L}{l} \frac{(-1)^l \left(e^{-\frac{I_{\rm th}(K-L+l)}{P_{\rm R}\pi_{\rm RP}}} - e^{-\frac{I_{\rm th}}{P_{\rm S}\pi_{\rm SP}}} \right)}{1 - \frac{(K-L+l)P_{\rm S}\pi_{\rm SP}}{P_{\rm R}\pi_{\rm RP}}}. \tag{6.9}$$

For $L = 0$, $\mathcal{P}_0$ is given by

$$\mathcal{P}_0 = \int_0^{I_{\rm th}} \left(e^{-\frac{I_{\rm th}-\beta}{P_{\rm R}\pi_{\rm RP}}} \right)^K \frac{e^{-\frac{\beta}{P_{\rm S}\pi_{\rm SP}}}}{P_{\rm S}\pi_{\rm SP}} \mathrm{d}\beta + \int_{I_{\rm th}}^{\infty} \frac{e^{-\frac{\beta}{P_{\rm S}\pi_{\rm SP}}}}{P_{\rm S}\pi_{\rm SP}} \mathrm{d}\beta \tag{6.10}$$

$$= \frac{P_{\rm R}\pi_{\rm RP} e^{-\frac{KI_{\rm th}}{P_{\rm R}\pi_{\rm RP}}} - KP_{\rm S}\pi_{\rm SP} e^{-\frac{I_{\rm th}}{P_{\rm S}\pi_{\rm SP}}}}{P_{\rm R}\pi_{\rm RP} - KP_{\rm S}\pi_{\rm SP}}. \tag{6.11}$$

Nakagami-m Fading

Similar to (6.7),

$$\mathcal{P}_{L|I_{\rm SP}}(\beta) = \binom{K}{L} \sum_{l=0}^{L} \binom{L}{l} (-1)^l \left(\frac{\mathbf{\Gamma}\left(m_{\rm RP}, \frac{I_{\rm th}-\beta}{P_{\rm R}\theta_{\rm RP}}\right)}{\mathbf{\Gamma}\left(m_{\rm RP}\right)} \right)^{K-L+l}, \tag{6.12}$$

Hence,

$$\mathcal{P}_L = \binom{K}{L} \sum_{l=0}^{L} \frac{\binom{L}{l}(-1)^l}{\mathbf{\Gamma}\left(m_{\rm SP}\right)\left(P_{\rm S}\theta_{\rm SP}\right)^{m_{\rm SP}}} \underbrace{\int_0^{I_{\rm th}} \left(\frac{\mathbf{\Gamma}\left(m_{\rm RP}, \frac{I_{\rm th}-\beta}{P_{\rm R}\theta_{\rm RP}}\right)}{\mathbf{\Gamma}\left(m_{\rm RP}\right)} \right)^{K-L+l} \beta^{m_{\rm SP}-1} e^{-\frac{\beta}{P_{\rm S}\theta_{\rm SP}}} \mathrm{d}\,\beta}_{\check{\mathcal{I}}_1}.$$

The integral in the last step can be evaluated with the aid of the multinomial theorem expansion as done in the previous chapter in (5.58). Specifically, it is given by

$$\check{\mathcal{I}}_1 = e^{-\frac{(K-L+l)I_{\rm th}}{P_{\rm R}\theta_{\rm RP}}} \sum_{\sum_{n=1}^{m_{\rm RP}} \check{k}_n = K-L+l} \check{C}_{\{\check{k}_n\}} \check{\mathcal{I}}_2, \tag{6.13}$$

where

$$\check{\mathcal{I}}_2 = \int_0^{I_{\rm th}} (I_{\rm th}-\beta)^{\check{D}_{\{\check{k}_n\}}} \beta^{m_{\rm SP}-1} e^{-\beta\check{\eta}_l} {\rm d}\beta, \tag{6.14}$$

$$\check{\eta}_l = \left(\frac{1}{P_{\rm S}\theta_{\rm SP}} - \frac{K-L+l}{P_{\rm R}\theta_{\rm RP}}\right), \tag{6.15}$$

$$\check{C}_{\{\check{k}_n\}} = \frac{\boldsymbol{\Gamma}\left(K-L+l+1\right)\left(\frac{1}{P_{\rm R}\theta_{\rm RP}}\right)^{\sum_{n=1}^{m_{\rm RP}}\check{k}_n(n-1)}}{\prod_{n=1}^{m_{\rm RP}}\left(\boldsymbol{\Gamma}\left(\check{k}_n+1\right)\boldsymbol{\Gamma}\left(n\right)^{\check{k}_n}\right)}, \tag{6.16}$$

$$\check{D}_{\{\check{k}_n\}} = \sum_{n=1}^{m_{\rm RP}} \check{k}_n(n-1), \tag{6.17}$$

with (6.13) obtained via the multinomial theorem [39, Section 24.1.2]. Now, the integral $\check{\mathcal{I}}_2$ in (6.14) is on the form of the Riemann-Liouville integral in [57, Eq. 3.383-1] when $\check{\eta}_l < 0$. Hence,

$$\check{\mathcal{I}}_2 = I_{\rm th}^{\check{D}_{\{\check{k}_n\}}+m_{\rm SP}} \boldsymbol{\mathcal{B}}\left(\check{D}_{\{\check{k}_n\}}+1, m_{\rm SP}\right) {}_1\boldsymbol{F}_1\left(m_{\rm SP}; \check{D}_{\{\check{k}_n\}}+m_{\rm SP}+1; -I_{\rm th}\check{\eta}_l\right). \tag{6.18}$$

When $\check{\eta}_l > 0$, we can again use the change of variables $y = I_{\rm th}-\beta$ then [57, Eq. 3.383-1] to get

$$\check{\mathcal{I}}_2 = e^{-I_{\rm th}\check{\eta}_l} I_{\rm th}^{\check{D}_{\{\check{k}_n\}}+m_{\rm SP}} \boldsymbol{\mathcal{B}}\left(m_{\rm SP}, \check{D}_{\{\check{k}_n\}}+1\right) {}_1\boldsymbol{F}_1\left(\check{D}_{\{\check{k}_n\}}+1; \check{D}_{\{\check{k}_n\}}+m_{\rm SP}+1; I_{\rm th}\check{\eta}_l\right). \tag{6.19}$$

Therefore, $\mathcal{P}_L$ is finally given as

$$\mathcal{P}_L = \binom{K}{L} \sum_{l=0}^{L} \frac{\binom{L}{l}(-1)^l e^{-\frac{(K-L+l)I_{\rm th}}{P_{\rm R}\theta_{\rm RP}}}}{\boldsymbol{\Gamma}\left(m_{\rm SP}\right)\left(P_{\rm S}\theta_{\rm SP}\right)^{m_{\rm SP}}} \sum_{\sum_{n=1}^{m_{\rm RP}}\check{k}_n = K-L+l} \frac{\boldsymbol{\Gamma}\left(K-L+l+1\right)}{\prod_{n=1}^{m_{\rm RP}}\left(\boldsymbol{\Gamma}\left(\check{k}_n+1\right)\boldsymbol{\Gamma}\left(n\right)^{\check{k}_n}\right)} \times \left(\frac{1}{P_{\rm R}\theta_{\rm RP}}\right)^{\check{D}_{\{\check{k}_n\}}} \check{\mathcal{I}}_2. \tag{6.20}$$

For $L=0$, $\mathcal{P}_0$ is given by

$$\mathcal{P}_0 = \int_0^{I_{\rm th}} \left(\frac{\mathbf{\Gamma}\left(m_{\rm RP}, \frac{I_{\rm th}-\beta}{P_{\rm R}\theta_{\rm RP}}\right)}{\mathbf{\Gamma}\left(m_{\rm RP}\right)} \right)^K \frac{\beta^{m_{\rm SP}-1} e^{-\frac{\beta}{P_{\rm S}\theta_{\rm SP}}}}{\mathbf{\Gamma}\left(m_{\rm SP}\right)\left(P_{\rm S}\theta_{\rm SP}\right)^{m_{\rm SP}}} {\rm d}\beta + \frac{\mathbf{\Gamma}\left(m_{\rm SP}, \frac{I_{\rm th}}{P_{\rm S}\theta_{\rm SP}}\right)}{\mathbf{\Gamma}\left(m_{\rm SP}\right)}. \quad (6.21)$$

Again, the integral involving higher powers of the upper regularized Gamma function is solved via its series expansion, multinomial theorem, then with the aid of the Riemann-Liouville integral in [57, Eq. 3.383-1] for $\left(\frac{1}{P_{\rm S}\theta_{\rm SD}} - \frac{K}{P_{\rm R}\theta_{\rm RP}}\right) < 0$ to yield

$$\begin{aligned}\mathcal{P}_0 &= \frac{\mathbf{\Gamma}\left(m_{\rm SP}, \frac{I_{\rm th}}{P_{\rm S}\theta_{\rm SP}}\right)}{\mathbf{\Gamma}\left(m_{\rm SP}\right)} + \frac{e^{-\frac{KI_{\rm th}}{P_{\rm R}\theta_{\rm RP}}}}{\mathbf{\Gamma}\left(m_{\rm SP}\right)\left(P_{\rm S}\theta_{\rm SP}\right)^{m_{\rm SP}}} \sum_{\sum_{n=1}^{m_{\rm RP}} \acute{k}_n = K} \frac{\mathbf{\Gamma}\left(K+1\right)}{\prod_{n=1}^{m_{\rm RP}} \left(\mathbf{\Gamma}\left(\acute{k}_n+1\right)\mathbf{\Gamma}\left(n\right)^{\acute{k}_n}\right)} \\ &\times \left(\frac{1}{P_{\rm R}\theta_{\rm RP}}\right)^{\acute{D}_{\{\acute{k}_n\}}} I_{\rm th}^{\acute{D}_{\{\acute{k}_n\}}+m_{\rm SP}} \boldsymbol{\mathcal{B}}\left(\acute{D}_{\{\acute{k}_n\}}+1, m_{\rm SP}\right) \\ &\times {}_1\boldsymbol{F}_1\left(m_{\rm SP}; \acute{D}_{\{\acute{k}_n\}}+m_{\rm SP}+1; -I_{\rm th}\left(\frac{1}{P_{\rm S}\theta_{\rm SD}} - \frac{K}{P_{\rm R}\theta_{\rm RP}}\right)\right), \end{aligned} \quad (6.22)$$

or, alternatively for $\left(\frac{1}{P_{\rm S}\theta_{\rm SD}} - \frac{K}{P_{\rm R}\theta_{\rm RP}}\right) > 0$, we get

$$\begin{aligned}\mathcal{P}_0 &= \frac{\mathbf{\Gamma}\left(m_{\rm SP}, \frac{I_{\rm th}}{P_{\rm S}\theta_{\rm SP}}\right)}{\mathbf{\Gamma}\left(m_{\rm SP}\right)} + \frac{e^{-\frac{KI_{\rm th}}{P_{\rm R}\theta_{\rm RP}}}}{\mathbf{\Gamma}\left(m_{\rm SP}\right)\left(P_{\rm S}\theta_{\rm SP}\right)^{m_{\rm SP}}} \sum_{\sum_{n=1}^{m_{\rm RP}} \acute{k}_n = K} \frac{\mathbf{\Gamma}\left(K+1\right)}{\prod_{n=1}^{m_{\rm RP}} \left(\mathbf{\Gamma}\left(\acute{k}_n+1\right)\mathbf{\Gamma}\left(n\right)^{\acute{k}_n}\right)} \\ &\times \left(\frac{1}{P_{\rm R}\theta_{\rm RP}}\right)^{\acute{D}_{\{\acute{k}_n\}}} e^{-I_{\rm th}\left(\frac{1}{P_{\rm S}\theta_{\rm SD}} - \frac{K}{P_{\rm R}\theta_{\rm RP}}\right)} I_{\rm th}^{\acute{D}_{\{\acute{k}_n\}}+m_{\rm SP}} \boldsymbol{\mathcal{B}}\left(m_{\rm SP}, \acute{D}_{\{\acute{k}_n\}}+1\right) \\ &\times {}_1\boldsymbol{F}_1\left(\acute{D}_{\{\acute{k}_n\}}+1; \acute{D}_{\{\acute{k}_n\}}+m_{\rm SP}+1; I_{\rm th}\left(\frac{1}{P_{\rm S}\theta_{\rm SD}} - \frac{K}{P_{\rm R}\theta_{\rm RP}}\right)\right), \end{aligned} \quad (6.23)$$

with

$$\acute{D}_{\{\acute{k}_n\}} = \sum_{n=1}^{m_{\rm RP}} \acute{k}_n (n-1). \quad (6.24)$$

6.3.2 Leveraging Direct S − D Link

The analysis of P_L follows directly from the no direct link case for $L = 1, 2, \cdots, K$. However, when a direct S − D link exists, communication can still take place even when no feasible relays exist. Thus, the event with probability $\mathcal{P}_0$ in the no direct link case is now further split into two sub-events. Specifically, communication can still succeed in the sub-event when the sum of the source and relay transmissions do not satisfy the interference constraint for all relays but the source alone does. Let us denote the probability of this sub-event by $\tilde{\mathcal{P}}_0$. It is then given by

$$\tilde{\mathcal{P}}_0 = \mathbb{P}\left\{\left(\bigcap_{k=1}^{K}(I_k > I_{\text{th}})\right) \cap (I_{\text{SP}} \leq I_{\text{th}})\right\}. \tag{6.25}$$

Note that I_k depends on I_{SP}. Nonetheless, $\{I_k\}_{k=1}^{K}$ are mutually independent given I_{SP}, and distributed as in (6.5).

Finally, when $I_{\text{SP}} > I_{\text{th}}$, with probability $\mathcal{P}_0 - \tilde{\mathcal{P}}_0$, communication fails resulting in an end-to-end SNR of $\gamma_{\text{e2e}} = 0$, and hence the distribution is a unit-step function at $\gamma_{\text{e2e}} = 0$. We can now write the end-to-end SNR CDF as

$$\begin{aligned} F_{\gamma_{\text{e2e}}}^{\text{IDL/DT}}(x) &= 1 \times \left(\mathcal{P}_0 - \tilde{\mathcal{P}}_0\right) + F_{\gamma_{\text{SD}}}(x)\,\tilde{\mathcal{P}}_0 + \sum_{L=1}^{K} F_{\gamma_{\text{e2e}}}^{\text{DL}}(x|L)\mathcal{P}_L \qquad (6.26)\\ &= \mathcal{P}_0 - \overline{F_{\gamma_{\text{SD}}}}(x)\,\tilde{\mathcal{P}}_0 + \sum_{L=1}^{K} F_{\gamma_{\text{e2e}}}^{\text{DL}}(x|L)\mathcal{P}_L. \qquad (6.27) \end{aligned}$$

$\tilde{\mathcal{P}}_0$ is given as follows for Rayleigh and Nakagami-m fading.

Rayleigh Fading

$$\begin{aligned}\tilde{\mathcal{P}}_0 &= \int_{\beta=0}^{I_{\rm th}} \left(e^{-\frac{I_{\rm th}-\beta}{P_{\rm R}\pi_{\rm RP}}}\right)^K \frac{e^{-\frac{\beta}{P_{\rm S}\pi_{\rm SP}}}}{P_{\rm S}\pi_{\rm SP}}{\rm d}\beta \\ &= \frac{P_{\rm R}\pi_{\rm RP}\left(e^{-\frac{KI_{\rm th}}{P_{\rm R}\pi_{\rm RP}}} - e^{-\frac{I_{\rm th}}{P_{\rm S}\pi_{\rm SP}}}\right)}{P_{\rm R}\pi_{\rm RP} - KP_{\rm S}\pi_{\rm SP}}, \qquad (6.28)\\ \mathcal{P}_0 - \tilde{\mathcal{P}}_0 &= e^{-\frac{I_{\rm th}}{P_{\rm S}\pi_{\rm SP}}}. \qquad (6.29)\end{aligned}$$

Nakagami-m Fading

$$\tilde{\mathcal{P}}_0 = \mathcal{P}_0 - \frac{\mathbf{\Gamma}\left(m_{\rm SP}, \frac{I_{\rm th}}{P_{\rm S}\theta_{\rm SP}}\right)}{\mathbf{\Gamma}\left(m_{\rm SP}\right)}. \qquad (6.30)$$

6.4 Numerical Evaluation

In this section, we numerically verify the theoretical findings derived in previous sections. All numerical results are evaluated by averaging over 10^7 sets of channel realizations with the parameters summarized in the caption of each figure. Also, for clarity of presentation, solid lines with unfilled marks are used to plot the theoretical results, while the same filled marks with no connecting lines are used for simulation results. Hence, curves with solid lines and filled marks indicate perfect matching between theoretical and simulation results.

6.4.1 End-to-End CDF

In Fig. 6.2, the CDF of the end-to-end SNR is plotted for the different relay selection protocols. As shown, since exact performance expressions were derived, the theoretical and simulation results match perfectly. It can be noticed that the CDF does not start from zero, which is typically encountered when the analysis involves mixed random variables. Specifically, this shift is due to the unit-step distributions in the events when the end-to-

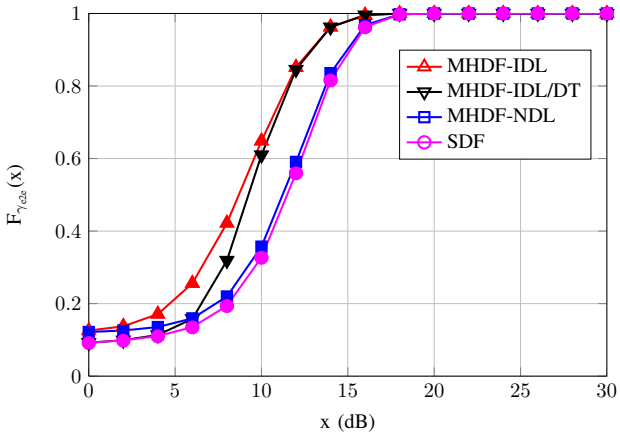

Figure 6.2: CDF of the end-to-end SNR, for $\pi_{\mathrm{SR}} = \pi_{\mathrm{RD}} = 15$ dB, $\pi_{\mathrm{RR}} = \pi_{\mathrm{SD}} = 5$ dB, $\pi_{\mathrm{SP}} = 2$ dB, $\pi_{\mathrm{RP}} = 4$ dB, $I_{\mathrm{th}} = 6$ dB, $m_{\mathrm{SR}} = m_{\mathrm{RD}} = 2$, $m_{\mathrm{RR}} = m_{\mathrm{SD}} = m_{\mathrm{SP}} = m_{\mathrm{RP}} = 1$, $\delta = 1$, $P_{\mathrm{S}} = P_{\mathrm{R}} = 1$, and $K = 5$ relays.

end communication totally fails due to the infeasibility of the relays/source transmissions, thereby yielding an SNR value of zero regardless of the secondary link gains. The event of total communication failure is less probable when a direct link exists, which can be easily noticed from the theoretic expressions, and hence, the shift has a lower value in the scenarios leveraging the direct link (IDL/DT and SDF). This shift is mainly controlled by I_{th}, and it decreases as I_{th} increases.

6.4.2 Outage Probability vs. No. of Relays

When a fixed-rate transmission is adopted, the SNR CDF directly yields the outage probability in the channel. In Fig. 6.3, we plot the outage probability versus the number of relays, K, with a source rate of $R = 1$ bpcu, yielding an SNR threshold of $\alpha = 2^R - 1$ below which outage is declared. There are two important observations in this figure that need to be highlighted. First, it is clear that relay selection has a promising potential to boost the performance of the secondary system in underlay networks, in both scenarios of coverage extension and throughput enhancement. Even when a high interference threshold I_{th} is allowed by the primary user, the performance can be seriously limited for single relay cooperation, while noticeable enhancements can be offered when more relays are available,

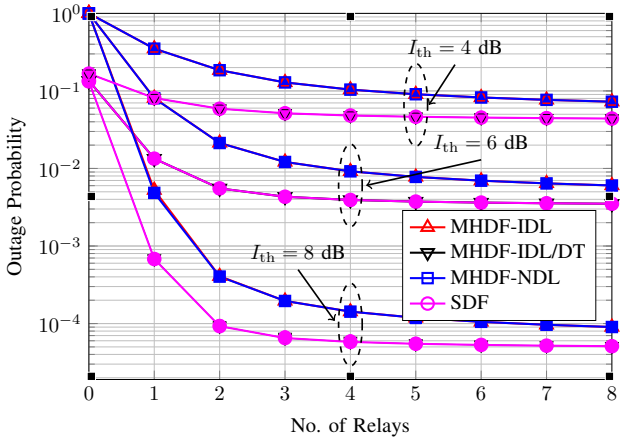

Figure 6.3: Outage probability vs. No. of Relays, for $\pi_{\text{SR}} = \pi_{\text{RD}} = 25$ dB, $\pi_{\text{RR}} = 3$ dB, $\pi_{\text{SD}} = 5$ dB, $\pi_{\text{SP}} = 0$ dB, $\pi_{\text{RP}} = 1$ dB, $m_{\text{SR}} = m_{\text{RD}} = m_{\text{RR}} = m_{\text{SD}} = m_{\text{SP}} = m_{\text{RP}} = 2$, $\delta = 1$, $P_{\text{S}} = P_{\text{R}} = 1$, $I_{\text{th}} \in \{4, 6, 8\}$ dB, and $R = 1$ bpcu.

especially when no direct link exists. Second, a plateau exists as K increases, and its value depends on the interference threshold and the average interference link gains. The average secondary link gains are found to only impact the behavior of how fast this plateau is eventually reached. Clearly, since the $\text{S} - \text{P}$ link is a common interfering link whenever any secondary communication occurs, its average gain significantly influences the value of such a plateau. This plateau effect can be considerably enhanced if means are proposed to make use of the diversity of the relays in the specific channel realizations of the $\text{S} - \text{P}$ link that exceed I_{th} and prevent any secondary system communication.

6.5 Conclusion

In this work, the performance of FDRS techniques was analyzed in underlay networks where a primary user dictates an interference threshold that cannot be exceeded by the secondary transmissions. The performance is analyzed for both relaying scenarios where either coverage extension or throughput enhancement is targeted. The derived exact analytical results are shown to perfectly match with those obtained via numerical simulations.

Part III

Buffer-Aided Relaying

Chapter 7

Buffer-Aided Half-Duplex Relaying

Until this point, it was assumed that no packet queuing is allowed at the relay. Such a physical restriction at the intermediate node causes two main performance limitations over fading channels:

1. **Instantaneous End-to-End Capacity Bottleneck:** First, the relay does not have information of its own, and hence, it can forward only what it has instantaneously received over its incoming link. Second, without a queuing capability, it cannot store any excess information that exceeds the capacity of its outgoing link. Hence, the instantaneous end-to-end capacity is limited by the minimum of the instantaneous capacities of the incoming and outgoing links. Accordingly, the average end-to-end capacity is the statistical average over such a minimum, multiplied by a factor of $\frac{1}{2}$ due to half-duplex relay operation.

2. **Round-Robin Listening/Forwarding:** The round-robin first-/second-hop activation is also a direct consequence of buffer-less relaying. After the relay forwards the packet it instantaneously received, it can do nothing except to listen again to the source. This happens regardless of the relative incoming/outgoing link qualities.

Keeping these two limitations in mind, we go over the main performance enhancement milestones in the available buffer-aided relaying literature in the following section.

7.1 Related Work

Buffer-aided relaying was first proposed in [84] in order to boost the *average* capacity of DF HDR, which is known to be limited by the minimum *instantaneous* capacity of the first and second hops. The idea can be easily explained as follows. As noted earlier in buffer-less relaying, the average end-to-end capacity can be simply given as the statistical average of the minimum of the relay's two instantaneous incoming/outgoing link capacities. Now, assume the relay is equipped with a sufficiently large buffer, and that a round-robin listening/forwarding is still adopted. If both the listening and forwarding phases are allocated a longer time that spans a sufficiently large number of channel realizations, with the received packets queued at the relay in the listening phase, the average capacity can be enhanced. Specifically, as the phase time and buffer size increase, the capacity of each hop approaches its statistical average. Accordingly, the average end-to-end capacity is hence enhanced to approach the minimum of the two link averages, multiplied by the half-duplex rate loss factor, i.e., $\frac{1}{2}$. Therefore, the buffering capability has relaxed the capacity bottleneck from being the average of the minimum to the *minimum of the averages*. In other words, the impact of packet loss at the relay due to instances of a severely attenuated $\mathrm{R}-\mathrm{D}$ link is mitigated by the ability to queue data until the link becomes reliable. Of course this comes at the expense of an increased end-to-end packet delay due to queuing.

Further capacity gains were demonstrated by Zlatanov *et al.* in [85] via the relaxation of the round-robin listening/forwarding phase allocation and adopting instead an adaptive link selection approach based on the instantaneous quality of the two hops. This adaptive link selection allowed for the further harvesting of the benefits of *multi-hop diversity* [86]. Through such an adaptive link selection, the instantaneous end-to-end capacity in essence tends to approach the *maximum* of the two instantaneous capacities, taking empty and full relay buffer states into account. The half-duplex rate loss of $\frac{1}{2}$ should be still taken into account.

Previous research on buffer-aided relaying with adaptive link selection only utilized the available CSI at the transmitters. In the available literature, however, the system performance did not exploit any possible knowledge of the BSI. In specific, the designed and analyzed protocols in the literature did not distinguish between the relay buffer states except for the full-buffer and empty-buffer ones. Such protocols first check to eliminate the outgoing link selection if the buffer is empty, and eliminate the incoming link selection if the buffer is full, then select the link with maximum instantaneous capacity out of the remaining. At channel instances where both links can be utilized, i.e., the buffer is neither full nor empty, the link with the maximum instantaneous capacity is always favored regardless of the number of packets in the relay's queue. From an average capacity perspective, this instantaneous maximization approach can be still a shortsighted one.

7.1.1 Potentials of Leveraging BSI

To easily imagine the behavior of the buffer-aided half-duplex two-hop channel with the knowledge of only full or empty buffer states, we examine two limiting cases. Let us call the specific probabilities of a buffer being in the full or empty state as the relay queue's *blocking* and *lacking* probabilities, respectively. In the limiting cases when either the first or the second hop has a much larger average gain, the average performance of buffer-aided relaying will end up to be very similar to buffer-less relaying, if only the full and empty buffer states are considered. On the one hand, if the $\mathrm{S}-\mathrm{R}$ link has a much larger gain on average, the $\mathrm{S}-\mathrm{R}$ link will be mostly favored, causing the relay to build up in the beginning, then continue to forward a packet and receive a packet in a round-robin fashion. This behavior is caused by the high blocking probability. On the other hand, when the $\mathrm{R}-\mathrm{D}$ link has a much larger average gain, the relay will be selected to forward as soon as it receives a packet. It is then expected to continue like that in the same round-robin manner due to the high lacking probability. This behavior is not limited only to such limiting cases, but it can be easily expected to exist at some level in any scenario with asymmetric average gains of

the two hops, while its effect becomes more severe as the asymmetry widens. Hence, when considering the optimization of the average performance over fading channels, it is important to minimize these blocking and lacking probabilities. The knowledge of all the buffer states can help in this direction. For instance, the system can *proactively* advise the relay node, based on the channel/buffer states and statistics, to either forward or listen early enough to minimize the blocking and lacking effects, respectively.

7.1.2 Leveraging BSI in Fixed-Rate Transmission

The previous work mainly discussed variable-rate transmission where the information content in each packet varies according to the instantaneous channel quality. To emphasize the idea that link selection based only on the instantaneous CSI can limit the performance, we add the following for fixed-rate transmission scenarios. In fixed-rate transmission systems, link selection based on the exact channel qualities is of less significance compared to variable-rate systems. Indeed, what matters most in the former systems is whether the link supports such a fixed-rate or not, i.e., its binary outage state. In other words, if the two links are outage-free, instantaneously favoring the stronger link over the other would be pointless, even from an instantaneous performance point of view. In this scenario, leveraging instantaneous BSI in addition to the outage state information can significantly boost the end-to-end throughput when taken into account.

7.1.3 Contribution

In this work, we consider exploiting both the BSI and partial transmit CSI (knowledge of binary outage state) at the transmitters in buffer-aided relaying. In this chapter, we study the impact of the additional utilization of BSI on the performance of buffer-aided HDR systems, followed by studying buffer-aided FDR in the following chapter.

7.2 System Model

7.2.1 Channel Model

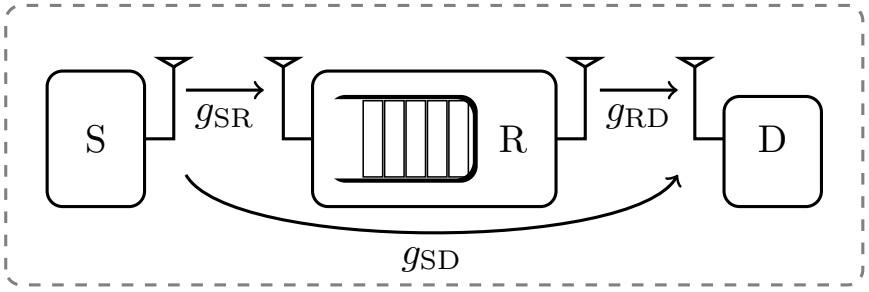

Figure 7.1: A buffer-aided half-duplex relay channel.

We study the two-hop cooperative setting depicted in Fig. 7.1, where a source S communicates with a destination D via a half-duplex DF relay R. The relay R is equipped with a buffer of size N data packets. As shown, g_{SR}, g_{RD} and g_{SD} denote the fading gains, i.e., the squared magnitude of the complex fading coefficients, for the $\mathrm{S}-\mathrm{R}$, $\mathrm{R}-\mathrm{D}$ and $\mathrm{S}-\mathrm{D}$ links, respectively. The channels are assumed to experience block fading, where the channel gains remain constant over one block, and vary independently from one block to another following a general probability distribution, i.e., the analysis to follow is not limited to a specific fading model.

It is assumed that the BSI is known at the source via acknowledgment (ACK)/negative acknowledgment (NACK) messages from the relay, like for instance in [87]. Also, CSI is assumed available at the transmitters, not necessarily of the exact channel state, but only of its outage state. This can be provided, for instance, via one-bit feedback messages. Finally, the link outage probabilities are calculated at the transmitters with their knowledge of the transmission rate and the channel statistics.

7.2.2 Signal Model

We assume that the source adopts a fixed rate transmission with a source rate of R bpcu. Unlike in the previous part where outage probability was taken as the main performance metric, it is more convenient in the subsequent queuing analysis to analyze the end-to-end throughput. Accordingly, when comparing DT, HDR, and FDR, or in hybrid systems that involve switching between more than one transmission scheme, we fix the source rate to that of DT, i.e., R, calculate the link outage probabilities, then account for the rate loss in HDR in the calculation of the final throughput expressions. The transmission power is fixed for the source and the relay to P_{S} and P_{R}, respectively. Also, the received signals at the relay and the destination are perturbed by AWGN with zero mean and variance σ_{R}^2 and σ_{D}^2, respectively.

The instantaneously received SNR via the S$-$R, R$-$D, or S$-$D link is given, respectively, by

$$\gamma_{\mathrm{SR}} = \frac{P_{\mathrm{S}} g_{\mathrm{SR}}}{\sigma_{\mathrm{R}}^2}, \qquad \gamma_{\mathrm{RD}} = \frac{P_{\mathrm{R}} g_{\mathrm{RD}}}{\sigma_{\mathrm{D}}^2}, \qquad \text{and} \quad \gamma_{\mathrm{SD}} = \frac{P_{\mathrm{S}} g_{\mathrm{SD}}}{\sigma_{\mathrm{D}}^2}. \tag{7.1}$$

7.3 Transmission Scheduling Scheme

The cooperative system seeks to adopt a source/relay transmission scheduling scheme that maximizes the end-to-end throughput. For this purpose, the access to the channel utilizes all the available BSI and/or CSI.

The packet queuing at the relay node can be modeled as a *birth-death Markov chain* as shown in Fig. 7.2, where the different states represent the number of packets in the relay's queue. The birth-death model is enforced by the fact that the relay neither receives nor transmits more than one packet in any given slot.

Let ϵ_n denote the steady-state probability of the queue being in state n, while λ_n and μ_n respectively denote the state increment and decrement probability when the queue is at

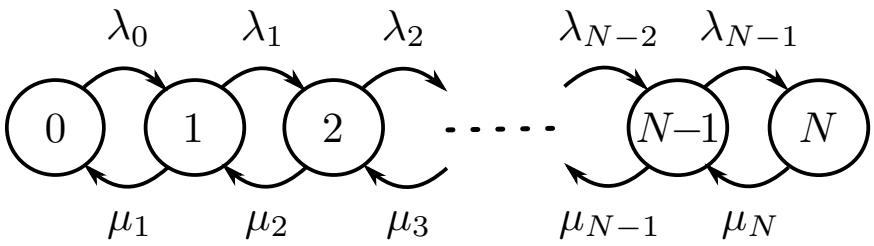

Figure 7.2: Birth-death Markov process. Transitions from a state to itself are omitted for visual clarity.

state n. The local balance equations of the Markov chain are given by

$$\epsilon_n \lambda_n \quad = \epsilon_{n+1} \mu_{n+1}, \quad 0 \leq n \leq N-1. \tag{7.2}$$

Since $\sum_{n=0}^{N} \epsilon_n = 1$, we have

$$\epsilon_n = \epsilon_0 \prod_{\ell=0}^{n-1} \frac{\lambda_\ell}{\mu_{\ell+1}}, \quad \text{with } \epsilon_0 = \left(1 + \sum_{n=1}^{N} \prod_{\ell=0}^{n-1} \frac{\lambda_\ell}{\mu_{\ell+1}}\right)^{-1}. \tag{7.3}$$

Based on the ACK/NACK messages sent by the destination near the end of the time slot, the relay decides whether or not to keep a correctly received packet in its buffer. Specifically, the relay keeps the packets that it decodes correctly, but have not been successfully decoded at the destination. If the relay can decode the source packet, it sends back an ACK; otherwise, it sends back a NACK. In case of failure in decoding the source's packet at both the relay and the destination, a re-transmission of the packet by the source is required in the following time slot.

In what follows, we study the queue dynamics based on the available BSI and/or CSI at the transmitters.

7.3.1 Transmit BSI/No Transmit CSI

We study here the buffer-aided relaying setting assuming only BSI knowledge at the source, with no available instantaneous CSI knowledge at the transmitters. Accordingly, the source/re-

lay channel access can be only based on the instantaneous BSI knowledge, in addition to statistical CSI. Specifically, when the relaying queue contains n packets, the channel is accessed by the source with probability $0 \leq \beta_n \leq 1$, while it is accessed by the relay when the source is inactive, i.e., with probability $\overline{\beta_n} = 1 - \beta_n$. If the buffer is empty, the source accesses the channel with probability 1, i.e., $\beta_0 = 1$. A handshaking mechanism is assumed available between the source and the relay, which can take place, for instance, via a dedicated low-rate control channel.

Let $Q(b)$ denote the number of packets in the queue at the beginning of block b. The transition probabilities of the states are given as follows.

$$\lambda_n = \mathbb{P}\{Q(b) = n+1 | Q(b-1) = n\} = \beta_n \overline{\mathcal{P}_{\mathrm{SR}}} \mathcal{P}_{\mathrm{SD}}, \quad 0 \leq n \leq N-1, \tag{7.4}$$

$$\mu_n = \mathbb{P}\{Q(b) = n-1 | Q(b-1) = n\} = \overline{\beta_n}\ \overline{\mathcal{P}_{\mathrm{RD}}}, \quad 1 \leq n \leq N. \tag{7.5}$$

The source throughput, $\mathcal{T}_{\mathrm{S}}$, is defined as the probability of successful packet delivery to the relay/destination. Hence, it is given by

$$\mathcal{T}_{\mathrm{S}} = (1 - \mathcal{P}_{\mathrm{SR}}\mathcal{P}_{\mathrm{SD}}) \sum_{n=0}^{N-1} \epsilon_n \beta_n + \overline{\mathcal{P}_{\mathrm{SD}}} \epsilon_N \beta_N. \tag{7.6}$$

The expression of $\mathcal{T}_{\mathrm{S}}$ can be explained as follows. A data packet is delivered successfully if either the S$-$D link or the S$-$R link is not in outage. If the buffer is full, it would not accept any extra packets from the source regardless of the S $-$ R link outage state. In this case, the transmitted packet must be delivered only through the S $-$ D link. It should be noted that the throughput calculated from (7.6) implicitly accounts for the HDR rate loss. Indeed, (7.6) only counts the time slots where the relay listens to the source, while ignoring those for relay forwarding to reflect the rate loss effect. It should be also noted that, since the relay has a finite buffer size, the throughput calculated from the source departures, i.e., $\mathcal{T}_{\mathrm{S}}$ in 7.6) is also equal to that calculated from the destination's perspective as arrivals, denoted as $\mathcal{T}_{\mathrm{D}}$. We analytically show this in Appendix 7.A.

7.3.2 Transmit BSI/Partial Transmit CSI

We assume here that the transmitters know the channel outage states in addition to the buffer state. This can be attained, for instance, via one-bit feedback messages from the receivers. Due to the existence of three fading links, each with a binary state space, a channel can fall into one out of eight possible states.

- If the $\mathrm{S}-\mathrm{D}$ link is not in outage, which covers four out of the eight possible channel states, then direct transmission is successful regardless of the state of the other two links.

- If the $\mathrm{S}-\mathrm{D}$ is in outage, then the access scheme depends on the outage states of the other two links as follows:

  - If the $\mathrm{S}-\mathrm{R}$ link is in outage, then the relay transmits if the $\mathrm{R}-\mathrm{D}$ link is not in outage and the buffer is nonempty.

  - If the $\mathrm{R}-\mathrm{D}$ link is in outage, then the source transmits if the $\mathrm{S}-\mathrm{R}$ link is not in outage and the buffer is not full.

  - If both the $\mathrm{S}-\mathrm{R}$ and $\mathrm{R}-\mathrm{D}$ links are not in outage, we use ξ_n to denote the probability of source transmission when the relay has n packets. Hence, the probability of relay transmission is $\overline{\xi_n} = 1 - \xi_n$ if the buffer has n packets. It is clear that $\xi_0 = 1$ and $\xi_N = 0$.

  - If both the $\mathrm{S}-\mathrm{R}$ and $\mathrm{R}-\mathrm{D}$ links are in outage, it is clear that the opportunity is missed and no communication can take place.

According to the explanation above, the transition probabilities of the birth-death process for state increments and decrements are given, respectively, by

$$\lambda_n = \mathcal{P}_{\mathrm{SD}}\overline{\mathcal{P}_{\mathrm{SR}}}\left(\mathcal{P}_{\mathrm{RD}} + \overline{\mathcal{P}_{\mathrm{RD}}}\xi_n\right), \quad 0 \leq n \leq N-1, \tag{7.7}$$

$$\mu_n = \mathcal{P}_{\mathrm{SD}}\overline{\mathcal{P}_{\mathrm{RD}}}\left(\mathcal{P}_{\mathrm{SR}} + \overline{\mathcal{P}_{\mathrm{SR}}}\ \overline{\xi_n}\right), \quad 1 \leq n \leq N. \tag{7.8}$$

It also follows that the source throughput is given as

$$\mathcal{T}_{\mathrm{S}} = \overline{\mathcal{P}_{\mathrm{SD}}} + \mathcal{P}_{\mathrm{SD}}\overline{\mathcal{P}_{\mathrm{SR}}}\mathcal{P}_{\mathrm{RD}}(1-\epsilon_N) + \mathcal{P}_{\mathrm{SD}}\overline{\mathcal{P}_{\mathrm{SR}}}\,\overline{\mathcal{P}_{\mathrm{RD}}}\sum_{n=0}^{N-1}\xi_n\epsilon_n, \tag{7.9}$$

with $\{\epsilon_n\}_{n=0}^{N}$ having the same form as in (7.3).

7.4 End-to-End Throughput Maximization

In this section, our objective is to design the source access probabilities in order to maximize the end-to-end throughput expressions given in (7.6) and (7.9).

7.4.1 Transmit BSI/No Transmit CSI

Our objective is to solve the following maximization problem:

$$\max_{0\leq\{\beta_n\}_{n=0}^{N}\leq 1} \mathcal{T}_{\mathrm{S}}, \text{ s.t. } \beta_0 = 1. \tag{7.10}$$

The objective function, $\mathcal{T}_{\mathrm{S}}$, in this optimization problem is not concave in the optimization variables, $\{\beta_n\}_{n=0}^{N}$. Fortunately, it can be solved as follows.

Let $K = \frac{\overline{\mathcal{P}_{\mathrm{SR}}}\mathcal{P}_{\mathrm{SD}}}{\overline{\mathcal{P}_{\mathrm{RD}}}}$. Using (7.3), (7.4), and (7.5), the term $\epsilon_n\beta_n$ can be written as

$$\epsilon_n\beta_n = \epsilon_0\prod_{\ell=0}^{n-1}\frac{\lambda_\ell}{\mu_{\ell+1}}\beta_n \quad = \epsilon_0 K^n\prod_{i=1}^{n}\frac{\beta_i}{\overline{\beta_i}} = \epsilon_0 K^n\Upsilon_n. \tag{7.11}$$

where $\Upsilon_n = \prod_{i=1}^{n}\frac{\beta_i}{\overline{\beta_i}}$. Note that $\Upsilon_0 = 1$, $\Upsilon_1 = \frac{\beta_1}{\overline{\beta_1}}$, $\Upsilon_2 = \Upsilon_1\frac{\beta_2}{\overline{\beta_2}}$, $\Upsilon_3 = \Upsilon_2\frac{\beta_3}{\overline{\beta_3}}$ and so on. Since $\Upsilon_n = \Upsilon_{n-1}\frac{\beta_n}{\overline{\beta_n}}$, then

$$\frac{\epsilon_n}{\epsilon_0} = K^n\frac{\Upsilon_n}{\beta_n} = K^n\left(\Upsilon_{n-1} + \Upsilon_n\right), \tag{7.12}$$

and

$$\beta_n = \frac{\Upsilon_n}{\Upsilon_n + \Upsilon_{n-1}}, \text{ for } n = 1, 2, ..., N. \tag{7.13}$$

With such an adopted substitution of variables, we can then write the throughput maximization problem as:

$$\max_{\{\Upsilon_n\}_{n=0}^{N} \geq 0} \mathcal{T}_{\mathrm{S}} = \frac{\overline{\mathcal{P}_{\mathrm{SR}}\mathcal{P}_{\mathrm{SD}}} \sum_{n=0}^{N-1} K^n \Upsilon_n + \overline{\mathcal{P}_{\mathrm{SD}}} K^N \Upsilon_N}{1 + \sum_{n=1}^{N} K^n \left(\Upsilon_n + \Upsilon_{n-1}\right)}, \text{ s.t. } \Upsilon_0 = 1. \tag{7.14}$$

Note that $\{\beta_n\}_{n=1}^{N-1}$ can be obtained back from the optimal values of $\{\Upsilon_n\}_{n=1}^{N-1}$ using (7.13).

In what follows, we provide an analytical solution to this problem. The denominator of the objective function of (7.14) can be rewritten as $(1+K)(1+\sum_{n=1}^{N-1} K^n \Upsilon_n + \frac{K^N}{1+K}\Upsilon_N)$. Therefore, the objective function becomes $\mathcal{T}_{\mathrm{S}} = \frac{\overline{\mathcal{P}_{\mathrm{SR}}\mathcal{P}_{\mathrm{SD}}}}{1+K} \frac{\theta+\vartheta\Upsilon_N}{\theta+\varepsilon\Upsilon_N}$, where $\theta = 1+\sum_{n=1}^{N-1} K^n \Upsilon_n \geq 1$, $\vartheta = \frac{\overline{\mathcal{P}_{\mathrm{SD}}}}{\overline{\mathcal{P}_{\mathrm{SR}}\mathcal{P}_{\mathrm{SD}}}} K^N$, and $\varepsilon = \frac{K^N}{1+K}$. The first derivative of $\mathcal{T}_{\mathrm{S}}$ with respect to Υ_N is given by

$$\frac{\partial \mathcal{T}_{\mathrm{S}}}{\partial \Upsilon_N} = \frac{\overline{\mathcal{P}_{\mathrm{SR}}\mathcal{P}_{\mathrm{SD}}}}{1+K} \frac{\theta(\vartheta - \varepsilon)}{(\theta + \varepsilon\Upsilon_N)^2}. \tag{7.15}$$

Note that given K, ϑ and ε, it is straightforward to show that $\vartheta < \varepsilon$ when $\mathcal{P}_{\mathrm{RD}} < \mathcal{P}_{\mathrm{SD}}$. In this case, the derivative with respect to Υ_N is always negative and the maximum of $\mathcal{T}_{\mathrm{S}}$ is attained when $\Upsilon_N = 0$. This means that when $\mathcal{P}_{\mathrm{RD}} < \mathcal{P}_{\mathrm{SD}}$, the optimal $\beta_N = 0$, and $\mathcal{T}_{\mathrm{S}} = \frac{(1-\mathcal{P}_{\mathrm{SR}}\mathcal{P}_{\mathrm{SD}})}{1+K}$ regardless of θ. This has the following intuitive explanation. When $\Upsilon_N = 0$, $\mathcal{T}_{\mathrm{S}}$ becomes independent of Υ_n and hence β_n for all $n \in \{1, 2, \ldots, N-1\}$. If $\{\beta_n\}_{n=1}^{N-1}$ are set to zero, then whenever the relay gets a packet, it will just attempt to transmit it to the destination while the source remains silent. Once it succeeds, the source transmits a new packet with probability one. If β_n, $n \in \{1, 2, \ldots, N-1\}$, are set to one, the source transmits with probability one in each time slot, any packet that fails to reach the destination but reaches the relay will be stored in the relay. Once the buffer is full, the relay transmits (and the source remains idle) with probability one. This renders the buffer size unimportant.

If $\vartheta > \varepsilon$, or equivalently if $\mathcal{P}_{\mathrm{RD}} > \mathcal{P}_{\mathrm{SD}}$, then the derivative is always positive and the maximum of $\mathcal{T}_{\mathrm{S}}$ is attained when $\Upsilon_N = \infty$ (or equivalently $\beta_N = 1$). It can be shown that, in this case, the corresponding optimal θ is [1] The optimal $\mathcal{T}_{\mathrm{S}}$ is thus given by $\frac{\overline{\mathcal{P}_{\mathrm{SR}}\mathcal{P}_{\mathrm{SD}}}}{1+K}\frac{\vartheta}{\varepsilon} = \overline{\mathcal{P}_{\mathrm{SD}}}$, thereby indicating that the relay is not helpful to the source in this case. This also has the following intuitive explanation. If the outage probability of the direct path is lower than that of the two-hop path, the source justifiably neglects the relay cooperation with the additional rate penalty it incurs due to two-hop transmission, where a packet needs at least two time slots to be delivered to the destination through the relay. Hence, it relies solely on the direct link which accordingly provides higher throughput. Therefore, the average throughput in this case is equal to the probability of the direct link being not in outage.

To summarize, the optimal throughput with BSI and without transmit CSI is given by

$$\mathcal{T}_{\mathrm{S}} = \begin{cases} \frac{\overline{\mathcal{P}_{\mathrm{SR}}\mathcal{P}_{\mathrm{SD}}}\,\overline{\mathcal{P}_{\mathrm{RD}}}}{\overline{\mathcal{P}_{\mathrm{RD}}}+\overline{\mathcal{P}_{\mathrm{SR}}}\mathcal{P}_{\mathrm{SD}}}, & \text{if } \mathcal{P}_{\mathrm{RD}} \leq \mathcal{P}_{\mathrm{SD}}, \\ \overline{\mathcal{P}_{\mathrm{SD}}}, & \text{if } \mathcal{P}_{\mathrm{RD}} > \mathcal{P}_{\mathrm{SD}}. \end{cases} \tag{7.16}$$

The optimal throughput is attained when $\mathcal{P}_{\mathrm{RD}} \leq \mathcal{P}_{\mathrm{SD}}$ via setting $\beta_0 = 1$ and $\beta_N = 0$ for any values of $\{\beta_n\}_{n=1}^{N-1}$, while it is attained at $\mathcal{P}_{\mathrm{RD}} > \mathcal{P}_{\mathrm{SD}}$ when the relay is deactivated.

7.4.2 Transmit BSI/Partial Transmit CSI

When outage state information is further supplied to the transmitters, the throughput in (7.9) can be written as

$$\mathcal{T}_{\mathrm{S}} = \overline{\mathcal{P}_{\mathrm{SD}}} + \mathcal{P}_{\mathrm{SD}}\overline{\mathcal{P}_{\mathrm{SR}}}\mathcal{P}_{\mathrm{RD}} + \mathcal{P}_{\mathrm{SD}}\overline{\mathcal{P}_{\mathrm{SR}}}\phi_{\mathrm{S}}, \tag{7.17}$$

[1] This can be shown using $\frac{\partial \mathcal{T}_{\mathrm{S}}}{\partial \theta}$. If $\varepsilon \geq \vartheta$, $\frac{\partial \mathcal{T}_{\mathrm{S}}}{\partial \theta}$ is always negative regardless of the other parameters, e.g., $\{\Upsilon_n\}_{n=1}^{N}$. Hence, the value of θ that maximizes $\mathcal{T}_{\mathrm{S}}$ is its lowest feasible value. Since $\theta = 1 + \sum_{n=1}^{N-1} K^n \Upsilon_n$, and $\sum_{n=1}^{N-1} K^n \Upsilon_n \geq 0$, then the lowest feasible value of θ is equal to 1.

where

$$\phi_{\mathrm{S}} = \frac{\overline{\mathcal{P}_{\mathrm{RD}}} + \overline{\mathcal{P}_{\mathrm{RD}}} \sum_{n=1}^{N-1} \xi_n \prod_{\ell=0}^{n-1} \frac{\lambda_\ell}{\mu_{\ell+1}} - \mathcal{P}_{\mathrm{RD}} \prod_{\ell=0}^{N-1} \frac{\lambda_\ell}{\mu_{\ell+1}}}{1 + \sum_{n=1}^{N} \prod_{\ell=0}^{n-1} \frac{\lambda_\ell}{\mu_{\ell+1}}}. \tag{7.18}$$

Maximizing $\mathcal{T}_{\mathrm{S}}$ is equivalent to maximizing ϕ_{S}. We define a new set of variables, $\{\Psi_n\}_{n=1}^{N}$, as

$$\Psi_n = \prod_{\ell=0}^{n-1} \frac{\lambda_\ell}{\mu_{\ell+1}} \text{ for } n = 1, 2, \ldots, N. \tag{7.19}$$

With the definition in (7.19), we can express (7.18) as

$$\phi_{\mathrm{S}} = \frac{\overline{\mathcal{P}_{\mathrm{RD}}} + \overline{\mathcal{P}_{\mathrm{RD}}} \sum_{n=1}^{N-1} \xi_n \Psi_n - \mathcal{P}_{\mathrm{RD}} \Psi_N}{1 + \sum_{n=1}^{N} \Psi_n}. \tag{7.20}$$

Now, by expressing $\{\xi_n \Psi_n\}_{n=1}^{N-1}$ as a linear combination of $\{\Psi_n\}_{n=1}^{N-1}$, the objective function of the optimization problem becomes a linear-fractional function in $\{\Psi_n\}_{n=1}^{N}$ that can be efficiently solved. From (7.19), and $\forall n \in \{2, 3, \cdots, N\}$, we get

$$\frac{\Psi_n}{\Psi_{n-1}} = \frac{\lambda_{n-1}}{\mu_n} = \frac{\overline{\mathcal{P}_{\mathrm{SR}}} \left(\mathcal{P}_{\mathrm{RD}} + \overline{\mathcal{P}_{\mathrm{RD}}} \xi_{n-1}\right)}{\overline{\mathcal{P}_{\mathrm{RD}}} \left(\mathcal{P}_{\mathrm{SR}} + \overline{\mathcal{P}_{\mathrm{SR}}}\, \overline{\xi_n}\right)} = \frac{\overline{\mathcal{P}_{\mathrm{SR}}} \left(\mathcal{P}_{\mathrm{RD}} + \overline{\mathcal{P}_{\mathrm{RD}}} \xi_{n-1}\right)}{\overline{\mathcal{P}_{\mathrm{RD}}} \left(1 - \overline{\mathcal{P}_{\mathrm{SR}}} \xi_n\right)}. \tag{7.21}$$

Therefore, we get the following recurrence relation between $\Psi_n \xi_n$ and $\Psi_{n-1} \xi_{n-1}$ as

$$\Psi_n \xi_n = a \Psi_n - b \Psi_{n-1} - \Psi_{n-1} \xi_{n-1}. \tag{7.22}$$

with $a = \frac{1}{\overline{\mathcal{P}_{\mathrm{SR}}}}$ and $b = \frac{\mathcal{P}_{\mathrm{RD}}}{\overline{\mathcal{P}_{\mathrm{RD}}}}$. Since $\Psi_1 = \frac{\lambda_0}{\mu_1}$ from (7.19), then by substituting for λ_0 and μ_1 from (7.7) and (7.8), we get

$$\Psi_1 \xi_1 = a \Psi_1 - \alpha, \tag{7.23}$$

where $\alpha = \frac{1}{\overline{\mathcal{P}_{\mathrm{RD}}}}$. Starting from (7.23), we can finally obtain $\Psi_n \xi_n$ as:

$$\Psi_n \xi_n = a\Psi_n + \textstyle\sum_{\ell=1}^{n-1} (-1)^{n-\ell}(a+b)\Psi_\ell + (-1)^n \alpha. \tag{7.24}$$

Noting that $\sum_{n=1}^{l} (-1)^n = -1$ when l is odd and 0 when l is even, we get

$$\sum_{n=1}^{N-1} \Psi_n \xi_n = \begin{cases} a\Psi_{N-1} - b\Psi_{N-2} + a\Psi_{N-3} - \cdots - b\Psi_1, & N \text{ odd}, \\ a\Psi_{N-1} - b\Psi_{N-2} + a\Psi_{N-3} - \cdots + a\Psi_1 - \alpha, & N \text{ even}. \end{cases} \tag{7.25}$$

Substituting (7.25) in (7.18), we obtain the following linear-fractional program:

$$\begin{aligned} \max_{\boldsymbol{\Psi}} \quad & \tfrac{\boldsymbol{c}^\dagger \boldsymbol{\Psi} + d}{\mathbf{1}^\dagger \boldsymbol{\Psi} + 1} \\ \text{s.t.} \quad & 0 \le \tfrac{\boldsymbol{c_n}^\dagger \boldsymbol{\Psi} + d_n}{\Psi_n} \le 1, \forall n \in \{1, 2, \cdots, N-1\}, \\ & \boldsymbol{c_N}^\dagger \boldsymbol{\Psi} + d_N = 0, \end{aligned} \tag{7.26}$$

where the superscript † denotes the vector transposition and

$$\boldsymbol{\Psi} = [\Psi_N, \Psi_{N-1}, \cdots, \Psi_2, \Psi_1]^\dagger, \tag{7.27}$$

$$\boldsymbol{c} = \overline{\mathcal{P}_{\mathrm{RD}}}[-b, a, -b, a, \cdots]^\dagger, \tag{7.28}$$

$$d = \begin{cases} \overline{\mathcal{P}_{\mathrm{RD}}}, & N \text{ odd}, \\ \overline{\mathcal{P}_{\mathrm{RD}}}(1-\alpha), & N \text{ even}, \end{cases} \tag{7.29}$$

$$\boldsymbol{c_n} = [\underbrace{0, \cdots, 0}_{N-n \text{ zeros}}, a, -(a+b), (a+b), \cdots]^\dagger, \tag{7.30}$$

$$d_n = (-1)^n \alpha. \tag{7.31}$$

Note that $\boldsymbol{\Psi}$, $\boldsymbol{c}$, and $\boldsymbol{c_n}$ are N-dimensional column vectors, while d and d_n are scalars. Linear-fractional programs like that in (7.26) are easily converted to standard linear programs [88], and hence, can be efficiently solved using standard numerical linear/convex programming tools. For instance, we used CVX, a MATLAB package for solving convex programs [89].

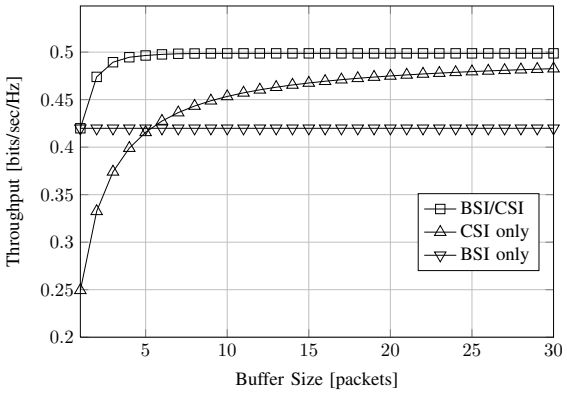

(a) $R = 1$ bpcu, $\gamma_{\mathrm{SR}} = 20$ dB, $\gamma_{\mathrm{RD}} = 5$ dB, and $\gamma_{\mathrm{SD}} = -10$ dB.

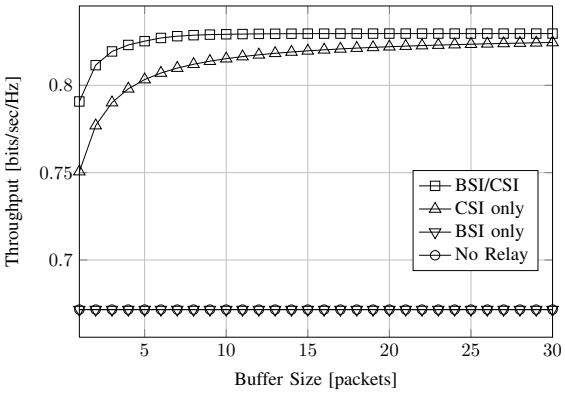

(b) $R = 1$ bpcu, $\gamma_{\mathrm{SR}} = 10$ dB, $\gamma_{\mathrm{RD}} = 3$ dB and $\gamma_{\mathrm{SD}} = 4$ dB.

Figure 7.3: Throughput vs. buffer size.

Afterwards, we obtain $\{\xi_n\}_{n=1}^{N-1}$ as

$$\xi_n \quad = \quad \frac{\boldsymbol{c_n}^{\dagger}\boldsymbol{\Psi} + d_n}{\Psi_n}, \forall n \in \{1, 2, \cdots, N-1\}. \tag{7.32}$$

7.4.3 Partial Transmit CSI only

For comparison purposes only, we consider the case where only partial CSI is available at the transmitters. Since the source cannot distinguish between the different queue states at the relay, the case of CSI-only can be simply obtained from the system with BSI and CSI via setting $\beta_n = \rho \in [0, 1]$ for all n and finding ρ that maximizes the throughput.

7.5 Numerical Results

In this section, we numerically evaluate the proposed access schemes for half-duplex buffer-aided relaying.

7.5.1 Throughput vs. Buffer Size

In Fig. 7.3a, we examine the case when no direct link exists (i.e., $\mathcal{P}_{\mathrm{SD}} = 1$) and investigate the impact of knowing the BSI as compared to the CSI-only system. In this case, the throughput

is ultimately limited to 0.5 packets/slot, or equivalently 0.5 bpcu when $R = 1$ bpcu, due to the half-duplex operation of the relay. The figure shows that knowing the BSI at the source with the availability of CSI improves the performance relative to the CSI-only and BSI-only cases. As shown in the figure, at low buffer size, specifically for $1 \leq N \leq 5$, the BSI-only system outperforms the CSI-only system. The behavior is reversed for $N > 5$. This behavior can be interpreted as follows. Since in the CSI-only system the source is oblivious to the relay's buffer state, a time slot is wasted when either 1) the source transmits and the buffer is full, or 2) the slot is dedicated for the relay at an empty buffer. At low buffer sizes, and for the same set of channel parameters, the probability of finding either a full or an empty buffer is higher than for those higher buffer sizes. Thus, knowing the BSI for the case of short buffer size is important to avoid wasted transmission instances. For the BSI/CSI case at $N = 5$, the optimal value of only $\xi_0 = 1$, while it is in the order of 10^{-6} for all higher states, as compared to an access probability of $\rho = 0.3193$ in the CSI-only case for all n. Since the second hop has much lower average gain than that of the first hop while the direct link experiences deep fading, this result agrees well with intuition where the BSI/CSI protocol allows the relay to drain its queue whenever it is possible so that it avoids building up and blocking future packets. This is further confirmed by knowing that the resulting full-buffer state probability, ϵ_N, is equal to 0.008 in the CSI/BSI case as compared to 0.167 when CSI only is available. The figure is generated using $R = 1$ bpcu, $\gamma_{\text{SD}} = -10$ dB, $\gamma_{\text{SR}} = 20$ dB, and $\gamma_{\text{RD}} = 5$ dB.

In contrast to Fig. 7.3a, which shows the case of $\mathcal{P}_{\text{SD}} > \mathcal{P}_{\text{RD}}$, in Fig. 7.3b, we plot the throughput versus the buffer size for the case $\mathcal{P}_{\text{SD}} \leq \mathcal{P}_{\text{RD}}$. The parameters used to generate the figure are: $R = 1$ bpcu, $\gamma_{\text{SR}} = 10$ dB, $\gamma_{\text{RD}} = 3$ dB and $\gamma_{\text{SD}} = 4$ dB. As shown in Fig. 7.3b, the proposed scheme with BSI and with or without the availability of CSI outperforms the case of no relay. The CSI-only system outperforms the BSI-only system for the used parameters. Knowing the BSI and CSI provides further gains. Like Fig. 7.3a, the figure also shows the fact that the BSI with no CSI does not change with the buffer size of the

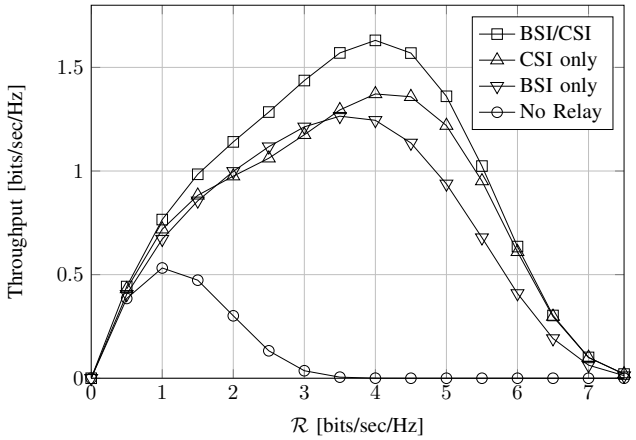

Figure 7.4: Throughput vs. rate for $N = 4$ packets, $\gamma_{\text{SR}} = 15$ dB, $\gamma_{\text{RD}} = 15$ dB and $\gamma_{\text{SD}} = 2$ dB.

relay. Consistent with the analytic result provided earlier, the figure shows the fact that for $\mathcal{P}_{\text{SD}} \leq \mathcal{P}_{\text{RD}}$, the relay provides no gains to the source when the BSI is known at the source and the CSI is unknown to transmitters. For the BSI/CSI case at $N = 5$, the optimal value of ξ_n is $\xi_0^* = \xi_1^* = 1$ and $\xi_n^* = 0$ for $n > 1$, while the optimal access probability for the CSI-only case is $\rho = 0.2272$.

7.5.2 Throughput vs. Source Rate

In Fig. 7.4, we show the source throughput versus R. We can notice that the CSI-only and BSI-only scenarios exchange the performance superiority over different transmission rate ranges. Specifically, the CSI-only scenario always yields higher throughput both at low and high transmission rates. This is due to the fact that, at low rates, the buffer occupancy is very low due to low link outage probabilities. Also, at high rates, the outage probability becomes higher, which also alleviates the load on the available buffer, and thus reduces the buffer size effect on the performance. Contrarily, the BSI becomes of immense importance at the intermediate rate range due to the higher buffer occupancy, and hence the BSI-only scenario performs better as explained earlier in Fig. 7.3a. The figure is generated using the following parameters: $N = 4$ packets, $\gamma_{\text{SR}} = 15$ dB, $\gamma_{\text{RD}} = 15$ dB and $\gamma_{\text{SD}} = 2$ dB.

7.6 Conclusion

In this chapter, we have studied buffer-aided HDR when BSI and/or partial CSI is available at the transmitters.

In the following chapter, buffer-aided FDR is further studied, where BSI and/or partial CSI is provided to the transmitters.

Appendix

Appendix 7.A Source/Destination Throughput

The average number of packets received successfully at the destination is given by

$$\mathcal{T}_{\mathrm{D}} = \overline{\mathcal{P}_{\mathrm{SD}}} \sum_{n=0}^{N} \epsilon_n \beta_n + \overline{\mathcal{P}_{\mathrm{RD}}} \sum_{n=1}^{N} \epsilon_n \overline{\beta_n}. \tag{7.33}$$

In (7.33), $\overline{\mathcal{P}_{\mathrm{SD}}} \sum_{n=0}^{N} \epsilon_n \beta_n$ denotes the average number of packets directly delivered from the source to the destination, while $\overline{\mathcal{P}_{\mathrm{RD}}} \sum_{n=1}^{N} \epsilon_n \overline{\beta_n}$ denotes those delivered to the destination through the relay. Summing both sides of (7.2) from $n = 0$ to $N - 1$, we get $\sum_{n=0}^{N-1} \epsilon_n \lambda_n = \sum_{n=1}^{N} \epsilon_n \mu_n$. Substituting by $\lambda_n = \beta_n \overline{\mathcal{P}_{\mathrm{SR}}} \mathcal{P}_{\mathrm{SD}}$ and $\mu_n = \overline{\beta_n}\ \overline{\mathcal{P}_{\mathrm{RD}}}$, we get the following:

$$\mathcal{P}_{\mathrm{SD}} \overline{\mathcal{P}_{\mathrm{SR}}} \sum_{n=0}^{N-1} \epsilon_n \beta_n = \overline{\mathcal{P}_{\mathrm{RD}}} \sum_{n=1}^{N} \epsilon_n \overline{\beta_n}. \tag{7.34}$$

Using (7.34) in (7.6), we reach

$$\mathcal{T}_{\mathrm{S}} = \overline{\mathcal{P}_{\mathrm{SD}}} \sum_{n=0}^{N} \epsilon_n \beta_n + \overline{\mathcal{P}_{\mathrm{RD}}} \sum_{n=1}^{N} \epsilon_n \overline{\beta_n} = \mathcal{T}_{\mathrm{D}}. \tag{7.35}$$

Hence, it is equivalent to calculate the throughput from the source or the destination perspectives.

Chapter 8

Buffer-Aided Full-Duplex Relaying

8.1 System Model

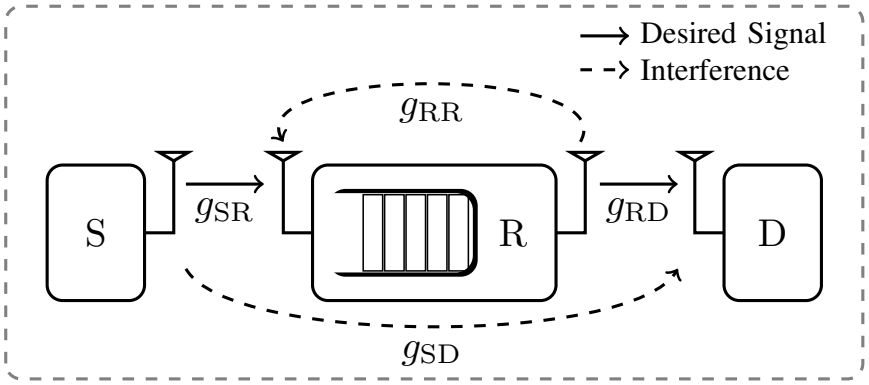

Figure 8.1: A buffer-aided full-duplex relay channel with self-interference.

We study the two-hop full-duplex cooperative setting depicted in Fig. 8.1. Now, the relay R is also equipped with a buffer of size N data packets, but suffers a residual level of self-interference while operating in the full-duplex mode. As shown, g_{RR} denotes the RSI fading gain.

In the presence of a direct source-destination link, the source is free to decide, according to channel and buffer states, whether to adopt DT or to seek the relay's cooperation for packet delivery. Further, while in the cooperative mode, the relay is assumed to adopt a hybrid HDR/FDR scheme according to the link outage states. For instance, when the $\mathrm{S}-\mathrm{R}$

link undergoes an outage while the relay is active due to RSI, time-orthogonal transmission, i.e., HDR, may still take place. In this channel state, the relay may either individually access the channel to forward the accumulated packets in its queue, or go into a listen-only mode while the source transmits. The latter case gives a higher chance for successful packet delivery from the source to the relay by eliminating the RSI effect. As commonly assumed in the literature, an *RF-chain conserved* scenario [33] is assumed when switching between HDR and FDR, i.e., the relay is equipped with exactly one transmit and one receive RF-chains. Therefore, single-antenna HDR is only possible when reverting to orthogonal transmission.

The received SINR at the relay when it is silent or active is given respectively by

$$\gamma_1 = \frac{P_{\mathrm{S}} g_{\mathrm{SR}}}{\sigma_{\mathrm{R}}^2}, \quad \text{and} \quad \gamma_2 = \frac{P_{\mathrm{S}} g_{\mathrm{SR}}}{P_{\mathrm{R}} g_{\mathrm{RR}} + \sigma_{\mathrm{R}}^2}. \tag{8.1}$$

Also, the received SINR at the destination when the source is silent or active is given by

$$\gamma_3 = \frac{P_{\mathrm{R}} g_{\mathrm{RD}}}{\sigma_{\mathrm{D}}^2}, \quad \text{and} \quad \gamma_4 = \frac{P_{\mathrm{R}} g_{\mathrm{RD}}}{P_{\mathrm{S}} g_{\mathrm{SD}} + \sigma_{\mathrm{D}}^2}. \tag{8.2}$$

The SNR via the direct link is also simply given by $\gamma_5 = \frac{P_{\mathrm{S}} g_{\mathrm{SD}}}{\sigma_{\mathrm{D}}^2}$. We use $\mathcal{O}_i$ for $i \in \{1, 2, 3, 4, 5\}$ to denote a link outage event where the link capacity $\log_2(1 + \gamma_i)$ falls below the source rate R, while $\mathcal{P}_i$ denotes the probability of occurrence of $\mathcal{O}_i$. In the sequel, $\overline{\mathcal{O}_i}$ will be used to denote the complementary event of $\mathcal{O}_i$. Also, $\overline{\mathcal{P}_i} = 1 - \mathcal{P}_i$. It should be noted that when both the source and relay simultaneously transmit, the $\mathrm{R} - \mathrm{D}$ and $\mathrm{S} - \mathrm{D}$ link outage events become correlated. Based on the following proposed transmission scheme and its entailed partitioning of the probability space, we are specifically interested in the probability of the $\mathrm{R} - \mathrm{D}$ outage event conditioned on the outage of the $\mathrm{S} - \mathrm{D}$ link. Hence, we take this fact into account in the specific definition of the event $\mathcal{O}_4$, and accordingly for calculating $\mathcal{P}_4$, while we keep the same notation of the other events for simplicity. Specifically, $\mathcal{O}_4$ is used to denote the *conditional* outage event in the $\mathrm{R} - \mathrm{D}$ link given an $\mathrm{S} - \mathrm{D}$ link outage.

8.2 Transmission Scheduling Protocol

Table 8.1: Proposed Transmission Scheduling Protocol

	(A) $\overline{\mathcal{O}_5}$	(B) $\mathcal{O}_5$					
		(i) $\mathcal{O}_1$	(ii) $\mathcal{O}_2 \cap \overline{\mathcal{O}_1}$		(iii) $\overline{\mathcal{O}_2}$		
			(a) $\mathcal{O}_3$	(b) $\overline{\mathcal{O}_3}$	(a) $\mathcal{O}_3$	(b) $\mathcal{O}_4 \cap \overline{\mathcal{O}_3}$	(c) $\overline{\mathcal{O}_4}$
Source	Active	Silent	Non-full buffer	w.p. β_n	Non-full buffer	w.p. β_n	Active
Relay	Silent	$\overline{\mathcal{O}_3}$ & Non-empty buffer	Silent	w.p. $\overline{\beta_n}$	Silent	w.p. $\overline{\beta_n}$	Non-empty buffer

In what follows, we carefully explain the proposed transmission scheduling and mode selection scheme. The probability space can be partitioned into two mutually exclusive events based on the outage state of the direct link, namely, (A) $\overline{\mathcal{O}_5}$, and (B) $\mathcal{O}_5$. When the direct link is in outage, event (B) can be further partitioned into the following three mutually exclusive events: (i) $\mathcal{O}_5 \cap \mathcal{O}_1$, (ii) $\mathcal{O}_5 \cap \mathcal{O}_2 \cap \overline{\mathcal{O}_1}$, and (iii) $\mathcal{O}_5 \cap \overline{\mathcal{O}_2}$. The proposed scheduling protocol is defined over these events as follows.

(A) When the $\mathrm{S}-\mathrm{D}$ link is not in outage, the source transmits directly to the destination without relay cooperation.

(B) When the direct link is found in outage, i.e., in $\mathcal{O}_5$, the access scheme is as follows:

(i) When the $\mathrm{S}-\mathrm{R}$ link is in outage even with a silent relay, i.e., in the $\mathcal{O}_1$ event, the source remains silent while the relay accesses the channel when the $\mathrm{R}-\mathrm{D}$ link is not in outage at a silent source (in $\overline{\mathcal{O}_3}$) and its buffer is non-empty.

(ii) When the $\mathrm{S}-\mathrm{R}$ link is in outage if the relay is active while it is not when the relay is silent, i.e., in $\mathcal{O}_2 \cap \overline{\mathcal{O}_1}$, the scheme further depends on the $\mathrm{R}-\mathrm{D}$ link outage state.

(a) When the $\mathrm{R}-\mathrm{D}$ link is in outage, i.e., in $\mathcal{O}_3$, only the source can transmit at non-full relaying buffer.

(b) When the $\mathrm{R}-\mathrm{D}$ link is not in outage, i.e., in $\overline{\mathcal{O}_3}$, the source and relay transmit in orthogonal time slots due to the RSI adverse effect on the $\mathrm{S}-\mathrm{R}$ link. Moreover, the access probability will depend on the state of the relay. Let the

probability that the source transmits be β_n when the buffer has n packets, while the relay transmits with probability $\overline{\beta_n} = 1 - \beta_n$. It is clear that $\beta_0 = 1$ and $\beta_N = 0$ when BSI is available.

(iii) When the S − R link is not in outage even with an active relay, i.e., in $\overline{\mathcal{O}_2}$, also the transmission scheme further depends on the R − D link outage state.

(a) In $\mathcal{O}_3$, the relay remains silent, while the source transmits provided that the relay's buffer is not full.

(b) In $\mathcal{O}_4 \cap \overline{\mathcal{O}_3}$, the source and the relay cannot transmit simultaneously since the source interference drives the second hop into outage. Nonetheless, they can still successfully transmit in orthogonal time slots exactly as in the event (B)-(ii)-(b). Hence, the source also transmits with probability β_n when the buffer has n packets, while the relay transmits with probability $\overline{\beta_n} = 1 - \beta_n$.

(c) In $\overline{\mathcal{O}_4}$, the source and relay can simultaneously transmit, taking advantage of FDR capability. Of course, the relay transmits when its buffer is non-empty. Due to FDR, the relay has an additional one-packet *transmission buffer*. If it transmits, the relay will take out the packet at the head of its main queue at the beginning of the time slot and put it in the transmission buffer. The source can then transmit concurrently with the relay even at a full-buffer state, since there is always a room for an upcoming packet.

The above proposed transmission scheduling protocol is summarized in Table 8.1.

A state increment occurs due to one of the events (B)-(ii)-(a), (B)-(ii)-(b), (B)-(iii)-(a), (B)-(iii)-(b), and (B)-(iii)-(c) with probability

$$\lambda_n \;=\; \mathcal{P}_5 \left(\overline{\mathcal{P}_1}\mathcal{P}_3 + (\overline{\mathcal{P}_1}\;\overline{\mathcal{P}_3} - \overline{\mathcal{P}_2}\;\overline{\mathcal{P}_4})\beta_n + \overline{\mathcal{P}_2}\;\overline{\mathcal{P}_4}\delta_{n,0} \right), \tag{8.3}$$

where

$$\delta_{n,j} = \begin{cases} 1 & \text{if } n = j, \\ 0 & \text{otherwise.} \end{cases} \tag{8.4}$$

The first term in (8.3) comes from the sum of the probabilities in the events (B)-(ii)-(a) and (B)-(iii)-(a), while the second comes from the events (B)-(ii)-(b) and (B)-(iii)-(b) after simple manipulation. The last term in (8.3) comes from the fact that a state increment occurs in the event (B)-(iii)-(c) only when the relay does not have packets in its queue to forward. Otherwise, simultaneous arrival/departure occurs in the full-duplex mode which contributes to the system throughput, however it does not alter the state of the queue. It should be noted that the queue state cannot be altered in the event (A) since the destination receives directly from the source while the relay remains silent.

A state decrement occurs due to the events (B)-(i), (B)-(ii)-(b), and (B)-(iii)-(b) with probability

$$\mu_n \;=\; \mathcal{P}_5 \left(\mathcal{P}_1 \overline{\mathcal{P}_3} + (\overline{\mathcal{P}_1}\ \overline{\mathcal{P}_3} - \overline{\mathcal{P}_2}\ \overline{\mathcal{P}_4})\ \overline{\beta_n} \right). \tag{8.5}$$

It is worth mentioning that no state decrement can occur in the event (B)-(iii)-(c) due to simultaneous departure/arrival, i.e., a transition can only take place from a state to itself, or to state 1 when the buffer is empty.

The source throughput is then given from all the events except for the event (B)-(i) as

$$\mathcal{T}_{\mathrm{S}} \;=\; \overline{\mathcal{P}_5} + \mathcal{P}_5 \Big(\overline{\mathcal{P}_1}\ \mathcal{P}_3(1-\epsilon_N) + \overline{\mathcal{P}_2}\ \overline{\mathcal{P}_4} + (\overline{\mathcal{P}_1}\ \overline{\mathcal{P}_3} - \overline{\mathcal{P}_2}\ \overline{\mathcal{P}_4}) \sum_{n=0}^{N-1} \epsilon_n \beta_n \Big), \tag{8.6}$$

where the first term in (8.6) comes from the event (A), the second is due to summing the events (B)-(ii)-(a) and (B)-(iii)-(a) over non-full queue states, the third comes from (B)-(iii)-(c) over all queue states, while the last term comes from the sum of the throughput

components in the events (B)-(ii)-(b) and (B)-(iii)-(b) also at non-full queue states.

The local balance equations of the birth-death Markov chain in Fig. 7.2 and the state probabilities are given, respectively, by (7.2) and (7.3).

In the following section, we design the access probabilities, $\{\beta_n\}_{n=0}^{N}$, to maximize the end-to-end throughput.

8.3 End-to-End Throughput Maximization

8.3.1 BSI and CSI at the Transmitter Side

When both the BSI and CSI are available at the transmitters, the end-to-end throughput maximization problem can be formally written as

$$\begin{aligned} \max_{\{\beta_n\}_{n=0}^{N}} \quad & \mathcal{T}_{\mathrm{S}} \\ \text{s.t.} \quad & \beta_0 = 1, \qquad \beta_N = 0, \\ & 0 \leq \beta_n \leq 1, \quad \text{for } n = 1, 2, \ldots, N-1. \end{aligned} \tag{8.7}$$

Note that the access probabilities, $\{\beta_n\}_{n=0}^{N}$, are only defined in the events where the system operates in the half-duplex cooperation mode. That is why the optimization problem in (8.7) has the constraints that the probability for the source to access the channel is equal to zero at a full buffer, while it is equal to unity at an empty buffer, i.e., $\beta_N = 0$ and $\beta_0 = 1$. As explained in the protocol, the source always transmits regardless of the buffer state for the event of full-duplex cooperation. For the rest of the events where one transmitter (either source or relay) is silent due to its own channel outage, the other transmitting node can always access the channel as explained earlier.

First, we define a new set of variables $\{\Psi_n\}_{n=1}^{N}$ as

$$\Psi_n \;=\; \frac{\epsilon_n}{\epsilon_0} = \prod_{k=0}^{n-1} \frac{\lambda_k}{\mu_{k+1}}. \tag{8.8}$$

It is clear that $\Psi_0 = \frac{\epsilon_0}{\epsilon_0} = 1$. We rewrite the throughput expression by substituting (7.2),(7.3), and(8.8) into (8.6) as

$$\mathcal{T}_{\mathrm{S}} \;=\; \overline{\mathcal{P}_5} + \mathcal{P}_5 \left(\overline{\mathcal{P}_1}\ \mathcal{P}_3 + \overline{\mathcal{P}_2}\ \overline{\mathcal{P}_4}\right) + \phi_{\mathrm{S}}, \tag{8.9}$$

where

$$\phi_{\mathrm{S}} \;=\; \frac{\mathcal{P}_5(\overline{\mathcal{P}_1}\ \overline{\mathcal{P}_3} - \overline{\mathcal{P}_2}\ \overline{\mathcal{P}_4}) \sum_{n=0}^{N-1} \Psi_n\beta_n - \mathcal{P}_5\overline{\mathcal{P}_1}\ \mathcal{P}_3\Psi_N}{\left(1 + \sum_{n=1}^{N} \Psi_n\right)}. \tag{8.10}$$

The new variables $\{\Psi_n\}_{n=1}^{N}$ can be written in terms of the old variables $\{\beta_n\}_{n=0}^{N}$ by substituting (8.3) and (8.5) into (8.8) as

$$\Psi_n \;=\; \prod_{k=0}^{n-1} \frac{\overline{\mathcal{P}_1}\mathcal{P}_3 + (\overline{\mathcal{P}_1}\ \overline{\mathcal{P}_3} - \overline{\mathcal{P}_2}\ \overline{\mathcal{P}_4})\beta_k + \overline{\mathcal{P}_2}\ \overline{\mathcal{P}_4}\delta_{k,0}}{\overline{\mathcal{P}_3} - \overline{\mathcal{P}_2}\ \overline{\mathcal{P}_4} - (\overline{\mathcal{P}_1}\ \overline{\mathcal{P}_3} - \overline{\mathcal{P}_2}\ \overline{\mathcal{P}_4})\ \beta_{k+1}}. \tag{8.11}$$

Maximizing $\mathcal{T}_{\mathrm{S}}$ is equivalent to maximizing ϕ_{S}. Moreover, we can notice in (8.10) that ϕ_{S} can be put in the form of a linear-fractional function in $\{\Psi_n\}_{n=1}^{N}$ if we manage to express $\{\Psi_n\beta_n\}_{n=0}^{N-1}$ in terms of $\{\Psi_n\}_{n=1}^{N}$ only. We have, for $n \in \{2, 3, \cdots, N\}$,

$$\frac{\Psi_n}{\Psi_{n-1}} \;=\; \frac{\overline{\mathcal{P}_1}\mathcal{P}_3 + (\overline{\mathcal{P}_1}\ \overline{\mathcal{P}_3} - \overline{\mathcal{P}_2}\ \overline{\mathcal{P}_4})\beta_{n-1}}{\overline{\mathcal{P}_3} - \overline{\mathcal{P}_2}\ \overline{\mathcal{P}_4} - (\overline{\mathcal{P}_1}\ \overline{\mathcal{P}_3} - \overline{\mathcal{P}_2}\ \overline{\mathcal{P}_4})\ \beta_n}, \tag{8.12}$$

while

$$\Psi_1 = \frac{\lambda_0}{\mu_1} = \frac{\overline{\mathcal{P}_1}\mathcal{P}_3 + (\overline{\mathcal{P}_1}\ \overline{\mathcal{P}_3} - \overline{\mathcal{P}_2}\ \overline{\mathcal{P}_4})\beta_0 + \overline{\mathcal{P}_2}\ \overline{\mathcal{P}_4}}{\overline{\mathcal{P}_3} - \overline{\mathcal{P}_2}\ \overline{\mathcal{P}_4} - (\overline{\mathcal{P}_1}\ \overline{\mathcal{P}_3} - \overline{\mathcal{P}_2}\ \overline{\mathcal{P}_4})\ \beta_1}. \tag{8.13}$$

Hence, for $n \in \{2, 3, \cdots, N\}$, we get the recurrence relation,

$$\beta_n \Psi_n = a\Psi_n - b\Psi_{n-1} - \beta_{n-1}\Psi_{n-1}, \tag{8.14}$$

with its initial value given by

$$\beta_1 \Psi_1 \;\; = \;\; a\Psi_1 - b_0 - \beta_0, \tag{8.15}$$

where

$$a = \frac{\overline{\mathcal{P}_3} - \overline{\mathcal{P}_2}\;\overline{\mathcal{P}_4}}{(\overline{\mathcal{P}_1}\;\overline{\mathcal{P}_3} - \overline{\mathcal{P}_2}\;\overline{\mathcal{P}_4})}, \qquad\qquad b = \frac{\overline{\mathcal{P}_1}\mathcal{P}_3}{(\overline{\mathcal{P}_1}\;\overline{\mathcal{P}_3} - \overline{\mathcal{P}_2}\;\overline{\mathcal{P}_4})}, \tag{8.16}$$

and

$$b_0 = \frac{\overline{\mathcal{P}_1}\mathcal{P}_3 + \overline{\mathcal{P}_2}\;\overline{\mathcal{P}_4}}{(\overline{\mathcal{P}_1}\;\overline{\mathcal{P}_3} - \overline{\mathcal{P}_2}\;\overline{\mathcal{P}_4})}. \tag{8.17}$$

From the recurrence relation in (8.14) and its initial value in (8.15), we can get $\beta_n\Psi_n$ in terms of $\{\Psi_k\}_{k=1}^{n}$ and β_0 only as

$$\beta_n \Psi_n = a\Psi_n + \sum_{k=1}^{n-1} (-1)^{n-k} (b+a)\Psi_k + (-1)^n(\beta_0 + b_0). \tag{8.18}$$

It can be shown that $\sum_{n=1}^{N-1} \beta_n\Psi_n$ is on the form

$$\sum_{n=1}^{N-1} \beta_n \Psi_n \;\; = \begin{cases} a\Psi_{N-1} - b\Psi_{N-2} + a\Psi_{N-3} - \cdots + a\Psi_1 - \beta_0 - b_0, & \text{if } N \text{ is even,} \\ a\Psi_{N-1} - b\Psi_{N-2} + a\Psi_{N-3} - \cdots - b\Psi_1, & \text{if } N \text{ is odd.} \end{cases} \tag{8.19}$$

When the BSI is available at the transmitters, the source always accesses the channel when the relay's buffer is empty, i.e., $\beta_0 = 1$. Hence, we can stack our remaining N optimization variables, i.e., $\{\Psi_n\}_{n=1}^{N}$, in a vector form as $\mathbf{\Psi} = (\Psi_N, \Psi_{N-1}, \cdots, \Psi_1)^T$, where $(\cdot)^T$ denotes

vector transposition. From (8.19), we can get $\phi_{\rm S}$ on the following desired form of a linear-fractional function:

$$\phi_{\rm S} \;=\; \frac{\boldsymbol{c}^{\dagger}\boldsymbol{\Psi}+d}{\mathbf{1}^{\dagger}\boldsymbol{\Psi}+1}, \tag{8.20}$$

where

$$\boldsymbol{c} \;=\; \begin{cases} \Big(q,\tilde{a},-\tilde{b},\tilde{a},-\tilde{b},\cdots,\tilde{a}\Big)^{\dagger}, & \text{if } N \text{ is even,} \\ \Big(q,\tilde{a},-\tilde{b},\tilde{a},-\tilde{b},\cdots,-\tilde{b}\Big)^{\dagger}, & \text{if } N \text{ is odd,} \end{cases} \tag{8.21}$$

$$q \;=\; -\overline{\mathcal{P}_1}\,\mathcal{P}_3, \quad \tilde{a}=\overline{\mathcal{P}_3}-\overline{\mathcal{P}_2}\,\overline{\mathcal{P}_4}, \quad \tilde{b}=\overline{\mathcal{P}_1}\mathcal{P}_3, \tag{8.22}$$

$$d \;=\; \begin{cases} (\overline{\mathcal{P}_1}\,\overline{\mathcal{P}_3}-\overline{\mathcal{P}_2}\,\overline{\mathcal{P}_4})-\overline{\mathcal{P}_1}, & \text{if } N \text{ is even,} \\ (\overline{\mathcal{P}_1}\,\overline{\mathcal{P}_3}-\overline{\mathcal{P}_2}\,\overline{\mathcal{P}_4}), & \text{if } N \text{ is odd,} \end{cases} \tag{8.23}$$

while $\mathbf{1}$ is an $N\times 1$ vector whose elements are all equal to unity. Also, the constraints are linear-fractional functions of $\{\Psi_k\}_{k=1}^{n}$. Specifically, from (8.18) and given $\beta_0=1$ we get

$$\beta_n \;=\; \frac{a\Psi_n+\sum_{k=1}^{n-1}(-1)^{n-k}\,(b+a)\Psi_k+(-1)^n(1+b_0)}{\Psi_n} \tag{8.24}$$

$$\;=\; \frac{\boldsymbol{c_n}^{\dagger}\boldsymbol{\Psi}+d_n}{\boldsymbol{1_n}^{\dagger}\boldsymbol{\Psi}}, \quad \text{for } n=1,2,\cdots,N, \tag{8.25}$$

where

$$\boldsymbol{c_n}=\Big(\underbrace{0,\cdots,0}_{N-n \text{ zeros}},a,-(a+b),\cdots,(-1)^k(a+b),\cdots\Big)^{\dagger}, \tag{8.26}$$

$$d_n=(-1)^n(1+b_0),\;\; \mathbf{1_n}=\Big(\underbrace{0,\cdots,0}_{N-n \text{ zeros}},1,\underbrace{0,\cdots,0}_{n \text{ zeros}}\Big). \tag{8.27}$$

Note that $\boldsymbol{c}$, $\boldsymbol{c_n}$, $\mathbf{1}$ and $\mathbf{1_n}$ are all N-dimensional column vectors. Now, since the objective and constraint functions are linear-fractional functions in $\boldsymbol{\Psi}$, the optimization problem in

(8.7) is now on the form of a linear-fractional program. After solving for the optimal $\mathbf{\Psi}$, $\{\beta_n\}_{n=1}^{N-1}$ can be directly obtained from (8.25), while the throughput can be readily computed from (8.9) and (8.20).

8.3.2 CSI Only at the Transmitter Side

For performance comparison purposes, we will briefly discuss the system where the transmitters are only provided with outage state information without BSI. In this case, the source becomes oblivious of the relay's queue state, and hence it cannot adapt its access probabilities accordingly. Specifically, in the event (ii)-(b), since the source cannot distinguish between the different states, β_n can be only set to a fixed value, $0 \leq \beta \leq 1$, for all $n \in \{0, 1, 2, \cdots, N\}$. In all events, the unawareness of the source about the queue state will only cause packet transmission and dropping at queue state N instead of remaining silent, which is equivalently accounted for in the given throughput expression. Hence, the throughput expression is given by

$$\mathcal{T}_{\mathrm{S}} \;=\; \overline{\mathcal{P}_5} + \mathcal{P}_5\overline{\mathcal{P}_2}\;\overline{\mathcal{P}_4} + \mathcal{P}_5(1-\epsilon_N)\Big(\overline{\mathcal{P}_1}\;\mathcal{P}_3 + (\overline{\mathcal{P}_1}\;\overline{\mathcal{P}_3} - \overline{\mathcal{P}_2}\;\overline{\mathcal{P}_4})\beta\Big). \tag{8.28}$$

where now the state transition probabilities and the state probabilities are calculated for $\beta_n = \beta, \forall n \in \{0, 1, \cdots, N\}$. The source can still optimize the value of β prior to communication in order to maximize the throughput.

8.4 Numerical Results

In this section, we numerically evaluate the theoretical results of the proposed scheme, and compare them to those obtained via event-based simulations. In the simulations part, we calculate the end-to-end throughput at the destination after the transmission of 10^5 packets. Since block fading channels are assumed, each packet experiences a different channel gain. For numerical evaluation purposes, we assume herein that the channels are Rayleigh fading.

Hence, the channel gain of the $i-j$ link, i.e., g_{ij}, is exponentially distributed with mean π_{ij}. Without loss of generality, we absorb the transmit powers into the channel coefficients, while noise variances are set to unity. The channel gains thus denote the received signal-to-noise ratio over each link. The channel outage probabilities, $\mathcal{P}_i = \mathbb{P}\{\gamma_i < 2^R - 1\}$, can be calculated as

$$\mathcal{P}_1 = 1 - e^{-\frac{\eta}{P_{\rm S}\pi_{\rm SR}}}, \quad \mathcal{P}_3 = 1 - e^{-\frac{\eta}{P_{\rm R}\pi_{\rm RD}}}, \quad \mathcal{P}_5 = 1 - e^{-\frac{\eta}{P_{\rm S}\pi_{\rm SD}}}, \tag{8.29}$$

where $\eta = 2^R - 1$, while $\mathcal{P}_2$ can be obtained as in [41] by

$$\mathcal{P}_2 = 1 - \frac{e^{-\frac{\eta}{P_{\rm S}\pi_{\rm SR}}}}{1 + \eta\frac{P_{\rm R}^{\delta}\pi_{\rm RR}}{P_{\rm S}\pi_{\rm SR}}}. \tag{8.30}$$

As mentioned earlier, $\mathcal{P}_4$ denotes the outage probability in the R $-$ D link conditioned on the S $-$ D link outage. It is shown in Appendix 8.A that it is given by

$$\mathcal{P}_4 \;=\; 1 - \frac{e^{-\frac{\eta}{P_{\rm R}\pi_{\rm RD}}}\left(1 - e^{-\eta\left(\frac{\eta}{P_{\rm R}\pi_{\rm RD}} + \frac{1}{P_{\rm S}\pi_{\rm SD}}\right)}\right)}{\left(1 + \eta\frac{P_{\rm S}\pi_{\rm SD}}{P_{\rm R}\pi_{\rm RD}}\right)\left(1 - e^{-\frac{\eta}{P_{\rm S}\pi_{\rm SD}}}\right)}. \tag{8.31}$$

We compare the performance of the proposed buffered hybrid HDR/FDR scheme with BSI/CSI with the following schemes: 1) buffered hybrid HDR/FDR with CSI only, 2) bufferless FDR, and 3) bufferless HDR. The throughput of the conventional bufferless schemes can be calculated as the probability of successful packet transmission (the complement of the outage probability) multiplied by the attempted source rate. The throughput of the bufferless HDR and FDR are hence given, respectively, by

$$\mathcal{T}_{\rm HDR} \;=\; R \times \frac{1}{2} \times \overline{\mathcal{P}_1}\,\overline{\mathcal{P}_3}, \tag{8.32}$$

$$\mathcal{T}_{\rm FDR} \;=\; R \times \overline{\mathcal{P}_2}\,\overline{\mathcal{P}_4'}, \tag{8.33}$$

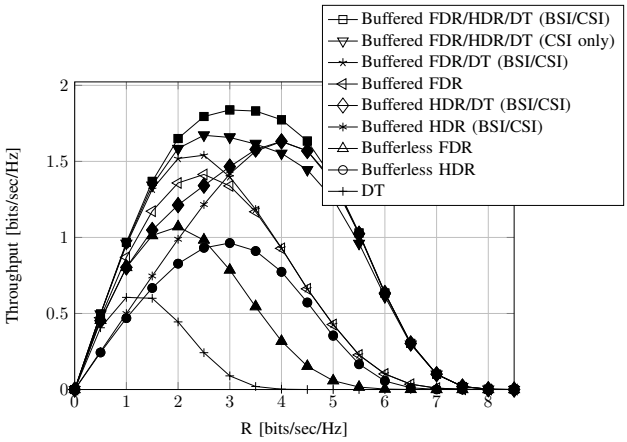

Figure 8.2: Throughput vs. source rate, for $\pi_{\mathrm{SR}} = \pi_{\mathrm{RD}} = 15$ dB, $\pi_{\mathrm{RR}} = 5$ dB, $\pi_{\mathrm{SD}} = 3$ dB, and $N = 4$ packets.

where $\mathcal{P}_4'$ is outage probability in the $\mathrm{R}-\mathrm{D}$ link which is given as in [41] by

$$\mathcal{P}_4' = 1 - \frac{e^{-\frac{\eta}{P_{\mathrm{R}}\pi_{\mathrm{RD}}}}}{1 + \eta\frac{P_{\mathrm{S}}\pi_{\mathrm{SD}}}{P_{\mathrm{R}}\pi_{\mathrm{RD}}}}. \tag{8.34}$$

Note that providing transmit CSI to bufferless systems does not offer any performance gains when fixed rate transmission is adopted. This is due to the causality of packet forwarding at the bufferless relay, where it is forced to wait for the event when the two hops are simultaneously outage-free to attain successful delivery. We summarize the used simulation parameters in the caption of each figure. Also, for all figures, we use unfilled plot marks with connecting lines to represent the theoretical results, while unconnected filled marks of the same shape are used for the simulations results. Hence, connected curves with properly filled marks reflect how well-matching the theoretical and simulation results are.

In Fig. 8.2, we plot the end-to-end throughput versus the source attempted rate R. As shown, the proposed buffered hybrid HDR/FDR scheme when it is only provided with transmit CSI outperforms both bufferless HDR and FDR. This is due to the ability of the scheme to jointly preserve three desirable aspects, namely, 1) the acceptance of additional packets and their storage at the relay's queue when the $\mathrm{R}-\mathrm{D}$ link experiences outage for possible future forwarding which increases the occupancy of the second hop and hence the

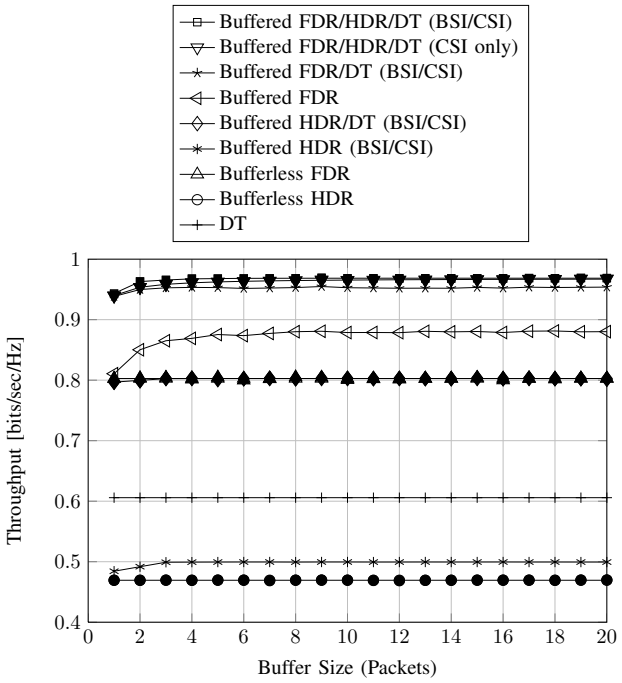

Figure 8.3: Throughput vs. buffer size, for $\pi_{\mathrm{SR}} = \pi_{\mathrm{RD}} = 15$ dB, $\pi_{\mathrm{RR}} = 5$ dB, $\pi_{\mathrm{SD}} = 3$ dB, and $R = 1$ bits/sec/Hz.

throughput, 2) the ability of the full-duplex relay to simultaneously listen and forward which avoids the known rate penalty in HDR, and 3) the agility of the relay to resort to half-duplex operation whenever the self-interference link prevents simultaneous transmission. Further, it can be noticed that providing the source with the BSI can offer further throughput gains. These gains arise from the additionally offered flexibility in link selection, where the source can now avoid transmission whenever the relay's queue is full, and give the opportunity for the relay to drain and recover a room in the queue to accept more packets.

We plot the throughput versus the size of the relay's buffer in Fig. 8.3. As shown, the throughput of the proposed hybrid scheme with either CSI only or BSI/CSI clearly outperforms that of the bufferless FDR and HDR schemes. Moreover, the throughput gains increase with increasing the buffer size. We can notice that the throughput of the CSI-only scheme approaches that of BSI/CSI as the buffer size increases. This behavior takes place due to the fact that the probability of a full buffer, ϵ_N, decreases with buffer size, and the need for the knowledge of BSI at the source diminishes.

8.5 Conclusion

In this work, we have proposed a hybrid half-/full-duplex buffer-aided relaying scheme that leverages the available outage and buffer state information to maximize the end-to-end throughput. The formulated optimization problem is put in a linear-fractional program form, which is in turn converted to a linear program that is efficiently solvable using standard numerical linear programming tools. Performance gains are shown to exist when the source is further provided with the relay's buffer state information, compared to systems with only outage state information at the transmitters, especially at low buffer sizes. The exact theoretical paper findings are validated via event-based simulations, which are shown to be in excellent agreement with theory.

Appendix

Appendix 8.A R − D Outage Probability Given S − D outage

The outage probability in the R − D link conditioned on the S − D link outage is given by

$$\mathcal{P}_4 \;= \mathbb{P}\{\gamma_4 < \eta \mid \mathcal{O}_5\} \;= \mathbb{P}\{\frac{g_{\mathrm{RD}}}{1+g_{\mathrm{SD}}} < \eta \mid g_{\mathrm{SD}} < \eta\}. \tag{8.35}$$

Since all link gains are exponentially distributed, we get

$$\mathcal{P}_4 = \frac{1}{\mathcal{P}_5}\int_0^{\eta} \mathbb{P}\{g_{\mathrm{RD}} < (x+1)\eta\}\frac{e^{-\frac{x}{P_{\mathrm{S}}\pi_{\mathrm{SD}}}}}{P_{\mathrm{S}}\pi_{\mathrm{SD}}}\mathrm{d}x \tag{8.36}$$

$$= \frac{1}{\mathcal{P}_5}\int_0^{\eta}\left(1-e^{-\frac{(x+1)\eta}{P_{\mathrm{R}}\pi_{\mathrm{RD}}}}\right)\frac{e^{-\frac{x}{P_{\mathrm{S}}\pi_{\mathrm{SD}}}}}{P_{\mathrm{S}}\pi_{\mathrm{SD}}}\mathrm{d}x, \tag{8.37}$$

which is readily given as in (8.31).

Part IV

General Conclusion and Future Work

Chapter 9

Conclusion

9.1 Summary of Results

In the presented thesis, several aspects of full-duplex cooperative communications have been studied when either buffer-less or buffer-aided relays are employed.

- **Buffer-less Relaying:**

– **Single Relay Cooperation:** Two selective cooperation protocols are proposed to enhance the end-to-end outage/throughput performance, and to boost the diversity order of the system. The end-to-end CDF SNR is derived in closed-form over Rayleigh and Nakagami-m fading channels. Also, several existing HDR and FDR protocols are studied in comparison, with the outage performance and diversity results summarized in Table 4.1.

– **Relay Selection:** The outage performance of FDRS was analyzed by deriving the end-to-end SNR CDF in closed-form over Rayleigh and Nakagami-m fading channels for several FDR protocols. The diversity order of each is also derived, with the results summarized in Table 5.1. It was shown that a significant diversity gain can be attained if the direct source-destination link is leveraged as an additional diversity branch, even for simple full-duplex cooperative protocols that treat the direct link as interference to each relayed path. Closed-form expressions were also presented for FDRS in cognitive underlay settings were

an interference threshold is imposed by the primary user of the spectrum.

• **Buffer-Aided Relaying:** Hybrid buffer-aided HDR/FDR was studied. In order to maximize the end-to-end throughput, protocols that utilize different combinations of BSI/CSI knowledge were studied and compared. It was shown that hybrid buffer-aided half-/full-duplex relaying with outage and buffer state information yields throughput values that outperform those of all pure half-duplex and full-duplex strategies, being either buffer-aided or buffer-less.

9.2 Future Research Work

Inspired by the results presented in this thesis as well as those in the recent literature, several research directions are yet to be investigated:

• **Hybrid FDRS/HDRS:** As shown earlier, the diversity order of FDRS depends on the RSI model. On the other hand, HDRS suffers from the known spectral efficiency loss. Using relay selection with adaptive duplexing mode selection would enjoy the benefits of both, while avoiding their drawbacks.

• **Buffer-aided Opportunistic Mode and Relay Selection in Underlay Networks:** In underlay networks with buffer-less relaying, being either full-duplex or half-duplex, the secondary system's throughput is limited by the $\mathrm{S}-\mathrm{P}$ interference link bottleneck regardless of the state of the $\mathrm{R}_k-\mathrm{P}$ interference links. Buffer-aided relaying can alleviate this limitation in such an interference limited setting since round-robin source/relay activation is no longer mandated. This can allow the existing multiple relay's not only to offer diversity to the end-to-end secondary communication, but also to allow the diversity effect to go beyond that to include the diversification of the interference link.

• **Network-wide Interference Management/Cell Association:** Even in non-cooperative settings, while a full-duplex (FD) BS can support uplink and downlink for one FD user or

two different/distant half-duplex (HD) users over the same resource, inter-cell interference from nearby BSs (macro, pico, femto) can seriously limit the potential gains.

– Advanced (Massive) MIMO techniques can be used for interference mitigation, e.g., Adaptive pencil-beamforming, also utilizing higher mmWave communication bands.

– Stochastic-geometric tools can be used to spatially analyze inter-cell interference coordination (ICIC)-enabled scenarios for UE/FD-BS association.

– Like in HD heterogeneous networks, a user may typically be better served with two different BSs, one for uplink (UL) and one for downlink (DL). Decoupled UL/DL association now needs to be studied.

– Further studies are also necessary for more advanced cooperative scenarios where FD relay tiers exist; which users to serve directly through BS, which to serve via relays,etc.

APPENDICES

Appendix A

Useful Probability Distributions

A.1 Sum of Two RVs: $S = X_1 + X_2$

A.1.1 Gamma Distributed X_1 and X_2

Theorem 3 (CDF of $S = X_1 + X_2$)**.** *For two independent Gamma RVs, $X_1 \sim \mathcal{G}(m_1, \theta_1)$ and $X_2 \sim \mathcal{G}(m_2, \theta_2)$, with integer shape parameters and possibly distinct scale parameters, $S = X_1 + X_2$ has the following CDF [56]:*

$$F_S(s; \boldsymbol{p}) = \frac{\boldsymbol{\gamma}\left(m_2, \frac{s}{\theta_2}\right)}{\boldsymbol{\Gamma}(m_2)} - \sum_{k=0}^{m_1-1} \frac{A}{\boldsymbol{\Gamma}(v)} \left(\frac{s}{\theta_1}\right)^k {}_1\boldsymbol{F}_1(u; v; w), \tag{A.1}$$

where $\boldsymbol{p} = (m_1, \theta_1, m_2, \theta_2)$ is a vector holding the shape and scale parameters, $A = \left(\frac{s}{\theta_2}\right)^{m_2} \exp\left(-\frac{s}{\theta_2}\right)$, $u = k + 1$, $v = m_2 + k + 1$, $w = \frac{\theta_1 - \theta_2}{\theta_1 \theta_2} s$ and ${}_1\boldsymbol{F}_1(u; v; w)$ is the Kummer's confluent hypergeometric function [39, Eq. 13.1.2].

A.1.2 Exponentially Distributed X_1 and X_2

Corollary 1 (Special case when $m_1 = m_2 = 1$)**.** *For two independent exponential RVs, $X_1 \sim \text{Exp}(\pi_1)$ and $X_2 \sim \text{Exp}(\pi_2)$, $S = X_1 + X_2$ is a hypoexponential RV which has the following CDF [55, Eq. (5.9)]:*

$$F_S(s) = 1 - \frac{\pi_1 e^{-\frac{s}{\pi_1}} - \pi_2 e^{-\frac{s}{\pi_2}}}{\pi_1 - \pi_2}. \tag{A.2}$$

A.2 Ratio of Two RVs: $Z = X_1/(X_2 + 1)$

A.2.1 Gamma-Distributed X_1 and X_2

Theorem 4 (CDF of $Z = \frac{X_1}{X_2+1}$)**.** *The CDF of $Z = \frac{X_1}{X_2+1}$, where $X_i \sim \mathcal{G}(m_i, \theta_i)$, for $i \in \{1, 2\}$, are independent but not identically distributed (i.n.i.d.) RVs, for general real-valued $m_1 \geq \frac{1}{2}$ and integer-valued $m_2 \geq 1$, is given by [42, 43]:*

$$F_Z(z; \boldsymbol{p}) = \frac{\boldsymbol{\gamma}\left(m_1, \frac{z}{\theta_1}\right)}{\boldsymbol{\Gamma}(m_1)} + B \sum_{k=0}^{m_2-1} \frac{c^{-d}}{{\theta_2}^k} \boldsymbol{W}_{a,b}(c), \tag{A.3}$$

where $\boldsymbol{p} = (m_1, \theta_1, m_2, \theta_2)$ is a vector of distribution parameters, $\boldsymbol{\gamma}(\alpha, \beta) = \int_0^\beta t^{\alpha-1} e^{-t} dt$ is the lower incomplete Gamma function, $\boldsymbol{W}_{a,b}(c)$ is the Whittaker function [39, Eq. 13.1.33], $a = \frac{m_1-k-1}{2}$, $b = \frac{-m_1-k}{2}$, $c = \frac{z}{\theta_1} + \frac{1}{\theta_2}$, $d = \frac{m_1+k+1}{2}$ and

$$B = \frac{\exp\left(-\frac{1}{2}\left(\frac{z}{\theta_1} - \frac{1}{\theta_2}\right)\right)}{\boldsymbol{\Gamma}(m_1)} \left(\frac{z}{\theta_1}\right)^{m_1}. \tag{A.4}$$

A.2.2 Gamma-Distributed X_1 and Exponentially-Distributed X_2

Corollary 2 (Special case when $m_2 = 1$)**.** *When $X_2 \sim \text{Exp}(\pi_2)$, i.e., $m_2 = 1$, the CDF of $Z = \frac{X_1}{X_2+1}$ is given, for $\boldsymbol{p} = (m_1, \theta_1, 1, \pi_2)$, by:*

$$F_Z(z;\boldsymbol{p}) = \frac{\boldsymbol{\gamma}\left(m_1, \frac{z}{\theta_1}\right)}{\boldsymbol{\Gamma}(m_1)} + \frac{e^{\frac{1}{\pi_2}}}{\left(\frac{\theta_1}{z\pi_2}+1\right)^{m_1}} \frac{\boldsymbol{\Gamma}\left(m_1, \frac{1}{\pi_2}+\frac{z}{\theta_1}\right)}{\boldsymbol{\Gamma}(m_1)}, \tag{A.5}$$

where $\boldsymbol{\Gamma}(a,b) = \int_b^\infty t^{a-1}e^{-t}dt$ and $\boldsymbol{\gamma}(a,b) = \boldsymbol{\Gamma}(a) - \boldsymbol{\Gamma}(a,b)$ denote the upper and lower incomplete Gamma functions [39], respectively.

Proof. By conditioning/deconditioning on X_1, we have

$$\begin{aligned} F_Z(z;\boldsymbol{p}) &= \int_0^\infty \mathbb{P}\left\{X_2 \geq \frac{x_1 - z}{z} | X_1 = x_1\right\} \frac{x_1^{m_1-1}e^{-\frac{x_1}{\theta_1}}}{\boldsymbol{\Gamma}(m_1)\theta_1^{m_1}} \mathrm{d}x_1 \\ &= \frac{\boldsymbol{\gamma}\left(m_1, \frac{z}{\theta_1}\right)}{\boldsymbol{\Gamma}(m_1)} + e^{\frac{1}{\pi_2}} \int_z^\infty \frac{x_1^{m_1-1}e^{-x_1\left(\frac{1}{z\pi_2}+\frac{1}{\theta_1}\right)}}{\boldsymbol{\Gamma}(m_1)\theta_1^{m_1}} \mathrm{d}x_1, \end{aligned} \tag{A.6}$$

which yields (A.5) using [57, Eq. 3.381-3]. This can be verified to be a special case of (A.3) when $m_2 = 1$ using the relation between Whittaker's function $\boldsymbol{W}_{\cdot,\cdot}(\cdot)$ and Tricomi's confluent hypergeometric function $\boldsymbol{U}(\cdot,\cdot,\cdot)$ in [39, Eq. 13.1.33] and the special case of Tricomi's function in [39, Eq. 13.6.28]. □

A.2.3 Exponentially-Distributed X_1 and X_2

Corollary 3 (Special case when $m_1 = m_2 = 1$)**.** *When $X_1 \sim \text{Exp}(\pi_1)$ and $X_2 \sim \text{Exp}(\pi_2)$, the CDF of $Z = \frac{X_1}{X_2+1}$ is given, for $\boldsymbol{p} = (1, \pi_1, 1, \pi_2)$, by [41]:*

$$F_Z(z;\boldsymbol{p}) = 1 - \frac{\exp\left(-\frac{z}{\pi_1}\right)}{1 + z\frac{\pi_2}{\pi_1}}. \tag{A.7}$$

Appendix B

Papers Submitted and Under Preparation

Journal Papers

[J.5] **M. G. Khafagy**, M.-S. Alouini, and S. Aïssa, "Full-Duplex Relay Selection in Cognitive Underlay Networks," submitted to *IEEE Transactions on Wireless Communications*, second round.

[J.4] **M. G. Khafagy**, A. El Shafie, A. Sultan, and M.-S. Alouini, "Buffer-aided hybrid half-/full-duplex relaying with self-interference," *IEEE Transactions on Wireless Communications*, in preparation.

[J.3] **M. G. Khafagy**, A. Ismail, M.-S. Alouini, and S. Aïssa, "Efficient cooperative protocols for full-duplex relaying over Nakagami-m fading channels," *IEEE Transactions on Wireless Communications*, vol. 14, no. 6, Jun. 2015.

[J.2] A. El Shafie, **M. G. Khafagy**, and A. Sultan, "Optimization of a relay-assisted link with buffer state information at the source", *IEEE Communications Letters*, Vol. 18, no. 12, pp. 2149-2152, Dec. 2014.

[J.1] **M. Khafagy**, A. Ismail, M.-S. Alouini, and S. Aïssa, "On the outage performance of full-duplex selective decode-and-forward relaying," *IEEE Communications Letters*, June 2013.

Conference Papers

[C.5] M. Gaafar, **M. G. Khafagy**, O. Amin, and M.-S. Alouini, "Improper Gaussian signaling in full-duplex relay channels with residual self-interference," *IEEE ICC16*, Kuala Lumpur, Malaysia, accepted for publication.

[C.4] **M. G. Khafagy**, M.-S. Alouini, and S. Aïssa, "On the performance of future full-duplex relay selection networks," in *Proc. IEEE CAMAD*, Guildford, United Kingdom, Sept. 2015 (**invited paper**).

[C.3] **M. G. Khafagy**, M.-S. Alouini, and S. Aïssa, "Full-duplex opportunistic relay selection in future spectrum-sharing networks," in *Proc. IEEE ICC'15 Workshops*, London, United Kingdom, Jun. 2015.

[C.2] **M. G. Khafagy**, A. El Shafie, A. Sultan, and M.-S. Alouini, "Throughput maximization for buffer-aided hybrid half-/full-duplex relaying with self-interference," in *Proc. IEEE ICC'15*, London, United Kingdom, Jun. 2015.

[C.1] **M. Khafagy**, A. Ismail, M.-S. Alouini, and S. Aïssa, "Energy-efficient cooperative protocols for full-duplex relay channels," in *Proc. IEEE GLOBECOM'13 Workshops*, Atlanta, GA, USA, Dec. 2013.

REFERENCES

[1] Report ITU-R M.2370-0, "IMT traffic estimates for the years 2020 to 2030," Jul. 2015. [Online]. Available: https://www.itu.int/pub/R-REP-M.2370-2015

[2] G. Fettweis and S. Alamouti, "5G: Personal mobile internet beyond what cellular did to telephony," *IEEE Commun. Mag.*, vol. 52, no. 2, pp. 140–145, Feb. 2014.

[3] N. Bhushan, J. Li, D. Malladi, R. Gilmore, D. Brenner, A. Damnjanovic, R. Sukhavasi, C. Patel, and S. Geirhofer, "Network densification: the dominant theme for wireless evolution into 5G," *IEEE Commun. Mag.*, vol. 52, no. 2, pp. 82–89, Feb. 2014.

[4] C.-L. I, C. Rowell, S. Han, Z. Xu, G. Li, and Z. Pan, "Toward green and soft: a 5G perspective," *IEEE Commun. Mag.*, vol. 52, no. 2, pp. 66–73, Feb. 2014.

[5] S. Hong, J. Brand, J. Choi, M. Jain, J. Mehlman, S. Katti, and P. Levis, "Applications of self-interference cancellation in 5G and beyond," *IEEE Commun. Mag.*, vol. 52, no. 2, pp. 114–121, Feb. 2014.

[6] Report ITU-R M.2243, "Assessment of the global mobile broadband deployments and forecasts for International Mobile Telecommunications," Nov. 2011. [Online]. Available: http://www.itu.int/pub/R-REP-M.2243

[7] Report ITU-R M.2290-0, "Future spectrum requirements estimate for terrestrial IMT," Dec. 2013. [Online]. Available: http://www.itu.int/pub/R-REP-M.2290

[8] Report ITU-R M.2320-0, "Future technology trends of terrestrial IMT systems," Nov. 2014. [Online]. Available: https://www.itu.int/pub/R-REP-M.2320

[9] Report ITU-R M.2376-0, "Technical feasibility of IMT in bands above 6 GHz," Jul. 2015. [Online]. Available: https://www.itu.int/pub/R-REP-M.2376

[10] A. Sabharwal, P. Schniter, D. Guo, D. W. Bliss, S. Rangarajan, and R. Wichman, "In-band full-duplex wireless: Challenges and opportunities," *IEEE J. Sel. Areas Commun.*, vol. 32, no. 9, pp. 1637–1652, Sep. 2014.

[11] G. Liu, F. R. Yu, H. Ji, V. C. M. Leung, and X. Li, "In-band full-duplex relaying: A survey, research issues and challenges," *IEEE Commun. Surveys Tuts.*, vol. 17, no. 2, pp. 500–524, Secondquarter 2015.

[12] D. Kim, H. Lee, and D. Hong, "A survey of in-band full-duplex transmission: From the perspective of PHY and MAC layers," *IEEE Commun. Surveys Tuts.*, vol. 17, no. 4, pp. 2017–2046, Fourthquarter 2015.

[13] Recommendation ITU-R M.2083-0, "IMT Vision Framework and overall objectives of the future development of IMT for 2020 and beyond," Sep. 2015. [Online]. Available: https://www.itu.int/rec/R-REC-M.2083

[14] Y. Yang, H. Hu, J. Xu, and G. Mao, "Relay technologies for WiMax and LTE-advanced mobile systems," *IEEE Commun. Mag.*, vol. 47, no. 10, pp. 100 –105, Oct. 2009.

[15] H. Ju, E. Oh, and D. Hong, "Catching resource-devouring worms in next-generation wireless relay systems: Two-way relay and full-duplex relay," *IEEE Commun. Mag.*, vol. 47, no. 9, pp. 58–65, Sep. 2009.

[16] Y. Zhu, Y. Xin, and P.-Y. Kam, "Outage probability of Rician fading relay channels," *IEEE Trans. Veh. Technol.*, vol. 57, no. 4, pp. 2648 –2652, Jul. 2008.

[17] J. I. Choi, M. Jain, K. Srinivasan, P. Levis, and S. Katti, "Achieving single channel, full duplex wireless communication," in *Proc. ACM MobiCom'10*, Chicago, IL, Sep. 2010.

[18] M. Duarte and A. Sabharwal, "Full-duplex wireless communications using off-the-shelf radios: Feasibility and first results," in *Proc. ASILOMAR'10*, Pacific Grove, CA, Nov. 2010.

[19] Z. Zhang, K. Long, A. V. Vasilakos, and L. Hanzo, "Full-duplex wireless communications: Challenges, solutions, and future research directions," *Proc. IEEE*, vol. PP, no. 99, pp. 1–41, 2016.

[20] M. Jain, J. Choi, T. Kim, D. Bharadia, S. Seth, K. Srinivasan, P. Levis, S. Katti, and P. Sinha, "Practical, real-time, full duplex wireless," in *Proc. ACM MobiCom'11*, Las Vegas, NV, Sep. 2011. [Online]. Available: http://doi.acm.org/10.1145/2030613.2030647

[21] M. Duarte, C. Dick, and A. Sabharwal, "Experiment-driven characterization of full-duplex wireless systems," *IEEE Trans. Wireless Commun.*, vol. 11, no. 12, pp. 4296–4307, Dec. 2012.

[22] D. Bharadia, E. McMilin, and S. Katti, "Full duplex radios," in *Proc. ACM SIGCOMM'13*. New York, NY, USA: ACM, 2013, pp. 375–386. [Online]. Available: http://doi.acm.org/10.1145/2486001.2486033

[23] E. Ahmed, A. M. Eltawil, and A. Sabharwal, "Rate gain region and design tradeoffs for full-duplex wireless communications," vol. 12, no. 7, pp. 3556–3565, Jul. 2013.

[24] E. Everett, A. Sahai, and A. Sabharwal, "Passive self-interference suppression for full-duplex infrastructure nodes," *IEEE Trans. Wireless Commun.*, vol. 13, no. 2, pp. 680–694, Feb. 2014.

[25] E. Ahmed and A. M. Eltawil, "All-digital self-interference cancellation technique for full-duplex systems," vol. 14, no. 7, pp. 3519–3532, Jul. 2015.

[26] E. Ahmed, A. M. Eltawil, Z. Li, and B. A. Cetiner, "Full-duplex systems using multi-reconfigurable antennas," vol. 14, no. 11, pp. 5971–5983, Nov. 2015.

[27] M. Jain, "Single channel full-duplex wireless radios," Ph.D. dissertation, Stanford University, Aug. 2011. [Online]. Available: https://stacks.stanford.edu/file/druid:zh047jt6489/thesis-augmented.pdf

[28] M. Duarte, "Full-duplex wireless: Design, implementation and characterization," Ph.D. dissertation, Rice University, Apr. 2012. [Online]. Available: https://scholarship.rice.edu/handle/1911/70233

[29] E. A. E. Ahmed, "Self-interference cancellation in full-duplex wireless systems," Ph.D. dissertation, University of California, Irvine, 2014.

[30] E. Everett, "Full-duplex infrastructure nodes: Achieving long range with half-duplex mobiles," Apr. 2012. [Online]. Available: https://scholarship.rice.edu/handle/1911/64704

[31] T. Riihonen, S. Werner, and R. Wichman, "Mitigation of loopback self-interference in full-duplex MIMO relays," *IEEE Trans. Signal Process.*, vol. 59, no. 12, pp. 5983 –5993, Dec. 2011.

[32] L. Jimenez Rodriguez, N. H. Tran, and T. Le-Ngoc, "Performance of full-duplex AF relaying in the presence of residual self-interference," *IEEE J. Sel. Areas Commun.*, vol. 32, no. 9, pp. 1752–1764, Sep. 2014.

[33] N. Shende, O. Gurbuz, and E. Erkip, "Half-duplex or full-duplex relaying: A capacity analysis under self-interference," in *Proc. CISS'13*, Baltimore, MD, USA, Mar. 2013.

[34] T. Riihonen, S. Werner, and R. Wichman, "Hybrid full-duplex/half-duplex relaying with transmit power adaptation," *IEEE Trans. Wireless Commun.*, vol. 10, no. 9, pp. 3074–3085, Sep. 2011.

[35] ——, "Optimized gain control for single-frequency relaying with loop interference," *IEEE Trans. Wireless Commun.*, vol. 8, no. 6, pp. 2801–2806, Jun. 2009.

[36] T. Riihonen, S. Werner, R. Wichman, and J. Hamalainen, "Outage probabilities in infrastructure-based single-frequency relay links," in *Proc. IEEE WCNC'09*, Budapest, Hungary, Apr. 2009.

[37] M. Nakagami, "The m-distribution, a general formula of intensity distribution of rapid fading," *Statistical Method of Radio Propagation*, 1960.

[38] M. K. Simon and M.-S. Alouini, *Digital communication over fading channels.* Wiley-Interscience, 2005, vol. 95.

[39] M. Abramowitz and I. A. Stegun, Eds., *Handbook of Mathematical Functions,* 10^{th} *Printing.* Dover Publications, Dec. 1972.

[40] H. Alves, G. Fraidenraich, R. D. Souza, M. Bennis, and M. Latva-aho, "Performance analysis of full duplex and selective and incremental half duplex relaying schemes," in *Proc. IEEE WCNC'12*, Paris, France, Apr. 2012.

[41] T. Kwon, S. Lim, S. Choi, and D. Hong, "Optimal duplex mode for DF relay in terms of the outage probability," *IEEE Trans. Veh. Technol.*, vol. 59, no. 7, pp. 3628 –3634, Sep. 2010.

[42] P. K. Sharma and P. Garg, "Outage analysis of full duplex decode and forward relaying over Nakagami-m channels," in *Communications (NCC), 2013 National Conference on*, New Delhi, India, Feb. 2013.

[43] H. Alves, D. da Costa, R. Souza, and M. Latva-aho, "Performance of block-Markov full duplex relaying with self interference in Nakagami-m fading," vol. 2, no. 3, pp. 311–314, Jun. 2013.

[44] B. Yu, L. Yang, X. Cheng, and R. Cao, "Power and location optimization for full-duplex decode-and-forward relaying," *IEEE Trans. Commun.*, vol. 63, no. 12, pp. 4743–4753, Dec. 2015.

[45] J. Laneman, D. Tse, and G. Wornell, "Cooperative diversity in wireless networks: Efficient protocols and outage behavior," *IEEE Trans. Inf. Theory*, vol. 50, no. 12, pp. 3062–3080, Dec. 2004.

[46] I. Krikidis, H. A. Suraweera, P. J. Smith, and C. Yuen, "Full-duplex relay selection for amplify-and-forward cooperative networks," *IEEE Trans. Wireless Commun.*, vol. 11, no. 12, pp. 4381–4393, Dec. 2012.

[47] P. J. Schreier and L. L. Scharf, *Statistical signal processing of complex-valued data: the theory of improper and noncircular signals.* Cambridge University Press, 2010.

[48] Y. Zeng, C. M. Yetis, E. Gunawan, Y. L. Guan, and R. Zhang, "Transmit optimization with improper Gaussian signaling for interference channels," *IEEE Trans. Signal Process.*, vol. 61, no. 11, pp. 2899–2913, Jun. 2013.

[49] C. Hellings, L. Gerdes, L. Weiland, and W. Utschick, "On optimal Gaussian signaling in MIMO relay channels with partial decode-and-forward," *IEEE Trans. Signal Process.*, vol. 62, no. 12, pp. 3153–3164, Jun. 2014.

[50] M. Gaafar, M. G. Khafagy, O. Amin, and M.-S. Alouini, "Improper Gaussian signaling in full-duplex relay channels with residual self-interference," in *Proc. IEEE ICC'16*, Kuala Lumpur, Malaysia, May 2016, accepted for publication.

[51] G. Kramer, M. Gastpar, and P. Gupta, "Cooperative strategies and capacity theorems for relay networks," *IEEE Trans. Inf. Theory*, vol. 51, no. 9, pp. 3037–3063, Sep. 2005.

[52] G. Kramer, "Topics in multi-user information theory," *Foundations and Trends in Communications and Information Theory*, 2008. [Online]. Available: http://dx.doi.org/10.1561/0100000028

[53] V. V. Prasolov, *Polynomials*. Springer Science & Business Media, 2009.

[54] W.-C. Yueh and S. S. Cheng, "Explicit eigenvalues and inverses of several toeplitz matrices," *The ANZIAM Journal*, vol. 48, no. 01, pp. 73–97, Jul. 2006.

[55] S. M. Ross, *Introduction to Probability Models*, 10th ed. New York: Academic Press, 2010.

[56] A. Chelli and M.-S. Alouini, "On the performance of hybrid-ARQ with incremental redundancy and with code combining over relay channels," *IEEE Trans. Wireless Commun.*, vol. 12, no. 8, pp. 3860–3871, Aug. 2013.

[57] I. S. Gradshteyn and I. M. Ryzhik, *Table of Integrals, Series, and Products, Seventh Edition*. Academic Press, 2007.

[58] A. Bletsas, A. Khisti, D. Reed, and A. Lippman, "A simple cooperative diversity method based on network path selection," *IEEE J. Sel. Areas Commun.*, vol. 24, no. 3, pp. 659–672, Mar. 2006.

[59] A. Bletsas, H. Shin, and M. Z. Win, "Cooperative communications with outage-optimal opportunistic relaying," *IEEE Trans. Wireless Commun.*, vol. 6, no. 9, pp. 3450–3460, Sep. 2007.

[60] D. S. Michalopoulos and G. K. Karagiannidis, "Performance analysis of single relay selection in Rayleigh fading," *IEEE Trans. Wireless Commun.*, vol. 7, no. 10, pp. 3718–3724, Oct. 2008.

[61] F. Xu, F. C. M. Lau, Q. F. Zhou, and D. W. Yue, "Outage performance of cooperative communication systems using opportunistic relaying and selection combining receiver," *IEEE Signal Process. Lett.*, vol. 16, no. 2, pp. 113–116, Feb. 2009.

[62] S. S. Ikki and M. H. Ahmed, "Performance analysis of adaptive decode-and-forward cooperative diversity networks with best-relay selection," *IEEE Trans. Commun.*, vol. 58, no. 1, pp. 68–72, Jan. 2010.

[63] K. Yan, J. Jiang, Y. G. Wang, and H. T. Liu, "Outage probability of selection cooperation with mrc in nakagami-m fading channels," *IEEE Signal Process. Lett.*, vol. 16, no. 12, pp. 1031–1034, Dec. 2009.

[64] G. C. Alexandropoulos, A. Papadogiannis, and K. Berberidis, "Performance analysis of cooperative networks with relay selection over nakagami-m fading channels," vol. 17, no. 5, pp. 441–444, May 2010.

[65] I. Krikidis, H. A. Suraweera, and C. Yuen, "Amplify-and-forward with full-duplex relay selection," in *Proc. IEEE ICC'12*, Ottawa, Canada, Jun. 2012.

[66] I. Krikidis, H. Suraweera, P. J. Smith, and C. Yuen, "Full-duplex relay selection for amplify-and-forward cooperative networks," *IEEE Trans. Wireless Commun.*, vol. 11, no. 12, pp. 4381–4393, Dec. 2012.

[67] J. Lee, H. Wang, J. G. Andrews, and D. Hong, "Outage probability of cognitive relay networks with interference constraints," *IEEE Trans. Wireless Commun.*, vol. 10, no. 2, pp. 390–395, Feb. 2011.

[68] M. G. Khafagy, A. Ismail, M.-S. Alouini, and S. Aïssa, "Efficient cooperative protocols for full-duplex relaying over nakagami-m fading channels," *IEEE Trans. Wireless Commun.*, 2015.

[69] J. Mitola and G. Q. Maguire, Jr, "Cognitive radio: Making software radios more personal," *IEEE Personal Commun. Mag.*, vol. 6, no. 4, pp. 13–18, Aug. 1999.

[70] A. Goldsmith, S. A. Jafar, I. Maric, and S. Srinivasa, "Breaking spectrum gridlock with cognitive radios: An information theoretic perspective," *Proc. IEEE*, vol. 97, no. 5, pp. 894–914, May 2009.

[71] K. Letaief and W. Zhang, "Cooperative communications for cognitive radio networks," *Proc. IEEE*, vol. 97, no. 5, pp. 878–893, May 2009.

[72] S. I. Hussain, M. M. Abdallah, M.-S. Alouini, M. Hasna, and K. Qaraqe, "Best relay selection using SNR and interference quotient for underlay cognitive networks," in *Proc. IEEE ICC'12*, Ottawa, Canada, Jun. 2012.

[73] S. I. Hussain, M.-S. Alouini, K. Qaraqe, and M. Hasna, "Reactive relay selection in underlay cognitive networks with fixed gain relays," in *Proc. IEEE ICC'12*, Ottawa, Canada, Jun. 2012.

[74] ——, "Outage analysis of selective cooperation in underlay cognitive networks with fixed gain relays and primary interference modeling," in *Proc. IEEE PIMRC'12*, Sydney, Australia, Sep. 2012.

[75] G. Chen, Y. Gong, and J. Chambers, "Study of relay selection in a multi-cell cognitive network," vol. 2, no. 4, pp. 435–438, Aug. 2013.

[76] Y. Zou, J. Zhu, B. Zheng, and Y.-D. Yao, "An adaptive cooperation diversity scheme with best-relay selection in cognitive radio networks," *IEEE Trans. Signal Process.*, vol. 58, no. 10, pp. 5438–5445, Oct. 2010.

[77] S. Sagong, J. Lee, and D. Hong, "Capacity of reactive DF scheme in cognitive relay networks," *IEEE Trans. Wireless Commun.*, vol. 10, no. 10, pp. 3133–3138, Oct. 2011.

[78] H. Chamkhia, M. O. Hasna, R. Hamila, and S. I. Hussain, "Performance analysis of relay selection schemes in underlay cognitive networks with decode and forward relaying," in *Proc. IEEE PIMRC'12*, Sydney, Australia, Sep. 2012.

[79] X. Zhang, Z. Yan, Y. Gao, and W. Wang, "On the study of outage performance for cognitive relay networks (CRN) with the Nth best-relay selection in rayleigh-fading channels," vol. 2, no. 1, pp. 110–113, Feb. 2013.

[80] G. Zheng, I. Krikidis, and B. Ottersten, "Full-duplex cooperative cognitive radio with transmit imperfections," *IEEE Trans. Wireless Commun.*, vol. 12, no. 5, pp. 2498–2511, May 2013.

[81] H. Kim, S. Lim, H. Wang, and D. Hong, "Power allocation and outage probability analysis for secondary users in cognitive full duplex relay systems," in *Proc. IEEE SPAWC'12*, Cesme, Turkey, Jun. 2012.

[82] ——, "Optimal power allocation and outage analysis for cognitive full duplex relay systems," *IEEE Trans. Wireless Commun.*, vol. 11, no. 10, pp. 3754–3765, Oct. 2012.

[83] Y. Shi, L. Zhang, Z. Chen, Y. Gong, and G. Wu, "Optimal power allocation for AF full-duplex relay in cognitive radio networks," in *Proc. IEEE GC Wkshps'13*, Atlanta, GA, USA, Dec. 2013.

[84] B. Xia, Y. Fan, J. Thompson, and H. V. Poor, "Buffering in a three-node relay network," *IEEE Trans. Wireless Commun.*, vol. 7, no. 11, pp. 4492–4496, Nov. 2008.

[85] N. Zlatanov, R. Schober, and P. Popovski, "Buffer-aided relaying with adaptive link selection," *IEEE J. Sel. Areas Commun.*, vol. 31, no. 8, pp. 1530–1542, Aug. 2013.

[86] J. Boyer, D. Falconer, and H. Yanikomeroglu, "Multihop diversity in wireless relaying channels," *IEEE Trans. Commun.*, vol. 52, no. 10, pp. 1820–1830, Oct. 2004.

[87] I. Krikidis, T. Charalambous, and J. S. Thompson, "Buffer-aided relay selection for cooperative diversity systems without delay constraints," *IEEE Trans. Wireless Commun.*, vol. 11, no. 5, pp. 1957–1967, May 2012.

[88] S. Boyd and L. Vandenberghe, *Convex optimization*. Cambridge University Press, 2004.

[89] M. Grant and S. Boyd, "CVX: Matlab software for disciplined convex programming, version 2.1," Mar. 2014. [Online]. Available: http://cvxr.com/cvx